UNIVERSITAT DE BARCELONA

Holography applications in the strongly coupled sector: from QCD to the new physics

Alisa Katanaeva

Holography applications to strongly coupled sectors: from QCD to New Physics

Alisa Katanaeva

PhD advisors:

Domènec Espriu Climent and Sergei Afonin

UNIVERSITAT DE BARCELONA

Holography applications in the strongly coupled sector: from QCD to the new physics

Memòria presentada per optar al grau de doctor per la
Universitat de Barcelona

Programa de Doctorat en Física

Autora:

Alisa Katanaeva

Directors:

Domènec Espriu Climent i Sergei Afonin

Tutor:

Domènec Espriu Climent

Departament de Física Quàntica i Astrofísica

UNIVERSITAT DE BARCELONA

Acknowledgments

While writing this thesis I required help not once because not always everything went on smoothly. Assistance came from different sources and, spectacularly, frequently a tiniest piece of advice pushed the research process much further. These instances showed me that discussion and exchange of opinions play an important role in the scientific process, and altogether it is undoubtedly great to be a part of the physics community.

From the personal perspective, I am obliged to my advisors Domènec Espriu and Sergei Afonin for endowing me with their knowledge and experience in physics and their profound interest in these research projects. Also, I would like to thank Alexander Andrianov for introducing me to the idea of having a PhD abroad and providing his professional opinion at different stages of my investigation.

This project received funding and support from the following grants:
MDM-2014-0369 (MINECO), FPA2016-76005-C2-1-P, PID2019-105614GB-C21 (MICINN), and 2017SGR0929 (Generalitat de Catalunya). The personal support to the doctorand was provided in the fellowship under the reference of BES-2015-072477.

Resumen

En esta tesis estudiamos sectores fuertemente acoplados en el Modelo Estándar (SM) y más allá (BSM) utilizando el enfoque holográfico. Nuestra estrategia es ensayar el método en aplicaciones donde la física mejor estudiada (cromodinámica cuántica (QCD)), y luego utilizar el conocimiento acumulado en un ámbito que esté fuera del alcance de los experimentos actuales (BSM).

Las ideas holográficas aparecieron después de la observación de Bekenstein y Hawking sobre la naturaleza de la entropía del agujero negro. El principio holográfico general se formuló de la siguiente manera: todo el contenido de información de una teoría de la gravedad cuántica en un volumen dado se puede codificar en una teoría efectiva sobre la frontera. La correspondencia anti-de Sitter / teoría conforme de campos (AdS/CFT) combinó holografía y dualidades (por esa razón también se conoce con el nombre de dualidad gauge/gravedad) en una interesante propuesta para la investigación tanto de la teoría de cuerdas como de aspectos de la gravedad cuántica.

Sin embargo, poco después se descubrió que la teoría supersimétrica $\mathcal{N} = 4$ de Yang-Mills, para la que Maldacena había encontrado la teoría dual de cuerdas, es en cierto modo similar a QCD en el régimen fuertemente acoplado. Eso desvió la atención a la parte gauge de la correspondencia. Sorprendentemente, la teoría de cuerdas es más fácil de resolver que la teoría habitual de quarks y gluones, porque según la conjetura AdS/CFT está en el límite semiclásico y débilmente acoplado.

Existen pocas herramientas teóricas para estudiar regímenes fuertemente acoplados. Para QCD, el más conocido es la formulación de primeros principios en el retículo (lattice). Esta formulación reveló mucho sobre la naturaleza de QCD. Por ejemplo, señaló que la transición de desconfinamiento de los estados de hadrones ligados al plasma de quark-gluones ocurre suavemente (crossover). Desafortunadamente, no es omnipotente: además de las restricciones tecnológicas y la complejidad cada vez mayor de los cálculos numéricos, existe, por ejemplo, un problema mucho más profundo relacionado con la inclusión del potencial químico de los

quarks finito. Este último define uno de los ejes del diagrama de fase QCD, de modo que lattice QCD no puede analizarlo en su totalidad.

A su vez, la holografía se puede utilizar para abordar varios aspectos de QCD: espectros de mesones, glueballs y bariones, interacciones hadrónicas y el proceso de hadronización en colisionadores, confinamiento y ruptura de simetría quiral, materia hadrónica en condiciones externas extremas. Sin embargo, existen varias limitaciones en QCD que aparecen en construcciones similares a AdS/CFT. Primero, se supone que debe estar en el límite de N_c grande. Independientemente de la holografía, se demostró que este límite puede verse como una versión deformada de QCD con $N_c = 3$ en la que el número de excitaciones radiales de un estado dado es infinito, cada una de ellas es infinitamente estrecha, el desconfinamiento representa una transición de fase real, etc. En segundo lugar, la propiedad de confinamiento no se puede combinar con CFT; uno debería encontrar una manera de romper la invariancia conforme e introducir una escala QCD Λ_{QCD}. No hace falta decir que se desconoce la teoría dual exacta para QCD, si es que existe.

En esta tesis utilizamos el llamado enfoque holográfico bottom-up (AdS/QCD) que fue desarrollado para rodear determinadas dificultades teóricas (la imposibilidad de encontrar un dual exacto de QCD) y que se busca sobre todo una descripción exitosa de la fenomenología de QCD.

En AdS/QCD se construyen modelos de cinco dimensiones siguiendo las reglas del diccionario AdS/CFT. Los campos $5D$ corresponden a los operadores de interpolación en 4D y pueden considerarse como la conexión entre la fuente sobre la frontera y un punto en el volumen. Las funciones de Green, que definen la teoría $4D$, se pueden calcular a partir de la acción $5D$ debido a la correspondencia entre las funciones de partición. Al mismo tiempo, la representación de Kaluza-Klein de un campo $5D$ contiene los grados de libertad físicos reales $4D$ con los números cuánticos de los operadores duales. Se puede extraer el espectro de masas de estos modos. La invariancia conforme del espacio AdS_5 se rompe mediante la introducción manual de una "pared" en la quinta dirección (z). Básicamente, se pueden considerar paredes de dos tipos: la pared dura (hard wall), que es solo un corte a una distancia finita en la dirección z, y la pared blanda (soft wall), donde se introduce un perfil exponencial en la acción para suprimir cualquier contribución en z -infinito.

Ha habido y hay innumerables esfuerzos para aplicar la holografía en muchos sistemas físicos fuertemente interactuantes, incluso aparentemente tan desconectados de la teoría de cuerdas como la física de la materia condensada. Nuestro interés

particular es la incorporación de modelos AdS/QCD en el ámbito de la física BSM. Hay varias ideas sobre cómo podrían producirse dinámicas fuertes allí. Nos centramos en los modelos de Higgs compuesto (CH), donde la nueva interacción fuerte une a los hiper-fermiones en estados compuestos a energías TeV, en paralelo a lo que ocurre en QCD, que une (de hecho confina) a los quarks del SM en mesones y bariones. Este nuevo sector a la escala energética de varios TeV podría resolver el problema de naturalidad del SM al precio de una afinación (fine tuning) relativamente pequeña. Además, proporciona predicciones BSM dentro de un alcance experimental relativamente cercano, lo que lo hace especialmente interesante.

Por lo tanto, en esta tesis presentamos nuestras investigaciones de QCD y de CH usando un enfoque holográfico bottom-up. Una revisión de una amplia gama de temas es un requisito previo en este tipo de estudio que combina construcciones teóricas sofisticadas y análisis de datos fenomenológicos. En el Capítulo 2 revisamos el formalismo teórico detrás de las dualidades gauge/gravedad. Los capítulos 3 y 4 se refieren a las características teóricas y fenomenológicas relevantes de la QCD. En el Capítulo 5 presentamos modelos simples de AdS/QCD y delineamos el análisis holográfico de los espectros de partículas. El Capítulo 6 contiene nuestros resultados originales sobre la determinación de la temperatura de desconfinación de QCD en el marco de AdS/QCD. El Capítulo 7 corresponde al artículo dedicado al estudio de la física de QCD de baja energía desencadenada por la implementación particular de la ruptura de simetría quiral en el modelo "soft wall". En el Capítulo 8 se presenta el trabajo sobre Higgs compuesto holográfico.

Comenzamos en el Capítulo 2 con una descripción del formalismo central, el de la correspondencia AdS/CFT. Las prescripciones holográficas generales se recopilan en el diccionario AdS/CFT. Luego, especificamos al caso la dualidad de Maldacena entre la teoría de cuerdas tipo IIB en $AdS_5 \times S_5$ espacio-tiempo y la teoría supersimétrica $\mathcal{N} = 4$ de Yang-Mills en cuatro dimensiones. Discutimos en qué sentido la parte gauge de esta dualidad es similar a large-N_c QCD y qué aspectos faltan.

En el Capítulo 3 discutimos algunos temas seleccionados de QCD. Revisamos varios métodos bien establecidos que permiten estudiar la QCD en diferentes regímenes: a gran número de colores, a bajas energías, centrándonos en las implicaciones de la simetría quiral y a temperatura finita. También cubrimos la expansión de productos del operador, la formulación lattice de QCD, sus predicciones e implicaciones.

Los observables fenomenológicos de hadrones se consideran en el Capítulo 4

e incluyen los espectros de las resonancias, los acoplamientos y los factores de forma. Investigamos en detalle la idea de excitaciones de mesones radiales que pertenecen a las trayectorias radiales lineales de Regge, y enfatizamos la noción de trayectorias universales de excitaciones radiales de los mesones. También se analizan los espectros de glueballs, estudiados en lattice QCD.

Habiendo resaltado las características fenomenológicas relevantes de QCD, pasamos a su implementación holográfica bottom-up. El formalismo general de incluir resonancias QCD en el volumen $5D$ se presenta en el Capítulo 5. Presentamos varios modelos simples de AdS/QCD: "hard wall", "soft wall" y "generalized soft wall". Se evalúan sobre la base de su éxito en la descripción de los espectros fenomenológicos. Los modelos de tipo "soft wall" exhiben la linealidad de las trayectorias radiales que se esperan en las teorías con la realización adecuada del confinamiento. Además, mencionamos la posibilidad de tener diversos perfiles de "soft wall" que conduzcan a los mismos espectros.

En AdS/QCD se asume que la transición de la fase de desconfinamiento es dual a la transición Hawking-Page entre diferentes geometrías en la teoría $5D$. Eso nos permite estimar la temperatura (pseudo) crítica de desconfinamiento, T_c. En el Capítulo 6 exploramos varios modelos holográficos con diferentes opciones para fijar sus parámetros con el fin de obtener el valor fenomenológico de T_c. Los resultados dependen bastante de la elección de los parámetros del modelo. Concluimos que hay un subconjunto que proporciona T_c cerca de las estimaciones de quenched lattice y large-N_c, y aquellas que predicen T_c en el rango físico (temperatura de freeze-out, estimaciones lattice con quarks dinámicos).

El mecanismo holográfico AdS/QCD para la implementación dual de la ruptura de la simetría quiral se desarrolla en el Capítulo 7. Elegimos el marco "soft wall" e introducimos varias características novedosas para acomodar mejor los modos Goldstone. El modelo resultante no tiene muchos parámetros libres y debido a este minimalismo proporciona interesantes interrelaciones entre diferentes sectores. Se extraen varios observables de interés. El resultado fenomenológico se da en términos del ajuste a quince QCD observables con el error cuadrático medio de $\sim 30\%$.

En el Capítulo 8 comenzamos con la motivación para la extensión de BSM con el sector fuertemente acoplado y enfatizamos las ventajas de los modelos CH. Además, nos especializamos en el caso de CH mínimo con el patrón de ruptura de la nueva simetría de sabor tipo $SO(5) \to SO(4)$. Allí aplicamos la técnica AdS/QCD y, en concreto, utilizamos la experiencia del capítulo anterior. Sin em-

bargo, las diferencias con el caso QCD no son tan simples como el intercambio de los grupos de ”sabor” y ”color”. La reconsideración de la realización holográfica y el papel de los bosones de Goldstone es un desarrollo importante del capítulo. Calculamos las masas de las nuevas resonancias compuestas, estimamos varios acoplamientos entre los nuevos estados del sector y los bosones electro-débiles y analizamos la realización holográfica de la primera y segunda reglas de suma de Weinberg.

Los límites experimentales de los observables de precisión electro-débil y el ángulo de desalineación, así como el valor conocido de la escala electro-débil, restringen el espacio de parámetros del modelo holográfico y especifican la escala de sus predicciones. Concluimos que el modelo es capaz de acomodar nuevas resonancias vectoriales con masas en el rango de 2-3 TeV sin encontrar otras dificultades fenomenológicas.

En conclusión, aunque los métodos AdS/QCD están lejos de ser precisos, son útiles aunque solo sea para proporcionar un marco bastante simple donde se pueden diseñar y probar diferentes escenarios. Al mismo tiempo, es fundamental tratar conscientemente la cantidad de libertad que otorga este marco fenomenológico. Nos esforzamos por encontrar este equilibrio y elaboramos para motivar bien las suposiciones y elecciones tomadas a lo largo de la construcción del modelo holográfico.

Contents

List of publications

The original contents of this thesis are based on the following publications.

In peer-reviewed journals:

1. S. S. Afonin and A. D. Katanaeva, Glueballs and deconfinement temperature in AdS/QCD, Physical Review D **98**, 114027 (2018) [arXiv:1809.07730 [hep-ph]].

2. S. S. Afonin and A. D. Katanaeva, Estimates of the deconfinement temperature in AdS/QCD, Theoretical and Mathematical Physics, **200(3)**: 1383–1400 (2019).

3. D. Espriu, A. Katanaeva, Effects of bulk symmetry breaking on AdS/QCD predictions, Physical Review D **101**, 074017 (2020) [arXiv:2001.08723 [hep-ph]].

4. D. Espriu, A. Katanaeva, Soft Wall holographic model for the minimal Composite Higgs, [arXiv:2008.06207 [hep-ph]].

Unpublished:

- D. Espriu, A. Katanaeva, Holographic description of $SO(5) \to SO(4)$ composite Higgs model, [arXiv:1706.02651 [hep-ph]].

Proceedings:

- D. Espriu and A. Katanaeva, Composite Higgs Models: a new holographic approach, Proceedings of Science (Confinement2018) 275 (2019), [arXiv:1812.01523 [hep-ph]];

- Afonin, S. S., Katanaeva, A. D., Prokhvatilov, E. V., Vyazovsky, M. I., Deconfinement Temperature in AdS/QCD from the Spectrum of Scalar Glueballs, Acta Physica Polonica B, Proceedings Supplement, **13**, 33-38 (2020);

- Afonin, S. S., Katanaeva, A. D., On holographic relation between radial meson trajectories and deconfinement temperature, Hadron Spectroscopy and Structure, 718-721 (2020).

List of abbreviations

AdS	Anti de Sitter
BSM	Beyond the Standard Model
CFT	Conformal Field Theory
CH	Composite Higgs
EFT	Effective Field Theory
EOM	Equations of Motion
EW	Electroweak
EWSB	Electroweak Symmetry Breaking
FF	Form Factor
GSW	Generalized Soft Wall
HP	Hawking–Page
HW	Hard Wall
IR	Infrared
KK	Kaluza–Klein
LHC	Large Hadron Collider
OPE	Operator Product Expansion
QCD	Quantum Chromodynamics
QFT	Quantum Field Theory
SCSB	Spontaneous Chiral Symmetry Breaking
SM	Standard Model
SW	Soft Wall
SYM	Supersymmetric Yang–Mills
UV	Ultraviolet
vev	vacuum expectation value
VMD	Vector Meson Dominance
YM	Yang–Mills

Chapter 1

Introduction

Physics is about discovering and systematising the laws of Nature, in that we agree with Eugene Wigner [1]. The utmost goal of a physicist is to learn to predict future based on the regularities studied in present or past. However, the laws are not necessarily fundamental, we would rather define them as a scientist's interpretation of the abstract logic behind the natural phenomena. The interpretation can be performed at different levels of detail and accuracy, taking into account limited sets of the world characteristics. That makes the laws of Nature conditional: a specific set of circumstances should take place so that they could be used to predict future. However, in exceptionally good interpretations a vast majority of the determinants of the present state of the world turns out irrelevant for the prediction. That is why the experiments, in which one intents to put most of the main relevant determinants into the scientist's direct control, play such an important role in physics. At the same time, we have to admit that the laws of Nature relate only to a very small part of our knowledge of the world. Moreover, nowadays we do not believe anymore in the precision of these statements: they are the probability laws making a specific statistical kind of prediction, which in common understanding could be seen just as an intelligent guess on future properties of the system.

Laws form theories. An interpretation (or realization) of the general law is made through a physical model and takes appearance of a stylized (in mathematical terms) description of a target system. More rigid definitions are developed in philosophy of science [2]. A *theory* is taken to be a (usually deductively closed) set of sentences in a formal language. A *model* is a structure that makes all sentences of a theory true when its symbols are interpreted as referring to objects, relations, or functions of a structure. In this point of view models are seen as subordinate to theory and as playing no role outside its context. But can we really understand

what are the models from these definitions? Are there some examples that are not described by them? Indeed, there exists a certain skepticism on whether models belong to a distinctive ontological category and whether, in fact, anything can be a model.

First, what it means for a model to represent and/or explain a target system? In physics we often work with *idealized* models, that involve a deliberate simplification or distortion of something complicated with the objective of making it more tractable or understandable. Idealizations are crucial to cope with systems that are too hard to study in their full complexity. However, we retain the belief that, in principle, it is possible to lift up the simplifications, and the predictions will not be drastically altered. The latter is no longer true for the *toy* models that are simplified to a degree when it is questionable whether they could be regarded as representational at all. They do not perform well in terms of prediction and empirical adequacy, but, as they keep some key features, may help, for instance, to outline the general calculation procedure. *Phenomenological* models are very frequent in particle physics. A general definition could be given as of the models that only represent specific known (observed or deduced) properties of their targets and refrain from containing any hidden mechanisms and the like [2]. They are not completely independent of theories and often incorporate principles and laws associated with them. To identify phenomenological models with models of a phenomenon is rather vague, because "phenomena" cover all relatively stable and general features of the world that are interesting from a scientific point of view.

Second, it is reasonable to classify some types of models as those being independent from theories. To start, some established theories may be too complicated to handle in particular cases. Then, a *complementary* model can provide a simplified version of the theoretical scenario that allows for a solution. There are various well-known phenomenological models complementary to quantum chromodynamics in this sense. *"Study"* or *probing* model do not perform a representational function and are not expected to instruct us about anything beyond the model itself. They are meant to be used to test new theoretical techniques that are used later on to build representational models. A φ^4 field theory is a prominent example.

Of course, in everyday communication (and even in this thesis) we frequently mix the terms "theory" and "model". However, we find it interesting to mention these several abstract concepts, though neither there exists a common philosophical view on the problem. There is even an idea that models are independent from both theories and their target systems, and should be seen as the instruments that mediate

between the two. That is reasoned, among other things, by the fact that models may be influenced by several theories.

Next, we would like to dwell on the notion of *duality*. In this thesis we study the applications of the AdS/CFT correspondence, also known as the gauge/gravity duality. The gravity side usually refers to the string theory in a many-dimensional spacetime (like $AdS_5 \times S_5$) that necessarily contains a graviton mode, while the gauge theory resides in a four-dimensional world. The pair should be further specified, for instance, as in the Maldacena realization of the duality [3]. The two theories are called dual because their symmetries, physically meaningful predictions and consequences coincide, though they are originally defined in different spacetimes and have different internal dynamics. One way to view such dual pairs is in terms of these two being distinct classical limits of a more all-encompassing quantum field theory. Unfortunately, it is problematic to construct and make sense of such fundamental theory.

A similar example concerns the dualities connecting physically distinct superstring theories between each other and to an assumed unifying eleven-dimensional theory, called the M-theory by Edward Witten. The S-duality, also known as weak/strong duality, plays an important role there. It allows to write the perturbation series in the unifying QFT in two equivalent ways, using distinct sets of fields and couplings. The duality states that the coupling constants are inversely proportional to each other. Quantum theory taken at a limit of small coupling is classical in a sense that the weight in path integral is contributing most when the action is evaluated on classical solutions. With S-duality there will be at least two such classical limits. Even the original wave-particle duality already can be regarded as an example of such duality [4]. One limit of QFT gives classical fields, the other classical particles, depending on what one holds fixed. Neither limit is fundamental, but the unifying QFT is, to the best of our knowledge. We will use the modification of this idea in applications of the AdS/CFT correspondence: calculations in the weakly coupled gravitational theory will be performed to explain the strongly-coupled dynamics on the gauge side.

How does the word "holography" emerge in this context? The term first appears in the work of 't Hooft [5], and is further popularized by Susskind [6]. They were motivated by the Bekenstein–Hawking formula for the entropy of a black hole $S_{BH} = \frac{A}{4G}$, where for a three-dimensional Schwarzschild black hole of mass M the area of the horizon is deined as $A = 4\pi r_s^2$, with the Schwarzschild radius $r_s = 2GM$, and the Newton constant can be given in units of the Planck length:

$G = l_P^2$. It was noted that S_{BH} puts a bound on the maximum entropy in a region of space (A =the boundary of the region). Intuitively one expects that, if the energy density is bounded, then the maximum entropy is proportional to the volume of the region V, but that is not the case for a quantum theory of gravity. Suppose that we found a region of space inside V to have $S > S_{BH}$ in a way that a would-be black hole is just big enough to fit in V but with smaller energy. By throwing in additional matter such black hole could be formed. Since the entropy of the black hole would be smaller than the original entropy the second law of thermodynamics would be violated.

According to the interpretation of 't Hooft, the Bekenstein bound implies that in a quantum gravity theory all physics within V can be described in terms of some other theory on the surface A. Moreover, the boundary theory has less than one degree of freedom per Planck area. This is the *"holographic principle"*, because the situation can be compared with a hologram of a three dimensional image on a two-dimensional surface [5]. The expected "blurring" of the image due to limitations of the "holographic technique" is assumed to be small compared to the uncertainties produced by the usual quantum mechanical fluctuations.

Indeed, we can claim that AdS/CFT correspondence gives a holographic description of physics in AdS spaces. It could be shown that the holographic bound of one degree of freedom per Planck area is saturated [7]. In fact, a peculiar property of AdS spaces is that V and A of a given region scale in the same fashion as we increase the size of the region. This way the number of degrees of freedom of any field theory within some (large enough) volume is proportional to the area (and also to the volume); and any theory in AdS would seem holographic [8]. However, we should take into account that V and A scale differently with R, the AdS radius. That allows us to understand whether the entropy goes in accordance with the Bekenstein formula.

These wonderful theoretical discoveries become even more valuable when applied to the actual problems in the particle physics. Strongly coupled theories such as QCD and Composite Higgs models will be in the focus of this thesis. Our motivation is quite contrary to the original goal of AdS/CFT of understanding string theory and quantum gravity by studying simpler (supersymmetry, conformality, *etc* notwithstanding) gauge theories. However, as it happens, these real world theories have no known exact holographic dual. That will not stop us. In fact, the theories that have sharp duals are always idealizations, and one must work to distinguish universal properties from artifacts of the model. To the same end, some conjectural

constructions can be used to probe the mentioned theories with the holographic techniques. Even the conformal AdS/CFT duality seems to capture some features of the strongly interacting systems produced at heavy ion accelerators. There is little doubt that dualities allow to study a range of phenomena in the strongly interacting theories in a novel way, and make predictions out of reach of the standard methods.

In this thesis we follow the so-called *bottom-up* approach to holography, which is often applied to the study of QCD and, hence, is also known as *AdS/QCD*. AdS/QCD holographic models are phenomenological and complementary in a sense given in the beginning of this chapter. These models are simple but endowed with specific properties expected for the QCD dual. The amount of fine tuning is purposefully constrained, and AdS/CFT-like prescriptions govern the model-building process. The validity of AdS/QCD models is checked by extracting holographic predictions for a range of physical quantities and comparing them to the ones observed experimentally or established with other standard methods. When applying the bottom-up approach to the theories without direct experimental confirmation, such as Composite Higgs, we rely on the self-consistency and prior attestation of the method. The results represent a pure prediction and are useful for the future experimental endeavours.

We proceed to describe the structure of this thesis.

In Chapter 2 we start with a formal description of AdS/CFT correspondence. The general holographic prescriptions are collected in the so-called AdS/CFT dictionary. Then, we specify to the case of Maldacena's duality between type IIB string theory in $AdS_5 \times S_5$ spacetime and $\mathcal{N} = 4$ supersymmetric Yang-Mills theory in four dimensions. We discuss in what sense the gauge part of this duality is similar to large-N_c QCD and which aspects are lacking.

In Chapter 3 we discuss some selected issues of QCD. We review several well-established methods that allow to study QCD in different regimes: at large number of colours, at small energies, focusing on the implications of the chiral symmetry, and at finite temperature. Many QCD phenomena require the usage of non-perturbative techniques. The operator product expansion provides a unique description of the QCD two-point functions in terms of the condensates. The lattice formulation of YM theories and full QCD reveals a lot about the confining properties of the strongly interacting theories and their behaviour under extreme external conditions.

Chapter 4 provides the information on the QCD states studied both experimen-

tally and on lattice. We focus on the lighter part of the QCD spectra. We cover light vector and scalar mesons, scalar glueballs and their radial excitations. The radial Regge trajectories are formed by the states of a given channel, and further generalization in terms of universal trajectories is discussed. We also present the expressions for the significative form factors and the main decay rates of the vector mesons. The results of this chapter are used both as the input and the reference data for the holographic models constructed further on.

In Chapter 5 we introduce particular five-dimensional AdS/QCD model. The Hard Wall and the Soft Wall-like types are under investigation. Holographic actions in AdS_5 are described for each kind of QCD resonance, as well as the procedure of obtaining the holographic mass spectra. The latter are analyzed in comparison with the experimental data, and the SW-like spectra are deemed more phenomenological due to the Regge linearity of the mass trajectories. The notion of isospectral potentials is discussed in the context of SW-like models.

We turn to the holographic description of the deconfinement phenomenon in Chapter 6. Finite temperature assumes switching to the Euclidean signature and introducing a black hole in AdS. The deconfinement is associated to the Hawking–Page phase transition between the thermal AdS and black hole geometries. To provide a numerical estimation of the deconfinement temperature the holographic model should be specified to reproduce some of the spectra of the previous chapter. We investigate various options and look for the best prediction that is both well-motivated and consistent (isospectrality called forward).

We mean to enrich the QCD description at zero temperature introducing the dynamics related to the chiral symmetry in Chapter 7. We put forward a new option for the chiral symmetry breaking in the five-dimensional bulk. The model assumes some generalization of the standard holographic prescriptions, but still leads to the correct phenomenology. Various QCD observables are evaluated and discussed in detail.

In Chapter 8 we apply the technique developed in the previous chapter to the theory of Composite Higgs. The differences are not limited just to the exchange of the "flavour" and "colour" groups, the reconsideration of the role of the Goldstone bosons is necessary. We present some results for the possible new heavy states bounded by the new strong interaction and attempt to make contact with the LHC experiments.

We conclude in Chapter 9. The results of the thesis are summed up and some speculation on the future of the bottom-up holography is given.

Chapter 2

AdS/CFT correspondence

Let us review the basic notions beyond the gauge/gravity formalism. We start with a more general description of the AdS/CFT formalism, and later turn to the specifics of the Maldacena conjecture and the possibility of its extension towards QCD.

Holography became increasingly popular in the last decades, so the literature on the subject is abundant. We will mostly refer to the reviews and lecture notes of Refs. [8–12].

2.1 Anti-de Sitter space

To start the discussion of anti-de Sitter (AdS) geometry let us first clarify some standard notations. Physics in d dimensions is invariant under the Lorentz group $SO(1, d-1)$ of generalized rotations. Specifically, it leaves invariant the line element

$$ds^2 = dt^2 - d\vec{x}^2 = \eta_{NM} dx^N dx^M, \tag{2.1}$$

here we take a notation $\eta_{NM} = \text{diag}(1, -1, ..., -1)$. A general curved spacetime is defined by a line element

$$ds^2 = g_{MN}(x) dx^N dx^M, \tag{2.2}$$

where $g_{MN}(x)$ are some functions called the metric. Geometry defines gravity because matter follows geodesics in a curved space, and to describe the dynamics of gravity one postulates the Einstein–Hilbert action

$$S_{EH} = -\frac{1}{16\pi G} \int d^d x \sqrt{-g} \mathcal{R}, \tag{2.3}$$

where G is the Newton constant in d dimensions, the invariant volume of integration appears with $g = \det g_{MN}$ and the Ricci scalar is obtained after contracting the Ricci tensor with the metric, $\mathcal{R} = R_{MN}g^{MN}$. The equations of motion (EOM) are

$$R_{MN} - \frac{1}{2}g_{MN}\mathcal{R} = 0. \tag{2.4}$$

The energy-momentum tensor T_{MN} may appear on the right-hand side if matter or a cosmological constant are put into the theory.

AdS is a space of Lorentzian signature and of constant negative curvature R. It can be visualized by an embedding in a flat space with one extra timelike dimension

$$ds^2 = dx_0^2 - \sum_{i=1}^{d-1} dx_i^2 + dx_{d+1}^2, \tag{2.5}$$

$$x_0^2 - \sum_{i=1}^{d-1} x_i^2 + x_{d+1}^2 = -R^2, \tag{2.6}$$

and can be regarded as a generalized Lorentzian analogue of a sphere. It is invariant under the group $SO(2, d-1)$. In the Euclidean signature ($x_0 \to -ix_0^E$) the AdS$_d$ space is described by

$$x_0^{E2} + \sum_{i=1}^{d-1} x_i^2 - x_{d+1}^2 = R^2. \tag{2.7}$$

The symmetry group is $SO(1, d)$ then.

Let us consider the following (Poincaré patch) coordinates

$$x_i \to \frac{R}{z}x_i, \ i = 0, .., d-2, \tag{2.8}$$

$$x_{d\mp1} \to \frac{1}{2}\left(z + \frac{x_0^2 - \sum\limits_{i=1}^{d-2} x_i^2 \pm R^2}{z} \right), \tag{2.9}$$

where z is restricted to the positive half of the axis $0 < z < +\infty$. The AdS$_d$ metric in these coordinates is

$$ds^2 = \frac{R^2}{z^2}\left(dx_0^2 - \sum_{i=1}^{d-2} dx_i^2 - dz^2 \right) = \frac{R^2}{z^2}\left(dx_\mu dx^\mu - dz^2 \right). \tag{2.10}$$

We see that up to a conformal factor AdS$_d$ is like a flat Minkowski space. The notation x_μ will look more natural later when the case $d = 5$ is specified. In the line element piece $dx_\mu dx^\mu$ we contract the indices standardly for the Minkowski spaces.

The metric can have a different form in another coordinate system. For instance, there exist global coordinates that cover the whole space. However, the metric of eq. (2.10) is sufficient for our discussion and applications. One can often see another variation of it where the radial coordinate r is introduced, $r = R^2/z$, and

$$ds^2 = \frac{r^2}{R^2}\left(dx_0^2 - \sum_{i=1}^{d-2} dx_i^2\right) - \frac{R^2}{r^2}dz^2. \tag{2.11}$$

$r = \infty$ (or $z = 0$) is the boundary of AdS, and $r = 0$ can be thought of as a horizon. Both are infinitely distant from any finite r, and for massive particles the AdS space represents a kind of a potential well inside which they move. In the same time, the boundary can be reached in finite time by radial light-like signals. These two facts are well-explained in the thought experiments of Ref. [10].

AdS space is a solution of the Einstein equation with a cosmological constant. Let us add to the action (2.3) another term: $\frac{1}{8\pi G}\int d^dx\sqrt{-g}\Lambda$, then the EOM is

$$R_{MN} - \frac{1}{2}g_{MN}\mathcal{R} = -\Lambda g_{MN} \tag{2.12}$$

The metric (2.10) of AdS$_d$ defines

$$R_{MN} = \frac{-(d-1)}{R^2}g_{MN},\ \mathcal{R} = -\frac{d(d-1)}{R^2}, \tag{2.13}$$

and hence we can specify the cosmological constant in terms of the AdS$_d$ parameters

$$\Lambda = -\frac{(d-1)(d-2)}{2R^2}. \tag{2.14}$$

2.2 Conformal Field Theories

Consider a quantum field theory in d dimensional flat space characterized by the coordinates x^μ. A theory can be invariant under the scale transformation $x'^\mu = \alpha x^\mu$. This can be expressed in terms of the theory β-function that shows the running of the coupling constant g with the renormalization scale μ,

$$\beta(g,\varepsilon) = \mu\left.\frac{dg}{d\mu}\right|_{m_0,g_0,\varepsilon}. \tag{2.15}$$

Here we specify the dependencies on the bare mass m_0 and coupling constant g_0, and on the cut-off ε. A scale invariant theory has a zero β function. It can either be that $\beta = 0$ everywhere or only in some fixed points $\beta(g_{f.p.}) = 0$.

It is believed [13] that unitary scale-invariant theories are also conformally invariant. Conformal transformations represent a generalization of the scale transformations. They are defined by $x^\mu \to x'^\mu(x)$ such that

$$dx'_\mu dx'^\mu = \Omega(x)^{-2} dx_\mu dx^\mu, \tag{2.16}$$

and the scaling factor now becomes an x-dependent function $\Omega(x)$. For $d > 2$ the generators of conformal transformations are:

- Lorentz rotations $M_{\mu\nu} = i(x_\mu \partial_\nu - x_\nu \partial_\mu)$,
- translations $P_\mu = i\partial_\mu$,
- dilatations $D = ix^\mu \partial_\mu$,
- special conformal transformations $K_\mu = i(2x_\mu x^\nu \partial_\nu - x^2 \partial_\mu)$.

One can assemble these generators in an antisymmetric $(d+2) \times (d+2)$ matrix,

$$M_{MN} = \begin{pmatrix} M_{\mu\nu} & M_{\mu,d+1} & M_{\mu,d+2} \\ -M_{\mu,d+1} & 0 & D \\ -M_{\mu,d+2} & -D & 0 \end{pmatrix}, \tag{2.17}$$

where the additional generators were defined as $M_{\mu,d+1} = \frac{K_\mu - P_\mu}{2}$, $M_{\mu,d+2} = \frac{K_\mu + P_\mu}{2}$, $M_{d+1,d+2} = D$. It can be shown [14] that the conformal algebra is equivalent to $SO(2,d)$, the symmetry group of AdS_{d+1}. This is already a hint on the similarity between a gravity theory in $d+1$ dimensional AdS space and a conformally invariant field theory on d dimensional Minkowski space.

The Hilbert space of states in CFT is related to the special way of foliation – by the $(d-1)$ spheres (instead of the surfaces of equal time in the Poincaré invariant theories), concentric at the origin $x = 0$. The dilatation operator D generates the evolution of states to different radial slices (instead of Hamiltonian). This is called radial quantization. In this quantization scheme the entire Hilbert space of CFT states is associated with an arbitrarily small region about the chosen point.

The states living on the spheres are classified according to their scaling dimension Δ

$$D|\Delta\rangle = -i\Delta|\Delta\rangle, \tag{2.18}$$

and their $SO(d)$ spin l

$$M_{\mu\nu}|\Delta, l\rangle_s = (\Sigma_{\mu\nu})^t_s |\Delta, l\rangle_t, \tag{2.19}$$

since $[D, M_{\mu\nu}] = 0$ and the two generators can bee simultaneously diagonalized. $\Sigma_{\mu\nu}$ are some matrices acting on spin indices, and they are non-trivial only for $l > 0$. For the sake of simplicity we provide most of the following formulas with the l index suppressed.

A state at the origin can be generated by the local operator $\mathcal{O}_\Delta(x)$ as $|\Delta\rangle = \mathcal{O}_\Delta(0)|0\rangle$, where the conformal vacuum state $|0\rangle$ is defined as the state that can be annihilated by any generator. This is an example of the local operator/state correspondence. The interesting representations of the conformal group involve such operators. The scaling dimension Δ is the factor appearing after a scale transformation

$$\mathcal{O}_\Delta(x) \to \mathcal{O}'_\Delta(x) = \lambda^\Delta \mathcal{O}_\Delta(\lambda x). \tag{2.20}$$

Δ, being the "radial quantization energy", can be increased by one unit with P_μ acting on $|\Delta\rangle$ as a consequence of $[D, P_\mu] = -iP_\mu$. This generates descendant states $|\Delta + 1\rangle,\ |\Delta + 2\rangle, ...$ On the other hand, the "energy" can be lowered by one with the K_μ due to $[D, K_\mu] = iK_\mu$. In unitary field theories there is a lower bound on the dimension of fields (will be mentioned further). Therefore, there must be a one-particle state with the minimal "energy" Δ_0 that cannot be lowered and hence is annihilated by K_μ: $K_\mu|\Delta_0\rangle = 0$. Such state and the corresponding operator are called primary. General state can be schematically constructed from the primary one as follows:

$$|\Delta_0 + 2n + l\rangle = (P^2)^n P_{\mu_1} \dots P_{\mu_l}|\Delta_0\rangle. \tag{2.21}$$

We observe "energy" levels that are integer spaced $E_{n,l} = \Delta_0 + 2n + l$; these are the eigenvalues of the "Hamiltonian" D.

The primary operator can be determined everywhere due to the known conformal transformation properties of the primary state it determines at the origin. In the end, we can say that there is a one-to-one correspondence between all the operators at any point x and all of the states in the Hilbert space [15].

One would wish to calculate the correlators of the primary operators. Afterwards the correlators of the descendants are obtained by taking derivatives. Conformal invariance dictates the form of the correlators. For instance, in the case of a single scalar field with dimension Δ we have

$$\langle\varphi(0)\varphi(x)\rangle = \frac{c}{(x^2)^\Delta}. \tag{2.22}$$

Also, a general property of local field theories is the existence of OPE (see also

Section 3.3). For the case of two scalar primaries it can be expressed as

$$\mathcal{O}_{\Delta_i}(x)\mathcal{O}_{\Delta_j}(0) = \sum_k c_{ijk}|x|^{-\Delta_i-\Delta_j+\Delta_k}(\mathcal{O}_{\Delta_k}(0) + \text{descendants}). \tag{2.23}$$

As any n-point correlator is determined by the OPE it would seem that sets of $\{\Delta_i, \text{spin}, c_{ijk}\}$ for all the primaries determine the CFT completely. However, the CFT imposes a lot of non-trivial relations and constraints on these sets. It is so difficult to solve that people started looking for a different approach. This leads us to AdS/CFT.

2.3 Connecting the partition functions

The definition of the partition function in the d-dimensional CFT is similar to that of a general QFT

$$\mathcal{Z}_{CFT}[\phi_{\Delta_j}] = \langle \text{Exp}\, i \int d^d x \sum_j \phi_{\Delta_j}(x)\mathcal{O}_{\Delta_j}(x)\rangle_{CFT}, \tag{2.24}$$

where $\langle \ldots \rangle_{CFT}$ signifies integrating over all fields with the weight of the CFT action. The n-point correlation function is obtained by taking derivatives of $\mathcal{Z}_{CFT}$ with respect to the classical sources ϕ_{Δ_j}

$$\langle \mathcal{O}_{\Delta_1}(x_1)\mathcal{O}_{\Delta_2}(x_2)\ldots\rangle = \left.\frac{\partial^n \mathcal{Z}_{CFT}[\phi_{\Delta_j}]}{\partial\phi_{\Delta_1}(x_1)\partial\phi_{\Delta_2}(x_2)\ldots}\right|_{\phi_{\Delta_j}=0}. \tag{2.25}$$

The conformal invariance of the correlators should be originated in that of $\mathcal{Z}_{CFT}$. Under scaling the sources must have some specific transformation in order to compensate that of the operator. In the scalar case eq. (2.20) leads to:

$$\phi_\Delta(x) \to \phi'_\Delta(x) = \lambda^{d-\Delta}\phi_\Delta(\lambda x). \tag{2.26}$$

Next, let us consider a $d+1$-dimensional AdS space. How can we construct a reminiscent conformally invariant functional there? A covariant function of some fields $\phi(x,z)$, living in the $d+1$-dimensional bulk, is conformally invariant. Additionally, one can show that the group of conformal isometries acts on the AdS boundary (at $z=0$) as the conformal group acts in d-dimensional spacetime. And hence the boundary values of the bulk fields $\phi_0(x) = \lim_{z\to 0}\phi(x,z)$ transform as representations of this group. This leads to a general class of appropriate functionals

$$\mathcal{Z}_{AdS}[\phi_0] = \left.\int [\mathcal{D}\phi(x,z)]\,\text{Exp}\, iS[\phi(x,z)]\right|_{\phi|_{\partial AdS}=\phi_0(x)}, \tag{2.27}$$

where we start with a generally covariant action of fields in the bulk of AdS_{d+1} and perform functional integration with a generally covariant measure while keeping the boundary values of the fields fixed.

The last step is to connect the boundary values to the sources $\phi_0 = \phi_\Delta$. However, we should take into account that $\mathcal{Z}_{AdS}$ should remain invariant under the scale transformation $\{x, z\} \to \{\lambda x, \lambda z\}$ while we already know the scaling of the sources, as in eq. (2.26). This imposes some restriction on the near boundary behaviour of the bulk fields $\phi(x, z)$.

As an example we can consider a standard QFT of a scalar fluctuating field with an action

$$S = \frac{1}{2}\int d^d x dz \sqrt{-g}(g^{MN}\partial_M\phi(x,z)\partial_N\phi(x,z) - m^2\phi^2(x,z)), \tag{2.28}$$

EOM for the field $\phi(x, z)$ is

$$z^{d+1}\partial_z(z^{1-d}\partial_z\phi(x,z)) - z^2\Box\phi(x,z) - m^2R^2\phi(x,z) = 0. \tag{2.29}$$

The near-boundary asymptotics of its solutions are [16]

$$\phi(x,z) \approx \phi_0(x)\cdot z^{\Delta_-} + \sigma(x)\cdot z^{\Delta_+}, \tag{2.30}$$

where the powers are the roots of the characteristic equation:

$$\Delta_\pm = \frac{d}{2} \pm \sqrt{\frac{d^2}{4} + m^2R^2}. \tag{2.31}$$

To coincide with eq. (2.26) we need $\Delta_- = d - \Delta$. This can be achieved if the mass m in terms of the original parameters Δ and d is given by

$$m^2R^2 = \Delta(\Delta - d). \tag{2.32}$$

The Δ_+ term turns out to be of a sub-leading order, $\Delta_+ = \Delta$. The physical meaning of $\sigma(x)$ could be given in terms of a condensate (one-point function of the corresponding operator) [16]; we provide some discussion of it for the case of QCD in Section 7.3.3.

Notice that the value of m^2 may be negative (and the field ϕ tachyonic). It is acceptable as long as we stay within the Breitenlohner–Freedman bound of a scalar field in AdS_{d+1} [17, 18]:

$$m^2R^2 \geq -\frac{d^2}{4}. \tag{2.33}$$

Below the Breitenlohner–Freedman bound the AdS_{d+1} background becomes unstable.

In the case of higher spin fields (p-forms) the appropriate bulk mass is defined as [8, 19]

$$m^2R^2 = (\Delta - p)(\Delta - p - d). \tag{2.34}$$

It is of further importance to notice that for the special case of $p = 1$, *i.e.* the bulk gauge field $A_M(x, z)$, we would write a boundary coupling of the corresponding source to the dual vector current $J_\mu(x)$ in a form $\int d^dx A^\mu J_\mu$. The gauge transformations, $\delta A_M = D_M\lambda$, should leave invariant both the bulk Lagrangian and the boundary term. We can write $0 = \int d^dx \delta A^\mu J_\mu = -\int d^dx \lambda D^\mu J_\mu$, that implies that J_μ must be a conserved current. Thus, we showed that the global symmetries in d dimensions correspond to the gauge symmetries in the higher dimensional theory.

To conclude, let us write down the main rules of the correspondence, also known as a holographic dictionary:

- One takes as truthful the conjecture that functionals of eq. (2.24) and eq. (2.27) describe the same physics [19, 20]. Specifically, they provide identical n-point functions when varied with respect to the sources.

- On the CFT side the sources are associated to the primary operators of the theory.

- The operators are distinguished by their scaling dimension Δ and spin p.

- The bulk action in AdS contains dynamical fields; each has a specific $z \to 0$ asymptotics, that provides dimensionality accordance in the source-operator coupling $\int d^dx \phi_\Delta \mathcal{O}_\Delta$.

- A given bulk field has a spin and a mass related to the characteristics of its dual operator, see eq. (2.34) and a fuller list in, *e.g.*, Ref. [8].

What kind of QFT could be living in the AdS bulk? It depends on the CFT one is interested in. However, there is something common to all of them. Any local field theory contains the stress tensor as an operator. In CFT there is always a two-index tensor with $\Delta = d$ among its primary operators. Its source $h_{\mu\nu}$ is the boundary value of the spin-2 bulk field with $m^2 = 0$. This is a graviton. Hence, one has to deal with a theory of quantum gravity in AdS.

2.4 String theory and its low-energy limit

In this context by quantum gravity one means a string theory. Strings are relativistic one-dimensional non-local objects characterized with tension T_s (=energy/length). A common notation is

$$T_s = \frac{1}{2\pi\alpha'}, \tag{2.35}$$

where $\alpha' = l_s^2$, α' is the Regge slope and l_s – the string length [21]. The string action is the one that minimizes the string trajectory through spacetime, this two-dimensional area is called a worldsheet.

While the classical description of a string is rather simple, the quantization procedure results in many constraints on the target spacetime the string moves in. Quantum consistency requires a bosonic closed string to be put into a Minkowski space of $d = 26$; this type of string is generally unstable. That is why a notion of supersymmetric strings appeared. $d = 10$ is sufficient there and one can get to a four dimensional theory utilizing the Kaluza–Klein idea of dimensional reduction.

The physical spectrum of the theory corresponds to different vibration modes of the string. From the spacetime viewpoint, each of these modes appears as a particle of a given mass and spin. The spectrum typically contains a finite number of massless modes and an infinite tower of massive modes with masses of order $m_s \sim 1/\sqrt{\alpha'}$. A closed superstring has three massless modes, one of which is a graviton. In the low-energy limit $E \ll m_s \;\Leftrightarrow\; \alpha' E^2 \to 0$ the massive string modes can be integrated out. The massless fields acquire vevs corresponding to classical backgrounds in which the string propagates. It turns out that requirements of quantum self-consistency define this background as a supersymmetric theory of gravity. That is: $\alpha' \to 0$ limit of string theory is supergravity in 10 dimensions.

The supergravity action necessarily contains the Einstein gravity

$$S_{SUGRA} = -\frac{1}{16\pi G}\int d^d x\sqrt{-g}\,(\mathcal{R} + ...)\,, \tag{2.36}$$

where dots stand for the terms with higher derivatives of the metric as well as the ones associated with the rest of massless modes. These terms could be represented as a double series: there are powers of $\alpha' E^2$ from integrating out the massive stringy modes, and powers of the string coupling g_s from loop corrections.

Interactions of strings can be introduced geometrically by postulating that the basic interactions are one string splitting into two and two strings merging into one. Every such triple vertex has a coupling g_s. The perturbative series in string theory is a topological expansion. The simplest loop "diagram" is formed by two

vertices and corresponds to a worldsheet that is a Riemann surface with a hole. In the topology of closed two-dimensional surfaces, the number h of holes of the surface is called the genus of the surface. In string perturbation theory, h is just the number of string loops. Qualitatively a perturbative expansion of some amplitude looks like

$$\mathcal{A} = \sum_{h=0}^{\infty} g_s^{2h-2} F_h(\alpha'). \tag{2.37}$$

So, the low-energy limit of $\alpha' E^2 \to 0$, or alternatively

$$l_s/R \ll 1,$$

allows us to avoid string corrections from the massive excitations and validates the supergravity limit. It can also be seen from the point of view that, because of the typical string size being much less than the scale of the bulk, the string can be approximated by a point particle. Let us formulate as well a similar condition of avoiding the quantum gravity corrections. For that we should demand gravity to be weakly coupled. This could be expressed by taking the limit $g_s \to 0$. Equivalently, we can understand that as smallness of the Newton's constant G. In d dimensions the Planck constant is defined as $l_P = G^{2-d}$. Taking into account that for AdS$_d$ $\mathcal{R} \sim R^{-2}$, $\sqrt{-g} \sim R^d$, the classical part of eq. (2.36) dominates when

$$l_P/R \ll 1.$$

The question of importance of these limits is related to the degree we believe the AdS/CFT correspondence to be valid. The strongest form of the correspondence implies that a quantum string theory with arbitrary g_s and α' has a QFT dual. As this is a gauge/gravity duality there exists a map between the characteristic parameters on two sides. More often, however, a weak form of the correspondence is studied; for it, at least, one can provide a sort of heuristic proof. In this form one takes the string theory in the aforementioned limits that make it a classical SUGRA. The map between the parameters of SUGRA and QFT should also be established. The distinct feature is that, as we will see in the next section, the dual counterpart of these limits exhibits this form of AdS/CFT correspondence to be a strong/weak gauge/gravity type of duality.

It is crucial that the semi-classical (saddle-point) approximation to the gravitational partition function is valid in these limits

$$\mathcal{Z}_{AdS}[\phi_0] \sim \sum_{\{\phi_{cl}\}} e^{iS_{EH}[\phi_{cl}]}, \tag{2.38}$$

where $\{\phi_{cl}\}$ is a set of classical fields, which represent the extrema of the action with some generalized boundary conditions. It should be understood that the classical metric is in this set, and the boundary condition is that the spacetime is asymptotically AdS. The dual fields should follow $\phi|_{\partial AdS} = \phi_0$. By S_{EH} we just assume that the quantum gravity and string corrections are dropped in eq. (2.36).

One would expect, of course, to find in eq. (2.38) in addition to S_{EH} some terms describing the fields related to the CFT operators in accordance with the rules of duality described previously. However, it is not that easy to find a string theory dual to a given CFT.

2.5 $\mathcal{N} = 4$ SYM and string theory on $AdS_5 \times S^5$

The most prominent example of AdS/CFT concerns the correspondence between type IIB string theory and $\mathcal{N} = 4$ SYM theory; it was originally studied in [3, 16, 19, 20]. To establish the duality we will follow a heuristic derivation that proposes two views on describing certain non-perturbative objects in the string theory.

We start with the type IIB string theory in 10 dimensions. The type refers to the amount of Majorana–Weyl fermions in a theory. Let us introduce new non-perturbative higher-dimensional objects, the Dp-branes, which are the $p + 1$ dimensional hypersurfaces on which the open strings can end. They are dynamical and have degrees of freedom living on them. The tension of the Dp-brane is given by [12]

$$T_{Dp} = \frac{1}{(2\pi)^p g_s l_s^{p+1}}. \tag{2.39}$$

The non-perturbative scaling $T_{Dp} \sim g_s^{-1}$ is very important. We will focus on $p = 3$.

Place a stack of N nearly coincident D3-branes in IIB string theory with weak enough string coupling g_s. The string endpoint may belong to any two of those N units (both to the same one as well). That means that a string state is described by $N \times N$ matrix, which can be proved to be a $U(N)$ matrix. Thus, one has a theory of open strings in the adjoint of $U(N)$ living on the D3-branes. In the low-energy limit $\alpha' E^2 \to 0$ we neglect the massive string excitations and are left with a supersymmetric $SU(N)$ Yang-Mills theory ($U(1) \subset U(N)$ effectively decouples in most issues) living in the worldvolume of the D3-branes [22]. The gauge fields correspond to the open string excitations parallel to the branes; there are also 6 scalar massless modes that are the transversal excitations. Together they fill out a massless four-dimensional $\mathcal{N} = 4$ vector supermultiplet of this theory. The

resulting SYM coupling is related to the open string coupling via

$$g_{YM}^2 = 4\pi g_s. \tag{2.40}$$

It was studied that one of the properties of this theory is the exactly vanishing beta function. Consequently, the coupling constant does not run with scale and the theory is conformally invariant.

The ten-dimensional Newton's constant G in the IIB supergravity can be expressed as

$$16\pi G = (2\pi)^7 g_s^2 l_s^8, \tag{2.41}$$

where the particular dependence on the string coupling can be understood contemplating two-to-two string scattering that should be equivalent to the graviton exchange in supergravity. The net strength of the D3-brane stack source goes as $G \times NT_{D3} \sim Ng_s$. Thus, the gravitational backreaction of the stack is negligible for $g_s N \ll 1$. In this limit the description of the D3-branes as just a boundary condition for the open strings is rather precise.

There are also 10-dimensional supergravity modes of the closed strings present. However, closed strings become non-interacting at the low energies because the interactions are controlled by a dimensionless coupling $\sim GE^8$. Thus, the supergravity sector is infrared-free. Interactions between closed and open strings are controlled by the same coupling. Therefore, at low energies closed strings decouple from open strings. We conclude that in the limit $g_s N \ll 1$ and at low energies the interacting sector of the effective action of the described system reduces to an $\mathcal{N} = 4$ $SU(N)$ SYM theory in four dimensions.

On the other hand, let us look at the system in the opposite limit, when the backreaction of the branes cannot be neglected. This would correspond to taking the strongly coupled limit $g_s N \to \infty$. In the low-energy limit the classical solution of the 10-dimensional supergravity EOM is given by [22]

$$ds^2 = (1 + R^4/r^4)^{-1/2}(dt^2 - d\vec{x}^2) + (1 + R^4/r^4)^{1/2}(dr^2 + r^2 d\Omega_5^2), \tag{2.42}$$

where $d\Omega_5^2$ is a unit length element of a sphere S^5, and it could be deduced that

$$R^4 = 4\pi g_s N l_s^4. \tag{2.43}$$

Consider taking the near-horizon limit $r \ll R$, and changing the variable as follows: $r = R/z$. Then, the metric acquires the form of the direct product $AdS_5 \times S^5$, the so-called AdS "throat"

$$ds^2 = \frac{R^2}{z^2}(dt^2 - d\vec{x}^2 - dz^2) + R^2 d\Omega_5^2. \tag{2.44}$$

On the other hand, at $r \gg R$ we have a 10-dimensional Minkowski space. Therefore, the background has two distinctive regions for small and large values of r.

What is the low energy effective description of physics in the geometry of eq. (2.42)? Specifically, we need to consider excitations that have arbitrarily low energy with respect to an observer in the asymptotically flat Minkowski region at $r = \infty$. The object energy E_* appears red-shifted to the observer as $E_\infty = \sqrt{g_{tt}}E_*$. At small enough r the observed energy $E_\infty \sim rE_*/R$ could be maintained low no matter how high the proper energy was. It means that the whole tower of massive string excitations may survive in the throat. In the Minkowski region the only modes that remain are those of the massless ten-dimensional graviton supermultiplet. They do not have self-interaction for the same reason as in the previous description. At lower and lower energies the throat modes become supported deeper and deeper and so they decouple from those in the asymptotic Minkowski region. Thus, from the perspective of the observer at infinity the system reduces to the interacting closed strings in $AdS_5 \times S_5$ and free supergravity in flat 10-dimensional spacetime.

Thus we have arrived to two distinct descriptions of a system: the open and the closed string pictures. First results in a gauge theory plus SUGRA in 10-dimensional Minkowski spacetime, second – in gravity theory on $AdS_5 \times S_5$ plus the very same SUGRA in the flat spacetime as in the previous picture. Maldacena [3] conjectured that the part present in both cases (SUGRA in Minkowski spacetime) can be lifted up, and the remaining theories are dual. However, one should check that couplings on both sides allow for the existence of the semi-classical low-energy solution of the string theory.

First, we note that eq. (2.43) imposes the connection $\left(\frac{R}{l_s}\right)^4 = Ng_{YM}^2$, that transforms into the following expression after the 't Hooft coupling is introduced $\lambda = Ng_{YM}^2$:

$$\left(\frac{l_s}{R}\right)^2 = \frac{1}{\sqrt{\lambda}}. \tag{2.45}$$

Second, we can recast the Newton's constant G in terms of g_{YM}: $G = l_P^8 = \frac{\pi^4}{2}g_{YM}^4 l_s^8$, and combine it with the previous equation to get

$$\left(\frac{l_P}{R}\right)^8 = \frac{\pi^4}{2N^2}. \tag{2.46}$$

In the end, type IIB string theory on $AdS_5 \times S_5$, being only really calculable in the classical SUGRA limit ($\alpha' E^2 \ll 1$ and $g_s \ll 1$), imposes the following conditions

on the four-dimensional $\mathcal{N} = 4$ SYM:

$$N \gg 1, \qquad \lambda \gg 1. \tag{2.47}$$

This is the Maldacena conjecture in the weak form: the duality between type IIB SUGRA on $AdS_5 \times S_5$ and $\mathcal{N} = 4$ SYM theory with limits of eq. (2.47). Relaxing the low-energy and small string coupling limits leads to the stronger equivalence with the quantum string theory on the gravity side.

The last step for a practical use is eliminating the S_5 manifold from $AdS_5 \times S_5$. This could be obtained after the Kaluza–Klein reduction, also called "compactification". It works schematically as follows [23]: AdS_5 and S_5 dependencies could be separated in a given EOM, the AdS_5-related components of a bulk field could be classified according to their harmonic dependence on the coordinates which parametrise the S_5. At low energies we keep the leading contribution from the lowest-lying harmonics: the modes with no dependence on the S_5 coordinates. At the gauge side it would correspond to the removal of some supersymmetries and results, effectively, in a simpler four-dimensional, conformal Yang-Mills field theory. After the reduction, AdS/CFT correspondence becomes a true realization of the holographic principle: the five-dimensional theory is mapped to a four-dimensional one that lives on its conformal boundary.

Further we would like to extrapolate the holographic methods on QCD, so that the parameter N will turn naturally into the number of colours N_c. It is also fortunate that in the Maldacena example of duality there is the $SU(N_c)$ group found on the gauge side of the theory. The large-N_c limit of $SU(N_c)$ was studied independently by 't Hooft [24] and though not met in Nature is known to be useful in description of certain characteristic aspects of QCD.

2.6 Steps towards QCD

There is no known stringy holographic dual to QCD. For a holography practitioner there are two approaches to the problem. In the so-called top-down approach one starts with the string theory and tries to engineer it so that the resulting dual gauge theory is more reminiscent to QCD. However, this way there is no precise control over obtaining specific QCD features. The antagonizing approach, the bottom-up one, puts its focus on the latter issue discarding attempts to find the consistent string formulation.

In both approaches the large-N_c limit plays an important role. By replacing the $SU(3)$ gauge group of QCD with $SU(N_c)$ and taking the limit $N_c \to \infty$ 't

Hooft introduced the expansion parameter $1/N_c$ to the theory. We discuss some interesting consequence of the limit in more detail in Section 3.1. For now we focus on how it motivates the notion of the QCD stringy dual.

Let us first examine the theory with only gluons; the quark degrees of freedom play a subleading role because their number scales as $N_f N_c$, while the amount of gluons is $\sim N_c^2$. The simplest Feynmann diagram, the gluon self-energy, scales as $\lambda = g_{YM}^2 N_c$. The limit of large N_c could be gained smoothly for $g_{YM} \to 0$ while keeping λ fixed. That is equivalent to λ having no N_c-dependent running and confinement scale Λ_{QCD} remaining fixed for any N_c.

The scaling of vacuum diagrams can also be understood in terms of N_c and λ. It was noted that the topological classification of such diagrams naturally appears. The planar diagrams (drawn on a two-dimensional plane without crossings in the 't Hooft's double line notation) are dominating in the large-N_c limit with the characteristic scaling $N_c^2 \times \lambda^n$. In the end, the expansion of a QCD amplitude in Feynman diagrams takes the form

$$\mathcal{A} = \sum_{h=0}^{\infty} N_c^{2-2h} \sum_{n=0}^{\infty} c_{h,n} \lambda^n, \tag{2.48}$$

where h is related to the topological genus of a three-dimensional Riemann surface drawn in the correspondence to a Feynman diagram. We recognize this expression as reminiscent to that of eq. (2.37) with $g_s \leftrightarrow 1/N_c$ and $\alpha' \leftrightarrow \lambda$.

Inclusion of quarks (matter in the fundamental representation with one colour index) corresponds to the appearance of boundaries in the Riemann surfaces. That is, the scaling of the diagram is given in general by N_c^{χ}, where the Euler number $\chi = 2 - 2h - b$ now counts the number of boundaries b as well. In the string framework it would correspond to an expansion with both close and open strings, the coupling constant of the latter $\sim N_f/N_c$.

The similarity between expansions (2.37) and (2.48) implies that treatment of QCD in the large-N_c limit following the lines of the previous section might be successful. However, there are important distinctions:

- QCD is not supersymmetric;
- QCD field content does not correspond to fermions and scalars in the adjoint representation of the gauge group;
- QCD has a discrete spectrum of physical states, with a finite mass gap and is not conformally invariant at the quantum level;

- in QCD the physical meaning belongs to a renormalized coupling, which runs with the momentum scale, and depends on the renormalization scheme.

It is sometimes argued that the latter point may be resolved by noting the connection between the 't Hooft coupling and the dilaton field $\Phi(z)$:

$$\lambda = e^{\Phi(z)}. \tag{2.49}$$

Interestingly, another way to find a similarity between QCD and $\mathcal{N} = 4$ SYM is to consider the case of non-zero temperature T. Introduction of the thermal excitation of SYM degrees of freedom is mirrored on the gravity side of conjecture with a modified AdS part of the metric

$$ds^2 = \frac{R^2}{z^2}\left(h(z)dx_0^2 - d\vec{x}^2 - \frac{dz^2}{h(z)}\right), \tag{2.50}$$

$$h(z) = 1 - \frac{z^4}{z_h^4}. \tag{2.51}$$

This solution is a black brane in AdS spacetime with a horizon at $z = z_h$. The temperature of the system is given by the Hawking temperature $T = 1/(\pi z_h)$.

Aside from temperature breaking supersymmetry and lifting up the scalar degrees of freedom, thus diluting some points in the aforementioned distinctions, there is a famous calculation of the ratio of shear viscosity to entropy density in $\mathcal{N} = 4$ plasma:

$$\frac{\eta}{s} = \frac{1}{4\pi} \simeq 0.08. \tag{2.52}$$

The importance of this result is caused by its universality for any large-N_c, strongly coupled, finite temperature gauge theories with a gravity dual. Presumably, the reason is that both quantities are related to the universal properties of black hole horizons [25]. It was also conjectured in Ref. [26] that in any sensible relativistic quantum field theory the value serves as the lower bound: $\frac{\eta}{s} \geq \frac{1}{4\pi}$.

Common fluids like water or liquid helium (being weakly coupled) have a much larger value of $\frac{\eta}{s}$. However, we should take into account the non-standard properties of the quark gluon plasma, a new state of matter produced in heavy-ion collisions. Elliptic flow seems to be best understood in terms of nearly ideal fluid dynamics. It was analysed from the data of the RHIC accelerator in Brookhaven that the small values $\frac{\eta}{s} \leq 0.25$ are favoured for the temperatures $T_c \lesssim T \lesssim 2T_c$, where T_c is the deconfinement temperature, confirming the strongly-coupled nature of the quark gluon plasma. The AdS/CFT prediction agrees excellently with these experimental results.

2.7 Conclusions

In this chapter we have described the basic ideas of the gauge-gravity duality. First, we have given a general outline of the AdS/CFT correspondence. Second, we have discussed a specific example of Maldacena's duality – between type IIB string theory $AdS_5 \times S_5$ and four-dimensional $\mathcal{N} = 4$ SYM. It is not just a beautiful theoretical construction but an important starting point to evolve holography towards phenomenologically interesting theories like QCD.

In the following chapters our investigation goes in the bottom-up style, and the developed holographic models have an undefined stringy origin. Nevertheless, the equality of the partition functions (2.24) and (2.27) is a cornerstone concept behind our calculations. $5D$ AdS space, specific limits, symmetry relations, the field-operator dictionary and other points developed in AdS/CFT lay the foundation of the bottom-up model-building. From the more general holographic concepts we will use the duality of the global symmetry in the boundary QFT to a gauge symmetry in the bulk [19].

Chapter 3

Some aspects of QCD phenomenology

3.1 Large-N_c QCD

There is a number of phenomenological consequences of the large-N_c limit that we would like to discuss. Specifically, we are interested in the large-N_c counting rules that help to understand the scaling of correlation functions, an example of that was given in eq. (2.48). Under the assumption that the 't Hooft limit of QCD is a confining theory, these rules can also be applied to physical hadronic states.

We will follow [27] in the description of the sensible large-N_c limit of QCD. The Lagrangian is

$$\mathcal{L}_{QCD} = -\frac{1}{2}\,\mathrm{Tr}\, G_{\mu\nu}G^{\mu\nu} + \sum_{f=1}^{N_f} \overline{\Psi}_f (iD_\mu \gamma^\mu - m_f)\Psi_f. \tag{3.1}$$

The gauge fields of $SU(N)$ are $A_\mu = A_\mu^a T^a$, with the generators that follow $\mathrm{Tr}\, T^a T^b = \frac{1}{2}\delta^{ab}$. The covariant derivative is $D_\mu = \partial_\mu + i\frac{g}{\sqrt{N_c}}A_\mu$, and the gluon field strength is $G_{\mu\nu} = \partial_\mu A_\nu - \partial_\nu A_\mu + i\frac{g}{\sqrt{N_c}}[A_\mu, A_\nu]$. Notice that instead of a simple g coupling we now have $\frac{g}{\sqrt{N_c}}$.

Next, we rewrite the QCD functional integral with N_c explicitly factored out in the exponent. That can be achieved with $\frac{g}{\sqrt{N_c}}A_\mu \to \widehat{A}_\mu$ and $\Psi \to \sqrt{N_c}\widehat{\Psi}$.

$$\mathcal{Z}_{QCD}[\phi] = \int \mathcal{D}\widehat{A}\mathcal{D}\widehat{\Psi}\mathcal{D}\widehat{\overline{\Psi}}\,\mathrm{Exp}\, iN_c \int d^4x \Bigg[\sum_{f=1}^{N_f} \widehat{\overline{\Psi}}_f (iD_\mu\gamma^\mu - m_f)\widehat{\Psi}_f \tag{3.2}$$

$$-\frac{1}{4g^2}\widehat{G}^a_{\mu\nu}\widehat{G}^{a\mu\nu} + \phi^a\widehat{\mathcal{O}}^a\Bigg]. \tag{3.3}$$

The fields and operators are properly rescaled, *i.e.* to go back to the standard normalization we have to take operators $\widehat{\mathcal{O}} = \mathcal{O}/N_c$. In what follows, we consider gauge invariant operators with at most one trace over colour indices. That includes operators like $\mathrm{Tr}\, G_{\mu\nu}G^{\mu\nu}(x)$. There is also a restriction that the number of fields inside the trace is kept finite so that the N_c-counting is not altered. For example, we do not include operators like $\det G_{\mu\nu}G^{\mu\nu}$. The operators with quark bilinears look like $\overline{\Psi}\Gamma\Psi$, where Γ is some matrix with flavour indices. If we assume that QCD remains confining at large N_c, these two types of operators create glueballs and mesons.

The connected correlators of such operators are obtained via the variation with respect to the appropriate sources

$$\langle\widehat{\mathcal{O}}_1(x_1)...\widehat{\mathcal{O}}_p(x_p)\rangle_{con} = (iN_c)^{-p}\,\frac{\partial}{\partial\phi_1(x_1)}...\frac{\partial}{\partial\phi_p(x_p)}\ln\mathcal{Z}_{QCD}[\phi]\Big|_{\phi=0} \tag{3.4}$$

Now we recall from Section 2.6, that the free energy (the sum of vacuum graphs) is dominated by diagrams of planar gluon loops, and is $O(N_c^2)$ in the case of purely gluonic operators (genus $g = 0$) or $O(N_c^1)$ when a quark bilinear is present ($g = b = 0$). Hence we can conclude that the generic p-point connected correlator is accordingly $O(N_c^{2-p})$ or $O(N_c^{1-p})$.

It could be seen that the leading contribution to any correlation function comes from disconnected diagrams, rather than connected diagrams. Let us restrict ourselves to the case of a Hermitian operator describing glueball states. Any two-point function has a disconnected piece $\langle\widehat{\mathcal{O}}_1\widehat{\mathcal{O}}_2\rangle \sim \langle\widehat{\mathcal{O}}_1\rangle\langle\widehat{\mathcal{O}}_2\rangle \sim N_c^2$, while the connected piece scales as $\langle\widehat{\mathcal{O}}_1\widehat{\mathcal{O}}_2\rangle_{con} \sim N_c^0$. This means that pure Yang-Mills at $N_c \to \infty$ is a free, classical theory. The quantum corrections are suppressed because

$$(\Delta\widehat{\mathcal{O}})^2 = \langle\widehat{\mathcal{O}}\widehat{\mathcal{O}}\rangle - \langle\widehat{\mathcal{O}}\rangle\langle\widehat{\mathcal{O}}\rangle = \langle\widehat{\mathcal{O}}\widehat{\mathcal{O}}\rangle_{con} \sim N_c^0 \Rightarrow \frac{(\Delta\widehat{\mathcal{O}})^2}{\langle\widehat{\mathcal{O}}\rangle^2} \sim 1/N_c^2. \tag{3.5}$$

The scaling of the connected correlator signifies that the operator $\widehat{\mathcal{O}}$ creates a glueball state with a unit amplitude when acting on the vacuum of the theory, $\widehat{\mathcal{O}}^G|0\rangle = |G\rangle$.

A similar discussion is valid for the correlators of purely fermionic operators. However, the scaling shows that to create a unit amplitude meson one should use $\sqrt{N_c}\widehat{\mathcal{O}}$, $\sqrt{N_c}\widehat{\mathcal{O}}^M|0\rangle = |M\rangle$. Further, it can be shown that the meson-glueball interactions are suppressed by a factor $1/\sqrt{N_c}$ [27]. Eventually, in the 't Hooft limit QCD, a strongly interacting theory of quarks and gluons, turns into a theory

Expression	Glueball	Meson
$\langle \mathcal{O}...\mathcal{O} \rangle_{con}$	N_c^2	N_c
M_n	N_c^0	N_c^0
F_n	N_c^1	$\sqrt{N_c}$
$\langle 0\|\mathcal{O}\|n_1 \dots n_m\rangle$	N_c^{2-m}	$N_c^{1-m/2}$
V_m	N_c^{2-m}	$N_c^{1-m/2}$
Γ	$1/N_c^2$	$1/N_c$
σ	$1/N_c^4$	$1/N_c^2$

Table 3.1: Dominant scalings in the large-N_c limit. V_m is a vertex between m hadrons. Here, Γ is the decay rate, and σ is the characteristic $2 \to 2$ scattering cross section.

of free, stable and weakly interacting hadrons. Quarks and gluons are bound into color singlet hadrons by the leading in N_c interactions, while the residual relations between these hadrons are suppressed.

In this weakly interacting theory, we can expand in the coupling constant $1/\sqrt{N_c}$. The leading order graphs are tree-graphs, and the only singularities are on-shell poles. Let us consider a one-loop graph with two particle cuts. In general QCD a two-point function $\langle \mathcal{O}\mathcal{O} \rangle_{con}$ comprises a lot of non-trivial diagrams, but now we know that the following representation should be correct:

$$\langle \mathcal{O}(k)\mathcal{O}(-k) \rangle_{con} = \sum_{n=0}^{\infty} \frac{F_n^2}{k^2 - M^2(n)} \tag{3.6}$$

Here $F_n = \langle 0|\mathcal{O}|n\rangle$, with $|n\rangle$ being single particle states of mass $M(n)$. Notice that the sum contains an infinite number of terms. That is related to the fact the two-point correlators in QCD are known to obtain a logarithmic scaling. The only way that to reproduce that with eq. (3.6) is to include an infinite number of stable intermediate states $|n\rangle$, with an infinite tower of masses $M(n)$. This construction is qualitatively similar to the Kaluza-Klein towers in extradimensional theories mentioned in Section 2.5.

We wrote eq. (3.6) with $\mathcal{O}$ instead of $\widehat{\mathcal{O}}$ because this is the form we are likely to meet in further chapters. Hence, let us provide a list of the scales for the standardly normalized meson and glueball operators in the upper part of Table 3.1. The mixing correlators (if even one fermionic operator is included) have the following behavior

$$\langle \mathcal{O}^M \dots \mathcal{O}^M \mathcal{O}^G \dots \mathcal{O}^G \rangle_{con} \sim N_c,$$

and the vertex between m mesons and p glueballs $\sim N_c^{1-p-m/2}$.

The lower part of Table 3.1 contains the scalings of quantities related to the physical hadron states. They can be easily deduced from the rules of creating states with $\widehat{\mathcal{O}}$. We observe that the resonances are narrow (their decay widths Γ vanish in the large-N_c limit), since all decay vertices V_3 are proportional to inverse powers of N_c and hadron masses in the phase space factors do not grow with N_c.

3.2 Chiral symmetry

3.2.1 Chiral symmetry breaking

Chiral symmetry is related to the flavour group of QCD. In case we consider only light u and d quarks, this is $SU(2)$. The generators of this group are related to the Pauli matrices

$$\sigma_1 = \begin{pmatrix} 0 & 1 \\ 1 & 0 \end{pmatrix},\ \sigma_2 = \begin{pmatrix} 0 & -i \\ i & 0 \end{pmatrix},\ \sigma_3 = \begin{pmatrix} 1 & 0 \\ 0 & -1 \end{pmatrix}.$$

Their algebra is described by

$$[\sigma_a, \sigma_b] = 2i\varepsilon_{abc}\sigma_c, \quad \mathrm{Tr}(\sigma_a\sigma_b) = 2\delta_{ab}.$$

The actual generators are $T_a = \sigma_a/2$, that follow

$$[T_a, T_b] = i\varepsilon_{abc}T_c, \quad \mathrm{Tr}(T_aT_b) = \delta_{ab}/2. \tag{3.7}$$

For the case of N_f flavours, the generators of $SU(N_f)$ will represent a generalization of the $SU(2)$ case. We will label them as T^a too ($a = 1, \ldots, N_f^2 - 1$) and assume that they are normalized as above.

Consider N_f Dirac fermions $\psi_i,\ i = 1, ..., N_f$. Each one belongs to a fundamental colour representation of $SU(N_c)$ (a complex representation).

Let us speak of the spinor indices. We take a chiral representation for the γ matrices

$$\gamma^0 = \begin{pmatrix} 0 & 1 \\ 1 & 0 \end{pmatrix},\ \gamma^i = \begin{pmatrix} 0 & \sigma_i \\ -\sigma_i & 0 \end{pmatrix},\ \gamma_5 = i\gamma^0\gamma^1\gamma^2\gamma^3 = \begin{pmatrix} -1 & 0 \\ 0 & 1 \end{pmatrix}, \tag{3.8}$$

they have the standard properties: $\{\gamma^\mu, \gamma_5\} = 0,\ \gamma_5^2 = 1$. Then, it is easy to distinguish a Dirac fermion to have a left-handed (χ_a) and a right-handed ($\eta_a^\dagger = [\eta_a]^\dagger$) Weyl component. We can rewrite a four-spinor in terms of two bi-spinors:

$$\psi_i = \begin{pmatrix} \chi_{i\ a} \\ \eta_i^{\dagger\dot{a}} \end{pmatrix},\ \overline{\psi}^i = (\eta^{ai}, \chi_{\dot{a}}^{\dagger i}),\ i = 1, ..., N_f. \tag{3.9}$$

Considering $\Psi = (\psi_1, ..., \psi_{N_f})^\top$ as a flavour vector we may construct a following Lagrangian:

$$\mathcal{L} = i\overline{\Psi}\partial_\mu\gamma^\mu\Psi - \overline{\Psi}M_Q\Psi, \quad M_Q = m_q \mathrm{Id}_{N_f\times N_f}. \tag{3.10}$$

The fundamental Lagrangian in terms of the Weyl spinors is ($\overline{\sigma}^\mu = (1, -\sigma^i)$):

$$\mathcal{L} = i\sum_{j=1}^{N_f}(\eta^{aj}\sigma^\mu_{a\dot{a}}\partial_\mu\eta_j^{\dagger\dot{a}} + \chi^{\dagger j}_{\dot{a}}\overline{\sigma}^{\mu\dot{a}a}\partial_\mu\chi_{aj}) - m_q\sum_{j=1}^{N_f}(\eta^{aj}\chi_{aj} + \chi^{\dagger j}_{\dot{a}}\eta_j^{\dagger\dot{a}}) \tag{3.11}$$

To have χ and η kinetic terms similar one can use the relation $\eta^{aj}\sigma^\mu_{a\dot{a}}\partial_\mu\eta_j^{\dagger\dot{a}} = \eta^\dagger_{\dot{a}j}\overline{\sigma}^{\mu\dot{a}a}\partial_\mu\eta^j_a +$ full divergence. With respect to the colour indices χ transforms as a fundamental representation $\mathbf{N_c}$, and η - as a conjugate representation $\overline{\mathbf{N}}_\mathbf{c}$. In the following we assume that the spinor indices are properly convoluted as ${}^a_a$ and ${}^{\dot{a}}_{\dot{a}}$, and abstain from mentioning them explicitly.

The Lagrangian (3.11) in the absence of a mass term exhibits a classical global symmetry $U(N_f)_L \times U(N_f)_R$. We can rotate separately a left-handed vector $X = (\chi_1, ..., \chi_{N_f})^\top$ as an $\mathbf{N_f}$ of $U(N_f)_L$ and a right-handed $H^\dagger = (\eta_1^\dagger, ..., \eta_{N_f}^\dagger)^\top$ as an $\mathbf{N_f}$ of $U(N_f)_R$ (H being a $\overline{\mathbf{N}}_\mathbf{f}$). It is also convenient to introduce the left and right projection operators $P_L = (1-\gamma_5)/2$, $P_R = (1+\gamma_5)/2$. When they act on a Dirac fermion of a given flavour they select the proper Weyl component

$$\psi_{iL} = P_L\psi_i = \begin{pmatrix}\chi_i\\0\end{pmatrix}, \ \psi_{iR} = P_R\psi_i = \begin{pmatrix}0\\\eta_i^\dagger\end{pmatrix}. \tag{3.12}$$

For such a global symmetry one would expect to have $2{\cdot}N_f^2$ conserved currents. Evidently, $U(N_f) \simeq SU(N_f) \times U(1)$, so we may write down $SU(N_f)$ related currents with proper generators

$$\mathcal{O}^{a\mu}_L = \overline{\Psi}_L\gamma^\mu T^a\Psi_L, \tag{3.13}$$

$$\mathcal{O}^{a\mu}_R = \overline{\Psi}_R\gamma^\mu T^a\Psi_R. \tag{3.14}$$

One often uses linear combinations of these operators

$$\mathcal{O}^{a\mu}_V = \mathcal{O}^{a\mu}_R + \mathcal{O}^{a\mu}_L = \overline{\Psi}\gamma^\mu T^a\Psi, \tag{3.15}$$

$$\mathcal{O}^{a\mu}_A = \mathcal{O}^{a\mu}_R - \mathcal{O}^{a\mu}_L = \overline{\Psi}\gamma^\mu\gamma_5 T^a\Psi. \tag{3.16}$$

The labels are due to their transformation properties under the parity as vector and axial-vector current densities:

$$P: \ \mathcal{O}^{a\mu}_V(\vec{x},t) \to \mathcal{O}^{a\mu}_V(-\vec{x},t) \tag{3.17}$$

$$P: \ \mathcal{O}^{a\mu}_A(\vec{x},t) \to -\mathcal{O}^{a\mu}_A(-\vec{x},t). \tag{3.18}$$

The remaining currents correspond to taking the $U(1)$ identity generator. A conserved singlet vector (axial) current results from a transformation of all left-handed quark fields by a given phase and all right-handed by the same (opposite) one:

$$\mathcal{O}_V^\mu = \overline{\Psi}_R \gamma^\mu \Psi_R + \overline{\Psi}_L \gamma^\mu \Psi_L = \overline{\Psi} \gamma^\mu \Psi, \tag{3.19}$$

$$\mathcal{O}_A^\mu = \overline{\Psi}_R \gamma^\mu \Psi_R - \overline{\Psi}_L \gamma^\mu \Psi_L = \overline{\Psi} \gamma^\mu \gamma_5 \Psi. \tag{3.20}$$

It is convenient then to write the classical chiral symmetry of massless N_f-flavour QCD as

$$SU(N_f)_V \times U(1)_V \times SU(N_f)_A \times U(1)_A. \tag{3.21}$$

However, upon quantization not all these symmetries remain. $SU(N_f)_V$ is an exact symmetry: in real-world QCD, it manifests itself in the approximate degeneracy of the proton and neutron masses. $U(1)_V$ symmetry is also preserved and corresponds to the baryon number conservation in QCD. That means that $\partial_\mu \mathcal{O}_V^{a\mu} = \partial_\mu \mathcal{O}_V^\mu = 0$. The divergence of $\mathcal{O}_A^\mu$ obtains quantum corrections due to anomalies, that phenomenon is responsible for the heaviness of η' meson.

Most interesting to us is that the ground state (the vacuum) of the quantum theory results to be not invariant under $SU(N_f)_A$ transformations. $N_f = 3$ QCD should properly describe the experimental hadron states. They could be classified in $SU(3)_V$ representations but degenerate multiplets with opposite parity do not exist. Moreover, the octet of pseudoscalar mesons happens to be much lighter than all the other hadronic states. That hints to the symmetry breaking pattern $SU(3)_L \times SU(3)_R \to SU(3)_V$, where a proper number of Goldstone bosons is produced. The general explanation is the appearance of non-vanishing chiral condensate. It transforms as the following representation

$$\langle \overline{\Psi}_R \Psi_L \rangle = (\mathbf{N_f}, \overline{\mathbf{N}}_\mathbf{f})_{SU(N_f)_L \times SU(N_f)_R},$$

that is only invariant under $SU(N_f)_V$ and thus produces the chiral symmetry breaking pattern

$$SU(N_f)_L \times SU(N_f)_R \to SU(N_f)_V. \tag{3.22}$$

In fact, it was shown under very general assumptions that the chiral symmetry must break down to the diagonal subgroup in the large-N_c limit [28].

The explicit symmetry breaking via the quark masses should also be taken into account. However, if all N_f quarks have the same mass the conditions $\partial_\mu \mathcal{O}_V^{a\mu} = \partial_\mu \mathcal{O}_V^\mu = 0$ remain intact [29].

3.2.2 Chiral perturbation theory

The dynamics of the Goldstone bosons is conveniently described by the so-called chiral Lagrangian. This EFT has the unitary matrix as an elementary building block

$$U(\phi) = \exp\left(\frac{2i\phi(x)}{f_\pi}\right),\ \phi(x) = T^a\phi_a(x), \tag{3.23}$$

where $\phi_a(x)$ is a set of Goldstone bosons, their amount depending on N_f. f_π is the pion decay constant in the chiral limit. In QCD one finds it defined as the matrix element related to the pion decay $\pi^+ \to \mu^+\nu_\mu$ process

$$\langle 0|\overline{\Psi}\gamma_\mu\gamma_5 T^a\Psi(0)|\pi^b(p)\rangle = ip_\mu f_\pi\delta^{ab}. \tag{3.24}$$

The experimental value is $f_\pi = 92.07 \pm 1.2$ MeV [30].

Let us name the chiral group as $\mathcal{G} \equiv SU(N_f)_L \times SU(N_f)_R$, and the resulting vector subgroup as $\mathcal{H} \equiv SU(N_f)_V$. $\phi_a(x)$ are the coordinates in the coset space $\mathcal{G}/\mathcal{H}$. We can choose a coset representative $\xi(\phi) = (\xi_L(\phi), \xi_R(\phi)) \in \mathcal{G}$. The changes under the chiral transformation $g \equiv (g_L, g_R) \in \mathcal{G}$ are $\xi_L(\phi) \xrightarrow{\mathcal{G}} g_L\xi_L(\phi)h^\dagger(\phi, g)$ and $\xi_R(\phi) \xrightarrow{\mathcal{G}} g_R\xi_L(\phi)h^\dagger(\phi, g)$. Since $h(\phi, g) \in \mathcal{H}$ appears in both sectors it is simpler to take the matrix $U(\phi) \equiv \xi_R(\phi)\xi_L^\dagger(\phi)$, that transforms as $U(\phi) \xrightarrow{\mathcal{G}} g_R U(\phi) g_L^\dagger$. Further, a canonical choice can be made that $\xi_L = \xi_R^\dagger = u(\phi)$. $U(\phi)$ transforms linearly under the chiral group, while the Goldstones themselves – non-linearly.

A general low-energy effective Lagrangian should involve $U(\phi)$ in a way consistent with chiral symmetry. It is standard to organize the Lagrangian in terms of the number of derivatives $\mathcal{L}_{eff}(U) = \sum_n \mathcal{L}_{2n}$. An even number is necessary to preserve parity. Due to the unitarity of the Goldstone matrix the lowest order term is the one with two derivatives:

$$\mathcal{L}_2 = \frac{f_\pi^2}{4}\,\mathrm{Tr}\,\partial_\mu U^\dagger\partial^\mu U. \tag{3.25}$$

$\mathcal{L}_2$ is also known as the Lagrangian of the non-linear sigma model.

One can also introduce couplings to external classical fields. The classical massless QCD Lagrangian can be augmented with terms

$$\mathcal{L}^0_{QCD} + \overline{\Psi}\gamma^\mu(v_\mu + \gamma_5 a_\mu)\Psi - \overline{\Psi}(s - i\gamma_5 p)\Psi. \tag{3.26}$$

There we have vector and axial vector sources with which to incorporate electromagnetic and semileptonic weak interactions. Equivalently, the right $r_\mu \equiv v_\mu + a_\mu$ and left sources $l_\mu \equiv v_\mu - a_\mu$ can appear as more convenient in some expressions.

The scalar source contains the quark mass matrix responsible for the explicit chiral symmetry breaking ($s = M_Q + \ldots$). It is also common to use the following related quantity $\chi = 2B_0(s + ip)$, where one introduces a constant B_0.

The transformation properties under the local chiral group that keep eq. (3.26) invariant are

$$\chi \to g_R \chi g_L^\dagger,\ l_\mu \to g_L l_\mu g_L^\dagger + i g_L \partial_\mu g_L^\dagger,\ r_\mu \to g_R r_\mu g_R^\dagger + i g_R \partial_\mu g_R^\dagger.$$

With them we can understand how the external sources enter into the EFT Lagrangian respecting the gauge invariance. The gauge fields enter through the covariant derivatives

$$D_\mu U = \partial_\mu U - i r_\mu U + i U l_\mu, \tag{3.27}$$

and the field strength tensors

$$l^{\mu\nu} = \partial^\mu l^\nu - \partial^\nu l^\mu - i[l^\mu, l^\nu],\ r^{\mu\nu} = \partial^\mu r^\nu - \partial^\nu r^\mu - i[r^\mu, r^\nu]. \tag{3.28}$$

In the end, at the lowest order in momenta we have

$$\mathcal{L}_2 = \frac{f_\pi^2}{4} \operatorname{Tr}\left(D_\mu U^\dagger D^\mu U + U^\dagger \chi + \chi^\dagger U \right). \tag{3.29}$$

It is important that the external fields in EFT (3.29) break the chiral symmetry the same way as in the fundamental Lagrangian (3.26).

Correlation functions can be calculated from the generating functional of the external sources $\mathcal{Z}[v, a, s, p]$ to provide some relations of interest. First, let us make a definition via the path integral

$$\exp i\mathcal{Z}[v, a, s, p] = \int \mathcal{D}U \exp i \int d^4x \mathcal{L}_{eff}[U, v, a, s, p], \tag{3.30}$$

and consider only the lowest order of $\mathcal{L}_{eff}$ given in eq. (3.29). Then, we can calculate the variations with respect to the gauge fields l_μ and r_μ. That would lead us exactly to eq. (3.24). In their turn, variations over χ and $\chi^\dagger$ show that the constant B_0 is related to the quark condensate as follows

$$\langle 0|\bar{\psi}^j \psi^i|0\rangle = -f_\pi^2 B_0 \delta^{ij}. \tag{3.31}$$

The non-derivative terms in eq. (3.29) with $s = M_Q,\ p = 0$ provide the relations for the Goldstone masses. Among those there is an expression for the masses of π mesons in terms of the quark masses:

$$M_\pi^2 = (m_u + m_d) B_0. \tag{3.32}$$

In $N_f = 3$ case the splitting between the masses of the charged and neutral pions appears. Combining eqs. (3.31) and (3.32) one gets the Gell-Mann–Oakes–Renner relation:

$$f_\pi^2 M_\pi^2 = -\frac{m_u + m_d}{2}\langle 0|\bar{u}u + \bar{d}d|0\rangle. \tag{3.33}$$

Other results from the lowest-order chiral Lagrangian can be found in Ref. [31]. The value of the method is substantiated by the fact that it encodes in a compact way various results of the current algebra.

Relation (3.33) is subject to chiral corrections: one needs to multiply the left-hand side by $1 - \delta_\pi$, where the coefficient could be expressed in terms of the low-energy constants that we proceed to define. The most general next-to-leading order $O(p^4)$ Lagrangian is given by [32]

$$\begin{aligned}
\mathcal{L}_4 = {} & L_1 \left(\mathrm{Tr}\, D_\mu U^\dagger D^\mu U\right)^2 + L_2\, \mathrm{Tr}\left(D_\mu U^\dagger D_\nu U\right) \mathrm{Tr}\left(D^\mu U^\dagger D^\nu U\right) \\
& + L_3\, \mathrm{Tr}\, D_\mu U^\dagger D^\mu U D_\nu U^\dagger D^\nu U + L_4\, \mathrm{Tr}\, D_\mu U^\dagger D^\mu U\, \mathrm{Tr}\left(U^\dagger\chi + \chi^\dagger U\right) \\
& + L_5\, \mathrm{Tr}\, D_\mu U^\dagger D^\mu U \left(U^\dagger\chi + \chi^\dagger U\right) + L_6\, \mathrm{Tr}^2\left(U^\dagger\chi + \chi^\dagger U\right) \\
& + L_7\, \mathrm{Tr}^2\left(U^\dagger\chi - \chi^\dagger U\right) + L_8\, \mathrm{Tr}\left(\chi^\dagger U\chi^\dagger U + U^\dagger\chi U^\dagger\chi\right) \\
& - iL_9\, \mathrm{Tr}\left(r^{\mu\nu} D_\mu U D_\nu U^\dagger + l^{\mu\nu} D_\mu U^\dagger D_\nu U\right) + L_{10}\, \mathrm{Tr}\, U^\dagger r^{\mu\nu} U l_{\mu\nu} \\
& + H_1\, \mathrm{Tr}\left(r^{\mu\nu} r_{\mu\nu} + l^{\mu\nu} l_{\mu\nu}\right) + H_2\, \mathrm{Tr}\,\chi^\dagger\chi
\end{aligned} \tag{3.34}$$

The chiral coefficients $L_i,\ H_1,\ H_2$ are the effective couplings parametrizing the low-energy Lagrangian. In analogy to f_π and B_0 they contain information on the underlying dynamics and should, in principle, be calculable in terms of the (remaining) parameters of full QCD. We notice that the terms with H_1 and H_2 contain only external modes.

However, to sum up all the contribution at $O(p^4)$ order we should also take into account loop graphs generated with $\mathcal{L}_2$. The Goldstone loops are divergent and need to be renormalized. We can introduce counterterms in each $\mathcal{L}_{2n}$, order by order. The dimensional regularization we would like to use preserves the symmetries of the theory. $\mathcal{L}_4$ of eq. (3.34) by construction contains all the terms permitted by the symmetry. So, the regularization is effectively taken into account in the renormalized chiral couplings:

$$L_i = L_i^r(\mu) + \Gamma_i\lambda, \quad H_i = H_i^r(\mu) + \widetilde{\Gamma}_i\lambda. \tag{3.35}$$

Here μ is the dimensional regularization scale, $\lambda \sim \mu^{d-4}$ and the specific values of $\Gamma_i,\ \widetilde{\Gamma}_i$ were first calculated in Ref. [32].

i	$L_i^r(M_\rho) \times 10^3$
1	0.4 ± 0.3
2	1.4 ± 0.3
3	-3.5 ± 1.1
4	-0.3 ± 0.5
5	1.4 ± 0.5
6	-0.2 ± 0.3
7	-0.4 ± 0.2
8	0.9 ± 0.3
9	6.9 ± 0.7
10	-5.5 ± 0.7

Table 3.2: The values of the couplings $L_i^r(\mu)$ at the scale $\mu = M_\rho$.

The main source of information about the chiral couplings is low-energy phenomenology of three-flavour QCD. The fist three terms of (3.34) are the only ones present in the absence of the external fields, they are responsible for the elastic scatterings of the pseudo-scalar modes. Couplings $L_{4,5}$ generate mass corrections to the meson decay constants, while $L_{6,7,8}$ affect the pseudoscalar masses. L_9 is closely related to the pion charge radius ($r_\pi = \sqrt{\langle r^2 \rangle^{\pi^\pm}} = 0.659 \pm 0.004$ fm [30]). L_{10} only contributes to amplitudes with at least two external vector or axial-vector fields, like the radiative semileptonic decay $\pi \to e\nu\gamma$. L_8^r and H_2^r appear in the chiral correction to the Gell-Mann–Oakes–Renner relation. In Table 3.2 we sum up the phenomenologically derived values of L_i [31].

The large-N_c counting rules can be applied to the coefficients L_i [27]:

$$\mathcal{O}(N_c^1): \qquad L_1,\ L_2,\ L_3,\ L_5,\ L_8,\ L_9,\ L_{10}; \tag{3.36}$$

$$\mathcal{O}(N_c^0): \qquad 2L_1 - L_2,\ L_4,\ L_6,\ L_7. \tag{3.37}$$

It is clear from Table 3.2 that the terms of order N_c are systematically larger than those of order unity. The general estimation of the couplings in terms of the scale of SCSB is $L_i \sim \frac{f_\pi^2/4}{\Lambda_{\chi SB}^2} \sim 2 \times 10^{-3}$ [31].

3.3 OPE in QCD

Chiral Lagrangians allow us to analyze the implications of QCD symmetries at low energies, and there is asymptotic freedom on the other side of the energy

scale, but in many applications one needs to combine the effective description in terms of hadrons with the high-energy (perturbative) one. For instance, to describe the lepton-nucleon scattering: the interaction photon can be highly virtual $Q^2 = -q^2 \to \infty$, while the nucleon is on-shell $p^2 = M^2$. Or we could be interested in the e^+e^- annihilation into hadrons. A technique that allows us to factorize the whole amplitude into the hadron Q^2-independent quantities (condensates) and the ones governed by the perturbative scaling is the operator product expansion (OPE).

The product of two local operators taken at the distance much smaller than the one characteristic to the system can be expressed as a linear combination of local operators:

$$\mathcal{O}_1(x)\mathcal{O}_2(0) \approx \sum_n C_{12}^n(x)\mathcal{O}_n(0). \tag{3.38}$$

The quantum number of the operators at the right hand side should correspond to those of the product on the left. The functions $C_{12}^n(x)$ are the c-number functions that can be singular. They are called the Wilson coefficients. In the renormalizable theories it was proved that the expansion (3.38) is valid at any finite order of the perturbation theory. Let us label the dimensionalities of the operators as d_1, d_2, d_n and fix some scale μ at which the operators are defined. The renormalization group equation could be applied to the Wilson coefficient, then at the leading order

$$C_{12}^n(x) \xrightarrow{x \ll 1/\mu} x^{d_n - d_1 - d_2} (\ln x\mu)^p [1 + O(x\mu)], \tag{3.39}$$

where p is a certain coefficient containing the anomalous dimensions. The higher the dimension of $\mathcal{O}_n$, the less singular is the Wilson coefficient. Hence, at large energies (small distances) the operators with the smallest dimensions dominate.

Let us have an example. For the hadron polarization of the vacuum one should consider a matrix element of the product of electromagnetic quark currents $J^\mu = \sum_j Q_j \overline{\Psi}_j \gamma^\mu \Psi_j$:

$$i\Pi_h^{\mu\nu}(q) = -e^2 \int d^4x e^{iqx} \langle 0|T\{J^\mu(x)J^\nu(0)\}|0\rangle. \tag{3.40}$$

As we need to take the vev, the operators in the OPE should be Lorentz and gauge invariant:

$$J_\mu(x)J_\nu(0) \sim C_{\mu\nu}^1(x) \cdot 1 + C_{\mu\nu}^{\bar{q}q}(x) m_q \bar{q}q(0) + + C_{\mu\nu}^{G^2}(x)(G_{\mu'\nu'}^a)^2 + \dots \tag{3.41}$$

Here we wrote down explicitly only dimension 0 and dimension 4 operators, the next order is dimension 6. $\bar{q}q$ operator violates chiral symmetry and its Wilson

coefficient must contain the quark mass; we choose to write it explicitly. The singularities of the Fourier transformed Wilson coefficients are

$$C^1 \sim (q^2)^0,\ C^{\bar{q}q} \sim (q^2)^{-2},\ C^{G^2} \sim (q^2)^{-2}. \tag{3.42}$$

Note that the quark condensate $\langle 0|\bar{q}q|0\rangle$ and the gluon condensate $\langle 0|G^2|0\rangle$ vanish by definition in perturbation theory. $\langle 0|\bar{q}q|0\rangle$ is the normalized single flavour version of $\langle 0|\overline{\Psi}_i\Psi_j|0\rangle$.

Instead of a model-dependent treatment in terms of constituent quarks, hadrons could be represented by their interpolating quark currents taken at large virtualities. We would be interested in the application of the OPE technique to the two-point functions of such currents.

The vector current of light quarks $J_\mu^{(\rho)} = \frac{1}{2}(\bar{u}\gamma_\mu u - \bar{d}\gamma_\mu d)$ corresponds to the neutral ρ meson and is equivalent to the third component of the operator in eq. (3.15). The one of eq. (3.16) has the quantum numbers of the a_1 meson. Let us consider the following matrix element where we have separated the Lorentz indices

$$\int d^4x e^{iqx}\langle 0|T\{J_\mu^{(\rho/a_1)}(x)J_\mu^{(\rho/a_1)}(0)\}|0\rangle = \left(\frac{q_\mu q_\nu}{q^2} - \eta_{\mu\nu}\right)\Pi_{V/A}(q^2). \tag{3.43}$$

The OPE for these correlators is well-known and could be found in Ref. [33, 34]. We will quote the results in the chiral limit ($m_q = 0$) for the dimensions of the operators not larger than six:

$$\begin{aligned}\Pi_{V,A}(Q^2)/Q^2 = &\frac{N_c}{24\pi^2}\left(1+\frac{\alpha_s}{\pi}\right)\ln\frac{Q^2}{\mu^2} - \frac{\alpha_s}{24\pi}\frac{N_c}{3}\frac{\langle G^2\rangle}{Q^4} \\ &+ c_{V,A}\frac{14N_c}{27}\frac{\pi\alpha_s\langle q\bar{q}\rangle^2}{Q^6}, \qquad c_V = 1,\ c_A = -\frac{11}{7}.\end{aligned} \tag{3.44}$$

Here $\langle G^2\rangle$ and $\langle q\bar{q}\rangle$ are the short names for the gluon and quark condensate, and α_s is the strong coupling constant.

Let us organize the scalar bilinears in the following operators

$$\mathcal{O}_S^a = \overline{\Psi}T^a\Psi = (T^a)_{jk}\left(\overline{\Psi}_R^j\Psi_L^k + \overline{\Psi}_L^j\Psi_R^k\right), \tag{3.45}$$

$$\mathcal{O}_P^a = \overline{\Psi}\gamma_5 T^a\Psi = i(T^a)_{jk}\left(\overline{\Psi}_L^j\Psi_R^k - \overline{\Psi}_R^j\Psi_L^k\right). \tag{3.46}$$

In the SU(2) case they would interpolate 0^{++} (σ or f_0) and 0^{-+} (π) states correspondingly. The two-point function of interest is defined as

$$\int d^4x e^{iqx}\langle 0|T\{J^{(f_0/\pi)}(x)J^{(f_0/\pi)}(0)\}|0\rangle = \Pi_{s/\pi}(q^2). \tag{3.47}$$

Applying the OPE and taking the vevs we can get:

$$\Pi_{s,\pi}(Q^2)/Q^2 = \frac{N_c}{16\pi^2}\left(1+\frac{11\alpha_s}{3\pi}\right)\ln\frac{Q^2}{\mu^2} + \frac{\alpha_s}{16\pi}\frac{N_c}{3}\frac{\langle G^2\rangle}{Q^4} - c_{s,\pi}\frac{11N_c}{9}\frac{\pi\alpha_s\langle q\bar{q}\rangle^2}{Q^6}, \qquad c_s = 1,\ c_\pi = -\frac{7}{11}. \tag{3.48}$$

The condensates are scale dependent quantities. In this type of calculations they are usually estimated at the scale of chiral symmetry breaking $4\pi f_\pi \sim 1$ GeV. There are different estimations for the value of the gluon condensate: in Ref. [33] they use $\langle\frac{\alpha_s}{\pi}G^2\rangle = 0.012$ GeV^4, but there is also a lattice result $\langle\frac{\alpha_s}{\pi}G^2\rangle = 0.10$ GeV^4 [35]. The quark condensate was evaluated to be $\langle q\bar{q}\rangle = -(242\pm 15)^3$ MeV^3 [36] or $-(235\pm 15)^3$ MeV^3 [37].

We should mention that to actually start evaluating the experimental cross-sections of the type $e^+e^- \to$ hadrons one needs to use additional methods, such as dispersion relations and sum rules.

3.4 QCD on lattice

QCD has a running physical coupling. For $\alpha_s = g^2/4\pi$ at the one-loop level:

$$\alpha_s(\Lambda^2) = \frac{\alpha_s(\Lambda_0^2)}{1+\beta_0\alpha_s(\Lambda_0^2)\ln(\Lambda^2/\Lambda_0^2)}, \tag{3.49}$$

where $\beta_0 = \left(11-\frac{2}{3}N_f\right)/4\pi$. A conventional choice is to take $\Lambda_0 = M_Z = 91.2$ GeV. The most recent world average from PDG [30] is $\alpha_s(M_Z^2) = 0.1179(10)$.

In the high energy limit (at energies higher than $\sim$ 2 GeV) the theory permits perturbative computations, and asymptotic freedom in QCD was proven by Gross, Wilczek and Politzer. At low energies, at a typical scale Λ_{QCD}, the coupling is large and the colour degrees of freedom are confined into colour-singlet states (mesons, baryons, glueballs). To deal with this regime the lattice regularization of QCD was proposed [38]. It represents a unique non-perturbative, gauge-invariant formulation of QCD from its firsts principles.

The lattice formulation is based on the Feynman path integral approach. The starting point is the partition function

$$\mathcal{Z} = \int \mathcal{D}A_\mu \mathcal{D}\overline{\psi}\mathcal{D}\psi \exp\left(iS\right),\ \mathcal{L} = -\frac{1}{4}G_{\mu\nu}^2 + \overline{\psi}M_D\psi \tag{3.50}$$

where M_D is the Dirac operator. To avoid a complex weight factor it is traditional to perform a Wick rotation and rewrite the former expression as

$$\mathcal{Z} = \int \mathcal{D}A_\mu \mathcal{D}\overline{\psi}\mathcal{D}\psi \exp\left(-S_E\right),\ \mathcal{L}_E = \frac{1}{4}G_{\mu\nu}^2 - \overline{\psi}M_D\psi \tag{3.51}$$

The fermions can be integrated out exactly with the result [39]

$$\mathcal{Z} = \int \mathcal{D}A_\mu \det M_D \exp\left(-\frac{1}{4}\int d^4x G_{\mu\nu}G^{\mu\nu}\right). \tag{3.52}$$

This move is useful because the path integral over Grassmann variables does not admit a computer implementation. However, the fermionic determinant is a non-local function of the gauge fields, and this leads to various complications in comparison to the simulations of pure YM theory. For this reason, most of the early lattice QCD computations were performed in the so-called quenched approximation ($\det M_D = 1$). There the effect of dynamical quarks is completely neglected, and the evaluation of quantities containing valence quarks happens with a quantum weight depending only on the pure YM action. Further we will refer to various results obtained in this approximation, though nowadays technology makes the unquenched computations a standard thing.

The lattice formulation makes the QCD calculations with eq. (3.51) mathematically rigorous. As the name suggests the theory is put on a discrete space-time greed, with the characteristic lattice spacing a. The functional integral (continuum) formulation can be replaced with a product of ordinary integrals. In addition, there is a natural cutoff $\sim 1/a$.

The continuum limit is recovered taking $a \to 0$. On one hand, a should be understood in terms of some dimensionful observable with a known physical value. On the other, in the continuum limit the ratio of this observable to a should diverge. This means that the lattice theory should have a continuous transition, characterized by a diverging correlation length. In QCD, and $4D$ non-Abelian theories in general, it is possible due to the presence of the UV fixed point at the value of the coupling tending to zero. In lattice QCD the bare lattice coupling, g, describes the strength of the physical gauge interaction at the distance a. As $a \to 0$ asymptotic freedom implies $g \to 0$ [40].

The lattice regularization explicitly breaks translational and rotational symmetries. Let us consider for simplicity a hypercubic lattice. There, the group of traditional translations is broken down to its subgroup of translations by integer multiples of the lattice spacing (in each direction), while the group of rotations is broken down to rotations by angles which are integer multiples of $\pi/2$. However, gauge symmetry is kept at every point of the lattice. This is achieved by the gauge degrees of freedom being different from the continuum gauge fields. The YM sector of QCD is defined in terms of parallel transporters along the oriented

links joining nearby lattice sites [40]:

$$U_\mu(x) = \exp[igaA_\mu(x + a\hat{\mu}/2)]. \tag{3.53}$$

Such link variable signifies the transportation form the sit x to the closest one in a direction of the unit vector $\hat{\mu}$ (that form a basis in the Euclidean spacetime). Under a gauge transformation χ the lattice variable transforms as

$$U_\mu(x) \to \chi(x)U_\mu(x)\chi^\dagger(x + a\hat{\mu}). \tag{3.54}$$

Gauge-invariant, purely gluonic lattice operators are given by traces of path-ordered products of $U_\mu(x)$ around closed contours. The simplest of them is the trace of the plaquette $U_\square$, for which the contour goes around an elementary $a \times a$ square on the lattice.

The simplest lattice action for the purely gluonic theory is the Wilson action, given by the sum over all lattice plaquettes

$$S_W = \frac{2}{g^2} \sum_\square \mathrm{Re}\,\mathrm{Tr}(1 - U_\square). \tag{3.55}$$

Taking the trace insures gauge invariance, and taking the real part is equivalent to averaging the loop and its charge conjugate. It could be shown that the Wilson action has the Euclidean YM action in its continuum limit.

In fact any gauge invariant action for QCD has to be built out of two types of objects: Wilson loops and Wilson/Polyakov strings. The latter are given by the path-ordered product of links capped by a fermion and an antifermion; or can appear on lattices with periodic boundary conditions.

The Wilson loops [38] are the generalization of the plaquette on the contours of arbitrary sizes:

$$\mathcal{W}(r, L) = \mathrm{Re}\,\mathrm{Tr} \prod U_\mu(x). \tag{3.56}$$

Specifically, one can associate a rectangular Wilson loop of sizes r and L, lying in a plane parallel to the Euclidean time direction, to the process of creation, propagation over a Euclidean time interval L and annihilation of an infinitely heavy (static) quark-antiquark pair with a relative distance r. The potential $V(r)$ of the pair is expressed as

$$V_{Q\bar{Q}}(r) = -\lim_{L\to\infty} \frac{1}{L} \ln\langle \mathcal{W}(r, L)\rangle. \tag{3.57}$$

Polyakov loops $\mathcal{P}$ [41, 42] are similar to the Wilson ones, but they wind around some periodic direction (of extent L) in the system, so that they cannot be contracted. The periodicity in the Euclidean time signifies that the system is at finite

temperature $T \sim 1/L$. The Polyakov loop expectation value can be interpreted as a partition function in the presence of a static-quark source. Then, the single-quark free energy F at temperature T follows from standard thermodynamics

$$F_q = -T \ln\langle \mathcal{P}(r, L)\rangle. \tag{3.58}$$

In the deconfined phase of YM theory at sufficiently high temperatures both $\langle\mathcal{P}\rangle$ and F_q are finite. In the confining phase (at zero or low temperatures): $\langle\mathcal{P}\rangle \to 0$ and $F_q \to \infty$, meaning that quarks cannot exist as asymptotic states. This behaviour is in accordance with Wilson's standard confinement criterion [38].

Linear combinations of gauge-invariant, purely gluonic lattice operators that belong to a specific well-defined irreducible representations of the group of discrete spatial rotations and have the well-defined parity and charge conjugation quantum numbers correspond to glueball operators, *i.e.* operators creating gauge-invariant, color-singlet states with well-defined J^{PC} quantum numbers. Further studies allow to extract the spectrum of these physical states.

Finally, we need to mention a standard non-perturbative way to define the value of a in physical units at a given g. First, one carries out simulations at a given value of g on a lattice of given sizes, computing the expectation values of large Wilson loops, $\langle\mathcal{W}(r, L)\rangle$ at $r \gg a,\ L \gg a$. Then, these values can be fitted to the expected area-law behaviour

$$\langle\mathcal{W}(r, L)\rangle \propto \exp\left(-\sigma a^2 \cdot \frac{r}{a}\frac{L}{a}\right). \tag{3.59}$$

Here appears a parameter σ, that has a certain phenomenological value [1]. That allows to obtain a certain numerical value of a in fm. The continuum extrapolation corresponds to $\sigma a^2 \to 0$. σ parameter frequently appears in heuristic discussions of the confinement related to the stretching of the flux tube of length l between two static sources (quarks). The thermodynamic weight of such a configuration depends on the string energy $E(l) = \sigma l$, and hence σ is known as the string tension.

3.5 QCD at finite temperature

QCD at finite temperature has been actively studied during the last several decades. However, the deconfinement transition in the QCD matter remains a complicated and largely not-understood process. Basically, we presume that with the temperature growth the description in terms of hadronic states becomes worse and worse

[1] Usually $\sigma = (440\ \text{MeV})^2$, but the value may vary slightly from paper to paper.

until finally one should turn to consider the hadron matter as the Quark-Gluon Plasma (QGP).

It is known that QCD properties change drastically when temperature of the system grows. At zero and small temperatures we have a gas of colour-bound hadronic states. That is the standard matter, the eigenstates of the zero temperature QCD Hamiltonian. The content of such gas is rather determined because of the exponential suppression $\sim \exp(-M/T)$ of large mass modes. At small temperatures this would be a pion gas. Its density is rather low as there is not enough temperature excitation and the pions do not interact with each other. As temperature grows the pion gas more dense and the interactions become stronger. That means that starting from some critical temperature T_c(=temperature of deconfinement) the hadron degrees of freedom no longer provide a valid basis to describe the physics of the system, and an analytic calculation is impossible.

Theoretical analysis becomes meaningful again at very high energies (much larger than the characteristic hadron scale of 1 GeV). In this region one should use a basis of quarks and gluons, the fields of the fundamental QCD Lagrangian. The system represents a thermodynamically stable medium in which these particles propagate freely. The possible interactions between quarks and gluons have a weak effective coupling in the near-asymptotic regime and could be taken into account perturbatively. The properties of this system make it akin to the non-relativistic plasma of charged particles bound by the weak Coulomb interaction. That is why it is called Quark Gluon Plasma. It is important to take notice that, though one often calls the state of the matter QGP as soon as the deconfinement takes place, there is no common plasma behaviour in between the extreme regimes, and asymptotic freedom is reached rather slowly. In fact, at the temperatures $T_c \lesssim T \lesssim 4T_c$ QGP stays strongly-coupled [25].

So, we expect to obtain different characteristics of the QCD matter on the edges of the temperature scale. One would assume that a thermodynamical transition happens at some point, but is it a sharp phase transition (non-analytic behaviour of some observables) or a more smooth crossover (analytic behaviour with rapid changes)?

Let us start with the pure YM theory that fulfills the criterion of the Polyakov loop behaviour. It is proved to be confining both theoretically [43] and on lattice [44, 45]. The confined phase corresponds to the bound glueball states, while the deconfined – to the gluon plasma. There exists a heuristic proof [43] of the phase transition between these phases. At zero temperature the confinement is

exhibited in the linearity of the potential between heavy quark and anti-quark

$$T = 0: \quad V_{Q\bar{Q}}(r) \sim \sigma r, \quad r \to \infty. \tag{3.60}$$

At higher temperatures a screening effect is present

$$T \gg \Lambda_{hadr}: \quad V_{Q\bar{Q}}(r) \sim \frac{g^2(T)}{r} e^{-m_D r}, \tag{3.61}$$

where $m_D \sim gT$ is the Debye mass; no confinement is present at large T. Hence, there should be a point T_c where the phase transition happens.

On the lattice the deconfinement of gluons was originally seen as onset of color screening and rapid increase in the energy density that indicate liberation of many new degrees of freedom. It turns out that in $SU(2)$ there is a second order phase transition [46–48], while in $SU(3)$ – it is of a first order [49]. The lattice studies of $SU(3)$ theory provide the specific values $T_c \sim 260 - 270$ MeV [44],[45].

In full QCD there is also a number of valid approaches. At such high temperature that gluons and quarks interact weakly calculations using a perturbative expansion in the QCD coupling must work. Their main problem, however, is very poor convergence and large dependence on the renormalization scale. A reorganization programme, called the hard thermal loop resummed perturbation theory (HTLpt) provides a quantitatively controlled application of the idea [50]. Depending on the thermodynamic function at hand, the agreement between lattice simulations and the results from HTLpt is very good down to temperatures of approximately 250 MeV. Besides, the method allows the study of QCD thermodynamics not only at finite temperature, but at finite baryon, strangeness, and isospin chemical potentials [51]. However, the HTLpt results concern specific properties of QGP, and in the end shed no light on the nature of deconfinement phase transition.

Research on the confining properties near and below T_c require non-perturbative approaches. The lattice-QCD simulations are the most successful as long as the quark chemical potential is sufficiently smaller than the temperature.

It was found out that the nature of transition in QCD depends a lot on the role of the quark mass. The accumulated knowledge is illustrated in the so-called Columbia plot of Figure 3.1. In the limit of massless quarks chiral symmetry restoration is expected to happen at sufficiently high temperatures, and indeed several observables (like chiral susceptibility and chiral condensate) signal the chiral phase transition on lattice. For $N_f = 3$ massless quarks it is shown that the transition should be first order. In case of just two massless quarks both possibilities (second or first order) are realized depending on the value of the strange quark

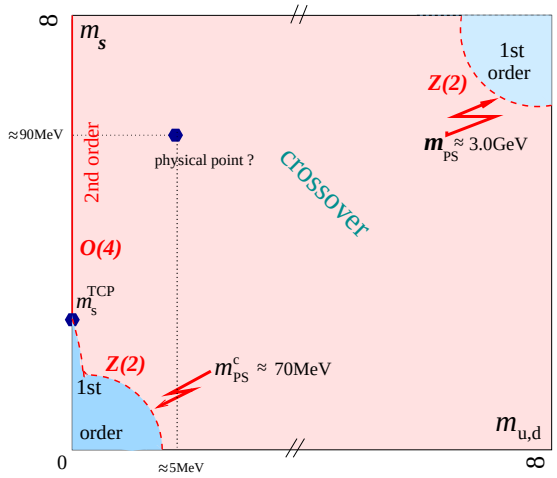

Figure 3.1: Phase transition in QCD. Figure taken from Ref. [52]

.

mass and/or the quark chemical potential. That implies the existence of tricritical point.

In the opposite limit of three infinitely massive quarks the QCD partition function has $Z(3)$ symmetry. The breaking of this symmetry at high temperatures due to colour screening takes place as a first order phase transition. The order parameter for this deconfinement phase transition is the Polyakov line, it shows a non-analytic behaviour.

The highly non-trivial result for the QCD with physical quark masses is that all of the characteristic observables show continuous, smooth, but rapidly changing temperature dependencies, and none can be regarded as an order parameter. Investigations on lattice with physical quarks leave no doubt to the fact that the deconfinement represents rather a smooth crossover than a phase transition [53, 54]. Hence, the notion of the critical parameter is substituted with the pseudo-critical temperature. The pseudo-critical temperature is well defined for a given observable, but it is not unique. The value may vary in almost 20% range. In Ref. [54] they argue that the more observables are studied, the broader picture on the QCD transition is obtained. They use the chiral susceptibility/condensate, the Polyakov loop, the strange quark number susceptibility and the energy density or trace anomaly to signal the transition. Such lattice simulations provide the critical temperature is the range $T_c \sim 145 - 165$ MeV [54–57]. Among the most recent

data the value $T_c = 156.5 \pm 1.5$ MeV is reported by the hotQCD collaboration [58]. However, strictly speaking, these arguments apply to the crossover nature of the chiral transition, and its connection to the deconfinement is not fully understood theoretically [59].

For a complementary viewpoint, we turn to the experimental data on heavy ion collisions. The experiments undertaken at such facilities as SPS and ALICE at LHC and RHIC in Brookhaven National Laboratory have gathered valuable information on the QGP. The future experiments at FAIR (GSI) and NICA (JINR) are aimed to broaden the current knowledge. The analysis of data on hadron production in ultra-relativistic nuclear collisions is made in the framework of the statistical hadronization approach. On the theory side it relies on an assumption that low temperature QCD (its partition function) can be well-described in terms of the hadron resonance gas (HRG) model, that is also called the hadron-parton duality. This hypothesis was checked by comparing the equation of state as evaluated in HRG model and on lattice. Agreement between the two methods was found for temperatures up to the lattice-estimated values of T_c (see, *e.g.*, [56, 57]). On the other hand, the observed hadron yields in central collisions can be very well described by computing particle densities from the hadronic partition function with the necessary parameters fitted to the experiment at the surface of "chemical freeze-out". In particular, the chemical freeze-out temperature is $T_{CF} \simeq 160$ MeV (*e.g.* see [59–61]). The value is close to that of the pseudo-critical temperature on lattice, and thus, the chemical freeze-out takes place close to hadronization of the QGP.

There exists, however, another limit of QCD with well-defined phase transition. That is the already discussed large-N_c limit. As the number of gluons $\mathcal{O}(N_c^2)$ suppresses any effect of quarks $\mathcal{O}(N_c)$, the quenched approximation works correctly there. The pressure of the hadronic matter at lower temperature is $\mathcal{O}(1)$, while the deconfined matter, dominantly gluonic, has $\mathcal{O}(N_c^2)$. The pressure jumps between the two limits and hence we have a phase transition, not a crossover. This should be naturally interpreted as the first order transition but, in fact, the issue remains a matter of some discussion [62].

The studies of finite temperature QCD in the large-N_c limit were performed in various papers [63–66]. They prove, indeed, that all $SU(N)$ Yang-Mills theories undergo a physical deconfining transition at a critical temperature T_c, which remains finite when expressed in some appropriately defined non-perturbative scale of the theory (*e.g.* the zero-temperature string tension σ). In particular, the deconfinement transition can be associated with the spontaneous breakdown of the exact

global center symmetry of the pure-glue theory, and takes place at temperatures which, if the scale is expressed in physical units, are in the range between 250 and 300 MeV, depending on the number of colors.

The estimation at $N_c \to \infty$ is done as a certain fit of the continuum limit data achieved for the theories with finite number of colours. In recent studies, like that of Ref. [66], they include $N_c = 2, .., 8$ and fit two factors in the linear approximation

$$\left.\frac{T_c}{\sqrt{\sigma}}\right|_{N_c} = \left.\frac{T_c}{\sqrt{\sigma}}\right|_{N_c=\infty} + \frac{c}{N_c^2} + \mathcal{O}(N_c)^{-4}. \tag{3.62}$$

They predict large-N_c result of $T_c/\sqrt{\sigma} = 0.5949 + 0.458/N_c^2$ with $\chi^2/dof = 1.18$. With the standard choice $\sqrt{\sigma} = 420 \div 440$ MeV we get $T_c \sim 250 \div 260$ MeV at the leading in $1/N_c$ order.

3.6 Conclusions

In this chapter we have scoped a number of QCD related topics. Large-N_c limit provides an interesting insight by itself and is an indispensable component of holographic models. In eq. (3.6) we have seen that the two-point correlator in large-N_c QCD takes the form of the infinite sum of infinitely narrow resonances.

Chiral symmetry and associated QCD currents belong to the construction ground of the $5D$ models. The chiral symmetry breaking due to the appearance of the non-vanishing chiral condensate agrees with the experimental data, and thus the symmetry breaking pattern for the descriptive models is set in eq. (3.22). The description of the low-energy QCD phenomenology is a primary goal of the developed AdS/QCD models. The comparison of their predictions to the universal ones of the chiral perturbation theory will be made. On the other hand, the OPE results for QCD also set some of the key features of the holographic models.

Lattice QCD is another interesting framework providing various reference results. Among them the understanding of the nature of deconfinement process in QCD and the estimation of the associated deconfinement temperature. In real QCD the process represents a smooth crossover, but in the large-N_c limit or in pure YM theory there is a phase transition.

Chapter 4

QCD spectra, couplings and form factors

In this chapter we would like to cover the necessary phenomenological information over the QCD states, that we will need to use in order to compare with our holographic computations. We are interested in the light non-strange mesons and scalar glueballs.

We focus on studying the pattern radial excitations fill in, and expect equidistant Regge trajectories. For the mesons the QCD phenomenon of the linearity of the kind

$$M^2(n) = M_0^2 + \mu^2 \cdot n, \quad n = 0, 1, 2, \ldots, \tag{4.1}$$

with n being the radial quantum number, could be seen in the quasiclassical stringy explanation (see, *e.g.* Ref. [67] and appendix of Ref. [68]) and in the experimental data (as analysed in Ref. [69]).

4.1 $J = 1$ mesons

4.1.1 Masses

The light non-strange 1^{--} mesons are ρ and ω mesons, while the a_1 meson has the quantum numbers 1^{++}. One can find information on their masses and those of their radial excitations in the PDG database [30]. We would focus mostly on the ρ meson case, and most conclusions are valid for the ω case as well.

The first three states of the ρ meson, $\rho(770),\ \rho(1450),\ \rho(1700)$ $(n = 0, 1, 2)$ are considered well-established. They make a blue trajectory in Fig. 4.1, that is obtained with the least square method and the weights are inversly proportional

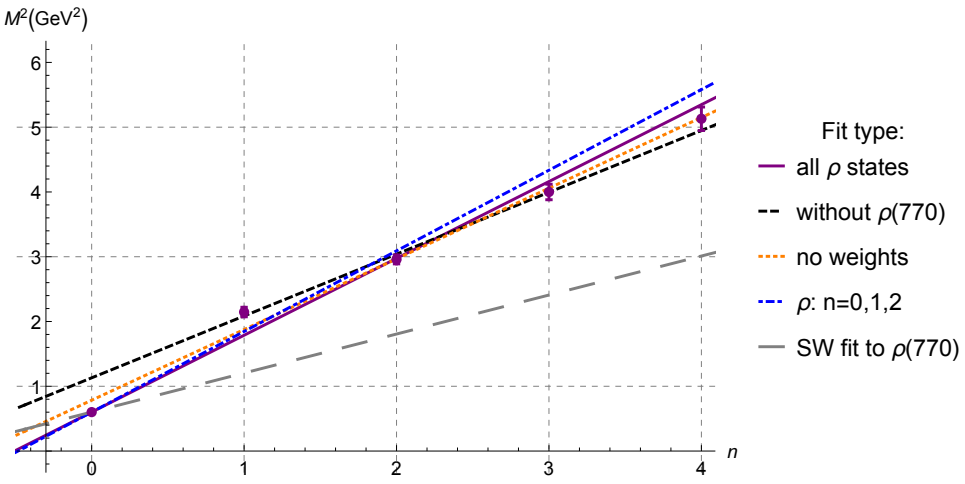

Figure 4.1: Possibilities for the radial Regge trajectories of the ρ meson radial excitations. The last option (SW fit) is derived in the AdS/QCD model and is explained in Section 5.4.

to the square of the experimental mass uncertainty. However, if we pay closer attention, the determination of the linear vector Regge trajectory is far from simple.

There is a well-known peculiarity in the ρ spectrum: the ground state lies notably below the linear trajectory if one considers adding further states $\rho(2000)$, $\rho(2270)$ ($n = 3, 4$). On one hand, $\rho(770)$ (or $\omega(782)$) have the most established mass values, being most useful for the numerical estimations. That is clear from comparing the error bars in $m_{\rho(770)} = 775.26 \pm 0.25$ MeV and in, *e.g.*, $m_{\rho(1450)} = 1465 \pm 25$ MeV. On the other, it is evident that the trajectories with (purple) and without $\rho(770)$ (black trajectory in Fig. 4.1) are significantly different.

Moreover, the first radially excited state $\rho(1450)$ is situated unnaturally higher the linear trajectory for $n = 0, 1, 2$ and has a PDG status of the namesake for broad resonance region. Its mass value is "only an educative guess". This resonance seems to have some admixture of the strange quark (enlarging its mass) and its decays show characteristics of hybrids (see the review "$\rho(1450)$ and $\rho(1700)$" in [30]). The resonance $\rho(1700)$ is often interpreted as the D-wave vector state. In the compilations [69–71] it belongs to the second radial vector trajectory (the first one contains the S-wave states). $\rho(2000)$ and $\rho(2270)$ are also ascribed to this second trajectory in Ref. [71].

The development of this problem depends on the way one obtains the averaged trajectory. For instance, we can introduce no weights (yellow trajectory in Fig. 4.1), making all the states equally significant. We will see that sometimes this type of

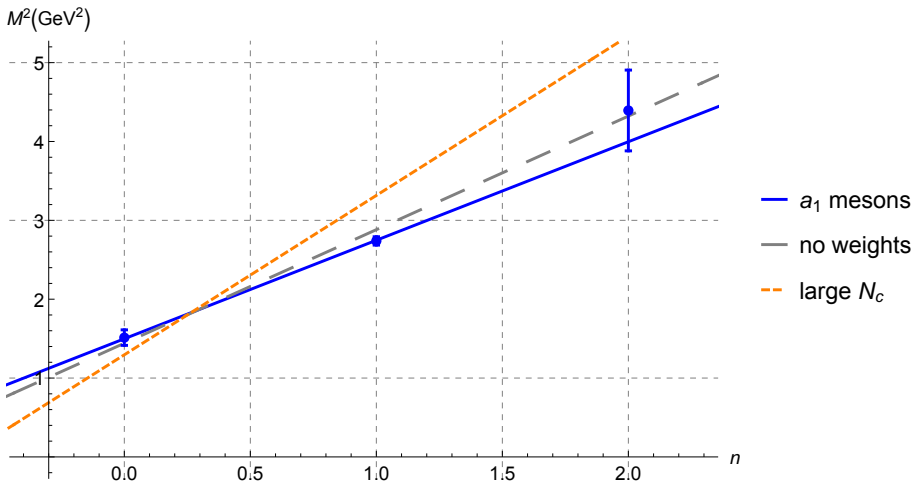

Figure 4.2: The radial Regge trajectory of the a_1 meson excitations. Large N_c trajectory is constructed for the states described in Section 4.3.

average can be useful. The ground state mass in this case weights ~ 1 GeV.

In the axial vector sector we have $a_1(1260)$, $a_1(1640)$ and $a_1(2095)$ ($n = 0, 1, 2$) belonging to one radial Regge trajectory. They are depicted in Fig. 4.2. Fortunately, there is less controversy on the issue as to which quantum numbers should be assigned to the states.

An interesting approach to look for the systematics in the meson spectra was started in Refs. [69, 70]. Among other things, they noticed the phenomenon of "universal" slope (μ^2 in eq. (4.1)) in the radial trajectories of various light non-strange mesons. This observation is also favoured by the hypothesis arising in the hadron string models that the slope is mainly determined by the gluodynamics. It was estimated that $\mu^2 = 1.25 \pm 0.15$ GeV^2 [69] and $\mu^2 = 1.143 \pm 0.013$ GeV^2 [70]. The idea was further advocated in many studies [67, 72–80]. We would also be interested in the generalizations to the trajectories with the universal intercept presented in

$$\text{Ref. [81]}: \quad M^2(n) = 1.14(n + 0.54)\ (\text{GeV}^2), \tag{4.2}$$

$$\text{Ref. [71]}: \quad M^2(n) = 1.38(4)n + 1.12(4)J + 0.13(4)\ (\text{GeV}^2). \tag{4.3}$$

As one can notice, it was proposed in Ref. [71] that no full spin J universality can be achieved. Also, both analyses result in the value of the slope similar to the ones of Refs. [69, 70].

4.1.2 Decay constants and decay rates

There are other phenomenologically relevant quantities characterizing the states in the vector and axial vector sectors. First, we discuss the vector meson decay constants. The following matrix elements define the experimentally observed quantities F_ρ and F_{a_1}:

$$\langle 0|\mathcal{O}_V^{a\,\mu}(x)|\rho^b(p)\rangle = \epsilon^\mu \delta^{ab} F_\rho e^{-ipx}, \tag{4.4}$$

$$\langle 0|\mathcal{O}_A^{a\,\mu}(x)|a_1^b(p)\rangle = \epsilon^\mu \delta^{ab} F_{a_1} e^{-ipx}, \tag{4.5}$$

where the operators are those defined in eqs. (3.15) and (3.16). We could have the n-the radial excitation of the meson in the matrix element, and the constants would be generalized to $F_\rho(n)$ and $F_{a_1}(n)$.

To understand the scale of these constants consider the leptonic decay of the neutral ρ excitation, described by the following diagram:

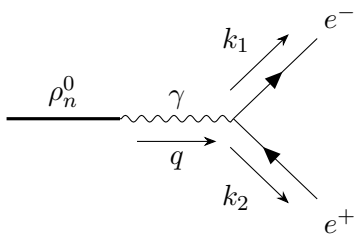

With the standard photon-e^+e^- vertex we have the amplitude

$$i\mathcal{M} = \bar{u}^s(k_1)(-ie\gamma^\mu)v^s(k_2)\frac{-i\eta_{\mu\nu}}{q^2}\left(ieq^2\frac{F_\rho(n)}{m_\rho^2(n)}\right)\epsilon^\nu(q), \tag{4.6}$$

that determines the decay rate

$$\Gamma_{\rho_n\to e^+e^-} = \frac{|\vec{k_1}|}{8\pi m_{\rho_n}^2}\cdot\frac{1}{3}\sum_{pol}|\mathcal{M}|^2 = \frac{\sqrt{m_{\rho_n}^2/4 - m_e^2}}{8\pi m_{\rho_n}^2}\cdot\frac{4}{3}e^4\frac{F_\rho^2(n)}{m_{\rho_n}^2}. \tag{4.7}$$

Neglecting the electron mass, we can equate the $\rho(770)$ decay amplitude to its experimental value [30] ($\alpha = e^2/4\pi$)

$$\Gamma_{\rho\to e^+e^-} = \frac{4\pi\alpha^2 F_\rho^2}{3m_\rho^3} = 7.04 \pm 0.06 \text{ KeV}. \tag{4.8}$$

This relation provides a high precision estimate $F_\rho|_{exp} = 0.12124 \pm 0.00002$ GeV^2.

The experimental value of $F_{a_1}|_{exp} = 0.177 \pm 0.014$ GeV^2 can be obtained in the study of the $\tau \to \nu_\tau\pi\pi\pi$ decay [82]. On the lattice, Ref. [83] provides

0.21 ± 0.02 GeV^2. We can also refer to a theoretical (extra-dimension) work of Ref. [84], where they estimate $F_{a_1} = 0.26$ GeV^2.

The full width of $\rho(770)$ is $\Gamma_\rho = 149.1 \pm 0.8$ MeV. Let us consider the main decay channel $\rho \to \pi\pi$. In general, for the n-th resonance we can include two diagrams:

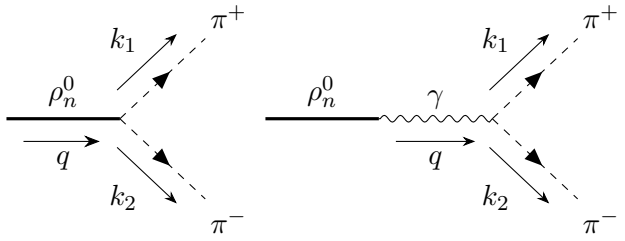

The corresponding amplitude is

$$i\mathcal{M} = ig_{\rho_n,\pi,\pi}(k_1-k_2)^\mu\epsilon_\mu(q)+ie(k_1-k_2)^\mu\frac{-i\eta_{\mu\nu}}{q^2}\left(ieq^2\frac{F_\rho(n)}{m_\rho^2(n)}\right)\epsilon^\nu(q); \quad (4.9)$$

and the decay rate of $\rho(770)$ is given by

$$\Gamma_{\rho\to\pi^+\pi^-} = \frac{(m_\rho^2-4m_\pi^2)^{3/2}}{48\pi m_\rho^2}\left(g_{\rho,\pi,\pi}+e^2\frac{F_\rho(n)}{m_\rho^2(n)}\right)^2 = 147.5 \pm 0.8\,\text{MeV}. \quad (4.10)$$

The processes $\rho^+ \to \pi^0\pi^+$ and $\rho^- \to \pi^0\pi^-$ receive no electromagnetic contribution and the difference with the neutral decay is estimated as follows [30]:

$$\Gamma(\rho(770)^0) - \Gamma(\rho(770)^\pm) = 0.3 \pm 1.3\,\text{MeV}. \quad (4.11)$$

We also remark that the ratio of the leptonic ρ decay to the pion one has been separately evaluated [30]:

$$\frac{\Gamma_{\rho\to e^+e^-}}{\Gamma_{\rho\to\pi^+\pi^-}} = (0.40 \pm 0.05)\cdot 10^{-4}. \quad (4.12)$$

Let us turn to the axial vector sector. The full $a_1(1260)$ width, as averaged by PDG, is given by $\Gamma_{a_1} = 389 \pm 29$ MeV. Their general estimate, however, is much broader $\Gamma_{a_1} = 250 \div 600$ MeV.

Experiments show that the dominant channel is the decay into the pair of $\rho(770)$ and π in the S-wave configuration, that is studied in the processes $e^+e^- \to \tau^+\tau^-$ or $\tau^- \to \pi^-\pi^0\pi^0\nu_\tau$. The partial width of $a_1 \to (\rho\pi)_{\text{S-wave}}$ is $60.19\% \times \Gamma_{a_1} \simeq 233$ MeV $\in 150 \div 360$ MeV. The next in significance is the decay $a_1 \to f_0(500)\pi$, with the width of order $18.76\% \times \Gamma_{a_1}$. In both these decays, as well as in several subleading ones, the final state contains three pions.

The diagram for the $a_1 \to \rho\pi$ process is

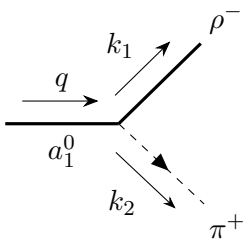

The amplitude is simple

$$i\mathcal{M} = g_{\rho,a_1,\pi}\epsilon_\mu(q)\epsilon'^{*\mu}(k_1), \tag{4.13}$$

but the decay rate is complicated by the more involved phase space factor

$$\Gamma_{a_1\to\rho\pi} = \frac{\sqrt{(m_a^2-(m_\rho+m_\pi)^2)(m_a^2-(m_\rho-m_\pi)^2)}}{48\pi m_a^3} \times\left(2+\frac{(m_a^2+m_\rho^2-m_\pi^2)^2}{4m_a^2m_\rho^2}\right)g_{\rho,a_1,\pi}^2. \tag{4.14}$$

For the charged decays $a_1^+\to\rho^0\pi^+$, $a_1^-\to\rho^0\pi^-$ there is a possible electromagnetic contribution from the $\gamma-\rho^0$ mixing resulting in $\Gamma_{a_1\to\rho\pi}\times(1-\frac{\alpha}{4\pi})^2$.

4.1.3 Pion and axial form factors

We also would like to examine the electromagnetic form factor (FF) of the pion $G_\pi(q^2)$:

$$\langle\pi^a(k_1)|\mathcal{O}_V^{3\mu}(q)|\pi^b(k_2)\rangle = i\varepsilon^{ab3}\delta(k_1+k_2+q)(k_1+k_2)^\mu G_\pi(q^2), \tag{4.15}$$

and the axial form factor $G_{a_1}(q^2)$:

$$\langle a_1^{a\nu}(k_1)|\mathcal{O}_V^{3\mu}(q)|\pi^b(k_2)\rangle = i\varepsilon^{ab3}\eta^{\mu\nu}\delta(k_1+k_2+q)G_{a_1}(q^2). \tag{4.16}$$

Generally, the electromagnetic current $\mathcal{J}_\mu^{em}$ in the case of two-flavour QCD is

$$\mathcal{J}_\mu^{em} = \mathcal{O}_{V\mu}^3+\frac{1}{6}\mathcal{O}_{V\mu} = \frac{2}{3}\overline{u}\gamma^\mu u-\frac{1}{3}\overline{d}\gamma^\mu d, \tag{4.17}$$

where $\mathcal{O}_{V\mu}$ is an Abelian current from eq. (3.19). However, it is omitted in the definitions of eqs. (4.15) and (4.16) because the corresponding matrix element is zero due to the isospin or G-parity conservation.

The two form factors are depicted schematically in the diagrams of Fig. 4.3. We would assume that there are two types of contribution: the direct one, and the one governed by the propagation of massive ρ excitations. For the case of the pion FF there are these two diagrams to be considered:

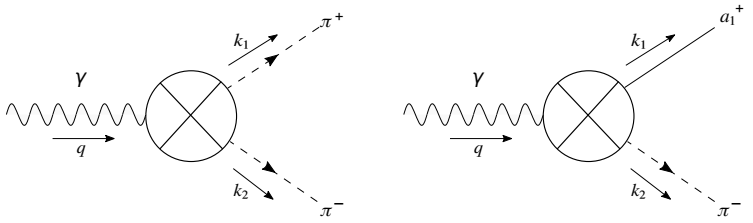

Figure 4.3: Pion (left) and axial (right) form factors. The effective coupling $\bigotimes$ comprises the direct contribution and the one mediated through the ρ meson radial excitations.

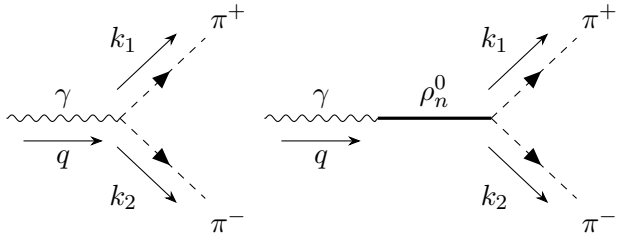

And the similar ones can be given in the axial case. In the end the expressions of the FFs are:

$$G_\pi(q^2) = 1 - \sum_n \frac{q^2 F_\rho(n)}{m_\rho^2(n)} \frac{g_{\rho_n,\pi,\pi}}{q^2 - m_\rho^2(n)}, \tag{4.18}$$

$$G_{a_1}(q^2) = g_{a_1,\pi,\gamma} - \sum_n \frac{q^2 F_\rho(n)}{M_D^2(n)} \frac{g_{\rho_n,a_1,\pi}}{q^2 - m_\rho^2(n)}, \tag{4.19}$$

where we introduced the three-point hadron couplings $g_{\rho_n,\pi,\pi}$ and $g_{\rho_n,a_1,\pi}$; the contact term in the case of the pion FF is standardly normalized to one and for the axial FF is given by $g_{a_1,\pi,\gamma}$. The experimental data on the pion FF can be found in Section 7.5 (see Fig. 7.1).

We can now consider the decay process $a_1 \to \pi\gamma$:

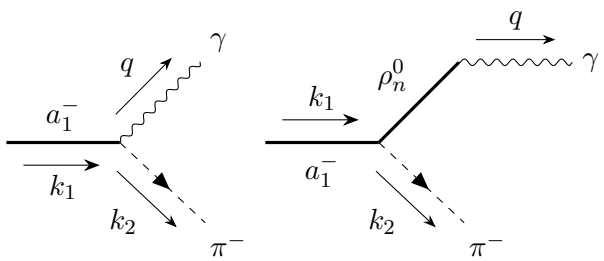

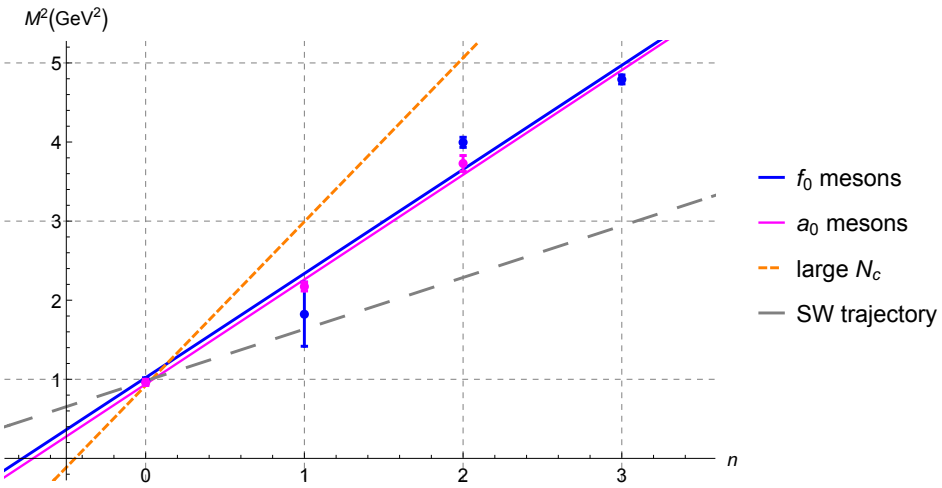

Figure 4.4: Our prescription of the states to the radial Regge trajectories of the scalar mesons. Large N_c trajectory of a_0 mesons is obtained from the data of Table 4.1. The SW trajectory of the scalar mesons is found out in Section 5.4.

The expression of the axial FF in eq. (4.19) allows us to estimate

$$\Gamma_{a_1\to\pi\gamma} = \frac{\alpha}{4}\frac{m_a^2 - m_\pi^2}{m_a^3} G_{a_1}^2(m_a^2/4) = 640 \pm 246 \text{ KeV}. \tag{4.20}$$

This PDG quoted experimental value is given in Ref. [85], it is also mentioned there that the radiative partial decay estimation is sensitive to the assumed a_1 resonance mass and the total width, and they use the parameters standard for their time (35 years ago). It is worth noticing that many holographic models predict zero value for this decay: either due to the absence of the direct term [86, 87] or to the exact cancellation of ρ and ρ' contributions [84].

4.2 $J = 0$ states

4.2.1 Masses

The 0^{++} states we are taking into account are the isosinglet f_0 and isotriplet a_0 mesons. There is a degree of uncertainty concerning which f_0 states belong to the radial trajectory of light quarks and which to the strange one. We follow mostly the reasoning from Ref. [71] and include as $q\bar{q}$ states $f_0(980)$, $f_0(1370)$, $f_0(2020)$, $f_0(2200)$. They are depicted in Fig. 4.4. The only difference from Ref. [71] is the substitution of $f_0(1500)$ with $f_0(1370)$ which will become clear after the discussion of scalar glueball states. Unfortunately, $f_0(1370)$ is much more wide and

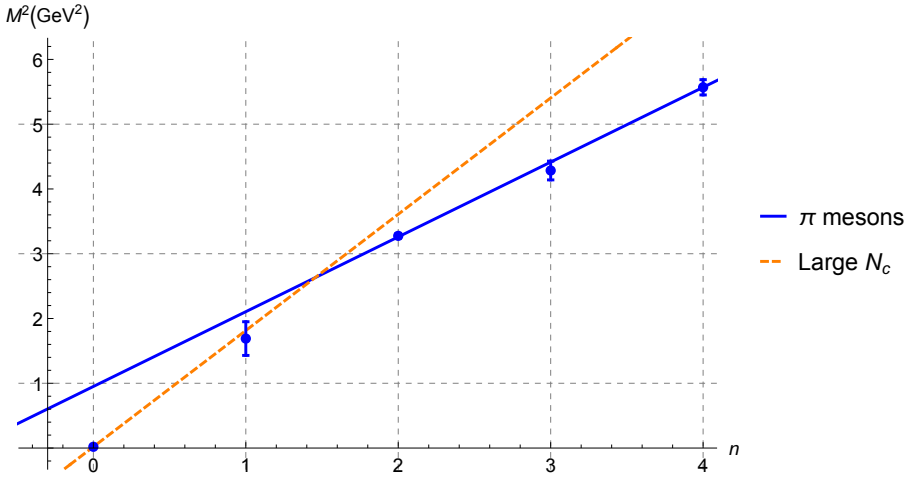

Figure 4.5: The radial Regge trajectory of the experimental π meson excitations (the ground state is excluded from the average) and the large N_c trajectory built on the data of Section 4.3.

ill-defined state. To compare the trajectories consider eq. (4.3) with $J = 0$ giving $1.38(4)n + 0.13(4)$ and our fit: $1.31(4)n + 1.02(2)$.

The trajectory of a_0 mesons consists of $a_0(980)$, $a_0(1450)$, $a_0(1950)$ states and follows the previous one closely, see Fig. 4.4. Notice, that we have omitted the $f_0(500)$ (σ) state because there is no counterpart for it in the isotriplet and as its pole position is poorly defined.

In the pseudoscalar sector of non-strange light mesons we have the π meson and its radial excitations. States $\pi(140)$, $\pi(1300)$, $\pi(1800)$, $\pi(2070)$ and $\pi(2360)$ are represented in Fig. 4.5. The pseudo-Goldstone nature of $\pi(140)$ makes the case quite different from the others. We did not include the ground state in the trajectory fit.

4.2.2 Decay constants

A very important quantity, the pion decay constant in the chiral limit, f_π, was defined in eq. (3.24):

$$\langle 0|\mathcal{O}_A^{a\mu}|\pi^b\rangle = ip^\mu f_\pi \delta^{ab}. \tag{4.21}$$

We could also introduce the decay constants similar to those of Eqs. (4.4) and

(4.5). The decay constants F_s and F_π appear in the one-point functions

$$\langle 0|\mathcal{O}_S^a(x)|a_0^b\rangle = \delta^{ab}F_s e^{-ipx}, \tag{4.22}$$

$$\langle 0|\mathcal{O}_P^a(x)|\pi^b\rangle = \delta^{ab}F_\pi e^{-ipx}. \tag{4.23}$$

The numerical information on the value of F_s could be found in the phenomenological studies, like those of Ref. [88]; they claim $F_s = 0.21 \pm 0.05$ GeV^2. F_π appears in various relations of the chiral perturbation theory, and in the chiral limit it can be related to the pion decay constant f_π and the quark condensate through the condition $f_\pi F_\pi = -\langle q\bar{q}\rangle$ [32, 89]. This condition appears in the chiral limit as a consequence of the equation that one gets considering the divergence of the axial vector current, $f_\pi m_\pi^2 = F_\pi(m_u + m_d)$, and the Gell-Mann–Oakes–Renner relation, $f_\pi^2 m_\pi^2 = -(m_u + m_d)\langle q\bar{q}\rangle$. The value of the chiral condensate could be estimated as $\langle q\bar{q}\rangle = -(235 \div 242 \text{ MeV})^3$[36, 37] and hence $F_\pi = 0.14 \div 0.15$ GeV^2.

4.3 Large-N_c lattice results for mesons

As an alternative to the experimental data we can turn to the meson spectroscopy on lattice at large N_c. From the discussion of previous chapter, we know that it should provide a valid input, especially in the context of the holographic part of our investigation. We follow the results of Ref. [90]. The quenched approximation is taken there and the predictions for $N_c = \infty$ are interpolated from those obtained at $N_c = 2, 3, 4, 5, 6, 7, 17$.

In Table 4.1 we present various results for the meson masses from Ref. [90]. They are given in terms of the dimensionless ratio $M/\sqrt{\sigma}$. The rough physical estimation with $\sqrt{\sigma} = 395$ MeV is also provided. The particular value of $\sqrt{\sigma}$ was advocated in Ref. [90] as making a better phenomenological fit than the ad hoc $\sqrt{\sigma} = 444$ MeV. The values of the pion and ρ decay constants are also estimated. $\hat{f}_\pi$ corresponds to our definition of f_π in eq. (3.24), while $\hat{F}_\rho = \sqrt{2}F_\rho/m_\rho$ with respect to eq. (4.4).

The resulting trajectories are marked in Figures 4.2, 4.4 and 4.5. We omitted the ρ meson case due to the unnaturally low value of the ground state mass. However, we can find a continuum limit result in Refs. [40, 91]

$$M_\rho = 1.79(5) \cdot \sqrt{\sigma}, \tag{4.24}$$

that is more in concordance with the physical mass of the ρ meson at usual $\sqrt{\sigma} \simeq 440$ MeV.

Particle	J^{PC}	M_{exp} (MeV)	$M_\infty/\sqrt{\sigma}$		M_∞ (MeV)	
			$m_q = 0$	$m_q = m_{ud}$	$m_q = 0$	$m_q = m_{ud}$
ρ	1^{--}	775.26	1.54	1.57	608	620
ρ'	1^{--}	1465	3.70	3.71	1462	1466
a_1	1^{++}	1230	2.86	2.88	1130	1138
a_1'	1^{++}	1655	4.59	4.61	1813	1821
π	0^{-+}	140	0	0.35	0	138
π'	0^{-+}	1300	3.39	3.41	1339	1347
a_0	0^{++}	980	2.40	2.43	948	960
a_0'	0^{++}	1474	4.36	4.38	1722	1730
$\hat{f}_\pi$	$-$	$92\sqrt{\frac{3}{N_c}}$	0.217	0.222	86	88
$\hat{F}_\rho$	$-$	$221\sqrt{\frac{3}{N_c}}$	0.572	0.576	226	228

Table 4.1: Large-N_c lattice estimation of light meson masses, pion and ρ decay constants. Last column is a rough dimensionful estimation for $\sqrt{\sigma} = 395$ MeV. The continuum limit has not been properly taken here, and one would expect a $5\ \%$ error associated to the values.

Overall, large-N_c lattice results seem rather close to the experimental ones, but the constructed radial trajectories show a significantly more rapid growth.

4.4 0^{++} glueballs

4.4.1 States on lattice

The masses of scalar glueballs on the lattice were widely studied in the quenched approximation. Here we present the results of several works devoted to the lattice simulations of $SU(3)$:

- Morningstar and Peardon [92] in 1999 have discovered a 0^{++} glueball with the mass of $1730(50)(80)$ MeV and its radial excitation 0^{++*}; together they form a linear radial Regge trajectory $m^2 = 4 \cdot (1017\text{ MeV})^2 \cdot (n + 0.72)$.
- Meyer in [93] has reported the ground state with the mass $1475(30)(65)$ MeV and three radial excitations that can be collected into the trajectory $m^2 = 4 \cdot (1094\text{ MeV})^2 \cdot (n + 0.46)$; at Fig. 4.6 it could be seen that the linear interpolation works well.

- Chen *et al.* in [94] have discussed the 0^{++} state of $1710(50)(80)$ MeV.

In Fig. 4.6 the full trajectories of Ref. [92] and Ref. [93] are in general accordance, while the ground state of Ref. [93] is ~ 250 MeV lower than both in Refs. [92] and [94]. It is noted in [95] that the possible source of a systematic difference in the results of Meyer with respect to the ones of Morningstar and Peardon and Chen *et al.* for the ground state is the usage by the former of the string tension σ instead of the hadronic scale parameter r_0 to determine the lattice spacing.

The unquenched approximation provides another interesting viewpoint. Though earlier it was supposed that glueball masses remain almost the same or get a $20-40\%$ suppression with respect to the quenched results, the authors of the more recent work on this subject, see Ref. [95], have reported on the ground state of $1795(60)$ MeV, that is greater than any aforementioned value. Together with the first excitation the unquenched method of Ref. [95] provides a trajectory $m^2 = 4 \cdot (1652 \text{ MeV})^2 \cdot (n + 0.30)$. There is a notable difference: the slope is much steeper than in the quenched approximation due to the 0^{++*} state of Ref. [95] being in the range of 0^{++***} of Ref. [93], as is clear from Fig. 4.6.

The studies of glueball masses in the large-N_c limit also present an interest to us. The results of Ref. [96] in terms of the string tension σ are: $\frac{m^2}{\sigma} = 4 \cdot 2.55^2 \cdot (n + 0.42)$ (an update of the widely cited result of [97]). In Ref. [93] the results for $SU(8)$ are claimed to be a valid approximation of $N_c \to \infty$ limit and are given by: $\frac{m^2}{\sigma} = 4 \cdot 1.67^2 \cdot (n + 0.99)$.

4.4.2 Candidate among f_0

The masses $m \simeq 1.5 - 1.7$ GeV are in the experimental reach. Moreover, there are known heavy 0^{++} states that do not fit into $q\bar{q}$ nonets. We refer to a hypothesis that $f_0(1370)$, $f_0(1500)$, $f_0(1710)$ states are a mixture of $\bar{u}u + \bar{d}d$, $\bar{s}s$ and glueball modes.

In one approach $f_0(1500)$ has the largest glueball component, while $f_0(1370)$ consists mostly of the up and down quarks and $f_0(1710)$ of the strange ones. In Ref. [98], that we take as an excellent typical example, there are two fits to existing data: Fit I gives $m_{gl} = 1464 \pm 47$ MeV, and Fit II – $m_{gl} = 1519 \pm 41$ MeV. The second way naturally proposes to exchange the roles of $f_0(1500)$ and $f_0(1710)$ and suggests that the latter has a predominant glueball component. In Ref. [99] the mass of the glueball is found to be $m_{gl} = 1674 \pm 14$ MeV .

However, a common viewpoint on the degree of the mixing, or on what state could be mostly glueballic, does not exist. For a variety of possibilities, in broader

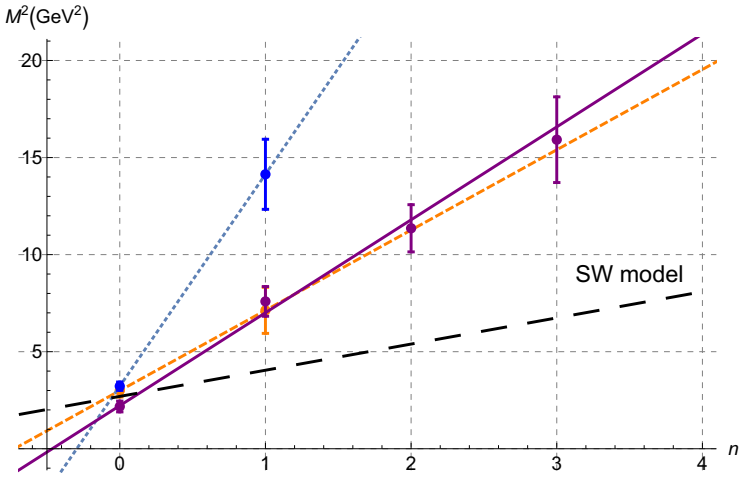

Figure 4.6: The radial Regge trajectories of lattice glueball states: orange – Morningstar and Peardon [92], purple – Meyer [93], blue – Gregory *et al.* [95]. Long dashes represent the SW trajectory going through the averaged 0^{++} state (see Section 5.4).

mass ranges as well, see, for instance, Ref. [100]. Taking the set of known f_0's, an attempt to separate those into the radial Regge trajectory of mesonic states and the one of glueballs from the point of view of rotated closed strings in the holographic background was made by the authors of Ref. [101]. Though various interesting fits to different glueball candidates are presented there, there is no final conclusion but that "an extension of experimental data on the spectrum of flavorless hadrons is needed" [101]. Here we do not try to cover all the options and will further stay in the limits of the two main hypotheses of the last paragraph.

Let us mention briefly the motivation on both sides. The first model is mostly supported by the fact that $f_0(1500)$ are not encountered in $\gamma\gamma$ reactions. In the same time the authors of Ref. [99] contradict that this fact does not necessarily imply a large glueball component there and advocate the $f_0(1710)$ option from the point of J/ψ decays. $f_0(1710)$ is also concluded to be a ground glueball state in some theoretical works (*e.g.* [102], [103]). From our point of view the option of $f_0(1500)$ appears as a favourite, because in this case the slope coefficient of the trajectory μ^2 is particularly close to the "universal" one previously highlighted in Section 4.1.1. The similarity is most acute for the Fit II of Ref. [98], which provides $\mu^2 \simeq 1.15$ GeV^2.

4.5 Summary

In this chapter we have discussed several issues related to the meson and glueball QCD spectra. The baryons are not reviewed because their holographic treatment lies beyond the scope of this thesis, and we provide no study of their phenomenology.

It is assumed that light non-strange mesons follow rather well the radial Regge trajectories. Though there are several complications, and a degree of uncertainty exist on the matter of prescribing certain states to certain trajectories. For the scalar f_0 mesons a persistent hypothesis is that some of them represent not the bound quark-antiquark states but the glueballs. The scalar glueball spectra is also well-studied on lattice and the Regge behaviour could be presumed based on the lattice data.

Moreover, the phenomenology of the discussed QCD states is not covered only by the spectra. We are also interested in the decay constants defined as the one-point functions of the interpolating operators corresponding to given meson states. In the vector sector we have considered the decay channels for ρ and a_1 mesons that are most contributing to their widths, as well as the electromagnetic pion and axial FFs.

Chapter 5

Bottom–up holographic models and their spectra

In this chapter we work on the dual description and physical interpretation of the fields immersed into the $5D$ framework that is commonly referred to as the bottom-up holography or AdS/QCD. We focus on building a $5D$ theory whose content makes it dual to QCD. However, in what follows the "QCD" label could be frequently understood in broader sense because the formalism can be easily generalized to the case of some other QCD-like strongly-interacting theory. A particular example of such application in the Composite Higgs models is given in Chapter 8.

5.1 General construction

Bottom-up holography is meant to be a phenomenological setup. We start with postulating the form of the $5D$ action:

$$S_{5D} = \int d^4x dz \sqrt{-g} p^2(z) \mathcal{L}, \tag{5.1}$$

where the metric is that of five-dimensional AdS given in Eq. (2.10) and $p(z)$ is the z-dependent profile intended to break the conformal invariance. The interval the fifth coordinate scopes is $z \in [\varepsilon, z_{max}]$, where we impose $\varepsilon = 0$ in the end of any calculation (unless the divergencies appear) and $z_{max} = \infty$ may be possible depending on the form of $p(z)$. We will describe several standard AdS/QCD frameworks: Hard Wall (HW), Soft Wall (SW) and Generalized Soft Wall (GSW). The matter content in $\mathcal{L}$ obeys the general rules set in Section 2.3.

To describe the QCD states one includes the cavity fields in the $5D$ bulk. Let us call a general $5D$ field with any set of quantum numbers as $\phi(x,z)$. Each such field is dual to some QCD operator $\mathcal{O}_j$ with a canonical dimension Δ_j at the $4D$ side. Instead of the CFT partition function of Eq. (2.24) the $5D$ action (5.1) taken properly to the boundary is dual to

$$\mathcal{Z}_{4D}[\phi_{\mathcal{O}}] = \int [\mathcal{D}\Psi][\mathcal{D}\overline{\Psi}] \,\mathrm{Exp}\, i \int d^4x [\mathcal{L}_{QCD}(x) + \sum_j \phi_{\mathcal{O}_j}(x)\mathcal{O}_j(x)], \quad (5.2)$$

where $\phi_{\mathcal{O}}$ are the sources of the corresponding operators.

Consider a standard Lagrangian containing the kinetic and the mass terms for an Abelian (for simplicity) vector field $A_M(x,z)$ and a scalar field $s(x,z)$

$$\begin{aligned}\mathcal{L}_v =& -\frac{1}{4g_5^2} g^{MP} g^{NQ} \left(\partial_M A_N - \partial_N A_M\right)\left(\partial_P A_Q - \partial_Q A_P\right) \\ &+ \frac{1}{2g_5^2} M_{5v}^2 g^{MN} A_M A_N, \quad (5.3)\\ \mathcal{L}_{sc} =& \frac{1}{2k_s}\left(g^{MN}\partial_M s \partial_N s - M_{5s}^2 s^2\right). \quad (5.4)\end{aligned}$$

Proper group indices and traces will be added when necessary. We introduce here the holographic parameters $[g_5^2] = [k_s] = E^{-1}$ in order to retain the standard dimensionalities of the fields. The bulk mass M^2 is canonically determined by the relation (2.34) from the AdS/CFT dictionary. For the scalar fields it gives $M_{5s}^2 R^2 = \Delta(\Delta-4)$ and for the vector ones $M_{5v}^2 R^2 = (\Delta-1)(\Delta-3)$.

We generally consider the two-flavour QCD and the following cases are covered in the QCD-related part of this thesis:

- The vector field A_M^a is dual to the conserved current of the chiral symmetry $\overline{\Psi}\gamma_\mu T^a \Psi$ with dimension 3. Such $5D$ vector field is massless $M_{5v}^2 R^2 = 0$. The standard holographic gauge choice is to impose $A_z = 0$. This represents the dual description of the light vector mesons ρ and ω (with $T^a \to \mathrm{Id}$).

- The vector field A_M^a is dual to the axial current $\overline{\Psi}\gamma_\mu\gamma_5 T^a \Psi$. The characteristics are identical to the previous case. a_1 meson is on the QCD side of duality.

- The scalar field s is dual to $G_{\mu\nu}G^{\mu\nu}$. That is the lowest-dimension ($\Delta = 4$) QCD operator with the quantum numbers 0^{++}, the ones of the scalar glueball. The dual $5D$ field should be massless $M_{5s}^2 R^2 = 0$.

- s^a is dual to the quark bilinear operator $\bar{\Psi}T^a\Psi$ with $\Delta = 3$. In this case we have $M_{5s}^2R^2 = -3$. The results should correspond to the f_0 and a_0 scalar mesons. Adding γ_5 to the operator we get the description of the pseudo-scalar QCD states (pions).

Vector mesons appear most frequently in the bottom-up description (see Ref. [86, 87, 104–106] and many others) due to their correspondence to the conserved currents. The scalar mesons appear, for instance, in Ref. [107, 108]. The bottom-up treatment of the glueballs was first realized in [109–112] and is still frequently discussed in the literature; it is worth to note some recent dynamical models such as Ref. [113, 114].

5.2 Bullk-to-boundary propagator and resonance description

Let us write the generalized equation of motion (EOM) for the Fourier transformation of the spin J field [1]:

$$\partial_z \frac{p^2(z)}{z^{3-2J}}\partial_z\phi(q,z) - \frac{M_5^2R^2}{z^{5-2J}}p^2(z)\phi(q,z) + \frac{p^2(z)}{z^{3-2J}}q^2\phi(q,z) = 0. \qquad (5.5)$$

In holography one gets from the EOMs information on two types of solutions [19, 116] (see also [117, 118]). Let us establish their interpretation within the AdS/QCD framework.

First, let us recall from Section 2.3 that the sources of the $4D$ operators appear as the boundary values of bulk fields. The correspondence also demands that the appropriate boundary conditions are imposed on the bulk field in order to correctly relate the bulk effective action to boundary correlation functions. Thus, the first type of solution is the bulk-to-boundary propagator $\widehat{\phi}$ that determines uniquely the evolution of the $5D$ field from its boundary value(=source) intowards the bulk: $\phi(x,z) = \widehat{\phi}(x,z)\phi_{\mathcal{O}}(x)$. It was originally constructed by Witten as a Green's function solution. To simplify the notation we further use the same symbol (no hat) for a $5D$ field and its propagator. In addition to the prescription on its UV ($z = \varepsilon$) asymptotics, this solution is restricted to be well-behaved in the interior of the bulk. The specific condition in the IR ($z = z_{max}$) depends on the type of AdS/QCD model. It allows to discard the irrelevant solution of eq. (5.5) and to

[1] We note that a general spin field ($J > 1$) may have a similar EOM. However, M_5^2 takes a wider meaning and turns out to be z dependent [115].

keep the correlation functions finite. The bulk-to-boundary propagator solutions are actively used in the calculations of Chapters 7 and 8; hence, we refer the reader there to find out more about their applications.

The other type we will call the Kaluza–Klein (KK) solution because it involves an effective reduction of the $5D$ field towards physically meaningful $4D$ modes and discretization with a new quantum number. However, the proper discussion of this solution requires a deeper look into the AdS/CFT correspondence and originally concerns the duality of the Hilbert spaces in two theories. Let us give it a brief theoretical overlook; Refs. [15, 17, 19, 116, 118] can provide additional details.

In Section 2.2 we discussed the Hilbert space construction in CFT with radial quantization. It could be seen that the AdS dual of radial quantization is the ordinary quantization in AdS global coordinates [15]. It is important that "ordinary quantization" is done in global coordinates that otherwise do not appear much in our applications. Their usefulness is related to the specific role of the time coordinate in the quantization process. Choosing the notion of time in accordance with the global time τ, one can also regard the dilatation operator D as the Hamiltonian for AdS physics.

The standard quantization requires a complete, normalizable set of field modes to decompose a general solution of the EOM. At the classical level:

$$\phi(\tau, x) = \sum_n \left(c_n \phi_n(\tau, x) + c_n^\dagger \phi_n^\dagger(\tau, x) \right). \tag{5.6}$$

Given some initial conditions, the series coefficients could be found with the use of the inner product defined on spacelike surfaces at fixed time (Cauchy surfaces Σ_τ). For the scalar fields in $d+1$ AdS it takes the form:

$$\langle \phi_1, \phi_2 \rangle = i \int_{\Sigma_\tau} d^{d+1}x \sqrt{-g} g^{\tau\tau} \left(\phi_1^\dagger \nabla_\tau \phi_2 - \phi_2 \nabla_\tau \phi_1^\dagger \right). \tag{5.7}$$

Free field in AdS becomes a quantum operator when the series coefficients c_n in front of the n-th classical harmonic modes are replaced with the annihilation and creation operators (up to the normalization constant). The satisfaction of canonical commutation relations could be checked with the use of the inner product of the normalizable modes $\langle \phi_n, \phi_m \rangle \sim \delta_{n,m}$.

In the example of Section 2.3 ($J = 0$ and $p(z) = 1$ in the notation of eq. (5.5)) the subleading mode $\phi_{s.l.} \sim z^\Delta$ turns out normalizable and can be considered as an element of the bulk Hilbert space, while the leading mode $\phi_{l.} \sim z^{d-\Delta}$ (bulk-to-boundary propagator) leads to the divergence in the inner product integral[2]. So, we

[2]In fact both modes are normalizable in the region $-\frac{d^2}{4} \leq M_5^2 R^2 \leq -\frac{d^2}{4} + 1$. The issue was

settle with the normalizable solution $\phi_{s.l.}$. The last step is to define on the boundary a new quantum operator $\mathcal{O}$ via compensating the near-boundary ε^{Δ} behaviour of the quantized $\phi_{s.l.}$. Due to the AdS isometries the resulting $\mathcal{O}$ represents a local CFT operator in the d-dimensional flat spacetime. Finally, we can return to what we have learned about the operator/state correspondence in Section 2.2. However, now it is more proper to speak of the one-to-one correspondence between AdS/CFT states in the Hilbert space and local operators acting at the boundary.

The roles of normalizable and non-normalizable modes in AdS spacetimes are excellently summarized in the study of Ref. [116]. Operator insertions in the boundary gauge theory provide non-trivial boundary conditions and originate the non-normalizable modes in the AdS. The normalizable modes fluctuate in the bulk; quanta occupying such modes have a dual description in the boundary Hilbert space.

In this chapter we are interested in studying the mass spectra of the states in various channels. One way to do that is to calculate the two-point correlation functions using the bulk-to-boundary propagators. The resulting expression $\langle \mathcal{O}(q)\mathcal{O}(-q)\rangle \sim \sum\limits_{n} \frac{a_n}{q^2-M^2(n)}$ contains the masses $M(n)$, $n = 0, 1, 2\ldots$, in its poles.

However, a more straightforward way is to solve eq. (5.5) as the eigenvalue problem that appears after imposing q^2 to take the discrete values $q^2 = M^2(n)$. The eigenfunctions $\phi_n(z)$ have the subleading asymptotics at small z. Hence, the $5D$ mode of the type

$$\phi(q,z) = \sum_{n=0}^{\infty} \phi_n(z)\phi^{(n)}(q) \tag{5.8}$$

represents the normalizable solution, and the free coefficients of this KK decomposition are the Fourier transformations of $\phi_{(n)}(x)$, the physical $4D$ degrees of freedom with proper quantum numbers. The sum in eq. (5.8) goes over the possible radial excitations n.

It is important to notice that due to the specifics of eq. (5.5) the discrete spectrum with a mass gap that is relevant for the description of the QCD-like theories becomes possible only for the AdS spaces that are cut off in the IR. Further we study several options to make this cut-off and discuss the differences they make in the particle spectra.

addressed to in Ref. [16], and we will give it no further consideration.

5.3 HW option

We begin with the Hard Wall model [86, 104] (its origins can be traced to the earlier work of Ref. [119]). This model is characterized by $p^2(z) = 1$ and an explicit IR cut-off of the z direction at some finite position z_{max}. The z-dependent part of the KK solution of Eqn. (5.5), $\phi_n(z)$, should be subject to the Dirichlet boundary condition in the UV, $\phi_n(0) = 0$, and the Neumann one on the IR cut-off, $\partial_z\phi_n(z_{max}) = 0$. The appropriate solution comes from the branch

$$\phi(q,z) \sim (qz)^{2-J} J_\alpha(qz), \quad \alpha = \sqrt{M_5^2 R^2 + (J-2)^2} \tag{5.9}$$

where J_α is a Bessel function of the first type. For the case of $M_5^2 R^2 = 0$ the recurrence relation for Bessel functions can be used, $\partial_z(z^\alpha J_\alpha) = z^\alpha J_{\alpha-1}$. The IR condition then could be formulated as $J_{\alpha-1}(M(n)z_{max}) = 0$. The first zeros of J_0 and J_1 fix the ground state masses:

$$m_{HW}^{J=1} = M_{J=1}(0) = \frac{2.405}{z_{max}}, \tag{5.10}$$

$$m_{HW}^{J=0,\Delta=4} = M_{J=0,\Delta=4}(0) = \frac{3.832}{z_{max}}. \tag{5.11}$$

For the scalar mesons the Neumann condition is given by the following equation ($\hat{z}_{max} = M(n)z_{max}$):

$$J_1(\hat{z}_{max}) + \hat{z}_{max} J_0(\hat{z}_{max}) = 0,$$

the first zero on the left hand side gives

$$m_{HW}^{J=0,\Delta=3} = M_{J=0,\Delta=3}(0) = \frac{2.735}{z_{max}}. \tag{5.12}$$

Further radial excitations in the spectra are determined by the position of the next zeros that can be seen at Fig. 5.1. It is interesting that the holographic spectra of scalar and vector mesons are rather degenerate: starting from $n = 2 \div 3$ the blue and green dots at Fig. 5.1 coincide. That is interesting from the point of view of universality, but does not seem to be congruent with the mass prescriptions of the previous chapter.

There is no Regge-like spectrum (4.1) in the HW model. In the vector meson case the HW spectrum goes as $M(0)\{1; 2.3; 3.6; ...\}$ featuring much faster growth than, for example, the actual ρ spectrum $M(\rho)\{1; 1.9; 2.0; ...\}$. For the scalar mesons we should compare the HW radial spectrum $M(0)\{1; 2.1; 3.2; ...\}$ with the f_0 spectrum $M(f_0)\{1; 1.4; 2.0; ...\}$, and they are inconsistent with each other as well.

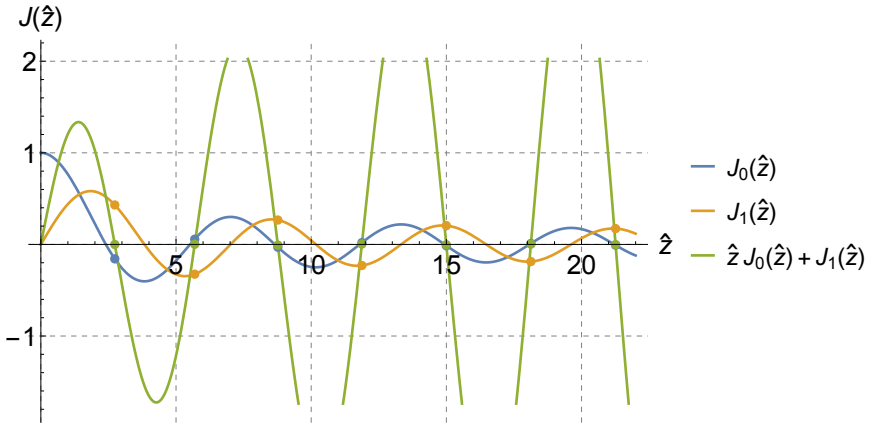

Figure 5.1: The Bessel functions, the zeros of which determine the mass spectra in the HW model. The plot is given in terms of dimensionless $\hat{z} = qz$. Blue line is relevant to the case of vector mesons, orange – scalar glueballs, and green – scalar mesons.

5.4 (G)SW option

The Soft Wall model [105] is of great interest to anyone perceiving uniformality in radial spectra as its main achievement is the reproduction of the linear radial Regge trajectories for mesons. This is an observed phenomenon discussed in Section 4.1.1. Also it naturally provides the linear trajectories for the scalar glueball and its radial excitation, the feature that may be hypothesized from some results on lattice (see Section 4.4.1).

The traditional SW model is characterized by an infinite IR cut-off, $z_{max} = \infty$, and the conformality is broken by the introduction of the dilaton profile $p^2(z) = e^{-\Phi(z)}$. In the simplest setups $\Phi(z) = \kappa^2 z^2$. On the UV brane the Dirichlet condition is imposed and good convergence is required in the IR (to be suppressed by the dilaton exponent). The normalizable discrete modes of Eqn. (5.5) are

$$\phi_n(z) = \mathcal{N}_n(\kappa z)^{2-J+\alpha} L_n^\alpha(\kappa^2 z^2), \quad \alpha = \sqrt{M_5^2 R^2 + (J-2)^2} \tag{5.13}$$

where L_n^m are the generalized Laguerre polynomials, and $\mathcal{N}_n$ are the normalization factors of little importance to us now. For the discrete parameter $n = 0, 1, 2, ...$ we obtain the SW spectra,

$$M_J^2(n) = 4\kappa^2 \left(n + 1 + \frac{\alpha - J}{2} \right). \tag{5.14}$$

We remind the reader that there are following cases: vector mesons $J = 1, \alpha = 1$; scalar mesons $J = 0, \alpha = 1$; scalar glueballs $J = 0, \alpha = 2$.

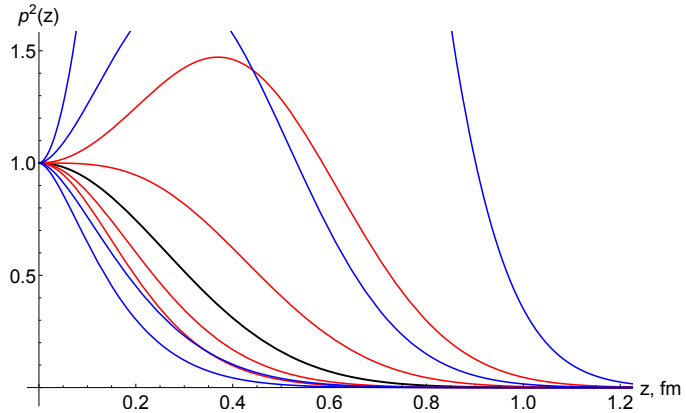

Figure 5.2: The normalized profile function $p^2(z)$ in the GSW model. The SW option ($b = 0$) is given in black, the blue profiles – $J = 1$ case, red – $J = 0$. We fix $\kappa = 534$ MeV and take several values of b: $b < 0$ results in a profile higher than the SW one, $b > 0$ – in a lower one.

A natural generalization toward a meson or glueball spectrum with an arbitrary intercept parameter b,

$$M_J^2(n) = 4\kappa^2 \left(n + 1 + b + \frac{\alpha - J}{2} \right), \tag{5.15}$$

may be achieved using the Generalized Soft Wall profile proposed in [120] (see also [121]):

$$p^2(z) = e^{-\kappa^2 z^2} U^2(b, J-1; \kappa^2 z^2). \tag{5.16}$$

The modification consists in the Tricomi hypergeometric function U that provides the necessary free parameter b to the spectrum but does not change the SW asymptotes in UV and IR. That is due to $U(b, J-1; \kappa^2 z^2) \xrightarrow{z\to 0}$ const and $U(b, J-1; \kappa^2 z^2) \xrightarrow{z\to\infty} (\kappa^2 z^2)^{-b}$. As $U(0, J-1; x) = 1$, GSW with $b = 0$ reduces to the usual SW. We note that in Eqn. (5.16) there is no dependence on $M_5^2 R^2$ but for different J we get different dilaton functions. We depict $p^2(z)$ for several values of b under condition $|b| \leq 1$ in Fig. 5.2.

Several SW trajectories were presented in Fig. 4.1 and 4.4. The value of κ^2 there is fixed so that to reproduce the ground state mass. It is evident in both cases that the SW trajectory disagrees greatly with the real ones. That means that the introduction of the GSW parameter b is necessary to describe correctly the whole towers of radial excitations. However, there is an interesting feature noted in Ref. [108]. If we assume the slope parameter (κ) to be the same in ρ and f_0 holographic spectra and then construct the ratios of the squared masses of the ground

states and of the first excitations, we get $R = \frac{m_f^2}{m_\rho^2} = 3/2$ and $R' = 5/4$, respectively. The experimental quantities $R_{exp} \approx 1.6,\ R'_{exp} \approx 1.1$[3] turn out to be well-satisfied.

5.5 Isospectrality

It was recently noticed in [122] that the SW background is not fixed by the form of the linear spectrum because one can find an infinite number of one-dimensional potentials leading to the identical spectrum of the normalized modes. The corresponding family of potentials is referred to as isospectral potentials.

Further we show how the modification of the GSW dilaton profile is in accordance with the choice of a particular member of the isospectral family. For that we adopt the method of [122] to the $5D$ fields subject to the EOM (5.5).

First, we should rewrite the EOM (5.5) in a Schrödinger form. It is straightforward under a certain change of variables responsible for the appearance of the KK z-profiles $\psi_n(z)$:

$$\phi(q,z) = p^{-1}(z) z^{(3-2J)/2} \psi(q,z), \tag{5.17}$$

$$-\psi_n''(z) + \widehat{\mathcal{V}}_J(z)\psi_n(z) = M^2(n)\psi_n(z). \tag{5.18}$$

Here $\widehat{\mathcal{V}}_J(z)$ is the Schrödinger potential for a model with some dilaton function $p^2(z)$ describing the spin J states. It is specified as

$$\widehat{\mathcal{V}}_J(z) = \frac{(3-2J)(5-2J) + 4M_5^2 R^2}{4z^2} + \frac{p''(z)}{p(z)} - \frac{3-2J}{z}\frac{p'(z)}{p(z)}. \tag{5.19}$$

We introduce an analogous quantity without the hat for the dilaton profile of the GSW model

$$\mathcal{V}_J(z) = \frac{(3-2J)(5-2J) + 4M_5^2 R^2}{4z^2} + \kappa^4 z^2 + 2\kappa^2(1-J+2b). \tag{5.20}$$

Its eigenvalues are those of a $2D$ harmonic oscillator system and result in the spectrum of Eqn. (5.15).

According to [122] and the references therein, the following isospectral transformation between $\mathcal{V}_J(z)$ and $\widehat{\mathcal{V}}_J(z)$ exists:

$$\widehat{\mathcal{V}}_J(z) = \mathcal{V}_J(z) - 2\frac{d^2}{dz^2}\ln[I_J(z) + \lambda]. \tag{5.21}$$

[3] R'_{exp} is given for the f_0' excitation heavier (~ 1.5 GeV) than the ρ' state.

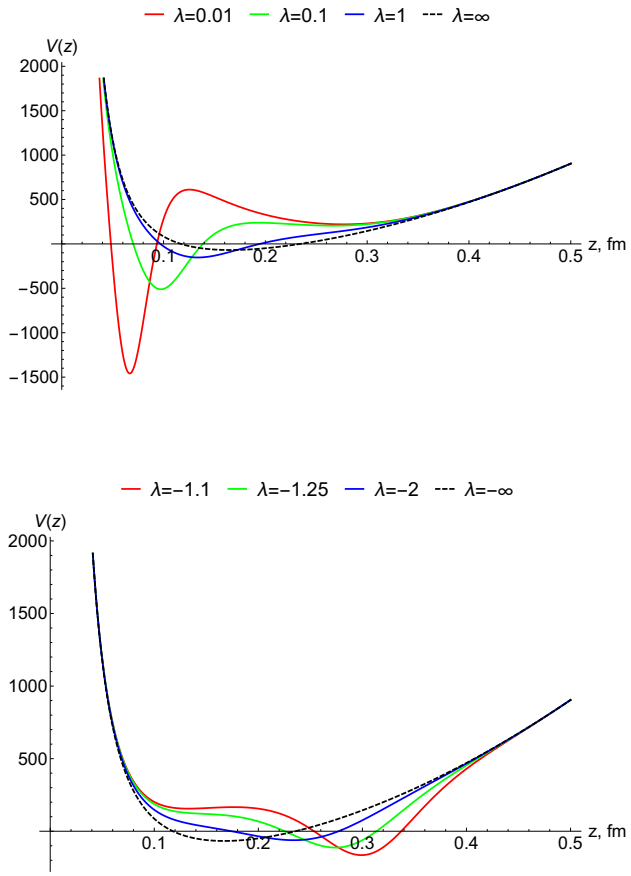

Figure 5.3: The dependence of the potential $\widehat{\mathcal{V}}_J(z)$ on the isospectral parameter λ. The particular GSW case is depicted: $J = 0,\ \kappa = 1652$ MeV, $b = -1.71$ (from the relevant glueball phenomenology). However, the main features are the same for other generations of $\widehat{\mathcal{V}}_J$.

This technique allows us to generate a family of dilaton functions $p(z)$ appearing in $\widehat{\mathcal{V}}_J(z)$, each member assigned to the value of the parameter λ. In general, the parameter can scope two unconnected regions $0 < \lambda < \infty$ and $-\infty < \lambda < -1$. The cases of $\lambda = \pm\infty$ correspond to the original $\mathcal{V}_J(z)$. The function $I_J(z)$ is defined through the ground eigenstate of $\mathcal{V}_J$, ψ_0, and is given by

$$I_J(z) \equiv \int_0^z \psi_0^2(z')dz' = 1 - \frac{\Gamma(\alpha+1, \kappa^2 z^2)}{\Gamma(\alpha+1)}. \tag{5.22}$$

Different λ provide slightly different forms of the potential (see Fig. 5.3), but the eigenvalues of Eqn. (5.18) and, hence, the spectrum remains the same. This ap-

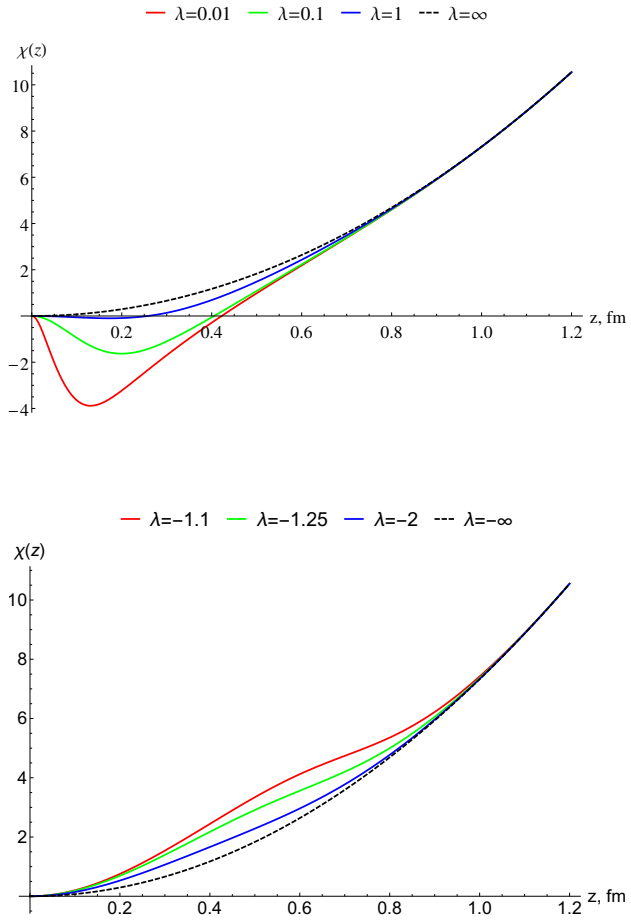

Figure 5.4: The interpolating function $\chi(\lambda, z)$ showing the isospectral variations of the dilaton. The case of SW with $J = 1,\ \kappa = 534$ MeV is depicted.

proach is well-known in the context of the supersymmetric quantum mechanics [123]. It realizes the following feature of one-dimensional potentials. The discrete spectrum of the normalized modes does not fix the potential uniquely, and there is an infinite family of isospectral potentials connected via relation of the type of Eq. (5.21). In this construction the parameter λ has no direct physical meaning and just reflects this special "symmetry" in the "space" of one-dimensional potentials.

We restrict the model to the deviations in the exponential factor only, *i.e.*, the isospectral profiles of a type

$$p^2(z) = \exp(-\chi(z))U^2(b, J-1; \kappa^2 z^2), \tag{5.23}$$

with the asymptotes fixed to $\chi(z \to 0) = \chi(z \to \infty) = \kappa^2 z^2$. Introducing an

argument $y = \kappa^2 z^2$ we may define the family of λ-dependent equations as follows

$$\frac{yp''(y) + (J-1)p'(y)}{p(y)} - b = \frac{y + 2(1-J)}{4} - \left(\frac{d}{dy} + 2y\frac{d^2}{dy^2}\right) \ln\left(I_J(y) + \lambda\right). \tag{5.24}$$

For a given set of b, J and λ the interpolating function $\chi(z)$ can be numerically calculated from this equation. A particular example is presented in Fig. 5.4. We will find an interesting use for this modulation of the (G)SW dilaton in the next chapter.

5.6 Summary

In this chapter we put forward the bottom-up realization of the QCD resonances in the $5D$ bulk. The confining property of QCD is introduced in the action with the z-dependent "wall", $p(z)$. We discuss several choices for this profile.

A five-dimensional field is dual to a specific interpolating operator at the $4D$ side. The bulk mass of the field is defined in accordance with the quantum numbers of this operator. The simplest bulk Lagrangian of non-interacting fields is invariant with respect to the AdS metric and contains just the kinetic and the mass terms. For each type of field we can extract the EOM from the $5D$ action. Imposing certain boundary conditions we determine the KK profiles and the spectrum of the resonance excitations. The outcome is highly model dependent. We favour the SW-like models because they predict the Regge-like radial spectra, *i.e.* show a proper realization of confinement.

We also noticed an interesting idea that could be applied in the SW-like holographic models. That is the introduction of the isospectral family of the dilaton profiles, all of which turn out to provide the common spectrum of states.

Chapter 6

Deconfinement in holography

6.1 Motivation

We would like to address the issue of deconfinement, the modern rendition of which was given in Section 3.5, within the five-dimensional AdS/QCD holographic framework. This approach proposes a connection between the deconfinement in a non-Abelian gauge theory and the Hawking–Page (HP) phase transition in the corresponding dual gravitational theory. The latter is characterized by a value of the critical temperature T_c interpreted as the temperature of transition from the confined to the deconfined phase of the quark-gluon matter.

The most general $5D$ model should describe many features of QCD: thermodynamical properties, confinement, chiral symmetry breaking, phenomenological spectra for all kind of resonances, *etc.* There is no unified way to describe them all in the conventional $4D$ QCD and in the $5D$ AdS/QCD neither, to the best of our knowledge.

However, our goal is to provide a self-consistent (both theoretically and phenomenologically) holographic estimation for the deconfinement temperature T_c with as few free parameters of the $5D$ model as possible. For that we find it practical and in the bottom-up spirit to make connections between different phenomena. Specifically, we will try to derive T_c from the holographic model the parameters of which are fixed to reproduce some particle spectra. Three major options for the matter content are investigated: the traditional consideration of the ρ and ω vector mesons; that of the scalar mesons, f_0 and a_0; the scalar glueballs. To guide us further we put forward several considerations.

The success of AdS/QCD is based on the consistent reproduction of the phenomenological hadron spectrum from the $5D$ model, see the discussion of the pre-

vious chapter. That should be understood in a rather generalized sense, as an effort to capture the qualitative features of the spectrum. By this we refer to the linear behavior of the radial Regge trajectories, and an obvious consequence is that we favour the SW-like models to the HW ones.

From the side of the theory, the first and major issue concerns the large-N_c limit naturally appearing at the $4D$ side of AdS/QCD models. It means that the QCD phase diagram we hope to get represents a study in pure gluodynamics. In this limit the glueballs dominate over the usual mesons and baryons, and the gluodynamics must dictate the overall mass scale and thereby the major contribution to the deconfinement temperature T_c. The dual $5D$ holographic description should be modelling the ground state gluodynamics and the glueball excitations. That brings particular attention to the AdS/QCD description of the glueballs and its relation to the thermodynamic properties. From another point of view, it signifies that the usage of the universal meson trajectories of Section 4.1.1 is justified. It was showed in Ref. [68] that the value $\mu^2 = 1.14 \pm 0.01$ GeV^2 leads to a consistent numerical estimation of the deconfinement temperature in the SW model. It is remarkable that a similar slope can be achieved considering the scalar resonance $f_0(1500)$ as the lightest glueball.

The second issue is connected to the isospectrality concept introduced in Section 5.5. We will demonstrate that in some cases different predictions for T_c may be obtained within one isospectral family. This fact provokes a doubt about the rigorous determination of T_c in terms of the spectra parameters. The criterion that the predicted values of T_c should be stable with respect to the isospectral modifications seems reasonable.

The numerical values of the deconfinement temperature T_c should be interpreted in comparison to the known lattice and experiment expectations, see Section 3.5. The lattice estimations in the quenched and large-N_c limit seem to be the most relatable to the holographic predictions. Also, it should be taken into account that the HP phase transition is of the first order. Thus, we would expect the values in a range $T_c \sim 250 - 270$ MeV. Nevertheless, it is often a practice to compare AdS/QCD predictions with the "real QCD" results of $150 - 170$ MeV. The "pro" arguments here are that the strict $N_c = \infty$ limit is almost always softened to achieve real phenomenology, that there is a relatively good description of hadron resonances in AdS/QCD, and that the final value of the critical parameter turns to be satisfactorily close to the pseudo-critical lattice one (in some numerical fits).

6.2 Hawking–Page phase transition

Let us introduce a universal gravitational term into the $5D$ holographic action:

$$S_{5D} = \int d^4xdz\sqrt{-g}p^2(z)\left(\mathcal{L}_{gravity}+\mathcal{L}_{matter}\right) \tag{6.1}$$

$$\mathcal{L}_{gravity} = -\frac{1}{2k_g}\left(\mathcal{R}-2\Lambda\right) \tag{6.2}$$

Here we keep the notations of Section 5.1, in addition, k_g is the coefficient proportional to the $5D$ Newton constant, $\mathcal{R}$ is the Ricci scalar and Λ is the cosmological constant. The matter part could be included following the lines of the previous chapter.

The assessment of the critical temperature is related to the leading contribution in the large-N_c counting. That is we focus on the $\mathcal{L}_{gravity}$ part scaling as $\frac{1}{2k_g}\sim N_c^2$ while the cavity modes in $\mathcal{L}_{matter}$, scaling as N_c, play a subleading role and can be neglected in the course of this section.

Witten used the three dimensional study of the black holes in AdS by Hawking and Page to make the connection between the HP phase transition in a higher dimensional gravity theory and the confinement phenomenon on the dual gauge side [124]. However, he worked in the framework of the AdS/CFT correspondence and was interested in the thermodynamics of the conformal $\mathcal{N}=4$ SYM. He argued that the confinement can only be achieved for a thermal SYM theory in the space with compact boundaries $S^3\times S^1$. Extending the radius of S^3 to infinity, thus approximating to R^3, results in a theory permanently at the high temperature side of the phase transition, *i.e.* deconfined.

Nevertheless, Herzog argued that the $5D$ AdS/QCD description provides both phases for the large-N_c QCD on the gauge side of the correspondence [125] and gave a recipe for the calculation of the critical temperature T_c. Moreover, in the study of Ref. [126] it is shown that the confinement criterion, proposed by Witten [124], is fulfilled in HW and SW models. The criterion concerns the estimation of the N_c scaling of the thermodynamic quantities: for a gauge theory in the large-N_c limit in the confined phase the present degrees of freedom give an order one contribution to the entropy density, in the deconfined – contribution is of order N_c^2.

We should mention that it is often a practice to use another type of criterion reflecting the confining force between quark and anti-quark in a more tangible fashion. That is, to define as confining the phase for which the Wilson loop expectation value satisfies the area law while for the Polyakov loop it vanishes (see Section 3.4). In holography the study of these loops can be performed because

the AdS/CFT correspondence provides an access to the free energy of the $q\bar{q}$ pair through the on-shell action of a fundamental string in the dual gravity background.

It is known that simplest HW and SW holographic models fail from this perspective – for the latter the perimeter law is non-confining due to the conformal background geometry (exact AdS_5), while in the former both the electric and the magnetic charges are confined [127]. However, many endeavors are made to modify the SW model so that it could be attested as confining following this criterion. First, in Ref. [128, 129] the dilaton (inversed) was embedded into the metric; then, with the evolution of the dynamical dilaton wall models, two problems are solved simultaneously: the background is non-conformal and it is a solution of the Einstein equations. There are many successes on this way: the description of the qualitatively different phase diagrams for the heavy [130] and the light mesons [131] just varying the ansatz within the same approach, or the anisotropic modifications [132] resulting in additional valuable specifics, such as the power of the energy dependence of the total multiplicity and the orientation of a quark-antiquark pair affecting the position of the critical points. We, however, devote our present analysis to the interplay between the more basic theoretical concepts in holography and the hadron phenomenology and leave the addition of the $q\bar{q}$ pair thermodynamics to future work.

We follow the approach laid in Ref. [124], [125] and [126]. There, the order parameter of the HP phase transition is the difference between free energy densities V's evaluated on different backgrounds corresponding to the two phases. We have encountered these metrics before, in Chapter 2.

First, the confined phase. It is given by the thermal AdS of radius R and defined by the general AdS line element in the Euclidean signature

$$ds^2_{Th} = \frac{R^2}{z^2}\left(dt_E^2 + d\vec{x}^2 + dz^2\right), \tag{6.3}$$

with the time direction restrained to the interval $[0, \beta]$. The metric of the Schwarzschild black hole in AdS describes the deconfined phase and is given by

$$ds^2_{BH} = \frac{R^2}{z^2}\left(h(z)dt_E^2 + d\vec{x}^2 + \frac{dz^2}{h(z)}\right), \tag{6.4}$$

where $h(z) = 1 - (z/z_h)^4$ and z_h denotes the horizon of the black hole. The corresponding Hawking temperature is related to the horizon as

$$T = \frac{1}{\pi z_h}. \tag{6.5}$$

The cosmological constant in $5D$ AdS is $\Lambda = -6/R^2$ and both these metrics are the solutions of the Einstein equations. They provide the same value of the Ricci scalar $\mathcal{R} = -20/R^2$. Hence, the free energy densities differ only in the integration limits,

$$V_{\text{Th}}(\epsilon) = \frac{4R^3}{k_g}\int_0^{\beta} dt \int_{\epsilon}^{z_{max}} dz p^2(z) z^{-5}, \tag{6.6}$$

$$V_{\text{BH}}(\epsilon) = \frac{4R^3}{k_g}\int_0^{\pi z_h} dt \int_{\epsilon}^{\min(z_{max}, z_h)} dz p^2(z) z^{-5}. \tag{6.7}$$

At the hypersurface of $z = \epsilon$ the two geometries have the same asymptotic but the local adjustment of the generally arbitrary periodicity β is needed: $\beta = \pi z_h \sqrt{h(\epsilon)}$. Then, the order parameter for the phase transition is constructed as follows,

$$\Delta V = \lim_{\epsilon \to 0} \left(V_{\text{BH}}(\epsilon) - V_{\text{Th}}(\epsilon) \right). \tag{6.8}$$

The thermal AdS is stable when $\Delta V > 0$; otherwise, the black hole is stable. The condition $\Delta V = 0$ defines the critical temperature T_c at which the transition between the two phases happens. Eq. (6.8) yields z_h as a function of the model-dependent parameters – z_{max} and/or those possibly introduced in $p(z)$.

It is interesting that in some works (*e.g.* [133],[130]) on dynamical bottom-up holographic models with finite chemical potential another stable geometry is found – a smaller size black hole. There the confinement/deconfinement transition is suggested to be associated to the small/large black hole phase transition on the gravity side. It is argued in [134], however, that the appearance of a smaller black hole could be a matter of the choice of ansatz, and even when it is present that the conventional loop criteria of confinement are not strictly satisfied. In the probe limit we work in this additional background does not exist.

6.3 T_c in different AdS/QCD models

We made a central decision assuming that $\mathcal{L}_{matter}$ and $\mathcal{L}_{gravity}$ should be introduced with the same holographic ansatz $p^2(z)$ in eq. (6.1). As a consequence T_c as expressed in terms of the model parameters becomes connected to a particular hadron description. One can use the simplest approach: to fix the model parameters so that the $\rho(770)$ mass is exactly experimental. That is the case with Ref. [125]. At first glance there seems to be no particular reason why $\rho(770)$ or the vector meson spectra in general should be used as an input to determine the deconfinement temperature. In our opinion, this is a necessary step, that is done in order

to give physical meaning to the model parameters appearing in the pure gravity action. However, to broaden the discussion we will include more options to fix the parameters introducing light scalar mesons and glueballs into consideration. In this section we only provide T_c as found in the models of Chapter 5.

Let us first consider the order parameter of the HP phase transition in the HW model. Solving eq. (6.8) with $p(z) = 1$ and finite z_{max} we obtain

$$\Delta V_{HW} = 0 \;\Leftrightarrow\; z_{max}^4 = 2z_h^4, \tag{6.9}$$

as has been found in Ref. [125] too. Then, the deconfinement temperature determined as the Hawking temperature at the horizon (eq. (6.5)) is given by

$$T_{HW}^{J=1} = \frac{2^{1/4}}{\pi z_{max}} = \frac{2^{1/4} m_{HW}^{J=1}}{2.405\pi} = 0.1574\, m_{HW}^{J=1}, \tag{6.10}$$

$$T_{HW}^{J=0,\Delta=4} = \frac{2^{1/4}}{\pi z_{max}} = \frac{2^{1/4} m_{HW}^{J=0,\Delta=4}}{3.832\pi} = 0.0988\, m_{HW}^{J=0,\Delta=4}, \tag{6.11}$$

$$T_{HW}^{J=0,\Delta=3} = \frac{2^{1/4}}{\pi z_{max}} = \frac{2^{1/4} m_{HW}^{J=0,\Delta=3}}{2.735\pi} = 0.1384\, m_{HW}^{J=0,\Delta=3}, \tag{6.12}$$

where we used the connections (5.10)–(5.12) between z_{max} and the ground state masses in different channels. Evidently, we do not get a universal estimation of T_c in HW models.

The estimation of ΔV from eq. (6.8) in case of GSW model is similar to the one performed in Ref. [68] and results in

$$\Delta V_{GSW} = \frac{\pi R^3}{2k_g z_h^3}\left(U^2(b, J-1; 0) - 4(\kappa z_h)^4 \int\limits_{\kappa^2 z_h^2}^{\infty} dt e^{-t} t^{-3} U^2(b, J-1; t)\right). \tag{6.13}$$

Numerically, one can find the value of z_h, as a function of κ (and b), that solves the equation $\Delta V_{(G)SW} = 0$. The result will also depend on J. With $b = 0$ we reproduce the expression of the deconfinement temperature in the SW model, it could be approximated by

$$T_{SW} \simeq 0.4917 \cdot \kappa. \tag{6.14}$$

In the GSW case the following numerical approximations are valid for the values of b corresponding to phenomenological spectra (to be discussed further):

$$T_{GSW}^{J=1}/\kappa \simeq 0.670 \cdot b + 0.496, \quad T_{GSW}^{J=0}/\kappa \simeq 0.123 \cdot b + 0.314. \tag{6.15}$$

See them depicted in Fig. 6.1.

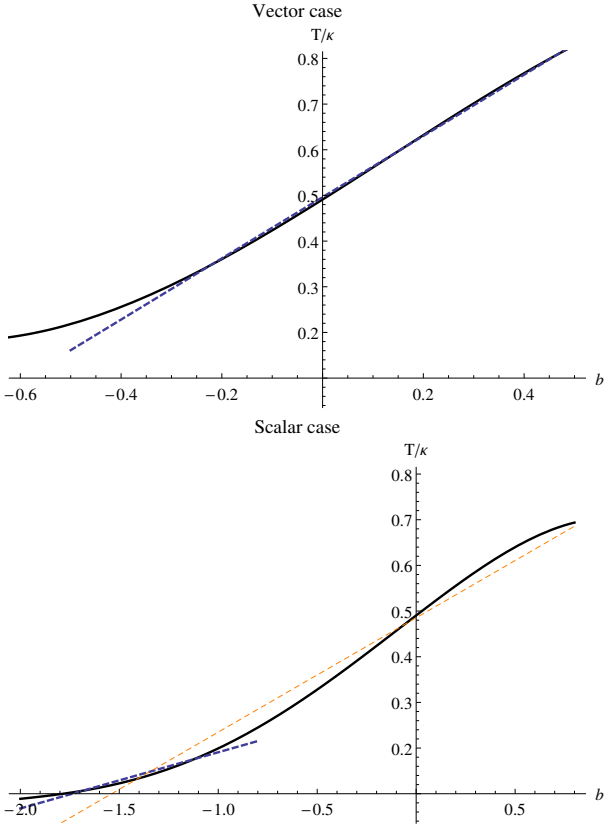

Figure 6.1: The deconfinement temperature in GSW model as a function of the intercept parameter b. The blue dashed lines are the linear interpolation functions given in eq. (6.15).

As was concluded in Section 5.5 the exponent argument in the GSW dilaton profile (5.16) can develop a dependence on a new parameter λ, specifying the member of the isospectral dilaton family. This interpolating function $\chi(z)$, found numerically for a given set of b, J and λ from eq. (5.24), should be substituted inside $p^2(z)$ when writing down eq. (6.8) in the case of GSW:

$$\Delta V_{GSW} = \frac{\pi R^3}{k_g z_h} \left[\frac{U^2(b,J-1,0)}{2} - p^2_{b,J,\lambda}(\kappa^2 z_h^2) - \kappa^2 z_h^2 \, p^2_{b,J,\lambda}(y)' \Big|_{y=\kappa^2 z_h^2} - (\kappa z_h)^4 \int_{\kappa^2 z_h^2}^{\infty} dy p^2_{b,J,\lambda}(y)'' y^{-1} \right]. \tag{6.16}$$

Equating this expression to zero leads to a λ-dependent prediction for T_{GSW}. We propose to investigate how the values of the critical temperature vary with this isospectral family parameter. Are these deviations of a large scale, or does isospec-

Hol. model	T_c (MeV)		
	ρ meson	ω meson	"universal" slope
HW	122.03 ± 0.04	123.19 ± 0.02	168.1 ± 0.7
SW	190.61 ± 0.06	192.43 ± 0.03	262.5 ± 1.2

Table 6.1: Vector meson predictions for the deconfinement temperature in HW and SW models with $\rho(770)$, $\omega(782)$ masses and the universal slope of Ref. [70].

trality preserve isothermality in general? If not, could we choose a correct family member with a 'physical' value of λ? May be there are some specific fits to (G)SW that provide more stable results than the others.

6.4 Meson fits

A general disclaimer for this and the next sections is that we consider all numerical results at the level of an estimation. The appearing error bars are only due to the uncertainty of the experimental or lattice determination of the input parameters. The holographic apparatus can only claim numerical validity on the semi-quantitative level and we cannot wholly estimate the theoretical error. Though for the well-known masses of the vector mesons the experimental error is definitely small and not comparable with the theoretical one, the lattice results are not that precise, and we find it useful to provide the minimal possible error that could be present.

Let us start with the classical AdS/QCD fits where the model is tuned to reproduce the masses of the lightest 1^{--} states. The resulting T_c is given in Table 6.1 and similar calculations can be found in Refs.[68, 125]. Another option is presented in the last column of Table 6.1. As argued in Ref. [68] we find the SW fit with "universal" slope $\mu^2 = 4\kappa^2 = 1.14$ GeV^2 [70] to be the most successful as it provides a unique $T_c \simeq 260$ MeV. This result being in range of lattice predictions with non-dynamical quarks allows us to claim that the fit defined from a gluodynamic insight provides the deconfinement temperature expected from the gluodynamics. We will also see that this fit corresponds to selecting $f_0(1500)$ meson as the lightest scalar glueball state.

The results for fuller trajectories are presented in Table 6.2. The weighted fits for ρ and ω including $n = 0$ rely on the non-standard position of the lightest state. They are close to the estimations in Table 6.1 and do not come close to any lattice prediction. The exclusion of $\rho(770)$ does not bring particularly satisfying results

Fit	T_{GSW} (MeV)	
	with Δm from PDG	equal weights
$\rho:\ n=0,1,2$	118 ± 3	143
$\omega:\ n=0,1,2$	121 ± 4	149
$\rho:\ n=0,1,2,3,4$	120 ± 2	163
$\rho:\ n=1,2,3,4$	303 ± 47	266
$a_1:\ n=0,1,2$	352 ± 55	294
universal [81]	~ 125	
universal [71], $J=1$	251 ± 11	

Table 6.2: Various vector meson predictions for T_c in GSW model.

either: the temperature becomes rather large. Additionally, the error bars in the T_c estimation for $\rho : n = 1, 2, 3, 4$ trajectory are much larger: though the fit in Fig. 4.1 looks well, the lack of well-established states is obvious. The equal weights fits are presented in the third column of Table 6.2 and surprisingly make better predictions proposing a balance of the including versus excluding $\rho(770)$ strategies. When the ground state is taken into account, but the trajectory is not rigorously fixed by its small experimental error, T_c tends to the physical values. When it is excluded the trajectory is almost SW-like: $4(500\ \text{MeV}^2)(n + 1.1)$; and T_c is close to the quenched large-N_c lattice results. We notice as well from Table 6.2 that the axial vector mesons serve poorly for the determination of T_c.

The trajectories with both universal slope and intercept are also quite remarkable. The prediction from the fit of Ref. [71] follows the success of the previously mentioned universal trajectory of Table 6.1. The one of [81] provides the T_c quite similar to those of ρ and ω fits with the ground state.

Now let us consider the families of isospectral dilatons and their impact on the value of T_c, that is provided in Table 6.3. The error bars in Table 6.3 are solely provided by the uncertainties in the trajectories. It is clear that for the vector mesons isospectrality does not come together with isothermality. We could speculate on the existence of a certain "physical" value of λ, that provides the "correct" value of T_c. However, for now we have neither the independent mechanism to choose a particular λ, nor the complete understanding on how to evaluate the result. One conclusion we can make is that the "physical" λ is not essentially the original $\lambda = \pm\infty$.

In the range of positive λ one gets smaller T_c going from $\lambda = +\infty$ to 0 . For the

λ	T_{SW} (MeV)	
	"universal" slope [70]	$\rho:\ n=0$
100	261.1 ± 1.2	189.7 ± 0.1
1	194.9 ± 0.9	141.5 ± 0.1
0.01	154.3 ± 0.7	112.0 ± 0.1
-1.1	421.1 ± 1.9	305.7 ± 0.1
-2	345.3 ± 1.5	250.7 ± 0.1
-100	263.8 ± 1.2	191.6 ± 0.1

λ	T_{GSW} (MeV)	
	"universal" traj. [71]	$\rho:\ n=1,2,3,4$
100	249.6 ± 10.8	302.3 ± 47.0
1	193.7 ± 6.2	218.2 ± 32.1
0.01	160.9 ± 3.4	154.8 ± 10.3
-1.1	435.1 ± 10.1	429.7 ± 33.2
-2	342.1 ± 11.9	372.7 ± 40.7
-100	252.2 ± 10.9	304.9 ± 47.0

Table 6.3: Variations of the deconfinement temperature estimations with the isospectral parameter λ in (G)SW models based on the vector meson fits.

"universal" trajectories both in SW and GSW we see a transition of the T_c from the region predicted on lattice with non-dynamical quarks (about 260 MeV) to the one of the unquenched approximation ($150 - 170$ MeV). For the standard SW model fit we can get a viable prediction in the latter range at some finite λ. For the GSW fit without $\rho(770)$ – we can go down to more natural values of T_c at finite λ.

In the range of negative λ we obtain an opposite behavior: T_c grows as one goes away from the initial $\lambda = -\infty$. Unfortunately, for the cases under consideration the resulting temperatures are not much relevant.

We can now turn to the fits of 0^{++} mesons. The masses of the ground states of f_0 and a_0 are very close and we give just the temperature estimation from the fit to the mass of $f_0(980)$:

$$T_{HW} = 156 \pm 3 \text{ MeV}, \quad T_{SW} = 199 \pm 4 \text{ MeV}. \tag{6.17}$$

Going down through the isospectral family of SW potentials the T_{SW} value lowers to $T_c = 155$ MeV at $\lambda = 1$ or grows towards $T_c = 250$ MeV at $\lambda = -2$.

The actual fits of Fig. 4.4 turn out to be more successful than the universal one as is shown in Table 6.4. The values of T_c are close to those on the lattice

	f_0 traj.	a_0 traj.	"universal" traj. [71], $J = 0$
T_{GSW} (MeV)	150 ± 5	140 ± 6	80 ± 1

Table 6.4: GSW predictions from the fit to the scalar mesons.

with physical quarks. Going through the family with the isospectral parameter λ, T_c shifts significantly toward lower values: ~ 126 GeV at $\lambda = 0.01$ for f_0's, for instance. Thus, no isothermality is observed once again.

The fit to the universal trajectory of eq. (4.3) with $J = 0$ results in very low T_c. This observation exemplifies how important the b parameter of the GSW trajectory is for the estimation of T_c: the slopes of this and previous trajectories almost coincide, but the final T_c is two times different.

Finally, we can consider an exotic option of the meson fits with large-N_c limit masses of Section 4.3. It is logical to make a holographic estimation of the relation T_c/m and compare it to the large-N_c lattice result that would be free of $\sqrt{\sigma}$. Combining the lattice predictions of [66] and [90] we get

$$\left.\frac{T_c}{m_\rho}\right|_{lat} = 0.3789, \quad \left.\frac{T_c}{m_{a_0}}\right|_{lat} = 0.2448. \tag{6.18}$$

The HW prediction is not so good:

$$\left.\frac{T_c}{m_\rho}\right|_{HW} = 0.1574, \quad \left.\frac{T_c}{m_{a_0}}\right|_{HW} = 0.1384. \tag{6.19}$$

While for the SW we obtain

$$\left.\frac{T_c}{m_\rho}\right|_{SW} = 0.2459, \quad \left.\frac{T_c}{m_{a_0}}\right|_{SW} = 0.2008, \tag{6.20}$$

where some more agreement with lattice can be distinguished, especially for the case of a_0. That is not surprising because large-N_c a_0 mass in physical scale is close to the experimental one (see Table 4.1). We have also observed that the large-N_c trajectories constructed from the states of Table 4.1 deviate a lot from the physical ones. Thus, we see no reason to look into the GSW/lattice comparison.

6.5 Glueball fits

We begin the scalar glueball estimations of T_c with the last exercise from the meson fit section. Let us combine lattice results in $N_c \to \infty$ limit for T_c [66] and m_{gl}

[96], where m_{gl} is the mass of the 0^{++} state:

$$\left.\frac{T_c}{m_{gl}}\right|_{lat} = 0.1799. \tag{6.21}$$

The HW and SW predictions are

$$\left.\frac{T_c}{m_{gl}}\right|_{HW} = 0.0988, \quad \left.\frac{T_c}{m_{gl}}\right|_{SW} = 0.1739. \tag{6.22}$$

The SW result is rather close to the lattice one. For a comparison with another holographic approach we can turn to the so-called models of Improved holographic QCD, which predict $\left.\frac{T_c}{m_{gl}}\right|_{IhQCD} = 0.167$ [135].

In the GSW model this ratio obtains dependence on the factor b. Considering the linear interpolations of eq. (6.15) we get:

$$\left.\frac{T_c}{m_{gl}}\right|_{GSW} \simeq \frac{0.123b + 0.314}{2\sqrt{2+b}}. \tag{6.23}$$

To satisfy the lattice condition (6.21) the glueball trajectory should be characterized by the intercept $b = -1.96$ (second solution lies outside the phenomenological range). If we use a higher order interpolation for the whole plot of Fig. 6.1, the almost SW value $b = 0.09$ can be reobtained as a proper solution. The previous result transforms into $b = -1.94$. It draws a rather non-standard trajectory $4\kappa^2(n + 0.06)$ and the spectrum $M(n) = M(0)\{1; 4.2; 5.9; ...\}$. We notice, however, that a certain tendency towards such significant gap between the ground state and the first resonance could be seen in the results on the unquenched lattice (see Ref. [95]).

If both states reported in [96] are taken into account and supposed to lie on the GSW trajectory, we get $\frac{T_c|_{GSW}}{\sqrt{\sigma}} = 0.2988$ to be compared with 0.5949 of Ref. [66]. The two values do not present a satisfying accordance, but remarkably the isospectral methods change this GSW result only in the last digit.

Utilizing the formulas of eq. (6.22) and taking the 0^{++} glueball mass in the physical scale we produce the variety of results in Table 6.5a. The isospectrality is considered for SW model and features similar behaviour to what we have seen in the vector meson case.

The HW results converge to a region of $150 - 170$ MeV, similar to that from the lattice with dynamical quarks and from the analysis of heavy-ion collisions.

In the range of the SW predictions there are those around $250 - 260$ MeV – the region preferred by the quenched lattice and the SW result for the "universal" vector trajectory fit. They are produced from the fits to somewhat lowly 0^{++}, like the dominantly glueball $f_0(1500)$ conjecture or the glueball from the large-N_c

lattice. The large N_c fit provides a similar number ~ 250 MeV in SW, showing nice concordance with large N_c predictions from the lattice. The glueballs of mass ~ 1.7 GeV produce a larger temperature estimation, up to 300 MeV, though it is possible to get the lower values changing the isospectral parameter λ. We see once more that the temperature varies vastly within the isospectral family.

Next, in Table 6.5b, we take the full spectra of radial excitations and define T_c through GSW formulas. From the various quenched lattice data one may extract the radial trajectories which are rather close in terms of the fit parameters κ and b. Hence, the temperature predictions are to some extent similar, lying in the range of $T_c \sim 130 - 150$ MeV. Also, it is interesting to see that among these there are cases stable under the isospectral modification of the dilaton profile.

The unquenched trajectory prediction in Table 6.5b looks qualitatively different. Its distinctly steep slope, evident in Fig. 4.6, results in $T_c = 175 \pm 16$ MeV. It is a value with a relatively small error, isospectrally stable and close to that expected from the recent lattice simulations with dynamical quarks [58].

The error bars in Table 6.5b are generally large as the higher glueball excitations are not that well-measured and usually only the masses of 0^{++} and 0^{++*} states are calculated. First, that does not allow us to be sure of the validity of linear Regge assumption for the radial excitations of the scalar glueballs. Second, the slope error may get rather significant. However, the only work reporting on more than two states, Ref. [93], gives a more well-defined trajectory (and rather linear, see Fig. 4.6). The T_c prediction there is rather low, but that is due to the fact that the ground state is calculated to have a mass ~ 1.5 GeV, which may be considered systematically lower than other lattice predictions for the masses.

Altogether, we find all T_c of Table 6.5b to be rather close to the results of unquenched lattice and collider predictions for the deconfinement temperature, especially it is significant to have this agreement for the unquenched fit of Ref. [95].

6.6 Summary

We explored various possibilities to make an estimation of the deconfinement temperature in AdS/QCD models associating the confinement/deconfinement threshold at the gauge side with the HP phase transition in AdS. The deconfinement temperature turned out either to be connected to the holographic parameters responsible for the particle spectra or to have an unpredictable value. We constrained the holographic models to be as simple as possible for the consistent description

Fit	m_{gl} (MeV)	T_{HW} (MeV)	T_{SW} (MeV)		
			$\lambda = \infty$	$\lambda = 1$	$\lambda = 0.1$
M & P [92]	1730(100)	171(10)	301(17)	253(15)	173(10)
Meyer [93]	1475(75)	146(7)	256(13)	215(11)	147(8)
Chen *et al.* [94]	1710(95)	169(9)	297(17)	250(14)	171(10)
Unquenched [95]	1795(60)	177(6)	312(10)	262(9)	179(6)
Large N_c [96]	1455(70)	144(7)	253(12)	212(10)	145(7)
$f_0(1500)$ meson [98]	1464(47)	145(5)	255(8)	214(7)	146(5)
	1519(41)	150(4)	264(7)	222(6)	152(4)
$f_0(1710)$ meson [99]	1674(14)	165(1)	291(2)	244(2)	167(1)

(a) From the reproduction of the ground glueball state.

Fit	$\sqrt{\sigma}$	$m^2 = 4\kappa^2(n+2+b)$		T_{GSW} (MeV)		
	(MeV)	κ (MeV)	b	$\lambda = \infty$	$\lambda = 1$	$\lambda = 0.1$
M & P [92]	410	1017(151)	−1.28(0.23)	153.6(39.2)	151.4(36.1)	149.9(34.1)
Meyer [93]	440	1094(49)	−1.54(0.07)	132.5(9.7)	132.3(9.5)	132.1(9.4)
Large N_c [96]	440	1120(88)	−1.58(0.08)	131.3(13.5)	131.1(13.4)	131.0(13.3)
Large N_c [93]	440	735(121)	−1.00(0.35)	142.8(55.3)	134.8(43.7)	129.7(36.6)
Unquenched [95]	420	1652(138)	−1.71(0.05)	174.6(16.4)	174.6(16.4)	174.5(16.4)

(b) From the towers of scalar glueballs.

Table 6.5: Predictions of T_c from different fits of the scalar glueball states in HW, SW and GSW model with isospectrality.

of the QCD spectra; and the investigated frameworks were the HW, SW and GSW models. The QCD resonances (and their radial excitations), described by the matter part of $5D$ action, scoped the scalar and vector mesons and 0^{++} glueballs. The consideration of the latter is related to the dominating role of the bound gluon states over the bound quark states in the large-N_c limit of QCD. For an optional check, in the SW-like models we proposed aspiring to the stable temperature predictions in a given isospectral family.

First, one can focus on the correct reproduction of the mass of the ground state in a channel. That is a sufficient fixation of the model parameters in HW or SW. Then in the HW model for scalars the T_c prediction is of order $150 - 170$ MeV close to the temperature on lattice with physical quarks. The vector meson ground states are systematically low and that affects the corresponding T_c value. But interestingly the SW model for the observed vector and scalar mesons provides similar $T_c \sim 190 - 200$ MeV.

Another observation can be made considering a mean vector radial trajectory with the "universal" slope value. Our interest in this option is motivated by: a) the perception that in the planar limit one should not be concerned with the particularities of the meson trajectory, b) the similarity of the slope to that in the $f_0(1500)$ glueball hypothesis. The result of $T_c \simeq 260$ MeV corresponds exceedingly well to the lattice results for pure $SU(3)$ and the large-N_c limit. It is the least model- and channel-dependent result in our study. However, the general lack of isothermality in the isospectral families of a simple SW is a downside unless we can prove the isospectral parameter to mimic various regimes of lattice predictions.

Second, one can try to have a better description of a trajectory of many states. We use the GSW model to have an additional intercept parameter in the trajectories. In the case of mesons we are in a situation of having a rather big amount of data on higher excitations but, in the same time, not knowing of their belongings to the particular trajectories. It is easy to get quite different predictions, but in some cases under consideration we can achieve $140 - 150$ MeV from the vector and scalar meson fits. In the GSW with the "universal" slope and intercept we find the results for the vector case to be similar to those of SW, though the result for the scalar mesons is unsatisfactory.

In the case of the scalar glueball trajectories GSW shows a uniform convergence in the quenched case to $T_c \sim 130 - 150$ MeV and in the unquenched – to 175 MeV. We find the latter to be a rather successful result. Additionally, it is noteworthy that T_c is isospectrally stable only for the GSW glueball fits.

In summary, we tried to demonstrate that, although there exists a huge number of various holographic possibilities to estimate the deconfinement temperature, some sensible theoretical and phenomenological restrictions on holographic models lead to reasonable and rather stable predictions for the range of temperatures in the deconfinement crossover region at small baryon densities. A general tendency is that the more particularities about the QCD states are introduced into the holographic model the more T_c strays from the quenched or large-N_c limit lattice predictions.

Our analysis may be viewed from the opposite side: the query to reproduce the temperature range efficiently restricts the possible bottom-up holographic models; this way it may have a serious predictive power for the hadron spectroscopy.

Chapter 7

Holographic description of chiral symmetry breaking

7.1 Motivation

In this chapter we would like to display a more complex holographic picture of QCD: the concordant five-dimensional dual description of the light vector and scalar mesons in association with a realization of the chiral symmetry and the products of its breaking. In the simplest HW and SW setups it was attempted to describe the phenomenology of the vector sector and its interaction with the pions in Refs. [86, 87, 104–106]. Various modification and extensions followed (see Refs. [136–138], *etc.*). It could be observed that in the mentioned papers the exact realization of the chiral symmetry breaking turns out to be model dependent.

In order to build a $5D$ model within the bottom-up approach one mixes the established AdS/CFT prescriptions of Chapter 2 with various assumptions. The latter might have a theoretical motivation, but the ultimate criterion for their validity is leading to a better phenomenological description for one or another aspect of QCD. This said, we believe that the field of viable model modifications is not exhausted yet and present our approach here.

In this chapter we construct and investigate a new holographic framework that is based on the SW setup and is dual to $SU(2)$ QCD. From a theoretical point of view, our goal is a new consistent description of the Goldstone states (pions). In the common holographic setup the Goldstone bosons turn out to be a part of the gauge field (playing the role of the "Higgs"). This is not the way chiral symmetry is broken in real QCD. One way around would be introducing some symmetry break-

ing terms: $5D$ vector meson masses in order to prevent Goldstones being eaten, and extra scalar term to make the Goldstone masses (m_π) lower than the natural scale of the composite states (m_ρ) and to fulfill the holographic requirements on the profile of the relevant mode in the extra dimension. Furthermore, by doing so we would be able to treat the Goldstones in a transparent and analytically tractable fashion that is often lacking in other approaches.

There is also an issue at the phenomenological side. Various low-energy observables have been calculated within one or another model and are claimed to be in agreement with experiment at level of $10 - 30\%$, but it is rather common that a given study is concentrated on a specific set of observables. The purpose of this work is to be as exhaustive as possible and to make as many predictions for the observables as can be extracted from this particular model of QCD with two flavors up to the three-point level.

We also realized that re-estimation and generalization of some concepts of the holographic model construction are necessary. The first one concerns the duality between the QCD operator and the five-dimensional field. Another, the mass prescriptions for these fields. Both are established in the previously discussed AdS/CFT dictionary, but we dispute its blind following in the phenomenology directed approach of AdS/QCD.

The dual operators in the dictionary are understood rather abstractly, for once they have no fixed normalizations attached. We suggest introducing some reference operators with free coefficients and studying whether they are eliminated from the physical quantities or not. The holographic prescriptions for the $5D$ masses in the dictionary are extremely stringent to the model. We argue that they should rather be considered as imposing boundary conditions on otherwise bulk coordinate-dependent mass (not the first attempt on this, see e.g. [139–141]). Obviously, a non-zero vector mass means that the local symmetry is not preserved in the holographic action in the bulk, but we will see that it is kept on the boundary. In addition to this, we also introduce an explicit breaking of the global chiral symmetry towards the vector subgroup in the scalar sector. That is not conventional but it turns out that this kind of symmetry breaking is crucial to achieve our goal regarding pions.

We would like to stress that the cumulative effect of all these modifications of the standard bottom-up framework turns out more interesting than was predesigned. For instance, just demanding the analyticity of solutions of the equations of motion results in a determined ansatz for the scalar vev, which is the driver

behind the chiral symmetry breaking in the holographic bulk. That leads us to question the common parametrization of the scalar vev in terms of the quark mass and chiral condensate (see also [136, 138, 142]). The two aforementioned non-standard symmetry violations and this particular choice of the scalar vev determines the novel phenomenology of our model. Besides, the appearance of several new parameters hints for a better fit to experiment. Moreover, after a close examination we will find out that the number of free parameters could be minimized to that of the traditional SW, while the described phenomenology remains richer.

7.2 Holographic model

The construction of the 5D model begins by selecting a collection of operators describing the 4D physics of interest. We use a standard set of QCD operators representative of the chiral two-flavour symmetry and its breaking. The $SU(2)$ group structure was defined in the beginning of Section 3.2.1.

Within the holographic approach the consideration of the partition function $\mathcal{Z}_{4D}$ is the cornerstone concept. Its conventional structure was given in eq. (5.2). Now $\phi_{\mathcal{O}}$ are the sources for the relevant operators. The vector and axial vector operators were introduced in (3.15) and (3.16). The symmetry breaking related operator is a bilinear. In terms of the flavour components of the Ψ spinor it is defined as $\overline{\Psi}^j_R \Psi^k_L$ and its conjugate is $\overline{\Psi}^j_L \Psi^k_R$. Its source should be a matrix, and we can make a following interpretation of it:

$$\phi_{\overline{\Psi}\Psi} = m_q \cdot \mathrm{Id} + \phi^a_S \cdot T^a - i\phi^a_P \cdot T^a, \tag{7.1}$$

where m_q is a physical source related to the quark mass. The other two non-physical sources in the expansion imply that we can introduce proper scalar (3.45) and pseudoscalar (3.46) operators. These four types of QCD operators (vector, axial vector, scalar and pseudoscalar) have some specific normalization, which we shall keep as a reference one.

We notice that to exploit the holographic procedure there is no necessity to talk about a particular normalization of a given operator, in the dictionary they are differentiated just by their canonical dimension and spin. However, some phenomenological observables in QCD may turn out dependent on the normalization. Thus, to see the possible impact of the normalization choice we introduce extra factors g_V and g_S in the vector and scalar operators respectively.

At the same time we would like to couple the QCD currents to the electroweak

bosons of the SM. There, the symmetry leaves no ambiguity for the couplings given in terms of the electroweak coupling constants e and g.

To conclude, in the partition function of eq. (5.2) the relevant QCD operators appear as follows in our setup

$$\begin{aligned}\sum_j \phi_{\mathcal{O}_j}(x)\mathcal{O}_j(x) &= \phi_V^{a\,\mu}(x)\cdot g_V\mathcal{O}_{V\,\mu}^a(x)+\phi_A^{a\,\mu}(x)\cdot g_V\mathcal{O}_{A\,\mu}^a(x)\\ &+ \phi_S^a(x)\cdot g_S\mathcal{O}_S^a(x)+\phi_P^a(x)\cdot g_S\mathcal{O}_P^a(x)\\ &+ e\mathcal{A}_\mu^{em}\cdot\mathcal{O}_V^{3\,\mu}\\ &- \frac{g}{2}W_\mu^{-/+}\cdot\mathcal{O}_A^{-/+\,\mu}+\frac{g}{2}W_\mu^{-/+}\cdot\mathcal{O}_V^{-/+\,\mu}+\ldots\end{aligned} \tag{7.2}$$

where we use the notation $\mathcal{O}^+=\frac{\mathcal{O}^1+i\mathcal{O}^2}{\sqrt{2}}$, $\mathcal{O}^-=\frac{\mathcal{O}^1-i\mathcal{O}^2}{\sqrt{2}}$.

7.2.1 Standard $5D$ construction

Applying the gauge-gravity correspondence to the aforementioned operators we obtain a theory for the left and right vector fields and a complex scalar field. The holographic dictionary provides relations between operators and $5D$ fields and dictates the bulk masses of the latter:

$$g_V\mathcal{O}_{L\,\mu}^a\leftrightarrow(A_L)_\mu^a,\ g_V\mathcal{O}_{R\,\mu}^a\leftrightarrow(A_R)_\mu^a,\qquad M_L^2R^2=M_R^2R^2=0; \tag{7.3}$$

$$g_S\overline{\Psi}_R^j\Psi_L^k\leftrightarrow\tfrac{R}{z}H^{jk},\ g_S\overline{\Psi}_L^j\Psi_R^k\leftrightarrow\tfrac{R}{z}H^{\dagger jk},\quad M_H^2R^2=-3. \tag{7.4}$$

The global symmetries of QCD translate into the local ones on the $5D$ side. Consideration of the transformation properties of different fields allows us to construct a gauge invariant Lagrangian with spontaneous symmetry breaking to the diagonal (vector) subgroup, $SU(2)_L\times SU(2)_R\to SU(2)_V$.

Let us denote the group transformations $g_L\in SU(2)_L,\ g_R\in SU(2)_R,\ h\in SU(2)_V$. The canonical choice for the coset representative $\xi(\pi)=(\xi_L(\pi),\xi_R(\pi))\in SU(2)_L\times SU(2)_R$ is to take $\xi_L=\xi_R^\dagger=u(\pi)$. Then the matrix of the Goldstone fields goes as follows under a chiral transformation: $u\to u'=g_Luh^\dagger=hug_R^\dagger$. The scalar degrees of freedom are collected in Σ transforming as $\Sigma\to\Sigma'=h\Sigma h^\dagger$. With these we construct a non-linear complex scalar field $H(x,z)$

$$H=u\Sigma u,\ \Sigma=f(z)\cdot\mathrm{Id}+T^as^a(x,z),\ u=\exp\left(\frac{i\pi^a(x,z)T^a}{\chi_\pi}\right), \tag{7.5}$$

for which we have $H\to H'=g_LHg_R^\dagger$. χ_π is a constant parameter used to normalize the dimensionality of the π fields. There is no reason to immediately

connect it to the QCD pion decay constant, the commonly used scale. The scalar vev, $f(z)$, implements chiral symmetry breaking in the bulk. This will be discussed in more detail further.

In the vector sector we have the non-Abelian fields $(A_L)_M$ and $(A_R)_M$, their kinetic terms given by the field strength tensor $F_{MN} = (\partial_M A^a_N - \partial_N A^a_M + C^{abc} A^b_M A^c_N) T^a$. The covariant derivative transforming as $D_M H \to g_L D_M H g_R^\dagger$ is

$$D_M H = \partial_M H - i A_{LM} H + i H A_{RM}. \tag{7.6}$$

The general dynamics is governed by the $5D$ action:

$$\begin{aligned} S_{5D} &= -\frac{1}{4g_5^2}\int d^5x\sqrt{-g}e^{-\Phi(z)}\,\mathrm{Tr}\left[F^L_{MN}F^{L\,MN} + F^R_{MN}F^{R\,MN}\right] \\ &\quad + \frac{1}{k_s}\int d^5x\sqrt{-g}e^{-\Phi(z)}\left[\mathrm{Tr}\, g^{MN}(D_M H)^\dagger (D_N H) - M_H^2\,\mathrm{Tr}\, H H^\dagger\right], \end{aligned} \tag{7.7}$$

where we introduce the usual holographic parameters g_5^2 and k_s. We have chosen to work within the SW setup that is implemented through the dilaton profile $\Phi(z) = \kappa^2 z^2$, where κ is a model parameter setting an overall energy scale [105].

7.2.2 Symmetry breaking in the bulk

The major disadvantage of the standard construction, from our point of view, is that pions, being introduced as they are, appear at the two-point level just in a combination $(\partial_M \pi - A_M)^2$. That makes them quite similar to the Goldstones in the Higgs mechanism and wrongly implies that they are fully dedicated to contribute to the axial two-point function (analogous to the mass of a gauge boson). It is known that the QCD pion should do more than that.

We want to make some changes in the setup so that the pion can no longer be eliminated by the gauge choice. The proposal consists in the introduction of a term providing a non-trivial diagonalization on $(A_M, \partial_M \pi)$ plane. The natural option is to add some z-dependence to the masses dictated by the holographic dictionary. Other authors [139, 141] have looked into this option motivated by a different reasoning, and the focus usually stays on the scalar mass [140, 141, 143] on the ground that its z-dependent part could be attributed to the anomalous dimension of the relevant quark operator. Obviously, by including masses for the $5D$ gauge fields we give up the local chiral gauge invariance. The following expressions for

the vector and scalar masses will be used in this work

$$M_L^2 R^2 = M_R^2 R^2 = M^2(z) R^2 = 0 + 4\mu_V \kappa^2 z^2, \tag{7.8}$$

$$M_H^2(z) R^2 = -3 + 4\mu_H \kappa^2 z^2. \tag{7.9}$$

The quadratic in z terms with μ_V and μ_H represent a minimal option to achieve the stated purpose while keeping the solutions analytically tractable.

For reasons that shall become clear further on we also include a scalar potential term containing a new function $b(z)$, that explicitly breaks the axial part of the symmetry. The total five-dimensional action of our model will be

$$\begin{aligned} S = -\frac{1}{4g_5^2} \int d^5x \sqrt{-g} e^{-\Phi(z)} \operatorname{Tr} \Big[& F_{MN}^L F^{L\,MN} + F_{MN}^R F^{R\,MN} \\ & - 2M^2(z)(A_M^L A^{L\,M} + A_M^R A^{R\,M}) \Big] \\ + \frac{1}{k_s} \int d^5x \sqrt{-g} e^{-\Phi(z)} \Big[& \operatorname{Tr}(D_M H)^\dagger (D^M H) - M_H^2(z) \operatorname{Tr} H H^\dagger \\ & - b(z) \operatorname{Tr}(H + H^\dagger) \Big]. \end{aligned} \tag{7.10}$$

To deal with the mixing term between the axial vector fields and the pions we make a redefinition of the vector fields inspired by their would-be gauge transformation property (in order to keep $F_{MN} = \widehat{F}_{MN}$):

$$(A_L)_M = \xi_G^\dagger (\widehat{A}_L)_M \xi_G - i \partial_M \xi_G^\dagger \xi_G, \tag{7.11}$$

$$(A_R)_M = \xi_G (\widehat{A}_R)_M \xi_G^\dagger + i \xi_G \partial_M \xi_G^\dagger, \tag{7.12}$$

$$\xi_G = \exp\left(\frac{i \pi^a T^a}{\widehat{\chi}_\pi} \right). \tag{7.13}$$

From now on we call "vector" the fields $V^a = \frac{\widehat{A}_L^a + \widehat{A}_R^a}{2}$ and "axial" the orthogonal combination $A^a = \frac{\widehat{A}_R^a - \widehat{A}_L^a}{2}$. The parameter $\widehat{\chi}_\pi$ is tuned in order to eliminate the mixing:

$$\widehat{\chi}_\pi = -\chi_\pi (1 + \beta), \quad \beta = \frac{k_s}{4g_5^2} \frac{M^2(z)}{f^2(z)}. \tag{7.14}$$

We assume that the factor β introduced here has no z-dependence. That is crucial to the determination of the possible z-dependencies of $f(z)$ and $b(z)$. The limit $\beta = \infty$ corresponds to the absence of the spontaneous breaking and signifies the restoration of the chiral symmetry.

7.3 Holographic equations of motion

The two types of solution to the holographic EOM were discussed in general in Section 5.2. Here we go immediately to the specifics of the model equations.

7.3.1 Vector and axial vector fields

Duality establishes the field-operator correspondence and the UV behaviour of the bulk-to-boundary propagators

$$V^a(x,\varepsilon) = 1 \cdot \phi_V^{a\,\mu}(x) \quad \leftrightarrow \quad g_V \mathcal{O}_{V\,\mu}^a(x) = g_V \overline{\Psi}\gamma^\mu T^a \Psi, \tag{7.15}$$

$$A^a(x,\varepsilon) = 1 \cdot \phi_A^{a\,\mu}(x) \quad \leftrightarrow \quad g_V \mathcal{O}_{A\,\mu}^a(x) = g_V \overline{\Psi}\gamma^\mu\gamma_5 T^a \Psi. \tag{7.16}$$

We work in a holographic gauge $A_z = V_z = 0$ and $\partial_\mu A^\mu = \partial_\mu V^\mu = 0$. The latter condition can be preserved on-shell only, and for the axial field it is necessary to have no mixing with the pions left. The EOMs for the transverse part of the vector and axial vector fields are

$$\left(\partial_z \frac{e^{-\Phi}}{z}\partial_z V_\mu^a(x,z) - \frac{e^{-\Phi}}{z}\Box V_\mu^a(x,z) - \frac{M^2(z)R^2 e^{-\Phi}}{z^3}V_\mu^a(x,z)\right)_\perp = 0, \tag{7.17}$$

$$\left(\partial_z \frac{e^{-\Phi}}{z}\partial_z A_\mu^a(x,z) - \frac{e^{-\Phi}}{z}\Box A_\mu^a(x,z) - \frac{M^2(z)R^2 e^{-\Phi}}{z^3}\frac{1+\beta}{\beta}A_\mu^a(x,z)\right)_\perp = 0. \tag{7.18}$$

Analytic solutions can be achieved for an ansatz of the form

$$M^2(z)R^2 = 4\mu_V \cdot \kappa^2 z^2. \tag{7.19}$$

The absence of the constant term is due to the holographic prescription for the vector mass in the UV, and it is a necessary choice for the correct behaviour of the vector bulk-to-boundary propagator on the boundary. After the Fourier transformation, we obtain

$$V(q,z) = \Gamma\left(1 - \frac{q^2}{4\kappa^2} + \mu_V\right)\Psi\left(-\frac{q^2}{4\kappa^2} + \mu_V, 0; \kappa^2 z^2\right),\ V(q,0) = 1. \tag{7.20}$$

The Tricomi function Ψ is the solution of the confluent hypergeometric equation with a proper behaviour at z-infinity. See Appendix A for more information about the solutions of EOMs of this type.

The difference in the axial vector case consists just in a constant shift $\mu_V \to \mu_V \frac{1+\beta}{\beta}$; and the axial vector propagator is:

$$A(q,z) = \Gamma\left(1 - \frac{q^2}{4\kappa^2} + \mu_V \frac{1+\beta}{\beta}\right) \Psi\left(-\frac{q^2}{4\kappa^2} + \mu_V \frac{1+\beta}{\beta}, 0; \kappa^2 z^2\right), \quad (7.21)$$
$$A(q,0) = 1.$$

The parameter μ_V remains free and also appears in the expression of the normalizable solutions. The orthogonality relation is

$$\frac{R}{g_5^2} \int_0^\infty dz e^{-\kappa^2 z^2} z^{-1} V_n/A_n(z) V_k/A_k(z) = \delta_{nk}. \quad (7.22)$$

Then the z profiles are determined from another branch of solutions of the EOMs, and the spectra can be expressed using the discrete parameter $n = 0, 1, 2, ...$:

$$V_n(z) = A_n(z) = \kappa^2 z^2 \sqrt{\frac{g_5^2}{R}} \sqrt{\frac{2}{n+1}} L_n^1(\kappa^2 z^2), \quad (7.23)$$

$$M_V^2(n) = 4\kappa^2(n + 1 + \mu_V), \quad M_A^2(n) = 4\kappa^2\left(n + 1 + \mu_V + \frac{\mu_V}{\beta}\right). \quad (7.24)$$

Here again $L_n^m(\kappa^2 z^2)$ are the generalized Laguerre polynomials. These solutions are analogous to those obtained in the standard framework (compare also with eq. 5.13) after $\mu_V \to 0$, $\frac{\mu_V}{\beta} \to$ constant. As was already discussed in detail in the previous chapters, the linearity of the radial Regge trajectories $M^2(n) \sim n$ is a distinctive feature of the SW model. We choose the SW setup because of this indication of a proper confinement realization.

The quantum numbers of the corresponding operators allow us to identify the boundary fields $(V/A)_{(n)}(x)$ and the masses $M_{V/A}(n)$ with the massive radial excitations of ρ and a_1 mesons.

Let us consider also an alternative treatment. Having computed the Green's function $G(q,z,z') = \sum_n \frac{\varphi_n^*(z)\varphi_n(z')}{q^2 - M^2(n)}$, one can arrive at the following expression for the propagators

$$V(q,z) = \sum_n \frac{F_V(n) V_n(z)}{-q^2 + M_V^2(n)}, \; A(q,z) = \sum_n \frac{F_A(n) A_n(z)}{-q^2 + M_A^2(n)}, \quad (7.25)$$

$$F_A^2(n) = F_V^2(n) = \frac{8R\kappa^4}{g_5^2}(n+1). \quad (7.26)$$

It can be proved that the UV boundary conditions are respected in this form as well.

Therefore, we have determined two kinds of phenomenologically relevant quantities: the masses and the decay constants related to the states in the vector and axial vector sectors. The following matrix elements define the experimentally observed quantities F_ρ and F_{a_1} (see Section 4.1.2) and can be expressed in the holographic framework as

$$\langle 0|\mathcal{O}_V^{a\,\mu}(x)|\rho^b(p)\rangle = \epsilon^\mu \delta^{ab} F_\rho e^{-ipx} \equiv \epsilon^\mu \delta^{ab} \frac{1}{g_V} F_V(0) e^{-ipx}, \quad (7.27)$$

$$\langle 0|\mathcal{O}_A^{a\,\mu}(x)|a_1^b(p)\rangle = \epsilon^\mu \delta^{ab} F_{a_1} e^{-ipx} \equiv \epsilon^\mu \delta^{ab} \frac{1}{g_V} F_A(0) e^{-ipx}. \quad (7.28)$$

Notice, that in our model, though the masses in the vector and axial vector channels are different, their decay constants coincide, while experimentally they are known to be distinct.

7.3.2 Scalar and pseudoscalar fields

Let us follow similar steps in case of spin zero fields. Due to the specifics of the linearized form of the H field

$$H(x,z) = f(z) + s^a(x,z)T^a + \frac{2if(z)}{\chi_\pi}\pi^a(x,z)T^a, \quad (7.29)$$

the correspondence in the scalar sector is the following

$$s^a(x,\varepsilon) = \frac{\varepsilon}{R}\phi_S^a(x) \quad \leftrightarrow \quad g_S \mathcal{O}_S^a(x) = g_S \overline{\Psi} T^a \Psi, \quad (7.30)$$

$$\pi^a(x,\varepsilon) = -\frac{\varepsilon}{R}\frac{\chi_\pi}{2f(\varepsilon)}\phi_P^a(x) \quad \leftrightarrow \quad g_S \mathcal{O}_P^a(x) = g_S \overline{\Psi} i\gamma_5 T^a \Psi. \quad (7.31)$$

The associated QCD states are a_0 and π mesons.

The EOMs for the scalar and pseudoscalar fields are

$$\partial_z \frac{e^{-\Phi}}{z^3}\partial_z s^a - \frac{e^{-\Phi}}{z^3}\Box s^a - \frac{M_H^2(z)R^2}{z^5}e^{-\Phi}s^a = 0, \quad (7.32)$$

$$\partial_z \frac{e^{-\Phi}}{z^3} f^2(z)\partial_z \pi^a - \frac{e^{-\Phi}}{z^3} f^2(z)\Box\pi^a + \frac{b(z)f(z)R^2}{z^5}e^{-\Phi}\frac{1+\beta}{\beta}\pi^a = 0. \quad (7.33)$$

In the pseudoscalar case we have to choose a function $b(z)$. The function $f(z)$ is already uniquely fixed by the ansatz selected for $M^2(z)$,

$$f(z)R = \sqrt{\frac{k_s}{g_5^2}\frac{\mu_V}{\beta}}\cdot \kappa z. \quad (7.34)$$

The condition (7.34) allows us to write the pion EOM in a form reminiscent of the vector EOM

$$\partial_z \frac{e^{-\Phi}}{z}\partial_z \pi^a - \frac{e^{-\Phi}}{z}\Box\pi^a + \frac{e^{-\Phi}}{z^3}(b_1 + 4b_2\cdot\kappa^2 z^2)\pi^a = 0, \quad (7.35)$$

where we have assumed that the function $b(z)$ is chosen so that

$$b(z)R^3 \cdot (1+\beta)\sqrt{\frac{g_5^2}{k_s \mu_V \beta}} = b_1 \kappa z + 4b_2 \cdot \kappa^3 z^3. \tag{7.36}$$

Any higher order terms would result in a non-analytic solution. We must impose $b_1 = 0$ in order to fulfill the boundary condition of eq. (7.31). Then, the bulk-to-boundary propagators are

$$s(q,z) = \frac{z}{R}\Gamma\left(\frac{3}{2} + \mu_H - \frac{q^2}{4\kappa^2}\right)\Psi\left(\frac{1}{2} + \mu_H - \frac{q^2}{4\kappa^2}, 0; \kappa^2 z^2\right), \tag{7.37}$$

$$\pi(q,z) = -\sqrt{\frac{g_5^2\beta}{k_s\mu_V}}\frac{\chi_\pi}{2\kappa}\Gamma\left(1 - b_2 - \frac{q^2}{4\kappa^2}\right)\Psi\left(-b_2 - \frac{q^2}{4\kappa^2}, 0; \kappa^2 z^2\right). \tag{7.38}$$

The EOMs and the orthogonality conditions,

$$\frac{R^3}{k_s}\int_0^\infty dz e^{-\kappa^2 z^2} z^{-3} s_n(z) s_k(z) = \delta_{nk}, \tag{7.39}$$

$$\frac{4\beta}{(1+\beta)\chi_\pi^2}\frac{R^3}{k_s}\int_0^\infty dz e^{-\kappa^2 z^2} z^{-3} f^2(z) \pi_n(z) \pi_k(z) = \delta_{nk}, \tag{7.40}$$

bring the following solutions for the KK z-profiles

$$s_n(z) = \frac{z}{R}\sqrt{\frac{k_s}{R}}\sqrt{\frac{2}{n+1}}(\kappa z)^2 L_n^1(\kappa^2 z^2), \tag{7.41}$$

$$\pi_n(z) = \frac{\chi_\pi}{\kappa}\sqrt{\frac{1+\beta}{\mu_V}}\sqrt{\frac{g_5^2}{2R}}(\kappa z)^2 L_n^1(\kappa^2 z^2), \tag{7.42}$$

$$M_s^2(n) = 4\kappa^2(n + 3/2 + \mu_H), \quad M_\pi^2(n) = 4\kappa^2\left(n + 1 - b_2\right). \tag{7.43}$$

Assuming $b_2 = 1$ makes the ground state Goldstones massless, $m_\pi = M_\pi(0) = 0$. This reveals the goal of $b(z)$ introduced in the scalar potential of the $5D$ action: with the analyticity of the solution imposed, it only serves to nullify the pion masses. However, even without it, we can generally distinguish the $m_\rho = M_V(0)$ and m_π scales due to the appearance of μ_V in the vector masses. Notice that we gain an analytic result for the whole tower of pion radial excitations, while in most holographic papers one finds an implicit equation defining numerically just the ground state.

The alternative expressions for the propagators are analogous to the ones found

in the vector sector

$$s(q,z) = \frac{1}{\sqrt{2}} \sum_n \frac{F_s(n) s_n(z)}{-q^2 + M_s^2(n)},\ \pi(q,z) = \sum_n \frac{F_\pi(n)\pi_n(z)}{q^2 - M_\pi^2(n)}, \tag{7.44}$$

$$F_s^2(n) = 16\kappa^4 \frac{R}{k_s}(n+1),\ F_\pi^2(n) = 8\kappa^4 \frac{\beta}{1+\beta}\frac{R}{k_s}(n+1). \tag{7.45}$$

The factor $1/\sqrt{2}$ in front of the scalar propagator is necessary to conform to the usual definition of the scalar decay constant. The true value of the decay constant is found only after one calculates the residue at $q^2 = M^2(n)$ of the corresponding two-point function. We follow the conventions of Ref. [108] and we use their definition of F_s. In Section 7.4, we will re-encounter this quantity in the residue of the scalar correlator, and the $1/\sqrt{2}$ factor ensures the agreement between both expressions.

The quantities in the last equations above are related to the decay constants F_s and F_π appearing in the one-point functions (see Section 4.2.2)

$$\langle 0|\mathcal{O}_S^a(x)|a_0^b\rangle = \delta^{ab} F_s e^{-ipx} \equiv \delta^{ab}\frac{1}{g_S} F_s(0) e^{-ipx}, \tag{7.46}$$

$$\langle 0|\mathcal{O}_P^a(x)|\pi^b\rangle = \delta^{ab} F_\pi e^{-ipx} \equiv \delta^{ab}\frac{1}{g_S} F_\pi(0) e^{-ipx}. \tag{7.47}$$

The numerical predictions for the decay constants are provided in Section 7.6.

7.3.3 Dynamics and interpretation of $f(z)$

In this analysis, we would like to stay within the chiral limit, where on the QCD side the breaking is generated dynamically by the chiral condensate $\langle q\bar{q}\rangle$. In the holographic bulk we have a sigma-model type theory, where the function $f(z)$ describes the spontaneous symmetry breaking in a non-dynamical fashion.

However, there is no clear holographic prescription on how the chiral symmetry breaking should be realized. In fact, the specifics of the realization define wholly different classes of models, *e.g.* in the framework with the IR cut-off one can choose between those of Refs. [104], [86] or [87]. In a general AdS/QCD framework (that of Refs. [104, 105]) the conventional understanding is that the scalar vev has the following form (see also Ref. [136])

$$f(z)R = m_q z + \frac{\sigma}{4} z^3, \tag{7.48}$$

where the parameters m_q and σ are believed to correspond to the physical current quark mass and the chiral condensate. This power behavior is a solution of the

EOM written for $f(z)$ in the case of the HW model with $\Phi(z) = 0$, while in the SW the powers get multiplied by the hypergeometric functions (see below). The interpretation in eq. (7.48) is motivated by the AdS/CFT correspondence [16, 116]: m_q is the physical source for the $\mathcal{O} = q\bar{q}$ operator and σ is a vev determined as a one-point function in the presence of a source, $\langle\mathcal{O}\rangle_\phi$. That means that if the source($= m_q$) goes to zero, the vev vanishes in the case of the normal-ordered observables $\langle\mathcal{O}\rangle_{\phi=0} = 0$. One has to admit that this is not compatible with QCD where the chiral condensate is non-zero in the chiral limit. Most authors do not try to explain this issue, though for instance, in the HW setup of Ref. [107] they introduce an extra scalar potential on the IR brane to get around the problem.

In the SW the function form (7.48) is not a solution of the EOM, but it is a common opinion that it should emerge in the UV asymptotics at least. The problem arises that while choosing a solution finite at $z \to \infty$, one is left with only one branch of the equation. Hence, the model bears a correlation in the definition of the coefficients at z and z^3 terms, mixing the coefficients associated in QCD with the explicit and spontaneous sources of the breaking. Various attempts were made to resolve this contradiction: from manually inserting a different ansatz [137] towards major modifications of the model dilaton and/or scalar potential to make a consistent dynamical solution for $f(z)$[138, 140, 144]. The latter models give independent predictions for m_q and σ, but in our opinion, they are no longer compatible with the strict AdS/CFT identification, not to mention its unclear realization in the chiral case.

It is evident that our ansatz for $f(z)$ given in eq. (7.34) does not follow the form of eq. (7.48). Nevertheless, the appearance of eq. (7.34) is related to the correct description of the vector sector. And we put reasonings on the analyticity and holographic consistency of the previous sections prior to the issue of possible identifications of the $f(z)$ parameters, especially in light of the discussion presented above. Let us mention several other arguments. First, it could be reasonable to demand $f(z \to \infty)R \sim z$ (as is done in Ref. [138]) that fixes the parallel slopes of the vector and axial vector trajectories in accordance with the idea of the chiral symmetry not being restored [145, 146]. We may attribute our ansatz (7.34) to the preservation of this quality in a simple manner. Second, one can speculate that a mass appearing at the linear in z order is not a current but a constituent one [147], that light quarks acquire in the presence of the quark condensate. We will show that, indeed, the factor could be of an order ~ 300 MeV for a natural value of g_S. And finally, we can refer to Ref. [142], in which it is concluded that because

the scale dependence is not systematically dealt with in the bottom-up holographic models, it might be advisable to give up on matching to such quantities as m_q and σ.

With a firm resolution to use the ansatz of eq. (7.34), let us nevertheless explore the case where $f(z)$ is a solution of the EOM. In our model this is not quite standard: there is a new coefficient μ_H and the scalar potential with $b(z)$ makes the equation inhomogeneous,

$$\partial_z \frac{e^{-\Phi(z)}}{z^3}\partial_z f(z) - \frac{e^{-\Phi(z)}M_H^2(z)R^2}{z^5}f(z) - \frac{b(z)}{z^5}e^{-\Phi(z)} = 0. \tag{7.49}$$

The homogeneous part coincides with the EOM of a conventional SW but for an addition of μ_H. The solution changes accordingly,

$$f_{hom}(z) \sim (\kappa z)^3 \cdot {}_1F_1\left(\frac{3}{2}+\mu_H, 2, \kappa^2 z^2\right) + \kappa z \cdot \Psi\left(\frac{1}{2}+\mu_H, 0; \kappa^2 z^2\right),$$

where ${}_1F_1$ and Ψ are confluent hypergeometric functions of different types.

With $b(z)$ taken from eq. (7.36) (though we might have used any arbitrary coefficient function $\sim b_1 z + b_2 z^3$, it would be necessary to have $b_1 = 0$ to get a finite result), the particular solution turns out to be (with the use of the relevant Green's function $G(z,z')$):

$$f_{part}(z)R = \int_0^\infty dz' \frac{b(z')e^{-\Phi(z')}}{z'^5} G(z,z') \tag{7.50}$$

$$= \frac{-\kappa b_2}{1+\beta}\frac{z}{\kappa^2 R^2}\sqrt{\frac{k_s}{g_5^2}\mu_V\beta}\left[\frac{1}{\mu_H+1/2} + \Gamma\left(\mu_H+\frac{1}{2}\right)\Psi\left(\mu_H+\frac{1}{2}, 0; \kappa^2 z^2\right)\right].$$

We can see that for $f(z) = f_{hom}(z) + f_{part}(z)$ a $f(z)R \sim z$ approximation is an appropriate one if we keep just the leading asympotics for $z \to 0$. Additionally, we have a separate source for the $\sim z$ terms aside from those coming from the Tricomi function.

Moreover, for specific values of μ_H we can simplify the EOM (7.49) so that a solution of the homogeneous part, that is finite in the IR, is either linear ($\sim z$) at $\mu_H = -1/2$ or cubic ($\sim z^3$) at $\mu_H = -3/2$. The case $\mu_H = -1/2$ seems most interesting, as it would prove our choice of the ansatz if no $b(z)$ were present; though the full solution is $f(z) \sim C_{hom} z + C_{part} z \ln z$. Furthermore, $\mu_H = -1/2$ makes the scalar tower $M_s^2(n) = 4\kappa^2(n+1)$ look exactly like a shifted pseudoscalar one, meaning $m_{a_0} = m_{\pi'}$. A finite pion mass could be a source of the splitting between them. We will use the assumption of fixing $\mu_H = -1/2$ in one of the phenomenological fits.

7.4 Two-point correlators

Following the duality connection between the $4D$ partition function and the on-shell holographic action we present a definition for the two-point functions, with $\mathcal{O}_\mu$ standing for spin one operators and $\mathcal{O}$ for spin zero,

$$\langle g_V\mathcal{O}^a_\mu(q)g_V\mathcal{O}^b_\nu(p)\rangle = \delta(p+q)\int d^4x e^{iqx}\langle g_V\mathcal{O}^a_\mu(x)g_V\mathcal{O}^b_\nu(0)\rangle = \frac{\delta^2 iS^{on-shell}_{5D}}{\delta i\phi^a_\mu(q)\delta i\phi^b_\nu(p)}, \tag{7.51}$$

$$i\int d^4x e^{iqx}\langle g_V\mathcal{O}^a_\mu(x)g_V\mathcal{O}^b_\nu(0)\rangle = \delta^{ab}\left(\frac{q_\mu q_\nu}{q^2}-\eta_{\mu\nu}\right)\Pi_{V,A}(q^2), \tag{7.52}$$

$$i\int d^4x e^{iqx}\langle g_S\mathcal{O}^a(x)g_S\mathcal{O}^b(0)\rangle = \delta^{ab}\Pi_{s,\pi}(q^2). \tag{7.53}$$

It is known that there could be divergences present in the functions of this type. If we perform a simple short-distance ε cut-off regularization as $z\to 0$ the resulting expressions are the following:

$$\Pi_V(q^2) = \frac{2\kappa^2 R}{g_5^2}\left(\mu_V - \frac{q^2}{4\kappa^2}\right)\left[\ln\kappa^2\varepsilon^2 + 2\gamma_E + \psi\left(1+\mu_V-\frac{q^2}{4\kappa^2}\right)\right], \tag{7.54}$$

$$\Pi_A(q^2) = \frac{2\kappa^2 R}{g_5^2}\left(\mu_V\frac{1+\beta}{\beta} - \frac{q^2}{4\kappa^2}\right)\left[\ln\kappa^2\varepsilon^2 + 2\gamma_E + \psi\left(1+\mu_V\frac{1+\beta}{\beta}-\frac{q^2}{4\kappa^2}\right)\right], \tag{7.55}$$

$$\Pi_s(q^2) = \frac{4\kappa^2 R}{k_s}\left(\frac{1}{2}+\mu_H - \frac{q^2}{4\kappa^2}\right)\left[\ln\kappa^2\varepsilon^2 + 2\gamma_E - \frac{1}{2} + \psi\left(\frac{3}{2}+\mu_H-\frac{q^2}{4\kappa^2}\right)\right], \tag{7.56}$$

$$\Pi_\pi(q^2) = \frac{2\kappa^2 R}{k_s}\frac{\beta}{1+\beta}\left(-1 - \frac{q^2}{4\kappa^2}\right)\left[\ln\kappa^2\varepsilon^2 + 2\gamma_E + \psi\left(-\frac{q^2}{4\kappa^2}\right)\right]. \tag{7.57}$$

The Π_s correlator also possesses a ε^{-2} singularity that is eliminated after the proper counterterm at the boundary is introduced. With the series representation of the digamma function $\psi\left(\frac{3}{2}+\mu_H-\frac{q^2}{4\kappa^2}\right) = -\gamma_E + \sum\frac{1}{n+1} + \sum\frac{4\kappa^2}{q^2-M_s^2(n)}$ we can check that the residue of Π_s is a quantity equal to F_s^2 as defined in eq. (7.45). The same procedure validates other decay constants.

Alternatively (and in need of a regularization) we can express the correlators

as follows

$$\Pi_V(q^2) = \sum_{n=0}^{\infty} \frac{F_V^2(n)}{-q^2 + M_V^2(n)},\ \Pi_A(q^2) = \sum_{n=0}^{\infty} \frac{F_A^2(n)}{-q^2 + M_A^2(n)}, \tag{7.58}$$

$$\Pi_s(q^2) = \sum_{n=0}^{\infty} \frac{F_s^2(n)}{-q^2 + M_s^2(n)},\ \Pi_\pi(q^2) = \sum_{n=0}^{\infty} \frac{F_\pi^2(n)}{-q^2 + M_\pi^2(n)}. \tag{7.59}$$

These expressions can be achieved using eqs. (7.25) and (7.44). Though in the case of Π_s the explicit derivation with $s(q,z)$ of eq. (7.44) leads as well to the ε^{-2} singularity and a non-pole term[1]; both are suppressed in eq. (7.59).

It is evident that the correlators of eqs. (7.54 – 7.57) and those of eqs. (7.58, 7.59) differ. However, it could be shown that the differences are encoded within the polynomial structure of a type $C_0 + C_1 q^2$. These are the known ambiguities of a two-point function. With those subtracted, we arrive at the convergent correlator that has a similar structure in all the cases,

$$\widehat{\Pi}(q^2) = \sum_{n=0}^{\infty} \frac{q^4 F^2(n)}{M^4(n)(-q^2 + M^2(n))}. \tag{7.60}$$

We would soon see that $F_{V/A}^2 \sim \frac{R}{g_5^2} \sim N_c$ and $F_{s/\pi}^2 \sim \frac{R}{k_s} \sim N_c$. Thus, the N_c scaling of the holographic two-point functions is in accordance with that of QCD in 't Hooft limit discussed in Section 3.1.

The most interesting and assumed regularization independent quantity in the spin one sector is the left-right combination Π_{LR}:

$$\Pi_{LR}(q^2) = \Pi_V(q^2) - \Pi_A(q^2). \tag{7.61}$$

In the region of small Euclidean momenta ($Q^2 = -q^2$) at the $(Q^2)^0$ order we obtain from Π_{LR} a constant coefficient that we call F^2. Both vector and axial vector correlators have some non-zero constant factor at this order. Their difference should establish the one free of the short-distance ambiguities. Nevertheless, the final quantity still contains the ε divergence:

$$F^2 = \frac{2R\kappa^2\mu_V}{g_5^2}\left[\psi\left(1+\mu_V\right) - \psi\left(1+\mu_V\frac{1+\beta}{\beta}\right) - \frac{1}{\beta}\left(\ln\kappa^2\varepsilon^2 + 2\gamma_E + \psi\left(1+\mu_V\frac{1+\beta}{\beta}\right)\right)\right] \tag{7.62}$$

[1]The derivation of the scalar two-point function, both in eq. (7.56) and in eq. (7.59), stands out among other cases. In $\Pi_s(q^2) \sim \varepsilon^{-3} s(q,\varepsilon)\partial_z s(q,\varepsilon)$, one has to include several orders in the series: $s(q,\varepsilon) \sim \varepsilon + \varepsilon^3$ and $\partial_z s(q,\varepsilon) \sim \varepsilon^0 + \varepsilon^2$. The estimation of $\partial_z s(q,\varepsilon)$ should be performed carefully in the case of the definition of eq. (7.44) because of taking the small z limit inside the infinite sum.

Otherwise it can be represented as a divergent series

$$F^2 = \sum_n \frac{F_V^2(n)\cdot 4\kappa^2\mu_V/\beta}{M_V^2(n)M_A^2(n)} \tag{7.63}$$

$$= \frac{2R\kappa^2\mu_V}{g_5^2\beta}\sum_n \frac{n+1}{(n+1+\mu_V)(n+1+\mu_V+\mu_V/\beta)}. \tag{7.64}$$

In QCD one finds a definition of $f_\pi \simeq 92$ MeV, the pion decay constant in the chiral limit, in the matrix element of eq. (3.24). To make the connection to the model-defined coefficient F, we have to first introduce some regularization in the latter, and second, take into account that the operators used in the construction of Π_{LR} differ from the one of the standard QCD definition by the yet undetermined factor ${g_V}^2$. Let us assume a vector meson dominance (VMD) like regularization, meaning cutting the sum in eq. (7.63) at the first ($n = 0$) term. Further we will use this VMD limit to estimate the experimental observable as $f_\pi = F_{reg}/g_V$. We will see that this assumption brings a good result for f_π.

The next term in the small-Q^2 expansion, $(Q^2)^1$ order, brings the L_{10} coefficient of the chiral Lagrangian (3.34):

$$g_V^2 L_{10} = \frac{1}{4}\frac{d}{dQ^2}\left(\Pi_V(Q^2)-\Pi_A(Q^2)\right)\Big|_{Q^2=0} \tag{7.65}$$

$$= \frac{R}{8g_5^2}\Bigg[\psi\left(1+\mu_V\right) - \psi\left(1+\mu_V\frac{1+\beta}{\beta}\right) + \mu_V\psi_1\left(1+\mu_V\right) - \mu_V\frac{1+\beta}{\beta}\psi_1\left(1+\mu_V\frac{1+\beta}{\beta}\right)\Bigg]. \tag{7.66}$$

The phenomenological value of L_{10} is given in Table 3.2.

Now let us consider the high-energy asymptotics of the calculated two-point functions. The QCD result for the OPE is well-known and was presented in Section 3.3. We should take into account that the expressions there were computed for the operators with $g_V = g_S = 1$.

The results from our model are the following (assuming that the logarithm regularization in eq. (7.54), in fact, can only be made up to a subtraction constant

[2]The factors g_V and g_S appear due to the conventions taken in eqs. (7.52,7.53). It turns out that they are reabsorbed (using the matching conditions of eq. (7.70)) in the physical parameters of this Section, but not in those related to the three-point correlators.

$\ln(Q^2\varepsilon^2) \to \ln\frac{Q^2}{\mu^2} + \lambda$)

$$\Pi_V(Q^2)/Q^2 = \frac{R}{2g_5^2}\left\{\ln\frac{Q^2}{\mu^2} + \lambda_V + \frac{2\kappa^2}{Q^2}\left[1 + 2\mu_V\left(\ln\frac{Q^2}{\mu^2} + \lambda_V + 1\right)\right] + \frac{4\kappa^4}{3Q^4}\left[-1 + 6\mu_V^2\right] + \frac{16\kappa^6}{3Q^6}\mu_V\left[1 - 2\mu_V^2\right] + \mathcal{O}\left(\frac{1}{Q^8}\right)\right\}, \quad (7.67)$$

and $\Pi_A(Q^2)$ is given by a similar expression with the change $\mu_V \to \mu_V + \frac{\mu_V}{\beta}$. For the spin zero two-point functions we have

$$\Pi_s(Q^2)/Q^2 = \frac{R}{k_s}\left\{\ln\frac{Q^2}{\mu^2} + \lambda_S + \frac{2\kappa^2}{Q^2}\left[1 + (1 + 2\mu_H)\left(\ln\frac{Q^2}{\mu^2} + \lambda_S + 1\right)\right] + \frac{2\kappa^4}{3Q^4}\left[1 + 12\mu_H(1 + \mu_H)\right] + \frac{4\kappa^6}{3Q^6}\left[1 + 2\mu_H\right]\left[1 - 4\mu_H(1 + \mu_H)\right] + \mathcal{O}\left(\frac{1}{Q^8}\right)\right\}, \quad (7.68)$$

$$\Pi_\pi(Q^2)/Q^2 = \frac{R}{2k_s}\frac{\beta}{1+\beta}\left\{\ln\frac{Q^2}{\mu^2} + \lambda_P + \frac{4\kappa^2}{Q^2}\left[\ln\frac{Q^2}{\mu^2} + \lambda_P + \frac{1}{2}\right] + \frac{20\kappa^4}{3Q^4} + \frac{16\kappa^6}{3Q^6} + \mathcal{O}\left(\frac{1}{Q^8}\right)\right\}. \quad (7.69)$$

Matching the corresponding leading logarithmic terms in eqs. (7.67,7.68) and eqs. (3.44,3.48) provides the values of the $5D$ coupling constants

$$g_V^2\frac{g_5^2}{R} = \frac{12\pi^2}{N_c}, \quad g_S^2\frac{k_s}{R} = \frac{16\pi^2}{N_c}. \quad (7.70)$$

However, the scalar and pseudoscalar correlators have different asympotics, and an alternative expression from matching eqs. (3.48) and (7.69) could be $g_S^2\frac{k_s}{R} = \frac{\beta}{1+\beta}\frac{8\pi^2}{N_c}$. The results for k_s coincide for $\beta = -2$ or in the case of the chiral restoration at $\beta = \infty$. Thus, we reach the conclusion that the consistency of the large-Q^2 asymptotics in the scalar sector fixes one of the model parameters to $\beta = -2$. We will see further that even in a global fit to the physical observables where β is allowed to vary its value settles close to this one.

For the left-right correlator, the model gives

$$\Pi_{LR}(Q^2)/Q^2 = -\frac{2R}{g_5^2}\left\{\frac{\kappa^2}{Q^2}\frac{\mu_V}{\beta}\left(\ln\frac{Q^2}{\mu^2} + \lambda_V + 1\right) + \frac{2\kappa^4}{Q^4}\mu_V^2\frac{1 + 2\beta}{\beta^2} + \frac{4\kappa^6}{3Q^6}\frac{\mu_V}{\beta}\left[1 - 2\mu_V^2\left(3 + \frac{3}{\beta} + \frac{1}{\beta^2}\right)\right] + \mathcal{O}\left(\frac{1}{Q^8}\right)\right\}, \quad (7.71)$$

Following eq. (3.44) we are supposed to obtain the manifestation of chiral symmetry breaking $-\eta_{\mu\nu}\Pi_{LR}(Q^2)/Q^2 = -g_V^2\eta_{\mu\nu}\frac{4\pi\alpha_s}{Q^6}\langle q\bar{q}\rangle^2$, while the other terms

should vanish in the chiral limit. The relevant combination is estimated in Ref. [148]: $-4\pi\alpha_s\langle q\bar{q}\rangle^2 = -(1.0 \pm 0.2) \times 10^{-3}$ GeV^6 (in the chiral limit), and in the holographic model we have

$$-4\pi\alpha_s\langle q\bar{q}\rangle^2 = \frac{8\kappa^6}{3}\frac{R}{g_V^2 g_5^2}\frac{\mu_V}{\beta}\left[1 - 2\mu_V^2\left(3 + \frac{3}{\beta} + \frac{1}{\beta^2}\right)\right]. \tag{7.72}$$

The other terms in eq. (7.71) have no counterpart in the chiral limit of QCD: λ in the logarithm regularization can be tuned to provide any constant piece in the $1/Q^2$ term, but the origin of $\ln Q^2/Q^2$ cannot be explained (the problem also encountered in [120]); and the $1/Q^4$ term can only be related to $m_q\langle q\bar{q}\rangle$.

It is a common problem that the holographic models fail to be a match to QCD in these large-Q^2 expansions of the correlators even on a qualitative level. In the setups with an IR cut-off [86, 87, 104] one faces the absolute lack of the next-to-leading order terms in the expansion, and the provided explanation is that the vector sector does not feel the symmetry breaking due to the scalar vev and the breaking effect of the cut-off is decoupling exponentially fast at high energies. Later it was proposed to introduce the condensates by hand in Ref. [149] or through a dynamical scalar with appropriate mass terms and potential coupled to gravity in a braneless approach in Ref. [150].

In the conventional SW model there appears no $1/Q^6$ term in the vector correlator. It is a general feature for the vector two-point functions saturated by the narrow resonances with a spectrum of a type $\sim \kappa^2(n+1)$ [151–153]. The left-right correlator in the SW acquires an order parameter of the chiral symmetry breaking only from the axial vector contribution. There are several propositions to make an improvement in the vector correlator [120, 154], and the appearance of μ_V in the intercept of the spectrum (7.24) can be considered as a possible solution too.

We can speculate on connecting separately the $1/Q^4$ and $1/Q^6$ terms in Π_V and Π_A to the condensates, but that does not sound reasonable. For instance, the gluon condensate prediction is distinct in the two channels, in contradiction to eq. (3.44); nor do we find a constant ratio between the $1/Q^6$ terms. After all, the condensates should manifest themselves as a result of the conformality violation, and both the HW and SW models propose just the simplest ways of doing it – maybe the leading order logarithm is the only term where enough precision can be claimed.

The situation does not become more consistent in the case of spin zero two-point functions. The $1/Q^4$ term in eq. (3.48), associated with the gluon condensate, is coincident in eqs. (7.68) and (7.69) just in the case of $\mu_H = -3/2$, rendering the a_0 state massless. And the constant ratio between the terms at $1/Q^6$ power can

only be achieved with a positive value of μ_H, which is not in the least favoured in other observables.

Let us instead consider an alternative large-Q^2 expansion using the two-point functions of eqs. (7.58) and (7.59). As was mentioned, they are in need of the regularization, and we assume to make it by cutting the tower of resonances at some finite number N_m. As the structure of the correlators (7.58,7.59) is the same, the following asymptotics is true for each one of them

$$\lim_{Q^2\to\infty} \Pi(Q^2)/Q^2 = \frac{\sum\limits_{n=0}^{N_m} F^2(n)}{Q^4} - \frac{\sum\limits_{n=0}^{N_m} F^2(n)M^2(n)}{Q^6} + \mathcal{O}\left(\frac{1}{Q^8}\right). \qquad (7.73)$$

This expression seems more appealing than those in eqs. (7.67-7.69): it has a unified form and there are no unexplicable terms. Furthermore, as in our model $F_V(n) = F_A(n)$ the large-Q^2 limit of Π_{LR}/Q^2 starts with $1/Q^6$. This is translated to the spin zero case, where $F_s^2(n) = 2\frac{1+\beta}{\beta}F_\pi^2(n)$ and the equality can be achieved for $\beta = -2$. This value of the β factor we have already seen in the comparison of the leading logarithmic terms. However, these logarithmic asymptotics themselves do not appear in this type of regularization, they need to have the whole infinite tower. Another drawback is that the gluon condensate comes with the wrong sign in the spin one cases and the quark condensate – in the vector and pseudoscalar channels.

Though these discrepancies are present, the situation for the $1/Q^6$ term with this regularization turns out to be more phenomenologically relevant. The coefficients at $1/Q^6$ power are the following:

$$\Pi_{LR}: \quad \frac{4\kappa^6\mu_V(N_m+1)(N_m+2)}{\pi^2\beta}, \qquad (7.74)$$

$$\Pi_s: \quad -\frac{\kappa^6(N_m+1)(N_m+2)(9+4N_m+6\mu_H)}{\pi^2}, \qquad (7.75)$$

$$\Pi_\pi: \quad -\frac{2\kappa^6 N_m(N_m+1)(N_m+2)}{\pi^2}\frac{\beta}{1+\beta}. \qquad (7.76)$$

Note that in the VMD limit of $N_m = 0$ there is no contribution of this order in the pion correlator due to $m_\pi = 0$. However, the logarithmic-independent quantity of Π_{LR} is not only correctly assessed in the qualitative behavior of its $\frac{1}{Q^2}$ expansion, but the estimate (7.74) in the VMD limit has a better agreement with Ref. [148] than that of eq. (7.72), as we will see in Section 7.6.

7.5 Three-point couplings, pion and axial form factors

The $\rho_n\pi_{n_1}\pi_{n_2}$ coupling is obtained from the $5D$ Lagrangian as an integral over the three KK z-profiles

$$g_{\rho_n,\pi_{n_1},\pi_{n_2}} = \frac{R}{k_s}\int dz e^{-\Phi(\kappa^2 z^2)}\frac{1}{z^3}\frac{2f^2(z)R^2\cdot\beta(1+2\beta)}{\chi_\pi^2(1+\beta)^2}V_n(z)\pi_{n_1}(z)\pi_{n_2}(z). \tag{7.77}$$

The calculation is straightforward for any given set of the radial numbers n, n_1, n_2. In the case that we are only interested in the ground state pions $n_1 = n_2 = 0$, the result is

$$g_{\rho_n,\pi,\pi} = \sqrt{\frac{2g_5^2}{R(n+1)}}\frac{1+2\beta}{1+\beta}(\delta_{n,0}-\delta_{n,1}). \tag{7.78}$$

We also can examine the electromagnetic FF of the pion $G_\pi(q^2)$ defined in eq. (4.15). In the model under investigation it receives two contributions

$$G_\pi(q^2) = \frac{1}{g_V}\frac{1+2\beta}{1+\beta}\sum_n \frac{\delta_{n,0}-\delta_{n,1}}{n+1+\mu_V}\left(1-\frac{q^2}{q^2-M_V^2(n)}\right), \tag{7.79}$$

that means that we go beyond the simplest $\rho(770)$-dominance (VMD) approximation. Moreover, a necessary condition is to normalize $G_\pi(0) = 1$. That allows us to fix the value of g_V,

$$g_V = \frac{1+2\beta}{(1+\beta)(1+\mu_V)(2+\mu_V)}. \tag{7.80}$$

Hereby, we notice that the introduction of this factor was of the outmost importance to the viability of the model, though we are yet to see its role in the phenomenological fits. The coupling of the $\rho(770)$ to the pions is then given by

$$g_{\rho,\pi,\pi} = \sqrt{\frac{24\pi^2}{N_c}}(1+\mu_V)(2+\mu_V). \tag{7.81}$$

The final expression for the pion FF is

$$G_\pi(q^2) = 1-\frac{1}{g_V}\sum_n \frac{q^2F_V(n)}{M_V^2(n)}\frac{g_{\rho_n,\pi,\pi}}{q^2-M_V^2(n)} \tag{7.82}$$

$$= 1-\frac{q^2}{q^2-M_V^2(0)}+\frac{q^2M_V^2(0)}{(q^2-M_V^2(0))(q^2-M_V^2(1))}, \tag{7.83}$$

and its plot can be seen in Fig. 7.1. There we also include as a marker the simplest case of the $\rho(770)$ dominated form factor, it provides a good interpolation

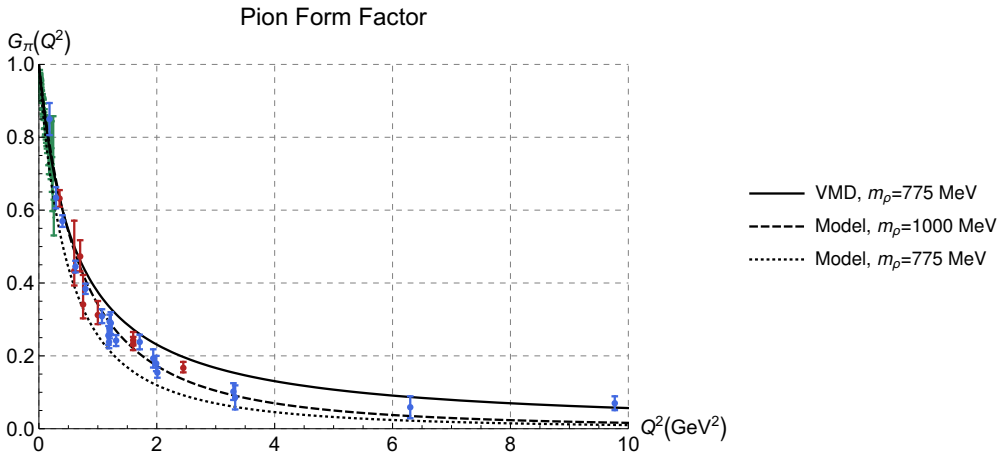

Figure 7.1: The pion form factor plot. The experimental points belong to CERN [155] (green), DESY and Jefferson Lab data [156] (red), and CEA/Cornell [157] (blue). The predicted lines are given for the cases with one vector meson exchange (solid), and two (the other two). The latter is the case of the model under consideration. $m_\rho = 775$ MeV or 1000 MeV and $m_{\rho'} = 1465$ MeV were assumed.

in the $Q^2 \lesssim 1$ GeV^2 region but fails at higher energies. The more conventional holographic models predict the pion FF above the VMD result at $Q^2 \gtrsim 1$ GeV^2 as is nicely displayed in a summary of HW and SW results in Ref. [137], the modified-dilaton SW of Ref. [138] shows a slight improvement, and some other modifications [141, 144] may bring it closer to but not below the VMD shape. A characteristic feature of our model is that it makes a prediction beyond the VMD result, and that brings it much closer to the experimental points in the most studied region $Q^2 \lesssim 3$ GeV^2. We only find an example of similar behavior achieved in the SW model with an additional quartic term in the scalar potential and a specific and rather complicated form of the scalar vev (model IIb of Ref. [144]). It is also obvious from Fig. 7.1 that a higher ρ mass gives a better prediction. The sensitivity to the variations in the ρ' mass is rather negligible. The notion of the value $m_\rho \simeq 1$ GeV origins in an assumption of the ground state positioned on the linear trajectory of the higher radial excitations. We have argued in Section 4.1.1 that this does not appear much irrelevant in a construction based on the reproduction of the linear Regge trajectories. We will come back to this option in Section 7.6.

The large-Q^2 asymptotics of eq. (7.83) is

$$Q^4 G_\pi(Q^2 \to \infty) = M_V^2(0)(M_V^2(0)+M_V^2(1))+\mathcal{O}\left(\frac{1}{Q^2}\right) \simeq 1.65\,\text{GeV}^2, \quad (7.84)$$

and that is not in accordance with the perturbative QCD expectation of $1/Q^2$ fall [158]. This is not really surprising after the discrepancies we have seen in the large-Q^2 behavior of the two-point functions.

At small q^2 we obtain

$$\begin{aligned} G_\pi(q^2) &= 1 + q^2 \frac{1}{g_V} \sum_n \frac{F_V(n) g_{\rho_n,\pi,\pi}}{M_V^4(n)} + \mathcal{O}(q^4) \\ &= 1 + q^2 \left(\frac{1}{M_V^2(0)} + \frac{1}{M_V^2(1)} \right) + \mathcal{O}(q^4) \end{aligned} \tag{7.85}$$

The coefficient at q^2 order is associated to the pion charge radius $r_\pi = \sqrt{\langle r^2 \rangle^{\pi^\pm}}$ and a chiral coefficient L_9 of eq. (3.34):

$$2L_9/f_\pi^2 = \tfrac{1}{6}\langle r^2 \rangle^{\pi^\pm} = \tfrac{1}{M_V^2(0)} + \tfrac{1}{M_V^2(1)}, \tag{7.86}$$

$$L_9 = \tfrac{f_\pi^2}{8\kappa^2} \tfrac{3+2\mu_V}{(1+\mu_V)(2+\mu_V)}. \tag{7.87}$$

The $\rho_n a_{1n_1} \pi_{n_2}$ coupling can also be found from the $5D$ Lagrangian,

$$g_{\rho_n,a_{1n_1},\pi_{n_2}} = \frac{4R}{k_s} \int dz e^{-\Phi(\kappa^2 z^2)} \frac{1}{z^3} \frac{f(z) R (f(z) + b(z)) R \cdot \beta}{\chi_\pi (1+\beta)} D_n(z) C_{n_1}(z) \pi_{n_2}(z). \tag{7.88}$$

For $n_1 = n_2 = 0$ we calculate

$$g_{\rho_n,a_1,\pi} = 4\kappa \sqrt{\frac{\mu_V}{1+\beta}} \sqrt{\frac{2g_5^2}{R(1+n)}} \left(\delta_{n,0} - \delta_{n,1}\right), \tag{7.89}$$

and using the value of g_V from eq. (7.80), the coupling between the three ground states is

$$g_{\rho,a_1,\pi} = 4\kappa \sqrt{\frac{\mu_V}{1+\beta}} \sqrt{\frac{24\pi^2}{N_c}} \frac{(1+\beta)(1+\mu_V)(2+\mu_V)}{1+2\beta}. \tag{7.90}$$

The axial form factor as defined by the diagram in Fig. 4.3 and eq. (4.16) is given by

$$\begin{aligned} G_{a_1}(q^2) &= \frac{2\kappa}{g_V} \sqrt{\frac{\mu_V}{1+\beta}} \sum_n \frac{\delta_{n,0} - \delta_{n,1}}{n + 1 + \mu_V} \left(1 - \frac{q^2}{q^2 - M_V^2(n)} \right) \\ &= \frac{2\kappa \sqrt{\mu_V (1+\beta)}}{1+2\beta} \left[1 - \frac{q^2}{q^2 - M_V^2(0)} + \frac{q^2 M_V^2(0)}{(q^2 - M_V^2(0))(q^2 - M_V^2(1))} \right]. \end{aligned} \tag{7.91}$$

Once the model parameters are fixed we can determine from the q^2 independent part of this expression the direct coupling in $a_1 \to \pi\gamma$ process and estimate the decay rate of eq. (4.20).

7.6 Fitting the observables

With the QCD parameters fixed, $N_c = 3,\ \alpha = \frac{1}{137}$, we have three major model parameters $\kappa,\ \mu_V,\ \beta$, and a free parameter μ_H, that is mostly used to set a_0 mass to the experimental value (if we neglect the chiral condensate prediction from the scalar two-point function).

Let us resume the estimates we have acquired.

Defined from the one-point functions are the constants $F_\rho,\ F_{a_1},\ f_\pi$ in the spin one sector, and $F_s,\ F_\pi$ in the spin zero sector. As was already mentioned our model implies $F_\rho = F_{a_1}$. However, it is shown further that the estimation achieved in some fits lies in between $F_\rho|_{exp}$ and $F_{a_1}|_{exp}$. It is a fair result for our holographic setup. For instance, the usual SW model predicts: $F_\rho|_{SW} = 0.07$ GeV^2, $F_{a_1}|_{SW} = 0.31$ GeV^2. The leptonic decay of ρ' is not as widely discussed, but we can predict, with the model's $F_{\rho'} = \sqrt{2}F_\rho$, the following decay rate $\Gamma_{\rho'\to e^+e^-} = 2 \div 3$ KeV in coincidence, for instance, with Ref. [152]. To evaluate f_π we will use the quantity from eq. (7.63) with just the first term in this generally diverging sum. This concession brings the model prediction close to the experimental value.

In the two-point functions there appear all the phenomenological masses and the aforementioned decay constants. As well there are the low-energy observable L_{10} and the controversially defined estimations for the condensates $\langle q\bar{q}\rangle$ and $\langle G^2\rangle$. At the same time, due to the general discordance in definitions related to the large-Q^2 limit, we find it instructive to evaluate separately f_π and F_π and use as an independent check the chiral limit condition $f_\pi F_\pi = -\langle q\bar{q}\rangle$.

Finally, there are several decay rates defined by the hadronic triple couplings: $\Gamma(\rho \to \pi^+\pi^-)$, $\Gamma(a_1 \to \pi\gamma)$, $\Gamma(a_1 \to \pi\rho)$. And the pion charge radius r_π could be extracted from the pion FF.

Next, we investigate several options to fix the model parameters. We would like to begin with β as a free parameter, thus giving priority to phenomenology over the large-Q^2 asymptotics of $\Pi_\pi(q^2)$. First, we can make a global fit to the highlighted observables. In holography to get the best fit one often minimizes the RMS (root-mean-squared) error, defined as $\varepsilon_{RMS} = \left(\sum_i \frac{(\delta O_i/O_i)^2}{n_{obs}-n_{par}}\right)^{1/2}$, where O_i is an experimental value of an observable, and δO_i is a difference between theoretical and experimental expressions. Naturally, this way the experimental errors are not taken into account at all. But the number ε_{RMS} still communicates the relative precision of the fit and is used to assess the experimental validity of the model

Observable	Experiment	RMS fit $\kappa = 532$ MeV $\beta = -2.12$ $\mu_V = -0.50$ $\mu_H = -0.65$	χ^2 fit $\kappa = 520$ MeV $\beta = -1.85$ $\mu_V = -0.48$ $\mu_H = -0.61$	χ^2 partial A $\kappa = 596$ MeV $\beta = -5.44$ $\mu_V = -0.58$ $\mu_H = -0.82$	χ^2 partial B $\kappa = 583$ MeV $\beta = -1.63$ $\mu_V = -0.46$ $\mu_H = -0.79$
m_ρ	775.26 ± 0.25 MeV	**751.4**	**753.5**	**775.2**	855.9
$m_{\rho'}$	1465 ± 25 MeV	1303.2	1283.8	1421.6	1445.8
m_{a_1}	1230 ± 40 MeV	**912.6**	**919.2**	**866.8**	**1056.3**
$m_{a_1'}$	1654 ± 19 MeV	1402.4	1387.6	1473.5	1572.8
$m_{\pi'}$	1300 ± 100 MeV	**1064.8**	**1039.5**	**1191.6**	1165.2
m_{a_0}	980 ± 20 MeV	**980**	**980**	**980**	**980**
$\rho \to e^+e^-$	7.04 ± 0.06 KeV	**8.56**	**7.72**	12.23	8.31
$\rho \to \pi^+\pi^-$	147.5 ± 0.8 MeV	**219.0**	**253.4**	**147.3**	309.2
$\Gamma(\rho^0) - \Gamma(\rho^\pm)$	0.3 ± 1.3 MeV	1.37	**1.40**	**1.34**	**1.60**
$\frac{\Gamma(\rho \to ee)}{\Gamma(\rho \to \pi\pi)} \cdot 10^4$	0.40 ± 0.05	**0.39**	**0.30**	0.83	**0.27**
$a_1 \to \pi\gamma$	640 ± 246 KeV	**396**	**396**	**202**	**463**
$a_1 \to \pi\rho$	252 ± 105 MeV	**75.9**	**87.3**	**19.7**	**110.3**
r_π	0.659 ± 0.04 fm	**0.742**	**0.744**	**0.710**	**0.656**
$L_{10} \cdot 10^3$	$-(5.5 \pm 0.7)$	**−8.4**	**−7.8**	**−7.2**	**−7.8**
f_π	92.07 ± 1.2 MeV	**96.4**	**92.5**	**92.2**	**104.6**
F_ρ	$0.121237(16)$ GeV^2	**0.1276**	**0.1216**	0.1598	0.1528
F_s	0.21 ± 0.05 GeV^2	**0.156**	**0.149**	0.196	0.187
F_π	0.14 ± 0.03 GeV^2	**0.152**	**0.155**	0.153	0.213

Table 7.1: Global fits. The quantities that were fitted are given in a bold script.

as a whole. Though holographic methods do not claim high accuracy and the experimental precision of some of the discussed observables is impossible to reach, we believe that the more conventional χ^2 method could also be used to provide some extra insight. Thus in Table 7.1 we present both approaches.

Some comments are in order. For the RMS minimization we have omitted the $\Gamma(\rho(770)^0) - \Gamma(\rho(770)^\pm)$ estimation because in this particular situation the error bars, being higher than the mean value, turn out to be particularly important. The inclusion of this observable affects the fit as a whole to the worse, and the model parameters lie in a very different region from any other fit. In this global fit of 15 observables with 4 parameters we get the best fit with $\varepsilon_{RMS} = 36\ \%$, and we consider it a rather good out-turn.

In the χ^2 minimization[3] the inclusion of the lepton decay of ρ and F_ρ puts a lot of constraint on the fit. Especially, it seems impossible to achieve simultaneously a good result for both the lepton and the pion ρ decays. The a_1 decays are also greatly affected by the matching of the model parameters to the more precisely measured ρ-related observables. We try to show to what degree some loosening of the fit affects the predictions. In the "partial A" fit the accuracy of $\rho \to \pi\pi$ rate dominates the fit and the a_1 decays receive an even worse description. In the "partial B" fit, we include the quantities with somewhat larger error bars. The most interesting effect there is a tendency for the higher ρ mass (resulting, of course, in a very high pion decay rate, though the coupling itself is moderate $g_{\rho,\pi,\pi} = 7.39$). The rates of $a_1 \to \rho\pi$ and $a_1 \to \pi\gamma$ come substantially closer to the experiment, as well as the a_1 mass itself. The increase of F_ρ towards $F_{a_1}|_{exp}$ once the lepton decay is out of focus is also evident in both partial fits.

The benefit that F_s gets from the freedom in β is not substantial, except perhaps for the "partial A" fit. Thus, though we introduced a potential difference between F_s and F_π, other observables turn out to outweigh this bit of phenomenology.

Next, we recall the theoretical motivation to implant $\beta = -2$ (coincidental large-Q^2 behavior in the scalar sector) and $\mu_H = -1/2$ (related to the choice of the $f(z)$ ansatz). We would also follow the tentative phenomenological preference for the value of μ_V to be close to $-1/2$, which can be seen in Table 7.1. This allows us to suggest a global fit to the observables with the single remaining free factor – the original SW scale κ. Table 7.2 shows the result of such fitting. We have

[3] Obviously, the values of χ^2_n are huge. We would like to avoid frightening the reader with such numbers and let him or her stay convinced that holographic models are $\sim 30\ \%$ accurate in *some* sense.

fixed $\beta = -2$, $\mu_V = \mu_H = -1/2$ and looked for the best fit minimizing the RMS error. It is provided by the value $\kappa = 527$ MeV. The relative error $\varepsilon_{RMS} = 32\ \%$ is not small, but it still manifests a slightly better agreement than that of a completely free RMS minimization due to the bonus of fitting 15 observables with just one parameter.

Using this fit, we can calculate the triple couplings

$$g_{\rho,\pi,\pi} = 6.66, \qquad (7.92)$$
$$g_{\rho,a_1,\pi} = 6.28 \cdot \kappa = 3.3 \text{ GeV}.$$

The experimental quantities (meaning the ones extracted from the decay rates for the experimental values of the interacting particles' masses) are $g_{\rho,\pi,\pi}|_{exp} = 5.94$, $g_{\rho,a_1,\pi}|_{exp} = 3.9 \div 6.0$ GeV. In light of the standard $g_{\rho,\pi,\pi}|_{SW} = 3.33$ [137] and $g_{\rho,\pi,\pi}|_{HW} = 4.28$ or 5.29 [104], the agreement for the $\rho\pi\pi$ coupling seems to be very good.

Observable	$\kappa = 527$ MeV $\beta = -2$ $\mu_V = \mu_H = -0.5$
m_ρ (MeV)	**745.3**
$m_{\rho'}$ (MeV)	1290.9
m_{a_1} (MeV)	**912.8**
$m_{a_1'}$ (MeV)	1394.3
$m_{\pi'}$ (MeV)	**1054.0**
m_{a_0} (MeV)	**1054.0**
$\rho \to e^+e^-$ (KeV)	**8.43**
$\rho \to \pi^+\pi^-$ (MeV)	**219.5**
$\Gamma(\rho^0) - \Gamma(\rho^\pm)$ (MeV)	1.36
$\frac{\Gamma(\rho\to ee)}{\Gamma(\rho\to\pi\pi)} \cdot 10^4$	**0.38**
$a_1 \to \pi\gamma$ (KeV)	**413**
$a_1 \to \pi\rho$ (MeV)	**80.8**
r_π (fm)	**0.749**
$L_{10} \cdot 10^3$	$\mathbf{-8.6}$
f_π (MeV)	**96.9**
F_ρ (GeV^2)	**0.1250**
F_s (GeV^2)	**0.153**
F_π (GeV^2)	**0.153**

Table 7.2: Single free parameter (κ) global fit. In bold are the fitted quantities. This is the best fit with $\varepsilon_{RMS} = 32\ \%$.

Let us also take this fit to calculate the gluon condensate $\langle \frac{\alpha_s}{\pi} G^2 \rangle$ from eqs. (7.67 – 7.69). The estimate with the correct sign is achieved only from the axial vector two-point function, 0.020 GeV^2 and the pseudoscalar one, 0.16 GeV^2. The predictions are an order different, but we notice that the former is closer to the Shifman-Vainshtein-Zakharov (SVZ) estimate [33], and the latter to the lattice one [35]. The other two give a negative sign for this particular fit, though, for instance, the expression in the scalar correlator provides 0.016 GeV^2 if $\mu_V = -1/2$, $\mu_H = 0$ and in principle can lie in the range of the SVZ estimate. We can also extract the gluon condensate from eq. (7.73), where the relevant term in the spin zero case provides 0.13 GeV^2.

Unfortunately, $\mu_V \simeq -1/2$ in the presented fits leads to the too small or even wrong sign value of $\langle q\bar{q}\rangle$ as defined from Π_{LR} in eq. (7.72). However, if we turn to the alternative expressions (7.74) and assume $N_m = 0$ (the VMD limit taken to determine f_π) the prediction with the fit of Table 7.2 is $4\pi\alpha_s\langle q\bar{q}\rangle^2 = 4.3 \times 10^{-3}$ GeV^6. If the proper term in the scalar correlator (7.75) is used, we get 7.1×10^{-3} GeV^6. These could be related to the assessment of Ref. [148]: $(1.0 \pm 0.2) \times 10^{-3}$ GeV^6. It is of interest that for the $\ln Q^2$ independent quantity such as Π_{LR} its holographic dual with the number of resonance cut-off demonstrates a qualitatively relevant behavior, while the ε cut-off fails. At last, estimating $\langle q\bar{q}\rangle$ as a product of f_π and F_π we get a rather fair result of $\langle q\bar{q}\rangle = -(241 \div 244 \text{ MeV})^3$ if the "partial B" fit is not taken into account.

Coming back to the interpretation of $f(z)$, we can now estimate the constant factor of eq. (7.34), tentatively related to the quark mass, $m_q = \sqrt{\frac{k_5}{g_5^2}\frac{\mu_V}{\beta}}\kappa = 2\kappa\frac{g_V}{g_S}\sqrt{\frac{\mu_V}{3\beta}}$. In the global fits of Table 7.1, $g_V = 3.7 \div 4.3$; assuming that $g_S \simeq g_V$, we can get $m_q \sim 220 \div 360$ MeV. Such values can only be related to the constituent quark mass, if any physical counterpart should be looked for at all.

Finally, we consider some more particular fits in Table 7.3, focusing on reproducing the masses of the states. It is a common practice to do so, especially normalizing to the experimental value of m_ρ like in the "Physical ρ" fit. In the "Heavy ρ" fit we pursue the idea of a higher ρ mass, that would put it on the radial Regge trajectory defined by the ρ excitations. The fits' parameters alter enough from those of the previous fits to make sizeable deviations for the values of the observables. Obviously, the results in Table 7.3 are generally less compatible with experiment. However, we notice that between the two fits the "Heavy ρ" one is significantly better in predicting the lepton ρ decay, the a_1 decays, L_{10} and f_π. It is naturally worse for the pion ρ decay, and the coupling itself is rather large too, $g_{\rho,\pi,\pi} = 8.3$.

7.7 Summary

We have constructed a new holographic model of the two-flavour QCD and have addressed multiple aspects of it. We have described the characteristics of dynamical fields in the scalar and vector sectors corresponding to $\rho,\ a_1,\ a_0$ and π mesons, analyzed the two-point functions and the structure of the pion and axial FFs, and calculated several hadronic couplings.

We questioned several steps in the common model-building strategies and looked

Observable	Physical ρ	Heavy ρ
	$\kappa = 650$ MeV	$\kappa = 650$ MeV
	$\beta = -1.19$	$\beta = -1.35$
	$\mu_V = -0.65$	$\mu_V = -0.41$
	$\mu_H = -0.93$	$\mu_H = -0.93$
m_ρ (MeV)	**775**	**1000**
$m_{\rho'}$ (MeV)	1514	1640
m_{a_1} (MeV)	**1230**	**1230**
$m_{a_1'}$ (MeV)	1790	1790
$m_{\pi'}$ (MeV)	**1300**	**1300**
m_{a_0} (MeV)	**980**	**980**
$\rho \to e^+e^-$ (KeV)	17.3	8.1
$\rho \to \pi^+\pi^-$ (MeV)	94.2	464.5
$\Gamma(\rho^0) - \Gamma(\rho^\pm)$ (MeV)	1.28	1.94
$\frac{\Gamma(\rho\to ee)}{\Gamma(\rho\to\pi\pi)} \cdot 10^4$	1.84	0.17
$a_1 \to \pi\gamma$ (MeV)	1.70	0.43
$a_1 \to \pi\rho$ (MeV)	84.4	129.9
r_π (fm)	0.701	0.566
$L_{10} \cdot 10^3$	-24.5	-6.7
f_π (MeV)	190.6	110.7
F_ρ (GeV^2)	0.190	0.190
F_s (GeV^2)	0.233	0.165
F_π (GeV^2)	0.409	0.325

Table 7.3: Particular fits. The model parameters are determined to provide the experimental masses marked as bold.

for possible generalizations there. At the same time, we required analyticity of our solutions that prohibited overcomplication of the model and even suggested some interrelations between its distinct sectors.

The primary framework is that of the Soft Wall model, the simplest one validating the confining properties of QCD in the linearity of the predicted Regge trajectories. The chiral symmetry breaking occurs as a result of the dual process in the bulk and is subject to the model specifics. Not everything turns up in the QCD-like fashion: there are massless Goldstones and splitting between the vector and axial vector masses, but the OPE-motivated appearance of the chiral condensate in

the two-point functions is not exactly met. One can speculate that introducing a more complicated structure of the scalar vev than that of eq. (7.34) may fix it. It could be also interesting to make simultaneous modifications of the dilaton profile, providing a way to stay consistent with the EOM (e.g., following the lines of [138]). However, first, we will lose the analyticity of the solutions, and second, we do not believe that the result will turn out significantly better. Treating the large-Q^2 limit of QCD in AdS/QCD is wielding a double-edged sword: on one side there is a near-conformality, but on the other is the sidestep from the strongly coupled regime. We cannot suggest any new route; matching the leading logarithms is very useful to establish the holographic couplings in terms of N_c, and the inconsistency of the subleading terms is to be tolerated. Moreover, in the presented model, the study of the leading logarithms of Π_s and Π_π allowed us to fix one of the parameters.

We developed a new approach to the description of the pions. They appear separated from the vector fields, though it obliges us to break the local gauge invariance in the bulk. We also introduced a specified scalar potential. Requirements of analyticity, masslessness of the pions and fulfillment of the holographic conditions on the boundary define it completely. Our prediction for the pion FF in the region $Q^2 \lesssim 3$ GeV^2 leads us to assume this new rendition as phenomenologically relevant.

The parametrization of the model is not quite traditional, because we forsake the use of the quark mass and chiral condensate in the scalar vev, exchanging those for β, and we introduce new parameters in the $5D$ masses: μ_V and μ_H. Mixing the theoretically and phenomenologically preferred values of these parameters, we came to a one-parameter fit of Table 7.2 that provides a fair description of the experimental quantities. Generally, we find that the typical SW scale, κ, can be of order $500 \div 600$ MeV.

We believe that the presented model is neither too artificial nor oversimplified. On the phenomenological level, it is certainly more successful than the traditional HW or SW models, while the motivation and assumptions beyond our modifications are easily accessible.

Among other interesting findings, we would like to mention our proposal to regularize some of the divergent at the boundary quantities via cutting the number of contributing resonances. That is an alternative we have not seen utilized often by other authors. It provides some interesting insight in the OPE-related structures and works genuinely well for the estimation of f_π.

Chapter 8

New Physics: Composite Higgs models

In this chapter we turn towards the study of New Physics. We would like to try using holographic methods to facilitate calculations in some beyond SM strongly-coupled theory. The most interesting candidate for the New Physics in this class is the Composite Higgs (CH). It is a fascinating extension that applies to at least two long-standing issues: naturalness of the EW scale, immediately related to the hierarchy problem, and dynamical generation of the electroweak-symmetry breaking (EWSB), that solves, for instance, the problem of the Higgs potential instability. CH models take a lot of inspiration in the QCD realizations, so we expect that the alternative AdS/QCD treatment could also be effective for this new strongly-coupled sector.

8.1 Motivation for a new strongly-coupled sector

So far the SM predictions are in concordance with all particle physics experiments. The last building block – the Higgs boson, was observed in 2012 with a mass of $m_h \sim 125$ GeV. In the same time, with more experimental data some BSM scenarios become ruled out or severely constrained. Hence, the more attention is put to the models where possible departures with respect to the predictions of the SM are small in a natural way. Misaligned Composite Higgs models [159–163] could be considered as a paradigm of this type of theories.

Despite the phenomenological success the SM suffers from a number of theoretical puzzles. The most prominent, and directly related to the Higgs boson, is the

hierarchy problem. That is the question on why the EW scale is so much smaller than the possible scale of the New Physics. The latter could be the Grand Unification scale $\sim 10^{16}$ GeV, or the Planck scale $\sim 10^{18}$ GeV. We relate the EW scale to the quantity $v = 246$ GeV that appears in the vev of the SM Higgs doublet, and fixes the masses of the W gauge boson, $m_W = \frac{gv}{2}$, and of the Higgs itself, $m_h = \sqrt{2\lambda}v$, where λ is the quartic coupling in the Higgs potential.

This is not a vain question as it is intertwined with the notion of naturalness. By the 't Hooft's definition [164]: at scale Λ a small parameter is technically natural if replacing it with zero would increase the symmetry of the system. For instance, gauge couplings when set to zero turn the gauge bosons into free particles that are separately conserved. Quark masses are natural because there is chiral symmetry. This means that, when quantum corrections to the quark mass are computed, they must be proportional to the bare parameter itself:

$$\delta m_q \propto m_q \log\left(\frac{\Lambda_{UV}}{m_q}\right) + \dots \tag{8.1}$$

where we use the UV cutoff at Λ_{UV} to regularise the loop integrals. In the limit $m_q = 0$, the chiral symmetry is restored and should remain exact, with $\delta m_q = 0$, to all orders in perturbation theory. A notorious problem is that one cannot get a relation like eq. (8.1) for scalar particles, specifically, there is no symmetry to protect the Higgs boson mass.

It is common for a Higgs to interact with Dirac fermions with mass m_f (SM leptons and quarks) through a vertex $-\lambda_f h f \bar{f}$. The corrections to the Higgs mass coming from a loop of these fermions could be estimated as

$$\delta m_h^2 = \frac{|\lambda_f|^2}{8\pi^2}\Lambda_{UV}^2 + \mathcal{O}\left(m_f^2 \log\left(\frac{\Lambda_{UV}}{m_f}\right)\right). \tag{8.2}$$

The largest correction comes from the top quark with $\lambda_f \approx 1$. For $\Lambda_{UV} \sim M_{Pl}$, δm_h^2 can be ~ 30 orders of magnitude larger than the observed value of the Higgs mass. The problem is not that easily solved by introducing some new heavy particles, because m_h^2 is sensitive to the masses of the heaviest particles that Higgs couples to.

SUSY provides a weakly-coupled solution due to the opposite sign loops of fermion superpartners. However, we are not observing in Nature any equal mass superpatners for the SM quarks as is expected from the straightforward SUSY realization. Hence, to make the model viable symmetry breaking terms should be introduced in a way that does not pose another hierarchy problem ("soft" terms).

Even then, one would like to understand the origin of these breaking terms. Nowadays, what was supposed to be the most natural realization of SUSY, the Minimal SUSY Standard Model, is largely disfavoured by the experiments, but there are still many extensions that are not ruled out.

We are more interested in a solution coming from the strongly-coupled sector of New Physics. Its appearance is logical when we recall that in QCD, the well-known strongly coupled theory, the spectrum contains scalar particles, and some of them are very light (pions). There is a simple reason we do not consider them problematic: they are not fundamental degrees of freedom of the SM. Their masses are not the SM parameters, but are related to the confinement scale of QCD, Λ_{QCD}. Hierarchy between Λ_{QCD} and the Planck scale can be easily generated due to the running of the QCD coupling and is considered natural.

Another useful observation about the QCD pions is that they are known to be pseudo–Nambu–Goldstone bosons emerging from the spontaneous breaking of the $SU(2)_L \times SU(2)_R$ chiral symmetry. Due to the explicit breaking by the quark masses pions are not massless Goldstone bosons. But there is a mass gap between them and the rest of the QCD resonances. This mechanism is useful for the explanation of why there are no more new-sector states at the energies of the Higgs mass.

In fact, why could not the quark condensate $\langle \bar{q}_L q_R \rangle$, triggering the spontaneous chiral symmetry breaking, be also responsible for the EW symmetry breaking? Left-handed quarks form weak doublets, while right-handed ones are singlets, hence, $\langle \bar{q}_L q_R \rangle \neq 0$ indeed breaks $SU(2) \times U(1)$. However, then the pion decay constant f_π should set the EW scale. We know from the phenomenology discussed in the previous chapters that it is of order ~ 0.1 GeV, while the true EW scale v should be three orders of magnitude larger to reproduce m_W.

Implementation of such QCD-like features for the sake of explaining the EWSB phenomenon resulted in two major scenarios: Technicolour (TC) and Composite Higgs. The idea of condensate-generated non-perturbative symmetry breaking is realized in both of them. Both speak of a new QCD-like sector with a confining technicolour or hyper-colour (in CH models) gauge group, that forms techni-fermions or hyper-fermions into the bound states. Their "flavour" structures, however, are quite distinct.

Original TC idea was to avoid completely the appearance of Higgs and realize EWSB in a fully dynamical fashion. The techni-fermion condensate was supposed to break the new chiral symmetry $SU(2N_f)_L \times SU(2N_f)_R$, containing the unbro-

ken electric charge $U(1)_{em}$, towards it diagonal subgroup at $\Lambda_{TC} \simeq 4\pi f_{TC}$. The relation to the EW scale is $v = f_{TC}\sqrt{N_{TC}}$. TC models faced various phenomenological challenges long before the Higgs was discovered experimentally and had to be accommodated in this framework, particularly, experimental constraints on flavour-changing neutral currents and precision electroweak measurements. We would not be much interested in this formalism further.

In CH models the breaking is realized in two steps. The global flavour symmetry group $\mathcal{G}$ is broken down to a subgroup $\mathcal{H}$, that contains the SM global group $SU(2) \times U(1)$, due to the condensation of hyper-fermions or some other non-perturbative mechanism at the scale $\Lambda_{CH} \simeq 4\pi f_{CH}$. However, this mechanism does not break EW symmetry, because, for instance, the hyper-fermions are assumed to be in a vectorial representation of $SU(2) \times U(1)$. EWSB is generated by vacuum misalignment: the SM gauge group itself lies in $\mathcal{H}'$ which is rotated with respect to $\mathcal{H}$ by a certain angle θ around one of the broken directions. Usually, the W mass could be expressed through $v = f_{CH} \sin\theta$. That sets a priori a large hierarchy between the symmetry breaking and EW scales. However, a large scale separation, *i.e.* $f_{CH} \gg v$, may lead to a sizeable amount of fine-tuning in order to keep light the states that should remain in the low energy part of the spectrum.

As a concluding remark, we mention the issue of UV completion in CH. Standardly, we assume that the hyper-fermions are charged under a simple hyper-color group, while SM fermions are neutral with respect to it. In general, one can have n_i fermions in each irreducible representation R_i of this gauge group. Let p be the number of different irreps in the model. Then the anomaly-free global symmetry group could only be [165]:

$$\mathcal{G} = SU(n_1) \times \ldots \times SU(n_p) \times U(1)^{p-1}. \tag{8.3}$$

8.2 Minimal Composite Higgs Model

The amount of Goldstones emerging after the symmetry breaking is equal to $dim\,\mathcal{G} - dim\,\mathcal{H}$. At least, we want that the four degrees of freedom of the Higgs doublet are accommodated in the coset space. There are two breaking schemes with exactly four Goldstone bosons: $SU(3) \to SU(2) \times U(1)$ [166] and $SO(5) \to SO(4)$ [167, 168]. The former generally provides large contributions to the Peskin–Takeuchi T parameter. It can be easily protected if we impose another condition on the CH models: that the unbroken subgroup $\mathcal{H}$ necessarily contains the custodial group,

$$\mathcal{H} \supset SU(2)_L \times SU(2)_R. \tag{8.4}$$

As $SO(4) \simeq SU(2) \times SU(2)$ this is fulfilled in the second breaking pattern. For this reasoning, the CH models with $SO(5) \to SO(4)$ are known as Minimal Composite Higgs Models (MCHM).

We notice that $SO(5)$ does not suffice the criterion of the UV completion (8.3). The simplest UV-completable theory will be the next-to-minimal CH with $SO(6) \to SO(5)$, featuring five Goldstone bosons. MCHM constitutes the primary working framework in this chapter because of its simplicity and illustrativeness. We do not dwell any more on its UV completion[1] and try to avoid direct need of knowing its fundamental structure.

Let us see explicitly how vacuum misalignment is realized in MCHM. First, we couple the electroweak sector of the SM to the conserved currents of the new strongly-interacting sector:

$$\mathcal{L} = \widetilde{\mathcal{L}}_{str.int.} + \mathcal{L}_{SM} + \widetilde{J}_L^{\alpha\,\mu} W_\mu^\alpha + \widetilde{J}^{Y\,\mu} B_\mu. \tag{8.5}$$

The currents of the strongly interacting sector $J_L^{\alpha\,\mu}$ and $J^{Y\,\mu}$ contain the generators of the $SU(2)_L \times U(1)$ global group that is necessarily included in $\mathcal{H}$. Moreover, these generators belonging to $\mathcal{H}$ are rotated (and marked with tildes) with respect to the SM gauge group $\mathcal{H}'$ containing the W_μ^α and B_μ electroweak gauge bosons. Similarly, we mark with a tilde $\mathcal{L}_{str.int.}$, corresponding to the strongly interacting sector.

We denote by $T^A,\ A = 1, ..., 10$, the ten generators of $SO(5)$, represented standardly by 5×5 matrices, which are traceless $\mathrm{Tr}\, T^A = 0$ and normalized as $\mathrm{Tr}(T^A T^B) = \delta^{AB}$. They separate naturally into two groups:

- the unbroken generators, in the case of MCHM those of $SO(4) \backsimeq SU(2)_L \times SU(2)_R$, we will call $T^a,\ a = 1, ..., 6$. They are specified as

$$T_L^\alpha = \begin{pmatrix} t_L^\alpha & 0 \\ 0 & 0 \end{pmatrix},\ T_R^\alpha = \begin{pmatrix} t_R^\alpha & 0 \\ 0 & 0 \end{pmatrix},\ \alpha = 1, 2, 3, \tag{8.6}$$

  where $(t_{L/R}^\alpha)_{jk} = -\frac{i}{2}(\varepsilon_{\alpha\beta\gamma}\delta_j^\beta\delta_k^\gamma \pm (\delta_j^\alpha\delta_k^4 - \delta_k^\alpha\delta_j^4))$, $j, k = 1, ..., 4$.

- the broken generators, corresponding to the coset $SO(5)/SO(4)$, are marked as $\widehat{T}^i,\ i = 1, 2, 3, 4$ and defined as follows

$$\widehat{T}_{IJ}^i = -\frac{i}{\sqrt{2}}(\delta_I^i\delta_J^5 - \delta_J^i\delta_I^5),\ \ I, J = 1, ..., 5. \tag{8.7}$$

[1] An interesting proposal is made in Ref. [169], that a certain mechanism can make some UV-complete CH models to be disguised as MCHM.

A quantity parametrizing EWSB is a rotation angle θ that relates the linearly-realized global group $\mathcal{H} = SO(4)$ and a gauged group $\mathcal{H}' = SO(4)'$ containing the electroweak bosons in its subgroup $SU(2)'_L \times U(1)'$. It is natural to denote the generators of $SO(5) \to SO(4)'$ as $\{T^a(0),\ \widehat{T}^i(0)\}$ and of $SO(5) \to SO(4)$ as $\{T^a(\theta),\ \widehat{T}^i(\theta)\}$ so that $\theta = 0$ is assigned to the SM.

We may choose any direction as the one preferred by the $SO(4)'$ and then make the misalignment occur with respect to it, this leads to a connection between the generators such as

$$T^\alpha(\theta) = r(\theta)T^\alpha(0)r^{-1}(\theta),\ \text{with}\ r(\theta) = \begin{pmatrix} 1_{3\times3} & 0 & 0 \\ 0 & \cos(\theta) & \sin(\theta) \\ 0 & -\sin(\theta) & \cos(\theta) \end{pmatrix}. \quad (8.8)$$

The value of θ is expected to be determined basically by a contribution from the top quark to the Higgs potential (that happens to break the custodial symmetry). However, no specific mechanism for the determination of θ will be assumed in this chapter.

The various couplings of the Higgs boson are usually parametrized as follows in EFT [30]:

$$\begin{aligned} \mathcal{L} =& \kappa_Z \frac{m_Z^2}{v} Z_\mu Z^\mu h + \kappa_W \frac{2m_W^2}{v} W_\mu^+ W^{-\mu} h + \kappa_3 \frac{m_h^2}{2v} h^3 && (8.9) \\ &+ \kappa_{VV} \frac{\alpha}{2\pi v} \left(\cos^2\theta_W Z_{\mu\nu} Z^{\mu\nu} + 2W^+_{\mu\nu} W^{-\mu\nu}\right) h && (8.10) \\ &+ \kappa_g \frac{\alpha_s}{12\pi v} G^a_{\mu\nu} G^{a\mu\nu} h + \kappa_\gamma \frac{\alpha}{2\pi v} \gamma_{\mu\nu}\gamma^{\mu\nu} h + \kappa_{Z\gamma} \frac{\alpha}{\pi v} \gamma_{\mu\nu} Z^{\mu\nu} h && (8.11) \\ &- \left(\kappa_t \sum_{f=u,c,t} \frac{m_f}{v} + \kappa_b \sum_{f=d,s,b} \frac{m_f}{v} + \kappa_\tau \sum_{f=e,\mu,\tau} \frac{m_f}{v} \right) f\bar{f}h. && (8.12) \end{aligned}$$

Here we have in the first line the couplings of the Higgs to the SM gauge bosons and the triple self-coupling. The next two lines parametrize couplings to the gauge boson, gluon and photon field strengths. Note, that in the SM, the Higgs boson does not couple directly to massless gauge bosons, hence $\kappa_g = \kappa_\gamma = \kappa_{Z\gamma} = 0$ at tree level. In the last line we have the couplings to the SM fermions.

As a consequence of the custodial symmetry $\kappa_Z = \kappa_W$ at the leading order, and these two parameters are commonly labeled as κ_V. The oblique parameter $T \propto \kappa_Z/\kappa_W - 1$ measures the degree of custodial symmetry breaking and is exactly zero in MCHM. Another relation imposed by this symmetry is

$$(1 - \cos^4\theta_W)\kappa_{VV} = \sin 2\theta_W \kappa_{Z\gamma} + \sin^2\theta_W \kappa_\gamma.$$

We would be interested in the experimental constraints imposed on the Higgs couplings in simplified models, where $\kappa_Z = \kappa_W \equiv \kappa_V$ and all Yukawa couplings scale with the same modifier κ_F. ATLAS and CMS provide results in the form of likelihood contour plots in the (κ_V, κ_F) plane. The latest ATLAS and CMS combined measurements with the LHC Run 1 dataset [30] lead to

$$\kappa_V = 1.04 \pm 0.05, \quad \kappa_F = 0.98^{+0.11}_{-0.10}. \tag{8.13}$$

The ATLAS analysis of Run 2 [30] yields

$$\kappa_V = 1.05 \pm 0.04, \quad \kappa_F = 1.05 \pm 0.09. \tag{8.14}$$

Both in eq. (8.13) and eq. (8.14) the error bars denote one standard deviation.

In MCHM these factors depend on the embedding of the SM fermions in $SO(5)$ representation. The common choices are: spinoral representation, MCHM4, and the fundamental one, MCHM5. In MCHM4: $\kappa_V = \kappa_F = \sqrt{1 - \sin^2\theta}$ [167], while in MCHM5: $\kappa_V = \sqrt{1 - \sin^2\theta}$ and $\kappa_F = \frac{1-2\sin^2\theta}{\sqrt{1-\sin^2\theta}}$ [170]. The trigonometric origin of the misalignment angle imposes $|\kappa_V| \leq 1$ in MCHM, while the best fit lies beyond 1. Nevertheless, the following restrictions could be established at the 95 % CL [171]:

$$\text{MCHM4:} \quad \sin^2\theta < 0.12, \tag{8.15}$$

$$\text{MCHM5:} \quad \sin^2\theta < 0.10. \tag{8.16}$$

The higher the permitted value of $\sin\theta$ the sooner the composite sector appears. For MCHM4, the condition (8.15) implies $f_{CH} > 710$ GeV.

In the alternative analysis of Ref. [172] they conclude that the present LHC data imposes somewhat weaker bounds:

$$\text{MCHM4:} \quad \sin^2\theta < 0.22, \tag{8.17}$$

$$\text{MCHM5:} \quad \sin^2\theta < 0.12. \tag{8.18}$$

They also predict the bounds that would be achieved at future colliders such HL-LHC, ILC, CLIC, *etc*. The future lepton machines are expected to lift f_{CH} to the order of $3 - 4$ TeV.

8.3 Holographic construction

Not much is known about the dynamics and the spectrum of these CH theories, particularly in the cases where the global symmetry $\mathcal{G}$ forbids the realization with

fermions at the microscopic level. Yet, due to the similarities in construction, it is often implicitly assumed that the spectrum in such models can be inferred from what we have learned from QCD. The lack of analytic tools to deal with strongly interacting theories is common to both situations. We have already witnessed the success of holographic techniques in the case of QCD and would like to apply them now in the CH framework.

In fact, MCHM scenario was realized first in Ref. [167, 168] using a HW model. These models have the following characteristics. The gauge symmetry of the SM is extended to the bulk and the symmetry breaking pattern totally relies on the two branes being introduced; the boundary conditions for the $5D$ fields determine whether they correspond to the dynamical fields or not. The Higgs is associated with the fifth component of gauge fields in the direction of the broken gauge symmetry. The Higgs potential is absent at the tree-level and is determined by quantum corrections (dominantly gauge bosons and top quarks at one-loop level). The extensive study in Ref. [167, 168] includes a complete calculation of the Higgs potential and an analysis of several electroweak observables ($S,\ T,\ Z \to b\bar{b}$). The stress is made on a way one embeds SM quarks into $5D$ model (choosing representation *etc.*) as their contribution is crucial for most of the mentioned computations.

In this chapter we use a SW model approach and lay emphasis on an alternative way to realize the global symmetry breaking pattern and to introduce spin zero fields. The $SO(5) \to SO(4)$ breaking happens in the bulk Lagrangian of the scalar fields, reminiscent to the one used for QCD in Chapter 7. The Goldstone bosons are introduced explicitly and their treatment is novel with respect to the former studies in the SW framework in Ref. [173]. Quite differently from the methods adopted in Ref. [167, 168, 173], the dynamics responsible for the $SO(5) \to SO(4)$ breaking is entirely "decoupled" from the SM gauge fields. The latter are treated in fact as external sources that do not participate in the strong dynamics (except eventually through mixing of fields with identical quantum numbers).

We do not consider SM fermion fields either, which in CH scenarios are essential to provide the Higgs potential giving the Higgs mass and self-couplings, among other things [174, 175]. We adopt the point of view that the said potential is of perturbative origin and holographic techniques are not applicable. Needless to say that no new insight into the naturalness problem nor the origin of the hierarchy of the various scales involved is provided. Our attempt is just to describe the strong dynamics behind the composite sector, the resulting spectrum and couplings. We also intend to verify the fulfillment of the expected current algebra properties, such

as the Weinberg sum rules, together with the existing constraints from electroweak precision measurements.

8.3.1 MCHM in $5D$

We would like to construct a $5D$ action with vector and Goldstone degrees of freedom in the spirit of Section 7.2.1. We also try to use similar notations. Let us denote the group transformations $R \in SO(5)$, $r \in SO(4)$. The matrix of the Goldstone fields goes as follows under the SO(5) transformation: $\xi \to \xi' = R\xi r^\top$. The scalar degrees of freedom are collected in Σ transforming as $\Sigma \to \Sigma' = r\Sigma r^\top$. And we can construct a proper combination leading to $H \to H' = RHR^\top$:

$$H = \xi\Sigma\xi^\top,\ \Sigma = \begin{pmatrix} 0_{4\times4} & 0 \\ 0 & f(z) \end{pmatrix} + \sigma^a(x,z)T^a,\ \xi = \exp\left(\frac{i\pi^i(x,z)\widehat{T}^i}{\chi_\pi}\right), \tag{8.19}$$

where $[\chi_\pi] = [f(z)] = E^1$. There scalar degrees of freedom introduced in Σ as σ^a will be further omitted in this study. It follows then that in this representation: $H = H^\top$ and the $\mathrm{Tr}\, HH^\top$ quadratic piece, that normally goes with the mass coefficient M_H^2, brings no field interaction.

The vector fields will be introduced as $A_M = -iA_M^A T^A$, where the upper index runs through both broken and unbroken indices $A_M^a T^a + A_M^i \widehat{T}^i$. We know that every global symmetry of the $4D$ model comes as a gauge symmetry of its $5D$ dual. Thus, to make the Lagrangian invariant under the gauge transformation $A_M \to A'_M = RA_MR^{-1} + iR\partial_M R^{-1}$ the covariant derivative is introduced:

$$D_M H = \partial_M H + [A_M, H], \quad D_M H \to g D_M H g^{-1}. \tag{8.20}$$

The field strength tensor that defines the vector field kinetic is

$$F_{MN} = \partial_M A_N - \partial_N A_M + [A_M, A_N]. \tag{8.21}$$

Finally, the following Lagrangian with $SO(5) \to SO(4)$ breaking defines our model:

$$\begin{aligned} S_{5D} = &-\frac{1}{4g_5^2}\int d^5x\sqrt{-g}e^{-\Phi(z)}\left[\mathrm{Tr}\, F_{MN}F_{KL}g^{MK}g^{NL}\right] + \\ &+\frac{1}{k_s}\int d^5x\sqrt{-g}e^{-\Phi(z)}\left[\mathrm{Tr}\, g^{MN}(D_M H)^\top (D_N H) - M_H^2\,\mathrm{Tr}\, HH^\top\right], \end{aligned} \tag{8.22}$$

with $[g_5^2] = [k_s] = E^{-1}$ and SW profile $\Phi(z) = \kappa^2 z^2$. The similarity of the construction to that of eq. (7.7) is evident. The difference is in the orthogonal symmetry group and the way the symmetry breaking with $f(z)$ is included.

However, closer examination shows that we cannot treat holographic MCHM completely in the AdS/QCD fashion of Chapter 7. That is due to the fact that we wish to abstract our mind from the particularities on the microscopic structure of the new composite states. At first glance, AdS/QCD construction depends very little on, *e.g.*, the quark substructure of mesons. In reality, the form of the operators is crucial. It determines the bulk masses and conditions on the UV behaviour of the bulk-to-boundary propagators, which in their turn affect all other holographic derivations.

In our holographic model for minimal CH we only use a single entry from the list of dualities

$$A_\mu^A(x,\varepsilon) = 1 \cdot \phi_\mu^A(x) \;\leftrightarrow\; O_\mu^A(x) \text{ with } \Delta = 3, \tag{8.23}$$

where O_μ^A are the unspecified conserved currents of the fundamental theory containing $SO(5)$ generators T^A. We take $\Delta = 3$ (and zero bulk mass of the vector fields) as a universal feature for the conserved vector currents, because it should be so both in the case of fermionic ($\overline{\Psi}\gamma_\mu T^A \Psi$) and bosonic ($\partial_\mu s^\top T^A s$) fundamental degrees of freedom. We cannot assume such feature in the scalar sector, and further construct the model so that this part of duality is regarded in an alternative way. The near-boundary behaviour of $\pi(x,z)$ will be determined from considerations of another type; M_H^2 stays free and does not affect any results until we are interested in the yet left out scalar degrees of freedom.

For the fifth component of the vector field we assume it indispensable that

$$A_z^A(x,\varepsilon) = 0, \tag{8.24}$$

because there is no $4D$ source for it to couple to. The common holographic gauge $A_z^A \equiv 0$ fulfills this condition, but this is not the only possibility.

We need to put special attention to the dynamics of the $5D$ fields governed by their EOMs. They are derived from the $5D$ action taken at the quadratic level:

$$\begin{aligned} S_{5D} = \int d^5x e^{-\Phi(z)} \Bigg\{ & -\frac{1}{4g_5^2}\frac{R}{z} F_{\mu\nu}^A F^{A\mu\nu} + \frac{1}{2g_5^2}\frac{R}{z}(\partial_z A_\mu^A - \partial_\mu A_z^A)^2 \\ & + \frac{f^2(z)}{k_s}\frac{R^3}{z^3}\left[\left(A_\mu^i - \partial_\mu \frac{\pi^i}{\chi_\pi}\right)^2 - \left(A_z^i - \partial_z \frac{\pi^i}{\chi_\pi}\right)^2\right]\Bigg\}. \end{aligned} \tag{8.25}$$

Here the sum over the coincident indices is assumed for $A = a, i = 1, \ldots, 10$ in the first line, and just the broken indices $i = 1, \ldots, 4$ in the second.

8.3.2 Unbroken equations of motion

Let us make no further assumptions and write down EOMs for the fields in the unbroken sector with $a = 1, .., 6$:

$$\partial_z \frac{e^{-\Phi(z)}}{z} \partial_z A^a_\mu - \frac{e^{-\Phi(z)}}{z} \Box A^a_\mu - \partial_z \frac{e^{-\Phi(z)}}{z} \partial_\mu A^a_z = 0, \tag{8.26}$$

$$\Box A^a_z = \partial^\mu \partial_z A^a_\mu. \tag{8.27}$$

If we act with ∂^μ on the first equation and substitute $\Box A^a_z$ from the second one, we would get the third term equal to the first one. Then, the result is

$$\Box \partial^\mu A^a_\mu = 0, \tag{8.28}$$

that implies either $\partial^\mu A^a_\mu = 0$ (transversality) or $q^2_{A^\parallel} = 0$ (longitudinal mode) and proposes the separation

$$A^a_\mu = A^{a\perp}_\mu + A^{a\parallel}_\mu, \tag{8.29}$$

with $A^{a\perp}_\mu = \mathcal{P}_{\mu\nu} A^{a\nu}$, $\mathcal{P}_{\mu\nu} = \left(\eta_{\mu\nu} - \frac{q_\mu q_\nu}{q^2}\right)$, and $A^{a\parallel}_\mu = \frac{q_\mu q_\nu}{q^2} A^{a\nu}$.

In return, the condition (8.28) means for the second equation in the system:

$$\Box^2 A^a_z = 0. \tag{8.30}$$

While acting with $\Box^2$ on eq. (8.26) and taking into account $q^2_{A^\perp} \neq 0$ we get the following equation for the transversal mode

$$\partial_z \frac{e^{-\Phi(z)}}{z} \partial_z A^{a\perp}_\mu - \frac{e^{-\Phi(z)}}{z} \Box A^{a\perp}_\mu = 0. \tag{8.31}$$

However, the result for the longitudinal mode with $q^2_{A^\parallel} = 0$ turns out trivial, meaning that the remaining system for $A^{a\parallel}_\mu$ and A^a_z is underdefined. We choose to work in a class of solutions where eq. (8.30) is fulfilled with the gauge

$$A^a_z(x, z) = 0. \tag{8.32}$$

The EOM for the longitudinal mode simplifies to

$$\partial_z A^{a\parallel}_\mu = 0. \tag{8.33}$$

We have the following boundary terms left in the on-shell action (8.25)

$$\begin{aligned} \frac{1}{2g_5^2} \quad & \int d^4x e^{-\Phi(z)} \tfrac{R}{z} A^{a\mu} (\partial_z A^a_\mu - \partial_\mu A^a_z)\big|^\infty_\varepsilon \\ & = -\tfrac{1}{2g_5^2} \int d^4x \, \tfrac{R}{z} A^{a\perp\mu} \partial_z A^{a\perp}_\mu \big|_{z=\varepsilon}. \end{aligned} \tag{8.34}$$

In the end, there is just the transversal term, giving rise to the corresponding two-point function.

From eqs. (8.31) and (8.33), the bulk-to-boundary solutions for the Fourier transformates $A^a_\mu(q,z)$ are

$$A^{a\perp}_\mu(q,z) = \phi^{a\perp}_\mu(q)\cdot V(q,z),\ V(q,z) = \Gamma\left(1-\frac{q^2}{4\kappa^2}\right)\Psi\left(-\frac{q^2}{4\kappa^2},0;\kappa^2 z^2\right), \tag{8.35}$$

$$A^{a\parallel}_\mu(q,z) = \phi^{a\parallel}_\mu(q)\cdot V^{\parallel}(q,z),\ V^{\parallel}(q,z) = 1, \tag{8.36}$$

where $\phi^{a\perp}_\mu$ and $\phi^{A\parallel}_\mu$ should be understood as projections of the original source on the relevant directions.

The subdominant solution of eq. (8.31) gives us the tower of massive states, identified with vector composite resonances at the boundary:

$$A^{a\perp}_\mu(q,z) = \sum_{n=0}^{\infty} V_n(z) A^{a\perp}_{\mu(n)}(q), \tag{8.37}$$

$$V_n(z) = \kappa^2 z^2 \sqrt{\frac{g_5^2}{R}}\sqrt{\frac{2}{n+1}} L^1_n(\kappa^2 z^2), \quad M_V^2(n) = 4\kappa^2(n+1). \tag{8.38}$$

The orthogonality relation is completely equivalent to that of eq. (7.22).

There is nothing new to this result, it could be achieved by imposing $A^a_z = 0$ from the start as is done in classical AdS/QCD papers. Nevertheless, we consider this exercise worthy for the further implementation in the broken sector.

8.3.3 Broken equations of motion

The EOMs for the broken sector with $i = 1,..,4$ are more complicated due to the appearance of mixing with π^i:

$$\partial_z \frac{e^{-\Phi(z)}}{z}\left(\partial_z A^i_\mu - \partial_\mu A^i_z\right) - \frac{e^{-\Phi(z)}}{z}\Box A^i_\mu - \frac{2g_5^2 f^2(z) R^2}{k_s}\frac{e^{-\Phi(z)}}{z^3}\left(A^i_\mu - \frac{\partial_\mu \pi^i}{\chi_\pi}\right) = 0 \tag{8.39}$$

$$\frac{e^{-\Phi(z)}}{z}\left(\partial^\mu \partial_z A^i_\mu - \Box A^i_z\right) - \frac{2g_5^2 f^2(z) R^2}{k_s}\frac{e^{-\Phi(z)}}{z^3}\left(A^i_z - \partial_z \frac{\pi^i}{\chi_\pi}\right) = 0 \tag{8.40}$$

$$\partial_z \frac{f^2(z) R^2 e^{-\Phi(z)}}{z^3}\left(A^i_z - \partial_z \frac{\pi^i}{\chi_\pi}\right) - \frac{f^2(z) R^2 e^{-\Phi(z)}}{z^3}\left(\partial^\mu A^i_\mu - \Box \frac{\pi^i}{\chi_\pi}\right) = 0 \tag{8.41}$$

Combining $\partial^\mu\times$ (8.39) with other two equations we again result in

$$\Box\partial^\mu A^i_\mu = 0, \tag{8.42}$$

with the same options $\partial^\mu A^i_\mu = 0$ and $q^2_{A\|} = 0$ as in the unbroken case. The condition on A^i_z is different though

$$\partial_z \frac{e^{-\Phi(z)}}{z}\Box^2 A^i_z - \frac{2g_5^2 f^2(z)R^2 e^{-\Phi(z)}}{k_s z^3}\Box^2\frac{\pi^i}{\chi_\pi} = 0. \tag{8.43}$$

We encounter the system on $A^{i\|}_\mu$, A^i_z and π^i insufficient for the reasons similar to the ones before, and are apt to solve the problem with appropriate gauge condition. There are various possible solutions of the system, but we find the option explained below the most useful for the physics we aspire to describe. To make sense of the condition (8.43) we impose

$$A^i_z(x,z) = \xi\partial_z\frac{\pi^i(x,z)}{\chi}, \tag{8.44}$$

where the parameter ξ is arbitrary at first. The fact that $\pi^i(x,z)$ appears both in the scalar part of the model Lagrangian and in this gauge condition makes it distinct from other $5D$ fields in the model. To analyze the Goldstone solution we assume that the corresponding EOM defines the z-profile $\pi(x,z)$ that couples to the physical mode $\pi^i(x)$ on the boundary. The Neumann boundary condition, $\partial_z\pi(x,z)|_{z=\varepsilon} = 0$, is imposed due to eq. (8.24).

Now both parts of eq. (8.43) have the same x-dependence, and $\Box^2$ can be taken out of the bracket. The rest of eq. (8.43) we postulate as the condition similar to $A^a_z = 0$. It results in the following equation on $\pi(x,z)$:

$$\partial_z\frac{e^{-\Phi(z)}}{z}\partial_z\pi(x,z) - \frac{2g_5^2 f^2(z)R^2}{\xi k_s}\frac{e^{-\Phi(z)}}{z^3}\pi(x,z) = 0. \tag{8.45}$$

In the same time it allows to get rid of A^i_z and $\partial_\mu\frac{\pi^i}{\chi_\pi}$ in eq. (8.39). Then,

$$\partial_z\frac{e^{-\Phi(z)}}{z}\partial_z A^{i\perp}_\mu - \frac{e^{-\Phi(z)}}{z}\Box A^{i\perp}_\mu - \frac{2g_5^2 f^2(z)R^2}{k_s}\frac{e^{-\Phi(z)}}{z^3}A^{i\perp}_\mu = 0, \tag{8.46}$$

$$\partial_z\frac{e^{-\Phi(z)}}{z}\partial_z A^{i\|}_\mu - \frac{2g_5^2 f^2(z)R^2}{k_s}\frac{e^{-\Phi(z)}}{z^3}A^{i\|}_\mu = 0. \tag{8.47}$$

At the boundary we have the following terms in the effective $4D$ action:

$$\int d^4x\left[\frac{R}{z}\frac{e^{-\Phi(z)}}{2g_5^2}A^{i\mu}(\partial_z A^i_\mu - \partial_\mu A^i_z) + \frac{f^2(z)R^2}{z^3}\frac{e^{-\Phi(z)}R}{k_s}\frac{\pi^i}{\chi_\pi}\left(A^i_z - \partial_z\frac{\pi^i}{\chi_\pi}\right)\right]\Bigg|_0^\infty$$

$$\xrightarrow{\xi=1} -\frac{1}{2g_5^2}\int d^4x\,\frac{R}{z}\left(A^{i\perp\mu}\partial_z A^{i\perp}_\mu + A^{i\|\mu}\partial_z A^{i\|}_\mu - A^{i\mu}\partial_\mu\partial_z\frac{\pi^i}{\chi_\pi}\right)\Bigg|_{z=\varepsilon} \tag{8.48}$$

The two-point function of the longitudinal mode is non-zero and that is the crucial difference from the previous sector. We explain the choice $\xi = 1$ in a minute. For now we observe that it makes identical the bulk EOMs for π^i and $A_\mu^{i\parallel}$ and eliminates the Goldstone mass term from the boundary: for $\xi = 1$ all the Goldstones (including the component associated to the Higgs) are massless.

It is also instructive to justify the system of EOMs (8.45)–(8.47) by deriving them in the model where we set from the start $\xi = 1$ in eq. (8.44) and implement it into eqs. (8.39)-(8.41). Then, the system on A_μ^i and π^i simplifies to

$$\partial_z \frac{e^{-\Phi(z)}}{z} \partial_z A_\mu^i - \frac{e^{-\Phi(z)}}{z} \Box A_\mu^i - \frac{2g_5^2 f^2(z) R^2}{k_s} \frac{e^{-\Phi(z)}}{z^3} A_\mu^i - \partial_\mu \left(\partial_z \frac{e^{-\Phi(z)}}{z} \partial_z \frac{\pi^i}{\chi_\pi} - \frac{2g_5^2 f^2(z) R^2}{k_s} \frac{e^{-\Phi(z)}}{z^3} \frac{\pi^i}{\chi_\pi} \right) = 0 \quad (8.49)$$

$$\partial^\mu A_\mu^i = \Box \frac{\pi^i}{\chi_\pi} \quad (8.50)$$

The condition of eq. (8.42) holds, and together with eq. (8.50) it implies that

$$\Box^2 \frac{\pi^i}{\chi_\pi} = 0. \quad (8.51)$$

With the use of the identity $A_\mu^{i\parallel} = \frac{\partial_\mu \partial^\nu}{\Box} A_\nu^i = \partial_\mu \frac{\pi^i}{\chi_\pi}$, the longitudinal part in eq. (8.49) transforms into

$$\partial_z \frac{e^{-\Phi(z)}}{z} \partial_z A_\mu^{i\parallel} - \frac{2g_5^2 f^2(z) R^2}{k_s} \frac{e^{-\Phi(z)}}{z^3} A_\mu^{i\parallel} - \partial_\mu \left(\partial_z \frac{e^{-\Phi(z)}}{z} \partial_z \frac{\pi^i}{\chi_\pi} + \frac{e^{-\Phi(z)}}{z} \Box \frac{\pi^i}{\chi_\pi} - \frac{2g_5^2 f^2(z) R^2}{k_s} \frac{e^{-\Phi(z)}}{z^3} \frac{\pi^i}{\chi_\pi} \right) = 0. \quad (8.52)$$

All things considered, one of the possible solutions is this set of simultaneously fulfilled equations

$$\partial_z \frac{e^{-\Phi(z)}}{z} \partial_z A_\mu^{i\parallel} - \frac{2g_5^2 f^2(z) R^2}{k_s} \frac{e^{-\Phi(z)}}{z^3} A_\mu^{i\parallel} = 0, \quad (8.53)$$

$$\partial_z \frac{e^{-\Phi(z)}}{z} \partial_z \frac{\pi^i}{\chi_\pi} - \frac{2g_5^2 f^2(z) R^2}{k_s} \frac{e^{-\Phi(z)}}{z^3} \frac{\pi^i}{\chi_\pi} = 0, \quad (8.54)$$

$$\Box \frac{\pi^i}{\chi_\pi} = 0, \quad (8.55)$$

while the transverse mode keeps being described by eq. (8.46). With this exercise we intend to be reassured that the masslessness of the Goldstones agrees with EOMs (8.45)–(8.47).

As in the unbroken case we perform the $4D$ Fourier transformation and establish the propagation between the source and the bulk for the transverse and longitudinal solutions:

$$A_\mu^{i\perp}(q,z) = \phi_\mu^{i\perp}(q)\cdot A(q,z),$$
$$A(q,z) = \Gamma\left(1-\frac{q^2}{4\kappa^2}+a\right)\Psi\left(-\frac{q^2}{4\kappa^2}+a,0;\kappa^2z^2\right), \quad (8.56)$$
$$A_\mu^{i\parallel}(q,z) = \phi_\mu^{i\parallel}(q)\cdot A^{\parallel}(q,z),\ \ A^{\parallel}(q,z) = \Gamma\left(1+a\right)\Psi\left(a,0;\kappa^2z^2\right). \quad (8.57)$$

Here we assumed just like in Chapter 7 the ansatz

$$f^2(z)R^2 = (fR)^2\cdot\kappa^2z^2, \quad (8.58)$$

and further collected the model parameters into the parameter

$$a = \frac{g_5^2(fR)^2}{2k_s}. \quad (8.59)$$

The KK expansion is similar to the unbroken sector but for the shifted masses:

$$A_\mu^i(q,z) = \sum_{n=0}^{\infty} A_n(z)A_{\mu(n)}^i(q), \quad (8.60)$$
$$A_n(z) = \kappa^2z^2\sqrt{\frac{g_5^2}{R}}\sqrt{\frac{2}{n+1}}L_n^1(\kappa^2z^2), \quad M_A^2(n) = 4\kappa^2(n+1+a). \quad (8.61)$$

These states are heavier than their unbroken counterparts just as in QCD axial vector mesons are heavier then the vector ones.

The Goldstone EOM (8.45) is the same as (8.47). However, we should normalize the Goldstone kinetic term in the $4D$ effective Lagrangian appearing after the integration over the z-dimension to $\frac{1}{2}(\partial_\mu\pi^i(x))^2$, and that fixes the constant factor differently:

$$\pi(x,z) = F^{-1}\chi_\pi\Gamma\left(1+a\right)\Psi\left(a,0;\kappa^2z^2\right), \quad (8.62)$$

where

$$F^2 = -\frac{2R\kappa^2a}{g_5^2}\left(\ln\kappa^2\varepsilon^2+2\gamma_E+\psi\left(1+a\right)\right). \quad (8.63)$$

In the next section we find the same F^2 in the residue of the massless pole of the broken vector correlator. The exact accordance is only possible for $\xi = 1$. Furthermore, solution (8.62) fixes the due boundary interaction

$$\int d^4x(-F)\partial^\mu\pi^i(x)\phi_\mu^i(x). \quad (8.64)$$

As a result of W_μ^α and B_μ couplings in eq.(8.5) the mixing in eq.(8.64) for $i = 1, 2, 3$ implies that the three Goldstones would be eaten by the SM gauge bosons to provide them masses proportional to F. Notice that there is no physical source to mix with the fourth Goldstone, it remains in the model as the physical Higgs particle $\pi^4(x) = h(x)$. The phenomenological discussion of its properties are postponed to a latter section.

As we have seen in the case of QCD, it is also convenient to use the bulk-to-boundary propagators given as the sum over the resonances. In our notation the definition is the same as before:

$$V(q,z) = \sum_{n=0}^{\infty} \frac{F_V(n)V_n(z)}{-q^2 + M_V^2(n)}, \quad A(q,z) = \sum_{n=0}^{\infty} \frac{F_A(n)A_n(z)}{-q^2 + M_A^2(n)}, \tag{8.65}$$

$$F_A^2(n) = F_V^2(n) = \frac{8R\kappa^4}{g_5^2}(n+1), \tag{8.66}$$

with $F_{V/A}(n)$ being the decay constants related to the states with the corresponding quantum numbers. For the longitudinal broken and Goldstone solutions we can use a representation of the Tricomi function given in eq. (A.7).

8.4 Two-point functions in the vector sector

From the general holographic prescriptions establish we can calculate the two-point correlation functions of two unbroken or two broken operators:

$$\langle \mathcal{O}_\mu^{a/i}(q)\mathcal{O}_\nu^{b/j}(p)\rangle = \delta(p+q)\int d^4x e^{iqx}\langle \mathcal{O}_\mu^{a/i}(x)\mathcal{O}_\nu^{b/j}(0)\rangle = \frac{\delta^2 i S^{5D}_{boundary}}{\delta i\phi_\mu^{a/i}(q)\delta i\phi_\nu^{b/j}(p)}. \tag{8.67}$$

Similarly to the QCD case (see Section 7.4), let us establish the definitions for the transverse part of the vector correlators:

$$i\int d^4x e^{iqx}\langle \mathcal{O}_\mu^{a/i}(x)\mathcal{O}_\nu^{b/j}(0)\rangle_\perp = \delta^{ab/ij}\left(\frac{q_\mu q_\nu}{q^2} - \eta_{\mu\nu}\right)\Pi_{unbr/br}(q^2). \tag{8.68}$$

We can calculate them using the bulk-to-boundary propagators given in the previous section:

$$\Pi_{unbr}(q^2) = -\frac{R}{2g_5^2}q^2\left[\ln\kappa^2\varepsilon^2 + 2\gamma_E + \psi\left(-\frac{q^2}{4\kappa^2}+1\right)\right], \tag{8.69}$$

$$\Pi_{br}(q^2) = -\frac{R}{2g_5^2}q^2\left(1-\frac{4\kappa^2 a}{q^2}\right)\left[\ln\kappa^2\varepsilon^2 + 2\gamma_E + \psi\left(-\frac{q^2}{4\kappa^2}+1+a\right)\right]. \tag{8.70}$$

The latter correlator brings the "pion decay constant" F of the composite sector as a first term in its small-q^2 expansion. It turns out exactly as in eq. (8.63).

In the "resonance" representation correlator expressions a-la eq. (7.58) are:

$$\Pi_{unbr}(q^2) = \sum_{n=0}^{\infty} \frac{F_V^2(n)}{-q^2 + M_V^2(n)},\ \Pi_{br}(q^2) = \sum_{n=0}^{\infty} \frac{F_A^2(n)}{-q^2 + M_V^2(n)}, \tag{8.71}$$

$$F_V^2(n) = F_A^2(n) = \frac{8R\kappa^4}{g_5^2}(n+1). \tag{8.72}$$

For both representations the result after neglecting the short-distance ambiguities of the type $C_0 + C_1 q^2$ is:

$$\widehat{\Pi}_{unbr}(Q^2) = \sum_n \frac{Q^4 F_V^2(n)}{M_V^4(n)(Q^2+M_V^2(n))}; \tag{8.73}$$

$$\widehat{\Pi}_{br}(Q^2) = \sum_n \frac{Q^4 F_A^2(n)}{M_A^4(n)(Q^2+M_A^2(n))} - F^2, \tag{8.74}$$

$$F^2 = \frac{2R\kappa^2 a}{g_5^2} \sum_n \frac{1}{n+1+a}. \tag{8.75}$$

Concordance in the ambiguity cancellation and between the definitions of F^2 in (8.63) and (8.75) is only achieved under condition connecting the UV regulator ε and the resonance cut-off N_{max}:

$$\log N_{max} = -2\gamma_E - \log \kappa^2 \varepsilon^2. \tag{8.76}$$

It is also relevant to establish the two-point function in the longitudinal direction:

$$i \int d^4x e^{iqx} \langle \mathcal{O}_\mu^i(x) \mathcal{O}_\nu^j(0) \rangle_\parallel = \delta^{ij} \frac{q_\mu q_\nu}{q^2} \Pi_{br}^\parallel(q^2). \tag{8.77}$$

Variation over the longitudinal modes in eq. (8.48) also brings the pion decay constant:

$$\Pi_{br}^\parallel(q^2) = F^2. \tag{8.78}$$

In the end, these correlation functions appear in the $4D$ effective Lagrangian as

$$\begin{aligned} \mathcal{L}_{eff} \supset & \frac{1}{2}\phi_\mu^a \left(\frac{q_\mu q_\nu}{q^2} - \eta_{\mu\nu} \right) \Pi_{unbr} \phi_\nu^a \\ & + \frac{1}{2}\phi_\mu^i \left(\left(\frac{q_\mu q_\nu}{q^2} - \eta_{\mu\nu} \right) \Pi_{br} + \frac{F^2 q^\mu q^\nu}{q^2} \right) \phi_\nu^i. \end{aligned} \tag{8.79}$$

8.4.1 Vacuum polarization amplitudes of the gauge fields

We started the discussion about CH with an idea of eq. (8.5) that the SM gauge fields couple to the currents of the strongly interacting sector $\widetilde{J}^{\alpha}_{L\mu}$ and $\widetilde{J}^{Y}_{R\mu} = \widetilde{J}^{3}_{R\mu}$. These currents are proportional to the ones dual to the $5D$ fields, $O^{a/i}_{\mu}$, with the EW couplings g and g' necessarily appearing, and the misalignment should be taken into account. A rotated operator can be given in terms of the original ones as ($i = 1, 2, 3$ here):

$$\widetilde{\mathcal{O}}^{\alpha}_{L/R\mu} = \frac{1 \pm \cos\theta}{2}\mathcal{O}^{\alpha}_{L\mu} + \frac{1 \mp \cos\theta}{2}\mathcal{O}^{\alpha}_{R\mu} \mp \frac{\sin\theta}{\sqrt{2}}\mathcal{O}^{i} \tag{8.80}$$

We introduce the factor g_V to quantify that proportionality to the EW couplings:

$$\widetilde{J}^{\alpha}_{L\mu} = \frac{g}{\sqrt{2}g_V}\widetilde{\mathcal{O}}^{\alpha}_{L\mu}, \quad \widetilde{J}^{3}_{R\mu} = \frac{g'}{\sqrt{2}g_V}\widetilde{\mathcal{O}}^{3}_{R\mu} \tag{8.81}$$

The two-point correlators of interest for us are:

$$i\int d^4x e^{iqx}\langle \widetilde{J}^{\alpha}_{L\mu}(x)\widetilde{J}^{\beta}_{L\nu}(0)\rangle = \delta^{\alpha\beta}\frac{g^2}{2}\left[\left(\frac{q_\mu q_\nu}{q^2} - \eta_{\mu\nu}\right)\Pi_{LL}(q^2) + \frac{q_\mu q_\nu}{q^2}\Pi^{\parallel}_{LL}(q^2)\right], \tag{8.82}$$

$$i\int d^4x e^{iqx}\langle \widetilde{J}^{\alpha}_{R\mu}(x)\widetilde{J}^{\beta}_{R\nu}(0)\rangle = \delta^{\alpha\beta}\frac{g'^2}{2}\left[\left(\frac{q_\mu q_\nu}{q^2} - \eta_{\mu\nu}\right)\Pi_{RR}(q^2) + \frac{q_\mu q_\nu}{q^2}\Pi^{\parallel}_{RR}(q^2)\right], \tag{8.83}$$

$$2i\int d^4x e^{iqx}\langle \widetilde{J}^{\alpha}_{L\mu}(x)\widetilde{J}^{\beta}_{R\nu}(0)\rangle = \delta^{\alpha\beta}\frac{gg'}{2}\left[\left(\frac{q_\mu q_\nu}{q^2} - \eta_{\mu\nu}\right)\Pi_{LR}(q^2) + \frac{q_\mu q_\nu}{q^2}\Pi^{\parallel}_{LR}(q^2)\right]; \tag{8.84}$$

where we defined the quantities

$$\Pi_{diag}(q^2) = \Pi_{LL}(q^2) = \Pi_{RR}(q^2) = \frac{1+\cos^2\theta}{2g_V^2}\Pi_{unbr}(q^2) + \frac{\sin^2\theta}{2g_V^2}\Pi_{br}(q^2), \tag{8.85}$$

$$\Pi_{LR}(q^2) = \frac{\sin^2\theta}{g_V^2}\left(\Pi_{unbr}(q^2) - \Pi_{br}(q^2)\right), \tag{8.86}$$

$$\Pi^{\parallel}_{LL}(q^2) = \Pi^{\parallel}_{RR}(q^2) = \frac{\sin^2\theta}{2g_V^2}F^2,\ \Pi^{\parallel}_{LR}(q^2) = -\frac{\sin^2\theta}{g_V^2}F^2. \tag{8.87}$$

The relevant quadratic contribution of the gauge bosons to the $4D$ partition function is:

$$\begin{aligned}\mathcal{L}_{eff} \supset & \left(\frac{q^\mu q^\nu}{q^2} - \eta^{\mu\nu}\right)\frac{1}{4}\Pi_{diag}(q^2)(g^2 W_\mu^\alpha W_\nu^\alpha + g'^2 B_\mu B_\nu) \\ & + \frac{F^2\sin^2\theta}{8g_V^2}\frac{q^\mu q^\nu}{q^2}(g^2 W_\mu^\alpha W_\nu^\alpha + g'^2 B_\mu B_\nu) \\ & + \left(\frac{q^\mu q^\nu}{q^2} - \eta^{\mu\nu}\right)\frac{1}{4}\Pi_{LR}(q^2) g g' W_\mu^3 B_\nu - \frac{q^\mu q^\nu}{q^2}\frac{F^2\sin^2\theta}{4g_V^2} g g' W_\mu^3 B_\nu.\end{aligned} \tag{8.88}$$

The mass terms in the effective Lagrangian can be determined from the lowest order in q^2. Both for the longitudinal and transverse W's and Z gauge bosons we get

$$M_W^2 = \frac{g^2}{4}\frac{\sin^2\theta}{g_V^2}F^2,\ M_Z^2 = \frac{g^2+g'^2}{4}\frac{\sin^2\theta}{g_V^2}F^2, \tag{8.89}$$

while the photon stays massless.

8.4.2 Left–right correlator and Weinberg sum rules

The oblique corrections to the SM physics [176, 177] are defined to follow the new physics contributions to the vacuum polarization amplitudes (new massive resonances in the loops). The S and T parameters of Peskin and Takeuchi [177] are the most relevant for the discussion of the CH models. However, due to the custodial symmetry of the strongly interacting sector the tree-level correction to the T parameter vanishes in the $SO(5) \to SO(4)$ model under consideration as we have already mentioned. The analysis of the next-to-leading-order corrections does not seem to be well-motivated as they are suppressed in the large-N_{tc} limit, where the holographic description is valid. Thus, we focus on the S parameter connected to the $\Pi_{LR}(q^2)$ as follows

$$S = -4\pi\Pi'_{LR}(0) = \frac{2\pi R}{g_5^2}\frac{\sin^2\theta}{g_V^2}\left[\gamma_E + \psi\left(1+a\right) + a\psi_1\left(1+a\right)\right]. \tag{8.90}$$

Alternatively, it could be expressed through masses and decay constants:

$$S = 4\pi\frac{\sin^2\theta}{g_V^2}\left[\sum_n \frac{F_V^2(n)}{M_V^4(n)} - \sum_n \frac{F_A^2(n)}{M_A^4(n)}\right]. \tag{8.91}$$

Let us now investigate the validity of the equivalent of the Weinberg sum rules that relate the imaginary part of $\Pi_{LR}(q^2)$ to the masses and decay constants of the vector resonances in the broken and unbroken channels. The way to proceed is to

equate Π_{unbr} to its subtracted counterpart given by eq. (8.73) and do the same with the equivalent expressions in the broken sector (*i.e.* take eq. (8.74). One selects a suitable integration circuit and formally

$$\frac{1}{\pi}\int_0^\infty \frac{dt}{t}\mathrm{Im}\Pi_{unbr}(t) = \sum_n \frac{F_V^2(n)}{M_V^2(n)}, \tag{8.92}$$

$$\frac{1}{\pi}\int_0^\infty \frac{dt}{t}\mathrm{Im}\Pi_{br}(t) = \sum_n \frac{F_A^2(n)}{M_A^2(n)} + F^2. \tag{8.93}$$

However, these expressions are ill-defined as neither the imaginary part of the poles has been properly defined (in the resonance expansions (8.73) and (8.74)) nor does the external contour vanish. Clearly, the left hand sides of the above expressions are generically divergent. In addition, the sum over resonances should possess an essential singularity on the real axis when the number of resonances N_{max} encircled in the contour tends to infinity.

In order to define the sum over the resonances more correctly we introduce the imaginary parts proportional to the masses following Vainshtein, *i.e.* we replace $M_V^2(n)$ in eq. (8.73) to $M_V^2(n)(1 - i\epsilon)$. This prescription reproduces the correct residues.

As is well known the convergence properties of the integrals on the left hand side of (8.92) and (8.93) are greatly improved if one considers the left-right combination. We introduce for uniformity the sum $F^2 = \sum_{n<N_{max}} F^2(n)$ (see eq. (8.75)) and therefore arrive at

$$\frac{1}{\pi}\int_0^{M^2(N_{max})} \frac{dt}{t}\mathrm{Im}\Pi_{LR}(t) = \frac{\sin^2\theta}{g_V^2}\sum_{n<N_{max}}\left(\frac{F_V^2(n)}{M_V^2(n)} - \frac{F_A^2(n)}{M_A^2(n)} - F^2(n)\right). \tag{8.94}$$

In QCD this integral vanishes because Π_{LR} decays fast enough to make the external contour contribution negligible if N_{max} is large enough. The equality of (8.94) to zero is the first Weinberg sum rule. The same argument works as well for the second sum rule to hold:

$$\frac{1}{\pi}\int_0^{M^2(N_{max})} dt\mathrm{Im}\Pi_{LR}(t) = \frac{\sin^2\theta}{g_V^2}\sum_{n<N_{max}}(F_V^2(n) - F_A^2(n)) = 0. \tag{8.95}$$

In fact, in QCD one gets a fairly good agreement with phenomenology by just including the first resonances [178]. In any case, the fact that the dispersion relation is convergent (no subtraction needed) indicates that the limit $N_{max} \to \infty$ could be taken.

We would like to understand the analogous situation in the present theory. Then, the two questions arise: (a) can the contour integral be neglected? (b) If this is the case, is the integral over the imaginary part along the real axis converging?

To answer the first question we derive the large-Q^2 expansion of $\Pi_{LR}(Q^2)/Q^2$. It is convenient to express

$$g_V^2\Pi_{LR}(q^2) = -\frac{R}{2g_5^2}q^2\sin^2\theta\Big\{\psi\left(1-\frac{q^2}{4\kappa^2}\right)-\psi\left(1-\frac{q^2}{4\kappa^2}+a\right) + \frac{4\kappa^2}{q^2}a\left[\ln\kappa^2\varepsilon^2+2\gamma_E+\psi\left(1-\frac{q^2}{4\kappa^2}+a\right)\right]\Big\}, \tag{8.96}$$

and use the Stirling's expansion of the ψ function in eq. (8.96) to get

$$\frac{g_V^2\Pi_{LR}(Q^2)}{Q^2} = \sin^2\theta\frac{2\kappa^2 a}{Q^2}\frac{R}{g_5^2} \times\left(\ln\frac{Q^2}{4\kappa^2}+\ln\kappa^2\varepsilon^2-\frac{2\kappa^2 a}{Q^2}\right)+\mathcal{O}\left(\frac{1}{Q^6}\right). \tag{8.97}$$

This limit is valid only in the (unphysical) region of $|\arg Q^2|<\pi$. The value on the physical axis ($0<q^2=-Q^2$) is ill-defined (needs a prescription, such as the one discussed above). However, to discuss the convergence of the outer part of the circuit in order to be able to derive eqs. (8.94) and (8.95) this is all we need. Unlike in the QCD case the correlator does not vanish fast enough due to the presence of the $\ln Q^2/Q^2$ and $1/Q^2$ terms. Therefore the corresponding dispersion relation requires one subtraction

$$\frac{\Pi_{LR}(Q^2)}{Q^2} = \int_0^\infty \frac{dt}{t+Q^2-i\epsilon}\frac{1}{\pi}\frac{\mathrm{Im}\Pi(t)}{t}+c, \tag{8.98}$$

c being the subtraction constant, *i.e.* the part of $\Pi_{LR}(Q^2)$ not determined by its imaginary part.

In the deep Euclidean region one could use an expansion

$$\frac{1}{t+Q^2} = \frac{1}{Q^2}-\frac{1}{Q^2}t\frac{1}{Q^2}+... \tag{8.99}$$

and then

$$\frac{\Pi_{LR}(Q^2)}{Q^2} = c+\frac{1}{Q^2}\frac{1}{\pi}\int_0^\infty\frac{dt}{t}\mathrm{Im}\Pi_{LR}(t)-\frac{1}{Q^4}\frac{1}{\pi}\int_0^\infty dt\mathrm{Im}\Pi_{LR}(t)+\ldots \tag{8.100}$$

Let us now consider a large, but finite, number of resonances in the analysis. That is, the theory is endowed with a cut-off that has to be connected to $N_{max}<\infty$ via the relation (8.76).

It is convenient to perform the large-Q^2 expansion of Π_{LR} of eq. (8.96) using the infinite series representation of the digamma function:

$$\lim_{Q^2\to\infty}\psi\left(\tfrac{Q^2}{4\kappa^2}+1\right)=-\gamma_E+\sum_{n,k=0}^{\infty}\tfrac{1}{n+1}\left(\tfrac{-M_V^2(n)}{Q^2}\right)^k;$$
$$\lim_{Q^2\to\infty}\psi\left(\tfrac{Q^2}{4\kappa^2}+1+a\right)=-\gamma_E+\left(1+\tfrac{4\kappa^2 a}{Q^2}\right)\times\sum_{n,k=0}^{\infty}\tfrac{1}{n+1}\left(\tfrac{-M_A^2(n)}{Q^2}\right)^k.$$

For $k=0$ we have $\lim\limits_{N\to\infty}\sum\limits_{n=1}^{N}\frac{1}{n}=\ln N+\gamma_E+\mathcal{O}(1/N)$.

Proper substitution in eq. (8.96) yields order by order for $g_V^2\Pi_{LR}(Q^2)/Q^2$:

$$\left(\frac{1}{Q^2}\right)^0:\quad \sin^2\theta\frac{R}{2g_5^2}\left(\sum_{n=0}^{\infty}\frac{1}{n+1}-\sum_{n=0}^{\infty}\frac{1}{n+1}\right); \tag{8.101}$$

$$\left(\frac{1}{Q^2}\right)^1:\quad 4\kappa^2\sin^2\theta\frac{R}{2g_5^2}\sum_{n=0}^{\infty}(1-1)-\sin^2\theta\kappa^2 a$$
$$\times\frac{2R}{g_5^2}\left(\ln\varepsilon^2\kappa^2+\gamma_E+\sum_{n=0}^{\infty}\frac{1}{n+1}\right); \tag{8.102}$$

$$\left(\frac{1}{Q^2}\right)^2:\quad 4\kappa^4\sin^2\theta a\frac{2R}{g_5^2}\sum_{n=0}^{\infty}(1-1). \tag{8.103}$$

Considering that 1 and -1 come together for any n, as well as the fractions in the difference between harmonic sums, we set these terms to zeros (certainly 0 for a finite sum). The remaining parentheses at $1/Q^2$ order cancels when infinite sum is replaced with the one up to N_{max} due to eq. (8.76). Thus, we show that the terms $1/Q^2$ and $1/Q^4$ are absent as long as $N_{max}<\infty$.

Let us compare this result with expansion (8.100) order by order. The dispersion relation should hold for a finite N_{max}, and a value for the constant c (that depends logarithmically on the cut-off) is provided. Since the $1/Q^2$ term in (8.102) is set to zero we have

$$\int_0^{M^2(N_{max})}\frac{dt}{t}\mathrm{Im}\Pi_{LR}(t)=0, \tag{8.104}$$

that establishes the formal validity of the first WSR

$$\sum_{n<N_{max}}\left(\frac{F_V^2(n)}{M_V^2(n)}-\frac{F_A^2(n)}{M_A^2(n)}-F^2(n)\right)=0. \tag{8.105}$$

We further stress that the situation is rather unsimilar to the one of real QCD, essentially because F^2 is logarithmically dependent on the cut-off. On the other hand,

the situation in the holographic CH scenario is quite analogous to the holographic QCD model of Chapter 7. We just proved that the sum over vector resonances $\sum\limits_{n<N_{max}}\left(\frac{F_V^2(n)}{M_V^2(n)}-\frac{F_A^2(n)}{M_A^2(n)}\right)$ is itself cut-off dependent for $N_{max}\to\infty$. This implies that symmetry restoration takes place very slowly in the UV and saturation with the ground state resonance is questionable both in holographic CH and holographic QCD. It seems fair to conclude that these peculiarities represent a pitfall of holography rather than a characteristic of the CH model.

Finally, regarding the second term in the expansion (8.100) – the nullification of the corresponding term in (8.103) leads to

$$\frac{1}{\pi}\int_0^{M^2(N_{max})}dt\mathrm{Im}\Pi_{LR}(t)=0, \tag{8.106}$$

that proves the second Weinberg sum rule to be present in our model under the same assumptions as for the first. Again, both the integral of the imaginary part over the real axis and the sum over resonances are logarithmically divergent unless a cut-off is imposed.

8.5 Higher order correlators and couplings

Let us write down explicitly several $5D$ interactions of further interest. At the three-point level they are:

$$\begin{aligned}S_{5D}^{(3)}\supset\quad & i\tfrac{R}{g_5^2}\int d^5x e^{-\kappa^2z^2}z^{-1}\Big(\partial_\mu A_\nu^A A^{B\mu}A^{C\nu}\,\mathrm{Tr}\,T^A[T^B,T^C] \\ & -\partial_z A_\mu^A A_z^i A^{B\mu}\,\mathrm{Tr}\,T^A[T^i,T^B]+\partial_\mu A_z^i A_z^j A^{A\mu}\,\mathrm{Tr}\,T^i[T^j,T^A]\Big) \\ & +(fR)^2\kappa^2\tfrac{R}{k_s}\int d^5x e^{-\kappa^2z^2}z^{-1}\tfrac{h(x,z)}{\chi_\pi}(A_L-A_R)_\mu^\alpha A_{br}^{\alpha\mu}.\end{aligned} \tag{8.107}$$

To prevent misunderstanding we specify the left, right or broken sectors of A where it is needed (they go with $\alpha=1,2,3$). Otherwise, the fields with $i=1,2,3,4$ are from the broken sector, and $A=1,\ldots,10$ ones encompass all options. At the four-point level we have:

$$\begin{aligned}S_{5D}^{(4)}\supset\quad & \tfrac{R}{4g_5^2}\int d^5x e^{-\kappa^2z^2}z^{-1}\Big(A_\mu^A A_\nu^B A^{C\mu}A^{D\nu}\,\mathrm{Tr}[T^A,T^B][T^C,T^D] \\ & -2A_z^i A_\mu^A A_z^j A^{B\mu}\,\mathrm{Tr}[T^i,T^A][T^j,T^B]\Big) \\ & +(fR)^2\kappa^2\tfrac{R}{4k_s}\int d^5x\tfrac{e^{-\kappa^2z^2}}{z}\tfrac{h^2(x,z)}{\chi_\pi^2}\left((A_{L\mu}^\alpha-A_{R\mu}^\alpha)^2-2A_{br\mu}^{\alpha 2}\right).\end{aligned} \tag{8.108}$$

The commutators there can be simplified with the Lie algebra of $SO(5)$

$$[T_L^\alpha, T_L^\beta] = i\varepsilon^{\alpha\beta\delta}T_L^\delta,\ [T_R^\alpha, T_R^\beta] = i\varepsilon^{\alpha\beta\delta}T_R^\delta,\ [T_L^\alpha, T_R^\beta] = 0,\ \alpha,\beta,\delta = 1,2,3$$
$$[T^a, \widehat{T}^i] = \widehat{T}^j(t^a)^{ji},\ [\widehat{T}^i, \widehat{T}^j] = (t_a)^{ji}T^a,\ a = 1,\ldots,6,\ i = 1,\ldots,4.$$

Here $t^a = \{t_L^\alpha, t_R^\alpha\}$, see the definition after Eqn. (8.6).

The expressions for $S_{5D}^{(3)}$ and $S_{5D}^{(4)}$ are already simplified with the gauge choice $A_z^a = 0$ in the unbroken channel. The Higgs-related terms proportional to $(fR)^2$ come from the square of the covariant derivative in Eqn. (8.22). Taking into account that in the broken sector imposed with $\xi = 1$ we had $A_z^i = \frac{\partial_z \pi^i}{\chi_\pi}$, we reveal the following interactions involving the Higgs from the F_{MN}^2 term

$$\frac{R}{2g_5^2}\int d^5x \frac{e^{-\kappa^2 z^2}}{z}\left[\frac{\partial_z h(x,z)}{\chi_\pi}\,(A_L - A_R)_\mu^\alpha \partial_z A_{br}^{\alpha\mu}\right.$$
$$\left. + \frac{1}{4}\left(\frac{\partial_z h(x,z)}{\chi_\pi}\right)^2\left((A_{L\mu}^\alpha - A_{R\mu}^\alpha)^2 + A_{br\mu}^{\alpha 2}\right)\right]. \tag{8.109}$$

8.5.1 Triple and quartic couplings of Higgs to SM gauge bosons

We are interested in triple and quartic couplings between the Higgs boson and the SM gauge bosons. In the standard MCHM picture these interactions have a given parametrization in the coordinate space:

$$g_{hWW}^{SM}\cos\theta W_\mu^+ W^{-\mu} h + g_{hZZ}^{SM}\cos\theta \tfrac{1}{2} Z_\mu Z^\mu h$$
$$+\tfrac{\cos 2\theta}{4}\left(g^2 W_\mu^+ W^{-\mu} + \tfrac{g^2+g'^2}{2} Z_\mu Z^\mu\right) hh, \tag{8.110}$$
$$g_{hWW}^{SM} = gM_W,\ g_{hZZ}^{SM} = \sqrt{g^2+g'^2}M_Z, \tag{8.111}$$

with $W_\mu^\pm = \frac{W_\mu^1 \mp i W_\mu^2}{\sqrt{2}}$ and $Z_\mu = \frac{1}{\sqrt{g^2+g'^2}}\left(gW_\mu^3 - g'B_\mu\right)$.

In our $5D$ model the effective couplings for hWW and $hhWW$ originate as follows:

$$\mathcal{L}_{eff} \supset i\frac{g^2}{4g_V^2} h(q) W^{\alpha\,\mu}(k_1) W^{\beta\,\nu}(k_2)\langle h(q)|\widetilde{\mathcal{O}}_{L\mu}^\alpha(k_1)\widetilde{\mathcal{O}}_{L\nu}^\beta(k_2)|0\rangle \tag{8.112}$$
$$+ i\frac{g^2}{4g_V^2} h(q_1)h(q_2) W^{\alpha\,\mu}(k_1) W^{\beta\,\nu}(k_2)\langle h(q_1)h(q_2)|\widetilde{\mathcal{O}}_{L\mu}^\alpha(k_1)\widetilde{\mathcal{O}}_{L\nu}^\beta(k_2)|0\rangle. \tag{8.113}$$

This expression shows that, in order to find the effective vertices, one extracts two-point functions from $S_{5D}^{(3)}$ and $S_{5D}^{(4)}$ while the Higgs field is taken on-shell. Z boson couplings can be taken into consideration after addition of the terms generated by

$\widetilde{\mathcal{O}}^3_{L\mu}\widetilde{\mathcal{O}}^3_{R\nu}$, $\widetilde{\mathcal{O}}^3_{R\mu}\widetilde{\mathcal{O}}^3_{L\nu}$ and $\widetilde{\mathcal{O}}^3_{R\mu}\widetilde{\mathcal{O}}^3_{R\nu}$ operator combinations. Their derivation follows closely that of the W^+W^-, so we just include them in the final result.

We can factorize the misalignment in (8.112) and (8.113), and come to the following equation:

$$\mathcal{L}_{eff} \supset \frac{g^2}{g_V^2}\frac{\sin 2\theta}{8\sqrt{2}}h(q)W^\alpha_\mu(k_1)W^\beta_\nu(k_2)\Bigg[\frac{\delta^2 S^{(3)}_{5D}}{\delta\phi^\alpha_{L\mu}(k_1)\delta\phi^\beta_{br\nu}(k_2)h(q)} \tag{8.114}$$

$$+\frac{\delta^2 S^{(3)}_{5D}}{\delta\phi^\alpha_{br\mu}(k_1)\delta\phi^\beta_{L\nu}(k_2)h(q)}\Bigg] \tag{8.115}$$

$$+\frac{g^2}{4g_V^2}h(q_1)h(q_2)W^\alpha_\mu(k_1)W^\beta_\nu(k_2)\left[\cos^2\theta\frac{\delta^2 S^{(4)}_{5D}}{\delta\phi^\alpha_{L\mu}(k_1)\delta\phi^\beta_{L\nu}(k_2)h(q_1)h(q_2)}\right. \tag{8.116}$$

$$\left.+\frac{\sin^2\theta}{2}\frac{\delta^2 S^{(4)}_{5D}}{\delta\phi^\alpha_{br\mu}(k_1)\delta\phi^\beta_{br\nu}(k_2)h(q_1)h(q_2)}\right]. \tag{8.117}$$

Note that to have all the physical fields out of the brackets we divided and multiplied the variations by $h(q)$. We also made use of the Lagrangian symmetry permitting to substitute $\langle h|\mathcal{O}^\alpha_{L\ \mu}\mathcal{O}^\beta_{br\ \nu}|0\rangle = -\langle h|\mathcal{O}^\alpha_{R\ \mu}\mathcal{O}^\beta_{br\ \nu}|0\rangle$ and $\langle hh|\mathcal{O}^\alpha_{L\ \mu}\mathcal{O}^\beta_{L\ \nu}|0\rangle = \langle hh|\mathcal{O}^i_{R\ \mu}\mathcal{O}^\beta_{R\ \nu}|0\rangle = -\langle hh|\mathcal{O}^\alpha_{L\ \mu}\mathcal{O}^\beta_{R\ \nu}|0\rangle$.

Let us explore the triple coupling first. The diagrammatic representation of (8.114) is given by

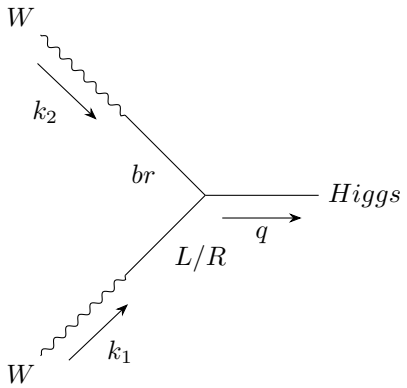

The $5D$ action provides two types of contributions

$$\frac{\delta^2 S^{(3)}_{5D}}{\delta\phi^\alpha_{L\mu}(k_1)\delta\phi^\beta_{br\nu}(k_2)h(q)} = \delta^{\alpha\beta}\eta_{\mu\nu}\frac{R}{g_5^2}\left(a\kappa^2\int dy\frac{e^{-y}}{y}\pi(y)/\chi_\pi V(k_1,y)A(k_2,y)\right.$$
$$\left.+\ \frac{1}{4}\int dy\frac{e^{-y}}{y}\partial_z\pi(y)/\chi_\pi V(k_1,y)\partial_z A(k_2,y)\right), \tag{8.118}$$

and the second variation in (8.115) evaluates the same but for exchange $k_1 \leftrightarrow k_2$.

Further, we would like to integrate analytically over y. As we substitute the Goldstone profile and the longitudinal vector propagators, all dependence on momenta disappears and the calculation can be performed. For the transverse modes we put the propagators on-shell with $k_1^2 = k_2^2 = M_W^2$ and consider the limit $M_W^2 \ll 4\kappa^2$. Indeed, we naturally expect the composite resonances to have rather large masses and that limit is substantiated numerically in Section 8.6. Essentially, we set $k_1^2 = k_2^2 = 0$, and the outcoming integral is analogous to the expression with the longitudinal propagators.

In the calculation it is convenient to use the definitions in terms of the resonance sums

$$\begin{aligned} A(0,z) = F\pi(z)/\chi_\pi = \Gamma(1+a)\Psi(a,0;\kappa^2 z^2) = \textstyle\sum_n \frac{\kappa^2 z^2 L_n^1(\kappa^2 z^2)}{n+1+a}, \\ \partial_z A(0,z) = F\partial_z\pi(z)/\chi_\pi = 2\kappa^2 z(-a)\Gamma(1+a)\Psi(a+1,1;\kappa^2 z^2) \\ = -2\kappa^2 z a \textstyle\sum_n \frac{L_n(\kappa^2 z^2)}{n+1+a}. \end{aligned}$$

Then, the previous variation could be estimated quite easily due to the orthogonality of the Laguerre polynomials:

$$\kappa^2 a F^{-1} \frac{R}{g_5^2} \sum_{n_1,n_2} \frac{\int dy e^{-y} y L_{n_1}^1(y) L_{n_2}^1(y) + a \int dy e^{-y} L_{n_1}(y) L_{n_2}(y)}{(n_1+a+1)(n_2+a+1)} \tag{8.119}$$

$$= \frac{1}{2F} \frac{2R\kappa^2 a}{g_5^2} \sum_n \delta_{n_1 n_2} \frac{n_1+1+a}{(n_1+a+1)(n_2+a+1)} = \frac{F}{2}. \tag{8.120}$$

Here we used for F^2 the definition of eq. (8.75).

We follow the same lines for the quartic coupling. Let us start with the variation of (8.116):

$$\begin{aligned} &\frac{\delta^2 S_{5D}^{(4)}}{\delta\phi_{L\mu}^\alpha(k_1)\delta\phi_{L\nu}^\beta(k_2)h(q_1)h(q_2)} \\ &= 2\delta^{\alpha\beta}\eta_{\mu\nu}\frac{R}{4g_5^2}\left(a\kappa^2\int dy \frac{e^{-y}}{y}(\pi(y)/\chi_\pi)^2 V(k_1,y)V(k_2,y)\right. \qquad (8.121) \\ &\qquad\left. + \frac{1}{4}\int dy \frac{e^{-y}}{y}(\partial_z\pi(y)/\chi_\pi)^2 V(k_1,y)V(k_2,y)\right) \\ &= \frac{1}{4}\delta^{\alpha\beta}\eta_{\mu\nu}F^{-2}\frac{2R}{g_5^2}a\kappa^2\sum_n \frac{n+1+a}{(n+1+a)^2} = \frac{1}{4}\delta^{\alpha\beta}\eta_{\mu\nu} \qquad (8.122) \end{aligned}$$

Unfortunately, the situation is not so clear with the variation over the broken sources

in (8.117) because the integrals there are quartic in Laguerre polynomials:

$$\frac{\delta^2 S^{(4)}_{5D}}{\delta\phi^{\alpha}_{br\mu}(k_1)\delta\phi^{\beta}_{br\nu}(k_2)h(q_1)h(q_2)} = \delta^{\alpha\beta}\eta_{\mu\nu}F^{-2}\frac{R}{g_5^2}a\kappa^2 \times \sum_{n_1,n_2}\frac{\int dy e^{-y}A^2(0,y)[a/2L_{n_1}(y)L_{n_2}(y) - yL^1_{n_1}(y)L^1_{n_2}(y)]}{(n_1+a+1)(n_2+a+1)} \tag{8.123}$$

We can make a calculation at $a=0$, with the result $\frac{\delta^2 S^{(4)}_{5D}}{\delta\phi^{\alpha}_{br\mu}(k_1)\delta\phi^{\beta}_{br\nu}(k_2)h(q_1)h(q_2)} = -\frac{1}{2}\delta^{\alpha\beta}\eta_{\mu\nu}$. We extrapolate this estimation to the case of general a when we present the quartic coupling in the effective Lagrangian.

In the end, the couplings to the EW gauge bosons appear in the effective Lagrangian as

$$\mathcal{L}_{eff} \supset \frac{g^{SM}_{hWW}\cos\theta}{\sqrt{2}g_V}\cdot\frac{1}{2}\left(W^{+\mu}(k_2)W^-_{\mu}(k_1) + W^{-\mu}(k_2)W^+_{\mu}(k_1)\right)h(q) \tag{8.124}$$

$$+ \frac{g^2\cos 2\theta}{8g_V^2}\cdot\frac{1}{2}\left(W^+_{\mu}(k_1)W^{-\mu}(k_2) + W^-_{\mu}(k_1)W^{+\mu}(k_2)\right)h(q_1)h(q_2) \tag{8.125}$$

$$+ \frac{g^{SM}_{hZZ}\cos\theta}{\sqrt{2}g_V}\cdot\frac{1}{2}Z^{\mu}(k_2)Z_{\mu}(k_1)h(q) \tag{8.126}$$

$$+ \frac{(g^2+g'^2)\cos 2\theta}{8g_V^2}\cdot\frac{1}{2}Z_{\mu}(k_1)Z^{\mu}(k_2)h(q_1)h(q_2), \tag{8.127}$$

$$g^{SM}_{hWW} = \frac{g^2\sin\theta F}{2g_V},\ g^{SM}_{hZZ} = \frac{(g^2+g'^2)\sin\theta F}{2g_V}, \tag{8.128}$$

where the factors in the last line indeed correspond to the SM definition of eq. (8.111) due to the definition of masses in eq. (8.89). The only thing missing to have the exact MCHM factors of eq. (8.110) is the proper choice of the model parameter:

$$g_V = \frac{1}{\sqrt{2}}. \tag{8.129}$$

We repeat that this value is obtained in the approximation $M_W^2 \ll 4\kappa^2$.

8.5.2 Triple couplings of heavy resonances to SM gauge bosons

Let us now turn to the part of eq. (8.107) independent of A_z and Higgs mode. A term relevant for the vector resonance-WW interaction is:

$$i\frac{R}{g_5^2}\int d^5x e^{-\kappa^2 z^2}z^{-1}\partial_{\mu}A^A_{\nu}A^{B\mu}A^{C\nu}\,\mathrm{Tr}\,T^A[T^B,T^C] \tag{8.130}$$

The commutator is proportional to the epsilon-tensor if none of the three fields is A^4_{br}. In the opposite case we rather obtain a Kronecker delta.

In eq. (8.130) we have an interaction between three vector $5D$ fields. In order to obtain a coupling of a vector resonance to a couple of EW gauge bosons one of them should be taken in its KK representation, while the other two should be given by their bulk-to-boundary propagators coupled later to the corresponding gauge field sources. In practice, we do the following steps. First, we are going to calculate the relevant three-point functions. Diagramatically, we obtain a vertex and three propagators with their residues attached to it. Second, we proceed with connecting two legs to the physical sources and reducing the third one via putting an n-th resonance on-shell.

There are not that many types of three-point functions that can be extracted from eq. (8.130):

$$\langle \mathcal{O}^\alpha_{L\mu_1}(q_1)\mathcal{O}^\beta_{L\mu_2}(q_2)\mathcal{O}^\gamma_{L\mu_3}(q_3)\rangle = \langle \mathcal{O}^\alpha_{R\mu_1}(q_1)\mathcal{O}^\beta_{R\mu_2}(q_2)\mathcal{O}^\gamma_{R\mu_3}(q_3)\rangle \tag{8.131}$$
$$= i\varepsilon^{\alpha\beta\gamma}\mathtt{Lor}_{\mu_1\mu_2\mu_3}\delta(q_1+q_2+q_3)T_{3V}(q_1,q_2,q_3);$$
$$\langle \mathcal{O}^\alpha_{L\mu_1}(q_1)\mathcal{O}^\beta_{br\mu_2}(q_2)\mathcal{O}^\gamma_{br\mu_3}(q_3)\rangle = \langle \mathcal{O}^\alpha_{R\mu_1}(q_1)\mathcal{O}^\beta_{br\mu_2}(q_2)\mathcal{O}^\gamma_{br\mu_3}(q_3)\rangle \tag{8.132}$$
$$= i\varepsilon^{\alpha\beta\gamma}\mathtt{Lor}_{\mu_1\mu_2\mu_3}\delta(q_1+q_2+q_3)\frac{1}{2}T_{V2A}(q_1,q_2,q_3);$$
$$\langle \mathcal{O}^4_{br\mu_1}(q_1)\mathcal{O}^\alpha_{br\mu_2}(q_2)\mathcal{O}^\beta_{R\mu_3}(q_3)\rangle = -\langle \mathcal{O}^4_{br\mu_1}(q_1)\mathcal{O}^\alpha_{br\mu_2}(q_2)\mathcal{O}^\beta_{L\mu_3}(q_3)\rangle \tag{8.133}$$
$$= i\delta^{\alpha\beta}\mathtt{Lor}_{\mu_1\mu_2\mu_3}\delta(q_1+q_2+q_3)\frac{1}{2}T_{V2A}(q_3,q_1,q_2).$$

The Lorentz structure of the vertex is collected into

$$\mathtt{Lor}_{\mu_1\mu_2\mu_3} = \eta_{\mu_1\mu_2}(q_1-q_2)_{\mu_3} + \eta_{\mu_1\mu_3}(q_3-q_1)_{\mu_2} + \eta_{\mu_2\mu_3}(q_2-q_3)_{\mu_1}.$$

There we defined the form factors

$$T_{3V}(q_1,q_2,q_3) = \frac{R}{g_5^2}\int dz e^{-\kappa^2 z^2} z^{-1} V(q_1,z)V(q_2,z)V(q_3,z), \tag{8.134}$$
$$T_{V2A}(q_1,q_2,q_3) = \frac{R}{g_5^2}\int dz e^{-\kappa^2 z^2} z^{-1} V(q_1,z)A(q_2,z)A(q_3,z). \tag{8.135}$$

Now, to consider the possible interactions with W and B bosons we write down the relevant three-point functions:

$$\langle \mathcal{O}^\alpha_{L/R\mu_1}(q_1)\widetilde{J}^\beta_{L\mu_2}(q_2)\widetilde{J}^\gamma_{L\mu_3}(q_3)\rangle = \frac{g^2}{8g_V^2} i\varepsilon^{\alpha\beta\gamma}\mathtt{Lor}_{\mu_1\mu_2\mu_3}(q_1,q_2,q_3)\delta(q_1+q_2+q_3)$$
$$\times\left[(1\pm\cos\theta)^2 T_{3V}(q_1,q_2,q_3) + \sin^2\theta T_{V2A}(q_1,q_2,q_3)\right]; \tag{8.136}$$

$$\langle \mathcal{O}^{\alpha}_{L/R\mu_1}(q_1)\widetilde{J}^{\beta}_{L\mu_2}(q_2)\widetilde{J}^{3}_{R\mu_3}(q_3)\rangle = \langle \mathcal{O}^{\alpha}_{L/R\mu_1}(q_1)\widetilde{J}^{3}_{R\mu_2}(q_2)\widetilde{J}^{\beta}_{L\mu_3}(q_3)\rangle$$
$$= \frac{gg'}{8g_V^2} i\varepsilon^{\alpha\beta 3}\mathtt{Lor}_{\mu_1\mu_2\mu_3}(q_1,q_2,q_3)\delta(q_1+q_2+q_3)$$
$$\times \left[(1-\cos^2\theta)T_{3V}(q_1,q_2,q_3) - \sin^2\theta T_{V2A}(q_1,q_2,q_3)\right]; \tag{8.137}$$

$$\langle \mathcal{O}^{\alpha}_{br\mu_1}(q_1)\widetilde{J}^{\beta}_{L\mu_2}(q_2)\widetilde{J}^{\gamma}_{L\mu_3}(q_3)\rangle = -\frac{g^2}{2g_V^2}\frac{\sin\theta}{\sqrt{2}} i\varepsilon^{\alpha\beta\gamma}\mathtt{Lor}_{\mu_1\mu_2\mu_3}(q_1,q_2,q_3)$$
$$\times \delta(q_1+q_2+q_3)\left[T_{V2A}(q_2,q_1,q_3) + T_{V2A}(q_3,q_2,q_1)\right]; \tag{8.138}$$

$$\langle \mathcal{O}^{\alpha}_{br\mu_1}(q_1)\widetilde{J}^{\beta}_{L\mu_2}(q_2)\widetilde{J}^{3}_{R\mu_3}(q_3)\rangle = \frac{gg'}{2g_V^2}\frac{\sin\theta}{\sqrt{2}} i\varepsilon^{\alpha\beta 3}\mathtt{Lor}_{\mu_1\mu_2\mu_3}(q_1,q_2,q_3)$$
$$\times \delta(q_1+q_2+q_3)\left[T_{V2A}(q_2,q_1,q_3) - T_{V2A}(q_3,q_2,q_1)\right]; \tag{8.139}$$

$$\langle \mathcal{O}^{4}_{br\mu_1}(q_1)\widetilde{J}^{\alpha}_{L\mu_2}(q_2)\widetilde{J}^{\beta}_{L\mu_3}(q_3)\rangle = \frac{g^2\sin 2\theta}{8\sqrt{2}g_V^2}\delta^{\alpha\beta}\mathtt{Lor}_{\mu_1\mu_2\mu_3}(q_1,q_2,q_3)$$
$$\times \delta(q_1+q_2+q_3)\left[T_{V2A}(q_3,q_1,q_2) - T_{V2A}(q_2,q_1,q_3)\right]; \tag{8.140}$$

$$\langle \mathcal{O}^{4}_{br\mu_1}(q_1)\widetilde{J}^{3}_{R\mu_2}(q_2)\widetilde{J}^{3}_{R\mu_3}(q_3)\rangle = \frac{g'^2\sin 2\theta}{8\sqrt{2}g_V^2}\mathtt{Lor}_{\mu_1\mu_2\mu_3}(q_1,q_2,q_3)$$
$$\times \delta(q_1+q_2+q_3)\left[T_{V2A}(q_3,q_1,q_2) - T_{V2A}(q_2,q_1,q_3)\right], \tag{8.141}$$

$$\langle \mathcal{O}^{4}_{br\mu_1}(q_1)\widetilde{J}^{3}_{L\mu_2}(q_2)\widetilde{J}^{3}_{R\mu_3}(q_3)\rangle = \frac{gg'\sin 2\theta}{8\sqrt{2}g_V^2}\mathtt{Lor}_{\mu_1\mu_2\mu_3}(q_1,q_2,q_3)$$
$$\times \delta(q_1+q_2+q_3)\left[T_{V2A}(q_3,q_1,q_2) - T_{V2A}(q_2,q_1,q_3)\right]. \tag{8.142}$$

Only a few BB–resonance interactions are possible due to the epsilon-tensor on the right-hand side of the holographic three-point functions.

Further, we reduce the leg corresponding with q_1 momenta and consider the limit $q^2_{2,3} \ll 4\kappa^2$ for other two momenta. For the n-th excitation of the left/right resonances of the unbroken sector that means:

$$T_{3V}(q_1,q_2,q_3) \to \sqrt{\frac{R}{2g_5^2(n+1)}}\int dy e^{-y}L^1_n(y) = \sqrt{\frac{R}{2g_5^2(n+1)}}, \tag{8.143}$$

$$T_{V2A}(q_1,q_2,q_3) \to \sqrt{\frac{R}{2g_5^2(n+1)}}\int dy e^{-y}L^1_n(y)\Gamma^2(1+a)\Psi^2(a,0;y), \tag{8.144}$$

where the latter integral can be calculated for a given n. For $n=0$: $1-2a+2a^2\psi_1(1+a)$.

For the n-th excitation of the resonances of the broken sector one of the broken

legs gets reduced, and we get:

$$\begin{aligned} T_{V2A}(q_2,q_1,q_3) \text{ or } T_{V2A}(q_3,q_2,q_1) &\rightarrow \\ \sqrt{\frac{R}{2g_5^2(n+1)}}\sum_{n'}\frac{\int dy e^{-y}L_n^1(y)L_{n'}^1(y)}{n'+1+a} &= \sqrt{\frac{R(n+1)}{2g_5^2}}\frac{1}{n+1+a}. \end{aligned} \tag{8.145}$$

Some triple couplings will not be included in the effective Lagrangian. These are: $A^4_{br}W^\alpha W^\alpha$, $A^4_{br}BB$, $A^4_{br}W^3B$, $A^\alpha_{br}W^\beta B$. The reason for it is that in the corresponding three-point functions the leading term in the limit $q^2_{2,3} \ll 4\kappa^2$ is zero due to the subtraction of the form factors. The first contribution is $\sim \frac{M_W^2}{4\kappa^2}$ and, thus, is strongly suppressed. We abstain from considering observables of this order in this work.

In the following, we limit ourselves to listing just the interactions for the ground states of the composite resonances:

$$\begin{aligned} \mathcal{L}_{eff} \supset\ & \frac{1}{2}W^\alpha_{\mu_2}(q_2)W^\beta_{\mu_3}(q_3)\mathtt{Lor}^{\mu_1\mu_2\mu_3}(q_1,q_2,q_3)(-i\varepsilon^{\alpha\beta\gamma}) && (8.146)\\ &\times \left(A^{L\,\gamma}_{\mu_1}(q_1)g_{LWW} + A^{R\,\gamma}_{\mu_1}(q_1)g_{RWW} - A^{Br\,\gamma}_{\mu_1}(q_1)g_{BrWW}\right) \\ &+ W^\alpha_{\mu_2}(q_2)B_{\mu_3}(q_3)\mathtt{Lor}^{\mu_1\mu_2\mu_3}(q_1,q_2,q_3)(-i\varepsilon^{\alpha 3\gamma}) && (8.147)\\ &\times \left(A^{L\,\gamma}_{\mu_1}(q_1)g_{LWB} + A^{R\,\gamma}_{\mu_1}(q_1)g_{RWB}\right), \end{aligned}$$

where we define

$$g_{L/RWW} = \tfrac{g^2}{4g_V^2}\sqrt{\tfrac{R}{2g_5^2}}\left[1 \pm \cos\theta + a\sin^2\theta(a\psi_1(1+a)-1)\right], \tag{8.148}$$

$$g_{BrWW} = \tfrac{g^2}{4g_V^2}\sqrt{\tfrac{R}{g_5^2}}\tfrac{\sin\theta}{1+a}, \tag{8.149}$$

$$g_{LWB} = g_{RWB} = \tfrac{gg'}{4g_V^2}\sqrt{\tfrac{R}{2g_5^2}}a\sin^2\theta\left[1 - a\psi_1(1+a)\right]. \tag{8.150}$$

If we switch to the vector/axial vector basis $A^L_\mu = \mathcal{V}_\mu - \mathcal{A}_\mu$, $A^R_\mu = \mathcal{V}_\mu + \mathcal{A}_\mu$, then there is only $\mathcal{V}_\mu$ appearing in the WB–resonance vertex. We can also change to the $Z-\gamma$ basis, then we have these couplings:

$$g_{\mathcal{V}WW} = \frac{g^2}{2g_V^2}\sqrt{\frac{R}{2g_5^2}}\left[1 - a\sin^2\theta(1 - a\psi_1(1+a))\right], \tag{8.151}$$

$$g_{\mathcal{V}WZ} = \frac{g}{2g_V^2}\sqrt{\frac{R}{2g_5^2}}\left[\frac{g^2}{\sqrt{g^2+g'^2}} - \sqrt{g^2+g'^2}a\sin^2\theta(1 - a\psi_1(1+a))\right], \tag{8.152}$$

$$g_{\mathcal{V}W\gamma} = \frac{g^2 g'}{2g_V^2}\sqrt{\frac{R}{2g_5^2(g^2+g'^2)}}, \tag{8.153}$$

$$g_{\mathcal{A}WW} = \frac{g^2}{2g_V^2}\sqrt{\frac{R}{2g_5^2}}\cos\theta. \tag{8.154}$$

For the couplings where there is no contribution from B, the relations including Z and γ are simple:

$$g_{\mathcal{A}WZ} = \frac{g}{\sqrt{g^2+g'^2}} g_{\mathcal{A}WW} \simeq 0.9 g_{\mathcal{A}WW}, \tag{8.155}$$

$$g_{\mathcal{A}W\gamma} = \frac{g'}{\sqrt{g^2+g'^2}} g_{\mathcal{A}WW} \simeq 0.5 g_{\mathcal{A}WW}, \tag{8.156}$$

and similarly for g_{BrWZ} and $g_{BrW\gamma}$.

The numerical values of the characteristic couplings will be estimated in the next section.

8.6 Applying the previous results to phenomenology

In this section we provide a numerical estimate of the masses and couplings of new composite states.

To have a contribution of the new physics at a realistic degree we start with the bounds on the S parameter, calculated using $5D$ techniques in eq. (8.90) or (8.91). It is experimentally constrained by the EW precision data (see Ref. [30] at $U = 0$) as

$$S = 0.02 \pm 0.07. \tag{8.157}$$

There are three model parameters in our expression for the S: $\sin\theta$, a and $\frac{R}{g_5^2}$, and g_V is assumed to be fixed as in eq. (8.129). a is related to the symmetry breaking by $f(z)$: at $a = 0$ there is no breaking, the unbroken and broken vector modes have the same mass. In principle, $\frac{R}{g_5^2}$ could be evaluated by comparing holographic two-point function to the perturbative calculation of the Feynman diagram (*e.g.*, of a hyper-fermion loop) at the leading order in large-Q^2, as it is usually done in the holographic realizations of QCD. As we would expect to get the hyper-color trace in the loop, it could be estimated that there is a proportionality $\frac{R}{g_5^2} \propto N_{hc}^p$ (power p depends on the particular representation). However, we deliberately made no hypothesis on the fundamental substructure, and could only expect that very large values of $\frac{R}{g_5^2}$ correspond to the large-N_{hc} limit. To have an idea of the scale of this quantity, we recall that in $N_c = 3$ QCD one has $\frac{R}{g_5^2} \sim 0.3$.

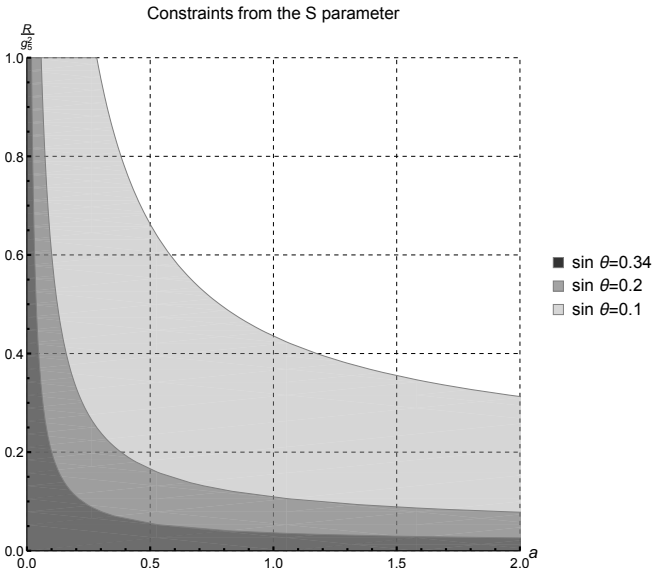

Figure 8.1: The $(\sin\theta, a, R/g_5^2)$ parameter region allowed by the S parameter restraints.

We present the effect of the current S-constraint on the $(\sin\theta, a, R/g_5^2)$ plane in Fig. 8.1. The larger the value of $\sin\theta$ the smaller the allowed region for a and R/g_5^2. We only consider $\sin\theta \leq 0.34$ due to the bounds on the misalignment given in eq. (8.15). That bound is valid under assumption that the coupling of the Higgs to gauge bosons is $\kappa_V = \sqrt{1-\sin^2\theta}$, and it was demonstrated in Section 8.5.1 that this is the case of our holographic model. LHC Run 1 estimation (8.13) at two standard deviations gives a similar maximal permitted $\sin\theta$.

We get no information on the mass scale κ from the EW precision data. However, we can relate it to the low-energy observables through the definition of the W boson mass in eq. (8.89). Standardly it is connected to the EWSB scale $v = 246$ GeV and we can equate

$$M_W^2 = \frac{g^2 v^2}{4} = \frac{g^2 \sin^2\theta F^2}{4 g_V^2}. \tag{8.158}$$

With F given in eq. (8.63), the following condition on κ is valid:

$$\frac{g_V^2 v^2}{\sin^2\theta} + \frac{2\kappa^2 R}{g_5^2} a \left(\ln \kappa^2 \varepsilon^2 + 2\gamma_E + \psi\left(1+a\right)\right) = 0. \tag{8.159}$$

Let us further set

$$\varepsilon = \frac{1}{\Lambda_{\text{cut-off}}} \simeq \frac{1}{4\pi f_{CH}} = \frac{\sin\theta}{4\pi v}. \tag{8.160}$$

Table 8.1: Different predictions of the minimal vector masses for $\sin\theta = 0.1,\ 0.2$ and 0.34.

$\sin\theta$	$\frac{R}{g_5^2}$	a	$M_* = M_V(0)$, TeV	$M_A(0)$, TeV	$\sim N_{max}$
0.1	0.1	266.3	0.22	3.68	>20 k
0.1	0.3	2.212	1.28	2.29	740
0.1	1	0.283	1.88	2.13	340
0.1	10	0.022	2.10	2.12	270
0.2	0.1	1.176	1.79	2.64	93
0.2	0.3	0.225	2.28	2.52	58
0.2	1	0.058	2.43	2.50	50
0.2	10	0.006	2.49	2.50	48
0.34	0.1	0.225	2.84	3.14	12
0.34	0.3	0.065	3.00	3.09	11
0.34	1	0.019	3.05	3.08	10
0.34	10	0.002	3.07	3.08	10

Here $\Lambda_{\text{cut-off}} = \Lambda_{\text{CH}} \simeq 4\pi f_{CH}$ is the range of validity of the effective theory of the composite resonances, which could be postulated as a natural cut-off in the present bottom-up model. We can also rework the connection between the number of resonances cut-off N_{max} and ε:

$$N_{max} = 16\pi^2 \frac{v^2}{\kappa^2 \sin^2\theta} e^{-2\gamma_E}. \tag{8.161}$$

Setting $g_V = \frac{1}{\sqrt{2}}$, we collect the results in Table 8.1. There we substitute the estimation of κ with that of the characteristic mass $M_* = \sqrt{4\kappa^2}$, the mass of the ground vector state, the lightest massive state in our spectrum. We take the values of a saturating the S-bound, thus, these are the minimal estimations for M_*. Should it be estimated that S is p times smaller, our estimates for M_* become roughly p times larger. For a given set of $\frac{R}{g_5^2}$ and $\sin\theta$ lower values of a are permitted and result in larger M_*. In addition, a larger a leads to a larger splitting between vector fields aligned in different (unbroken and broken) directions. It is evident from Table 8.1 that the splitting almost disappears starting from $\frac{R}{g_5^2} = 10$ for the demonstrated values of $\sin\theta$. We also noticed that the effective "N_{hc}-infinity" starts rather early because $\frac{R}{g_5^2} = 10$ bring similar results to, say, $\frac{R}{g_5^2} = 1000$. It is an interesting observation, because we know the limit $N \gg 1$ to be an important ingredient of the original AdS/CFT conjecture. Of course, in phenomenological

AdS/QCD models the duality is commonly extended for the finite values of N_c, so we take into consideration a set of smaller $\frac{R}{g_5^2}$ as well.

In Fig. 8.2 (see in the end of the chapter) we depict a broader range of M_* values. The dependencies on the model parameters could be easily traced from there. In the parameter space $(\sin\theta, a, \frac{R}{g_5^2})$ we can fix any two values, then the growth of the third parameter results in lower M_* (as long as it does not appear in the prohibited zone). Pursuing higher degree of breaking a results in unlikely small masses in the areas that are not well-restrained by the S parameter. We speak of masses below 2 TeV at smaller values of $\frac{R}{g_5^2}$ and $\sin\theta$. Higher values of other two parameters are more efficiently cut off by the S bound. In general, $2.0 - 4.0$ TeV states are expected. We also recollect that in a tower of resonances of one type we have a square root growth with the number of a resonance. Thus, for a lowish value of M_* there is a tower with several comparatively low-lying states. For instance, for the input set $(\sin\theta, a, R/g_5^2) = (0.1, 2.2, 0.3)$ we have $M_* = 1.3$ TeV and the tower masses are $M_V(n) = \{1.3, 1.8, 2.3, 2.6, \ldots\}$ TeV.

In Fig. 8.3a (printed in the end of the chapter) we present the numerical analysis resulting from eqs. (8.148), (8.149) and (8.150), showing the possible values of the couplings between the left, right and broken resonances and a W^+W^- or W^3B-pair. It is clear that the left resonances couple more strongly than the right ones thanks to the dampening the latter get with $\cos\theta$ being rather close to 1. All the WW couplings exhibit a logarithmic growth with $\frac{R}{g_5^2}$. The parameter a was taken to be saturating the S-bound of Fig. 8.1 and is rendered quite close to zero at higher values of R/g_5^2 especially for larger $\sin\theta$. The coupling including the B meson is rather small in comparison to the WW ones due to the direct proportionality to a, and it vanishes exactly for $a = 0$.

In Fig. 8.3b we present the same couplings but computed in the different basis as given by eqs. (8.151–8.154). There is only one reference line for the broken resonances – g_{BrWW}; the WZ and $W\gamma$ ones lie even lower. Due to the direct proportionality in eq. (8.154) (and related) to $\cos\theta$, the misalignment angle effect is demonstrated rather clear in this basis: the smaller it is the closer the axial vector couplings are to the vector ones.

In order to show the impact of a on the couplings to SM gauge bosons in more detail we provide the similar computation in Fig. 8.3c but imposing $a = 0$ by hand for the fits with $\sin\theta = 0.1$ (the most illustrative case). The difference between this and the left panel of Fig. 8.3a is only noticeable for $R/g_5^2 \lesssim 0.5$; and now the saturation is reached sooner. The difference in the basis of Fig. 8.3b is even less

perceptible. We conclude, that at the major part of the R/g_5^2 axis the scale of $SO(5)$ breaking is of little consequence for the couplings discussed. The importance of the S constraint at very small values of R/g_5^2 is doubtful. At the same time, this area turns out relevant if we assume that the CH value is close to the QCD one, or if we take into account the estimations of these couplings made in other studies.

It is not easy to make comparison between the values of the couplings obtained here and possible experimental bounds because in the analyses of the LHC experimental data on resonances decaying into WW or WZ pairs some benchmark signal models are normally used (Kaluza–Klein graviton in extra dimension, extended gauge model of W' and Z', and others). However, in a more model-independent framework of Ref. [179] we find that the characteristic scale for the couplings is of order $0.001 \div 0.010$. g_{LWW} and g_{BrWW} tend to be much larger unless computed at very small R/g_5^2. We can only speculate about the effect of including quantum corrections in our calculation. Barring large corrections, the comparison with Ref. [179] really indicates lowish values for R/g_5^2.

8.7 Summary

In this chapter we used the bottom-up holographic approach to have a fresh look at non-perturbative aspects of CH models with a global breaking pattern $SO(5) \to SO(4)$ and a gauge group misaligned with the unbroken group. With the purpose of being as close as possible to the characteristics of a confining theory (presumed to be underlying the EWSBS) we chose to work in a $5D$ SW framework inspired by effective models of QCD and consisting in a generalized sigma model coupled both to the composite resonances and to the SM gauge bosons. The $5D$ model is similar to that of successful AdS/QCD constructions, specifically to the one presented in Chapter 7, and depends on the two ansatze functions: the SW dilaton profile $\Phi(z)$ and the symmetry-breaking $f(z)$. The microscopic nature of the breaking, besides being triggered by some new strong interactions with an hyper-color group, is factored out and every effort have been taken to make predictions as independent of it as possible.

We investigated the dynamics of ten vector (unbroken and broken) and four Goldstone (one of them related to the Higgs) $5D$ fields. Though for the unbroken vectors the situation is much similar to a generic AdS/QCD model, in the broken sector we have developed a procedure that relates the Goldstone fields to the fifth component A_z^i. That is not just a gauge-Higgs construction because there are as

well definite independent Goldstone modes in the bulk. The resulting Goldstone description is quite different from that of the vector fields. The proposed procedure is ratified by the agreement of the hWW and $hhWW$ characteristic couplings to those of the general MCHM. The Higgs remains massless as long as we do not take into account the quantum corrections.

In the paper we lay emphasis on the following issues of phenomenological interest:

- derivation of the spectra of the new states in the broken and unbroken channels;
- connection to the EW sector (masses of the gauge bosons and electroweak precision observables);
- triple couplings of the new heavy resonances to the gauge bosons of SM;
- in-depth analysis of the realization of the first and second Weinberg sum rules and the study of their convergence.

The holographic effective theory describes the composite resonances; their maximum number N_{max} is found to be related to the theory natural UV cut-off ε. Adhering to one of these cut-offs is necessary to derive relations involving resonance decay constants and masses. The latter stay cut-off independent as befits physical observables. The only but very significant exception is the "pion decay constant" F. We made a hypothesis that ε can be taken as related to the characteristic range of the CH effective theory, and provided numerical estimations for the value of N_{max}. Moreover, the two Weinberg sum rules hold their validity just in a formal sense as the sum over resonances has to be cut off. The sum rules are logarithmically divergent, and this implies that they are not saturated at all by just the first resonance. We believe it to be a common feature of AdS/CFT models, detached from the particularities of our setup, as it is also present in holographic QCD. We can regard it as a general serious flaw of the bottom-up holographic models, and hence a realistic CH theory could also have the sum rules more similar to those of actual QCD.

The minimal set of input parameters in our model is: $\sin\theta$, a, and $\frac{g_5^2}{R}$. There are constraints coming from the W mass (EW scale), the S parameter and the existing experimental bounds on κ_V ($\sin\theta$). Their consideration allows us to estimate the masses for the composite resonances. It is not difficult to find areas in the parameter space where a resonance between 2 and 3 TeV is easily accommodated.

The presented technique offers the possibility of deriving trilinear couplings of a type WW, WB, WZ–new composite resonance. They are of interest because the SM gauge boson scattering is regarded as the process for the new vector resonance production in collider experiments.

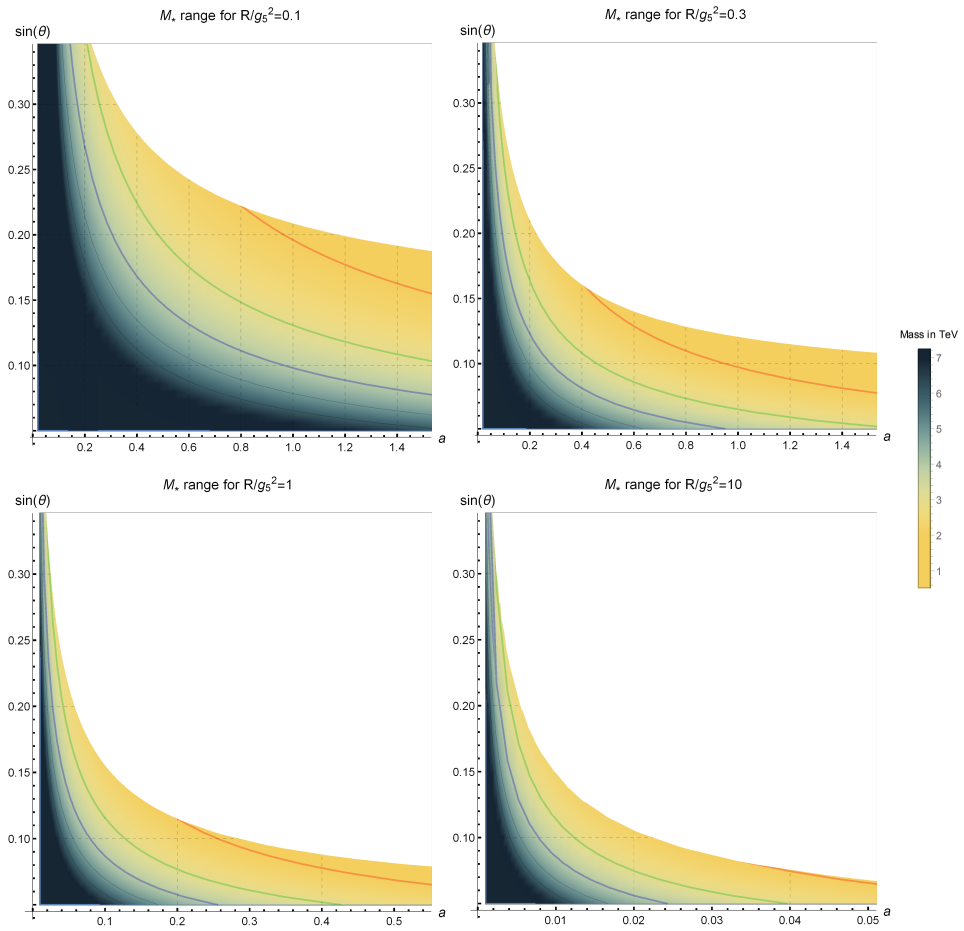

Figure 8.2: The density plots of M_* for different values of R/g_5^2. The coloured curves represent the lines of constant M_*: the red one – $M_* = 2$ TeV, the green one – $M_* = 3$ TeV, the blue one – $M_* = 4$ TeV and successive black curves for higher integer values. The white area represents the sector prohibited by the S bound.

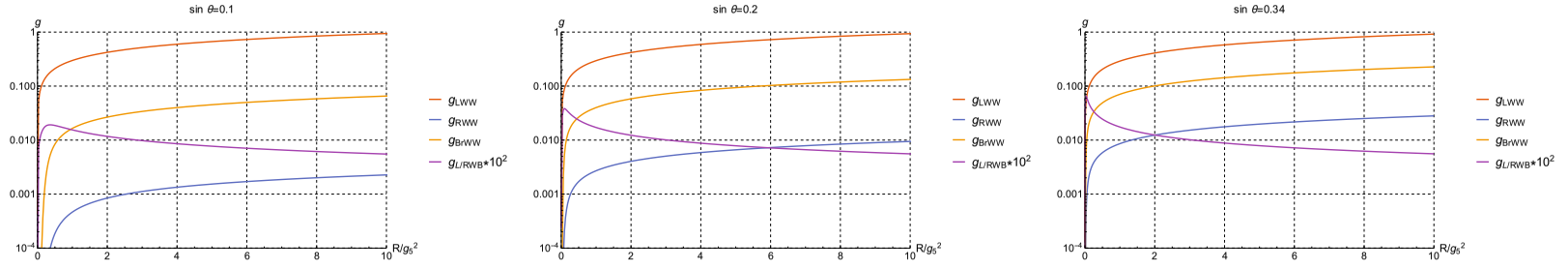

(a) Left, right and broken resonances to the W^+W^- and $W^\pm B$ pairs.

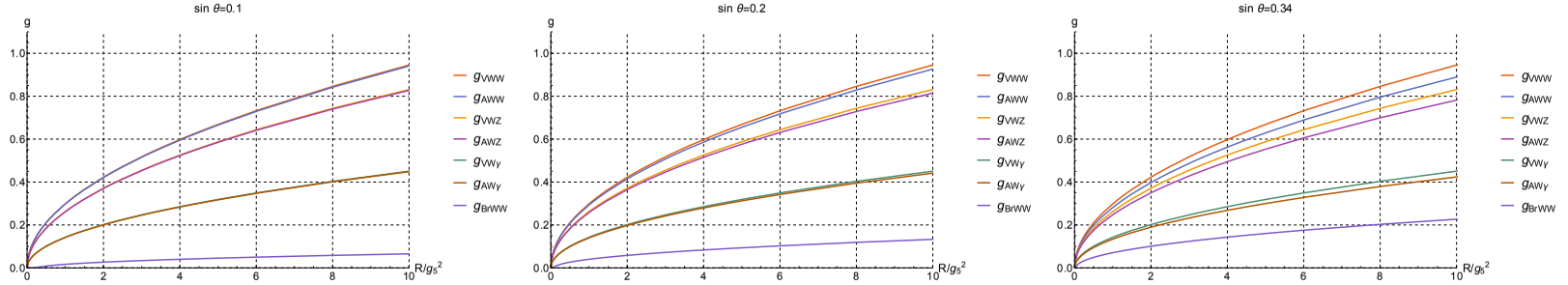

(b) Vector, axial vector and broken resonances to the W^+W^-, $W^\pm Z$, $W^\pm\gamma$ pairs.

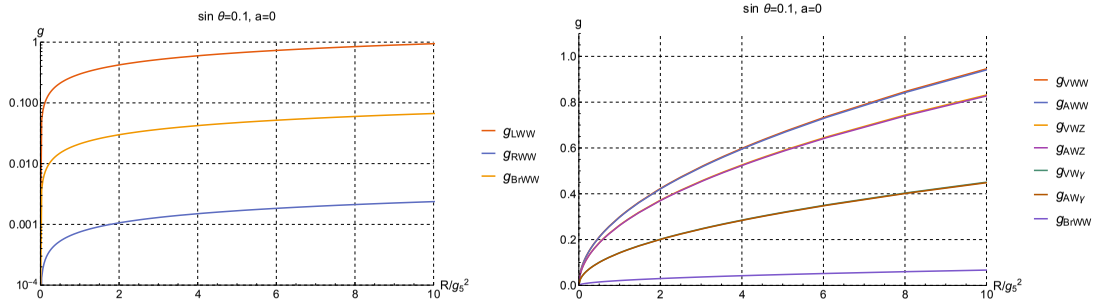

(c) Example for a completely vanishing value of a.

Figure 8.3: Couplings of composite resonances to the SM gauge bosons.

Chapter 9

Conclusions

Holography raised from the generalization of the Bekenstein–Hawking observation on the nature of the black hole entropy. Holographic principle has a general nature and states that the entire information content of a quantum gravity theory in a given volume can be encoded in an effective theory on the boundary.

String theory is a unique example where both bulk and boundary theories are known. Furthermore, it is endowed with dualities – there exist different equivalent formulations of its physics. These two ideas substantiate gauge/gravity duality. A gravity theory in the bulk is equivalent to a QFT on the boundary with some gauge symmetry. In addition, due to duality of coupling constant regimes, when the latter is strongly coupled the former is weakly coupled and vice versa. Theoretical physics lacks analytic tools for the study of the strongly coupled regime. At least, there is no such universally applicable and ubiquitous approach as perturbation theory. Thus, the usefulness of the duality is in making a definite proposal for how to compute in strongly coupled theories. The same fact, though, keeps the duality from being rigorously proved – it remains a conjecture.

The most famous and best understood case of gauge/gravity duality is the AdS/CFT correspondence. Its study was pioneered in late 90's by Juan Maldacena and gave boost to various further holographic advances and applications. These ideas promoted a lot of additional theoretical investigation in mathematical and string theory physics and provided new descriptions of many physical systems: QCD, relativistic hydrodynamics, cosmology and condensed matter physics.

There are many important strongly coupled systems in physics. However, chronologically and for the purpose of this thesis the first and obvious motivation to study holography is QCD. At low energies it is a non-supersymmetric strongly coupled $SU(3)$ gauge theory in which we cannot compute analytically,

though there exist first principle lattice calculations. Holography addresses various aspects of QCD: meson, glueball and baryon spectra, hadronic interactions and the hadronization process in colliders, confinement and chiral symmetry breaking, hadronic matter under extreme external conditions. As yet, there is no known precise dual of QCD. Nevertheless, we find the bottom-up holographic approach (AdS/QCD) most inspiring due to the fact that rather simple models turn out to reproduce the relevant QCD phenomenology quite successfully.

Another interesting application is in the realm of BSM physics. There are several ideas on how strong dynamics might occur beyond the SM. We focus on Composite Higgs models, where the new strong interaction binds hyper-fermions into composite states at TeV energies. The new sector at this energy scale can both solve the naturalness problem of the SM at the price of a relatively small tuning and provide signatures that can be observed experimentally in the near future. Among others, the High-Luminosity upgrade of LHC is expected to shed some light on the possibility of a non-standard Higgs sector by providing more precise determination of the Higgs couplings to gauge bosons and fermions, and by observing, hopefully, some BSM signals. Duality techniques improve the understanding in this area not only because they provide an analytic tool, but also due to the insight given by the holographic study of QCD. The AdS/QCD heritage plays an important role in the CH model-building presented in this thesis.

In this thesis we report on our investigations of QCD and CH within the bottom-up holographic approach. A review of a wide range of subjects was prerequisite to make sense of the particular holographic study. We started in Chapter 2 with description of the core formalism, that of the AdS/CFT correspondence. Though we utilized its phenomenological sibling, the AdS/QCD, the logic of general holographic constructions is best understood through the development of the original Maldacena conjecture. That happens thanks to a lot of theoretical effort that was directed on this case of gauge/gravity duality.

We cannot and do not need to cover all the aspects of QCD, so in Chapter 3 we selected the issues most relevant to the idea of the thesis. These are: large-N_c limit, chiral symmetry breaking, operator product expansion, QCD at finite temperature. We also needed to mention another non-perturbative approach – lattice simulations of QCD. Lattice results are referred to at various places in this thesis: as an input data, as a reference point, as a source to understand the nature of some phenomena.

We wanted our holographic models to be predictive. For AdS/QCD it means reproducing the phenomenological hadron observables. These were covered in

Chapter 4 and included the resonance mass spectra, couplings and form factors. We investigated in detail the idea of radial excitations belonging to the linear radial Regge trajectories, and emphasized the notion of universal radial meson trajectories. Glueballs also belong to the QCD resonances, their spectra were actively studied on the lattice.

Having thus highlighted the relevant phenomenological features of QCD, we turned towards their bottom-up holographic implementation. The general formalism of including QCD resonances in the $5D$ bulk was presented in Chapter 5. We introduced several simple AdS/QCD models: HW, SW and GSW. They were assessed on the basis of their success in description of the phenomenological spectra. The SW-like models demonstrate the expected linearity of the radial trajectories. Besides, we mentioned the possibility to acquire families of SW profiles leading to the same spectra.

Thermodynamic properties of QCD can also be studied in the bottom-up framework. It is assumed that the deconfinement phase transition is dual to the Hawking–Page transition between different geometries in the $5D$ theory. That allows to estimate the (pseudo) critical temperature of deconfinement, T_c. In Chapter 6 we explored several holographic models with different options for fixing their parameters in order to obtain the phenomenological value of T_c. The results turned out quite dependent on the choices of the model parameters. We concluded that there is a subset providing T_c close to the quenched and large-N_c lattice estimations, and those predicting T_c in the range of physical (freeze-out, lattice with dynamical quarks) T_c. We traced the theoretical motivation for the models to belong to one of these classes.

The AdS/QCD holographic mechanism for chiral symmetry breaking was developed in Chapter 7. We chose the SW framework there, and introduced several novel features to better accommodate the Goldstone modes. The resulting model had a few free parameters and provided not just separate resonance spectra, but an interesting interrelation between different sectors. We also extracted several interaction observables. The phenomenological outcome was given in terms of the fit to fifteen QCD observables with the RMS error of $\sim 30\%$.

Chapter 8 was wholly devoted to the application of the AdS/QCD technique and, specifically, of the models with symmetry breaking to the case of higher energy strongly coupled sector responsible for the formation of the Composite Higgs and concomitant heavy composite resonances. We reassessed employing the holographic technique to the description of 4D minimal composite Higgs model with

$SO(5) \to SO(4)$ global symmetry breaking pattern. The BSM signatures (masses, couplings, contribution to the EW precision observables) of the holographic CH model were studied in detail, and proper restrictions on the model were derived. We concluded that the model is able to accommodate new vector resonances with masses in the range 2 TeV to 3 TeV without encountering phenomenological difficulties.

This research can be continued in the following directions. The study of the deconfinement phase transition could be performed in a space of more thermodynamic parameters (quark and chiral chemical potentials, external magnetic field, *etc.*). The BSM investigation could be augmented with other symmetry breaking patterns giving rise to the Composite Higgs. Especially it is interesting to consider an UV-completable model, because some of the model parameters would be calculable in terms of the non-exotic fundamental theory, like in QCD. Another great improvement would be to generalize our results for the fully dynamical SW holographic models.

Holography is a relatively new tool that can be applied in different areas of theoretical physics to reveal the non-perturbative nature of some phenomena. Fortunately, we can generalize our experience in the fields where we already have some knowledge to give us intuition to build the models for the New Physics. Nevertheless, the QCD studies are valuable on their own. Despite its properties being a central issue of various holographic models, the completely satisfactory description (neither theoretically, nor phenomenologically) of QCD is not yet achieved. It means that further and alternative research strategies should be developed.

Appendix A

Some properties of the confluent hypergeometric functions

The confluent hypergeometric equation has the general form:

$$y\varphi''(y) + (c - y)\varphi'(y) - a\varphi(y) = 0. \tag{A.1}$$

Solutions of this equation depend crucially on the value of the a and c parameters. Here we provide a brief overlook of the properties of the confluent hypergeometric equation, focusing on the dependence on the different integer values of the c parameter [180].

For the positive integer values $c = 1, 2, 3, ...$ we have

$$\varphi(y) = C_1\ {}_1F_1(a, c; y) + C_2\Psi(a, c; y), \tag{A.2}$$

where ${}_1F_1(a, c; y)$ is called the Kummer (confluent hypergeometric) function and $\Psi(a, c; y)$ - the Tricomi (confluent hypergeometric) function.

However, all the cases mentioned in the paper lie in the region of the non-positive integer c, for which one of the expected solutions, ${}_1F_1(a, c; y)$, does not exist, because it has poles at $c = 0, -1, -2, ...$ In the same time the Tricomi function can be analytically continued to any integer c. Nevertheless, the fundamental system of solutions is rich enough and we are able to choose another two solutions:

$$\varphi(y) = C_1 y^{1-c}\ {}_1F_1(a - c + 1, 2 - c; y) + C_2\Psi(a, c; y). \tag{A.3}$$

Mark that the Tricomi function exhibits a logarithmic behaviour for all integer

c. Specifically for the case $c = 1 - n,\ n = 0, 1, 2, ...$ one can write:

$$\Psi(a, 1-n; y) = \frac{(n-1)!}{\Gamma(a+n)} \sum_{r=0}^{n-1} \frac{(a)_r y^r}{(1-n)_r r!} + \frac{(-1)^{n-1}}{n!\Gamma(a)} \Bigg({}_1F_1(a+n, n+1; x) \times y^n \ln y + \sum_{r=0}^{\infty} \frac{(a+n)_r}{(n+1)_r} [\psi(a+n+r) - \psi(1+r) - \psi(1+n+r)] \frac{y^{n+r}}{r!} \Bigg), \tag{A.4}$$

here the Pochhammer symbol is $(a)_n = 1 \cdot a \cdot (a+1)...(a+n-1) = \Gamma(a+n)/\Gamma(a)$, $\psi(a)$ is the digamma function; and the first sum is absent for the case $n = 0$. There exists also a useful equation relating the Tricomi functions of different arguments:

$$\Psi(a, c; y) = y^{1-c} \Psi(a - c + 1, 2 - c; y). \tag{A.5}$$

The Kummer function being an series solution ${}_1F_1(a, c; y) = \sum_{n=0}^{\infty} \frac{(a)_n}{(c)_n} \frac{y^n}{n!}$ has a natural connection with the generalized Laguerre polynomials (for integer $n > 0,\ m > 0$):

$$L_n^m(y) = \frac{(m+1)_n}{n!}\ {}_1F_1(-n, m+1, y). \tag{A.6}$$

In the same time, the Tricomi function has an infinite sum representation involving the Laguerre polynomials:

$$\Gamma(1+a)\Psi(a, 0; y) = \sum_{n=0}^{\infty} \frac{y L_n^1(y)}{n+1+a}. \tag{A.7}$$

List of Figures

List of Tables

Bibliography

1. E. P. Wigner, Communications on Pure and Applied Mathematics **13**, 1 (1960), https://onlinelibrary.wiley.com/doi/pdf/10.1002/cpa.3160130102 .
2. R. Frigg and S. Hartmann, in *The Stanford Encyclopedia of Philosophy*, edited by E. N. Zalta (Metaphysics Research Lab, Stanford University, 2020) spring 2020 ed.
3. J. Maldacena, Int. J. Theor. Phys. **38**, 1113 (1999), [Adv. Theor. Math. Phys.2,231(1998)], arXiv:hep-th/9711200 .
4. J. Polchinski, Stud. Hist. Phil. Sci. B **59**, 6 (2017), arXiv:1412.5704 [hep-th] .
5. G. 't Hooft, Conf. Proc. C **930308**, 284 (1993), arXiv:gr-qc/9310026 .
6. L. Susskind, J. Math. Phys. **36**, 6377 (1995), arXiv:hep-th/9409089 .
7. L. Susskind and E. Witten, (1998), arXiv:hep-th/9805114 .
8. O. Aharony, S. S. Gubser, J. M. Maldacena, H. Ooguri, and Y. Oz, Phys. Rept. **323**, 183 (2000), arXiv:hep-th/9905111 [hep-th] .
9. H. Nastase, (2007), arXiv:0712.0689 [hep-th] .
10. S. S. Gubser and A. Karch, Ann. Rev. Nucl. Part. Sci. **59**, 145 (2009), arXiv:0901.0935 [hep-th] .
11. P. C. Argyres, "Introduction to the AdS/CFT Correspondence," in *From Gravity to Thermal Gauge Theories: The AdS/CFT Correspondence: The AdS/CFT Correspondence*, edited by E. Papantonopoulos (Springer Berlin Heidelberg, Berlin, Heidelberg, 2011) pp. 57–75.
12. A. V. Ramallo, *Proceedings, 3rd IDPASC School: Santiago de Compostela, Spain, January 21-February 2, 2013*, Springer Proc. Phys. **161**, 411 (2015), arXiv:1310.4319 [hep-th] .
13. J. Polchinski, Nuclear Physics B **303**, 226 (1988).
14. S. Rychkov, *EPFL Lectures on Conformal Field Theory in D$\geq$ 3 Dimensions*, SpringerBriefs in Physics (2016) arXiv:1601.05000 [hep-th] .
15. J. Kaplan, "Lectures on AdS/CFT from the Bottom Up," (2016).

16. I. R. Klebanov and E. Witten, Nucl. Phys. B **556**, 89 (1999), arXiv:hep-th/9905104 .
17. P. Breitenlohner and D. Z. Freedman, Annals of Physics **144**, 249 (1982).
18. P. Breitenlohner and D. Z. Freedman, Phys. Lett. **115B**, 197 (1982).
19. E. Witten, Adv. Theor. Math. Phys. **2**, 253 (1998), arXiv:hep-th/9802150 .
20. S. Gubser, I. Klebanov, and A. Polyakov, Phys. Lett. B **428**, 105 (1998), arXiv:hep-th/9802109 .
21. B. Zwiebach, *A First Course in String Theory* (Cambridge University Press, 2004).
22. E. Witten, Nucl. Phys. B **460**, 335 (1996), arXiv:hep-th/9510135v2 .
23. H. Nastase, "Kaluza-Klein dimensional reduction," in *Introduction to the AdS/CFT Correspondence* (Cambridge University Press, 2015) pp. 87–97.
24. G. 't Hooft, Nuclear Physics B **72**, 461 (1974).
25. D. Mateos, *Strings, supergravity and gauge fields. Proceedings, European RTN Winter School, RTN 2007, Geneva, Switzerland, January 15-19, 2007*, Class. Quant. Grav. **24**, S713 (2007), arXiv:0709.1523 [hep-th] .
26. P. Kovtun, D. T. Son, and A. O. Starinets, Phys. Rev. Lett. **94**, 111601 (2005), arXiv:hep-th/0405231 .
27. A. V. Manohar, in *Probing the standard model of particle interactions. Proceedings, Summer School in Theoretical Physics, NATO Advanced Study Institute, 68th session, Les Houches, France, July 28-September 5, 1997. Pt. 1, 2* (1998) pp. 1091–1169, arXiv:hep-ph/9802419 [hep-ph] .
28. S. Coleman and E. Witten, Phys. Rev. Lett. **45**, 100 (1980).
29. S. Scherer, Adv. Nucl. Phys. **27**, 277 (2003), arXiv:hep-ph/0210398 [hep-ph] .
30. M. Tanabashi *et al.* (Particle Data Group), Phys. Rev. D **98**, 030001 (2018).
31. A. Pich, Rept. Prog. Phys. **58**, 563 (1995), arXiv:hep-ph/9502366 [hep-ph] .
32. J. Gasser and H. Leutwyler, Ann. Phys. **158**, 142 (1984).
33. M. Shifman, A. Vainshtein, and V. Zakharov, Nucl. Phys. B **147**, 385 (1979).
34. L. Reinders, H. Rubinstein, and S. Yazaki, Phys. Rep. **127**, 1 (1985).
35. M. Campostrini, A. D. Giacomo, and Y. Gunduc, Phys. Lett. B **225**, 393 (1989).
36. M. Jamin, Phys. Lett. B **538**, 71 (2002), arXiv:hep-ph/0201174 [hep-ph] .
37. G. Colangelo, J. Gasser, and H. Leutwyler, Phys. Rev. Lett. **86**, 5008 (2001), arXiv:hep-ph/0103063 [hep-ph] .
38. K. G. Wilson, Phys. Rev. D **10**, 2445 (1974).

39. R. Gupta, in *Probing the standard model of particle interactions. Proceedings, Summer School in Theoretical Physics, NATO Advanced Study Institute, 68th session, Les Houches, France, July 28-September 5, 1997. Pt. 1, 2* (1997) pp. 83–219, arXiv:hep-lat/9807028 [hep-lat] .
40. B. Lucini and M. Panero, Prog. Part. Nucl. Phys. **75**, 1 (2014), arXiv:1309.3638 [hep-th] .
41. A. Polyakov, Physics Letters B **72**, 477 (1978).
42. L. Susskind, Phys. Rev. D **20**, 2610 (1979).
43. A. V. Smilga, Phys. Rept. **291**, 1 (1997), arXiv:hep-ph/9612347 [hep-ph] .
44. G. Boyd, J. Engels, F. Karsch, E. Laermann, C. Legeland, M. Lutgemeier, and B. Petersson, Nucl. Phys. **B469**, 419 (1996), arXiv:hep-lat/9602007 [hep-lat] .
45. Y. Iwasaki, K. Kanaya, T. Kaneko, and T. Yoshie, *Lattice'96. Proceedings, 14th International Symposium on Lattice Field Theory, St. Louis, USA, June 4-8, 1996*, Nucl. Phys. Proc. Suppl. **53**, 429 (1997), arXiv:hep-lat/9608090 [hep-lat] .
46. J. Engels, J. Fingberg, F. Karsch, D. Miller, and M. Weber, Physics Letters B **252**, 625 (1990).
47. J. Fingberg, U. M. Heller, and F. Karsch, Nucl. Phys. **B392**, 493 (1993), arXiv:hep-lat/9208012 [hep-lat] .
48. J. Engels, F. Karsch, and K. Redlich, Nucl. Phys. **B435**, 295 (1995), arXiv:hep-lat/9408009 [hep-lat] .
49. S. Borsanyi, G. Endrodi, Z. Fodor, S. D. Katz, and K. K. Szabo, JHEP **07**, 056 (2012), arXiv:1204.6184 [hep-lat] .
50. J. O. Andersen, L. E. Leganger, M. Strickland, and N. Su, JHEP **08**, 053 (2011), arXiv:1103.2528 [hep-ph] .
51. J. O. Andersen, N. Haque, M. G. Mustafa, and M. Strickland, Phys. Rev. D **93**, 054045 (2016), arXiv:1511.04660 [hep-ph] .
52. P. Petreczky, J. Phys. **G39**, 093002 (2012), arXiv:1203.5320 [hep-lat] .
53. Y. Aoki, G. Endrodi, Z. Fodor, S. D. Katz, and K. K. Szabo, Nature **443**, 675 (2006), arXiv:hep-lat/0611014 [hep-lat] .
54. S. Borsanyi, Z. Fodor, C. Hoelbling, S. D. Katz, S. Krieg, C. Ratti, and K. K. Szabo (Wuppertal-Budapest), JHEP **09**, 073 (2010), arXiv:1005.3508 [hep-lat] .
55. A. Bazavov *et al.*, Phys. Rev. D **85**, 054503 (2012), arXiv:1111.1710 [hep-lat] .

56. S. Borsanyi, Z. Fodor, C. Hoelbling, S. D. Katz, S. Krieg, and K. K. Szabo, Phys. Lett. B **730**, 99 (2014), arXiv:1309.5258 [hep-lat] .
57. A. Bazavov *et al.* (HotQCD), Phys. Rev. D **90**, 094503 (2014), arXiv:1407.6387 [hep-lat] .
58. P. Steinbrecher (HotQCD), *Proceedings, 27th International Conference on Ultrarelativistic Nucleus-Nucleus Collisions (Quark Matter 2018): Venice, Italy, May 14-19, 2018*, Nucl. Phys. **A982**, 847 (2019), arXiv:1807.05607 [hep-lat] .
59. A. Andronic, P. Braun-Munzinger, K. Redlich, and J. Stachel, Nature **561**, 321 (2018), arXiv:1710.09425 [nucl-th] .
60. A. Andronic *et al.*, Nucl. Phys. **A837**, 65 (2010), arXiv:0911.4806 [hep-ph] .
61. M. Bluhm, M. Nahrgang, and J. M. Pawlowski, (2020), arXiv:2004.08608 [nucl-th] .
62. K. Fukushima, Journal of Physics G: Nuclear and Particle Physics **39**, 013101 (2011).
63. B. Lucini, M. Teper, and U. Wenger, JHEP **02**, 033 (2005), arXiv:hep-lat/0502003 [hep-lat] .
64. M. Panero, Phys. Rev. Lett. **103**, 232001 (2009), arXiv:0907.3719 [hep-lat] .
65. S. Datta and S. Gupta, Phys. Rev. **D82**, 114505 (2010), arXiv:1006.0938 [hep-lat] .
66. B. Lucini, A. Rago, and E. Rinaldi, Phys. Lett. **B712**, 279 (2012), arXiv:1202.6684 [hep-lat] .
67. M. Shifman and A. Vainshtein, Phys. Rev. D **77**, 034002 (2008), arXiv:0710.0863 [hep-ph] .
68. S. S. Afonin and A. D. Katanaeva, Eur. Phys. J. **C74**, 3124 (2014), arXiv:1408.6935 [hep-ph] .
69. A. V. Anisovich, V. V. Anisovich, and A. V. Sarantsev, Phys. Rev. D **62**, 051502 (2000).
70. D. Bugg, Physics Reports **397**, 257 (2004), arXiv:hep-ex/0412045 [hep-ex] .
71. P. Masjuan, E. Ruiz Arriola, and W. Broniowski, Phys. Rev. D **85**, 094006 (2012).
72. E. Klempt and A. Zaitsev, Physics Reports **454**, 1 (2007).
73. S. S. Afonin, Phys. Lett. **B639**, 258 (2006), arXiv:hep-ph/0603166 [hep-ph] .
74. S. S. Afonin, Mod. Phys. Lett. **A22**, 1359 (2007), arXiv:hep-ph/0701089

[hep-ph] .

75. S. S. Afonin, *41st Annual Winter School on Nuclear and Particle Physics (PNPI 2007) Repino, St. Petersburg, Russia, February 19-March 2, 2007*, Int. J. Mod. Phys. **A22**, 4537 (2007), arXiv:0704.1639 [hep-ph] .
76. S. S. Afonin, Int. J. Mod. Phys. **A23**, 4205 (2008), arXiv:0709.4444 [hep-ph] .
77. S. S. Afonin, Mod. Phys. Lett. **A23**, 3159 (2008), arXiv:0707.1291 [hep-ph] .
78. D. M. Li, B. Ma, Y. X. Li, Q. K. Yao, and H. Yu, Eur. Phys. J. C **37**, 323 (2004).
79. S. S. Afonin and I. V. Pusenkov, Phys. Rev. **D90**, 094020 (2014), arXiv:1411.2390 [hep-ph] .
80. S. S. Afonin and I. V. Pusenkov, Mod. Phys. Lett. **A29**, 1450193 (2014), arXiv:1308.6540 [hep-ph] .
81. S. S. Afonin, Phys. Rev. **C76**, 015202 (2007), arXiv:0707.0824 [hep-ph] .
82. N. Isgur, C. Morningstar, and C. Reader, Phys. Rev. D **39**, 1357 (1989).
83. M. Wingate, T. DeGrand, S. Collins, and U. M. Heller, Phys. Rev. Lett. **74**, 4596 (1995).
84. D. T. Son and M. A. Stephanov, Phys. Rev. D **69**, 065020 (2004), arXiv:hep-ph/0304182 .
85. M. Zielinski *et al.*, Phys. Rev. Lett. **52**, 1195 (1984).
86. L. Da Rold and A. Pomarol, Nucl. Phys. B **721**, 79 (2005), arXiv:hep-ph/0501218 .
87. J. Hirn and V. Sanz, J. High Energy Phys. **2005**, 030 (2005), arXiv:hep-ph/0507049 .
88. A. Gokalp and O. Yilmaz, Eur. Phys. J. C **22**, 323 (2001).
89. J. Gasser and H. Leutwyler, Phys. Rep. **87**, 77 (1982).
90. G. S. Bali, F. Bursa, L. Castagnini, S. Collins, L. Del Debbio, B. Lucini, and M. Panero, JHEP **06**, 071 (2013), arXiv:1304.4437 [hep-lat] .
91. G. S. Bali and F. Bursa, JHEP **09**, 110 (2008), arXiv:0806.2278 [hep-lat] .
92. C. J. Morningstar and M. J. Peardon, Phys. Rev. **D60**, 034509 (1999), arXiv:hep-lat/9901004 [hep-lat] .
93. H. B. Meyer, *Glueball Regge trajectories*, Ph.D. thesis, Oxford U. (2004), arXiv:hep-lat/0508002 [hep-lat] .
94. Y. Chen *et al.*, Phys. Rev. **D73**, 014516 (2006), arXiv:hep-lat/0510074 [hep-lat] .

95. E. Gregory, A. Irving, B. Lucini, C. McNeile, A. Rago, C. Richards, and E. Rinaldi, JHEP **10**, 170 (2012), arXiv:1208.1858 [hep-lat] .
96. B. Lucini, M. Teper, and U. Wenger, JHEP **06**, 012 (2004), arXiv:hep-lat/0404008 [hep-lat] .
97. B. Lucini and M. Teper, JHEP **06**, 050 (2001), arXiv:hep-lat/0103027 [hep-lat] .
98. F. E. Close and Q. Zhao, Phys. Rev. **D71**, 094022 (2005), arXiv:hep-ph/0504043 [hep-ph] .
99. H.-Y. Cheng, C.-K. Chua, and K.-F. Liu, Phys. Rev. **D92**, 094006 (2015), arXiv:1503.06827 [hep-ph] .
100. W. Ochs, J. Phys. **G40**, 043001 (2013), arXiv:1301.5183 [hep-ph] .
101. J. Sonnenschein and D. Weissman, JHEP **12**, 011 (2015), arXiv:1507.01604 [hep-ph] .
102. S. Janowski, F. Giacosa, and D. H. Rischke, Phys. Rev. **D90**, 114005 (2014), arXiv:1408.4921 [hep-ph] .
103. F. Brünner, D. Parganlija, and A. Rebhan, Phys. Rev. **D91**, 106002 (2015), [Erratum: Phys. Rev.D93,no.10,109903(2016)], arXiv:1501.07906 [hep-ph] .
104. J. Erlich, E. Katz, D. T. Son, and M. A. Stephanov, Phys. Rev. Lett. **95**, 261602 (2005), arXiv:hep-ph/0501128v2 .
105. A. Karch, E. Katz, D. T. Son, and M. A. Stephanov, Phys. Rev. D **74**, 015005 (2006), arXiv:hep-ph/0602229v2 .
106. H. R. Grigoryan and A. V. Radyushkin, Phys. Rev. D **76**, 115007 (2007), arXiv:0709.0500 [hep-ph] .
107. L. Da Rold and A. Pomarol, J. High Energy Phys. **01**, 157 (2006), arXiv:hep-ph/0510268 [hep-ph] .
108. P. Colangelo, F. D. Fazio, F. Giannuzzi, F. Jugeau, and S. Nicotri, Phys. Rev. D **78**, 055009 (2008), arXiv:0807.1054 [hep-ph] .
109. H. Boschi-Filho and N. R. F. Braga, Eur. Phys. J. **C32**, 529 (2004), arXiv:hep-th/0209080 [hep-th] .
110. P. Colangelo, F. D. Fazio, F. Jugeau, and S. Nicotri, Phys. Lett. B **652**, 73 (2007), arXiv:hep-ph/0703316 [hep-ph] .
111. H. Forkel, Phys. Rev. **D78**, 025001 (2008), arXiv:0711.1179 [hep-ph] .
112. P. Colangelo, F. De Fazio, F. Jugeau, and S. Nicotri, Int. J. Mod. Phys. **A24**, 4177 (2009), arXiv:0711.4747 [hep-ph] .
113. D. Li and M. Huang, JHEP **11**, 088 (2013), arXiv:1303.6929 [hep-ph] .

114. S. P. Bartz, A. Dhumuntarao, and J. I. Kapusta, Phys. Rev. **D98**, 026019 (2018), arXiv:1801.06118 [hep-th] .
115. S. J. Brodsky, G. F. de Teramond, H. G. Dosch, and J. Erlich, Phys. Rept. **584**, 1 (2015), arXiv:1407.8131 [hep-ph] .
116. V. Balasubramanian, P. Kraus, and A. Lawrence, Phys. Rev. D **59**, 046003 (1999), arXiv:hep-th/9805171 .
117. J. Polchinski, in *Theoretical Advanced Study Institute in Elementary Particle Physics: String theory and its Applications: From meV to the Planck Scale* (2010) pp. 3–46, arXiv:1010.6134 [hep-th] .
118. H. Nastase, "Gravity duals," in *Introduction to the AdS/CFT Correspondence* (Cambridge University Press, 2015) pp. 331–351.
119. J. Polchinski and M. J. Strassler, Phys. Rev. Lett. **88**, 031601 (2002), arXiv:hep-th/0109174 .
120. S. S. Afonin, Phys. Lett. **B719**, 399 (2013), arXiv:1210.5210 [hep-ph] .
121. S. S. Afonin, *Proceedings, International Meeting Excited QCD 2016: Costa da Caparica, Portugal, March 6-12, 2016*, Acta Phys. Polon. Supp. **9**, 597 (2016), arXiv:1604.02903 [hep-ph] .
122. A. Vega and P. Cabrera, Phys. Rev. **D93**, 114026 (2016), arXiv:1601.05999 [hep-ph] .
123. F. Cooper, A. Khare, and U. Sukhatme, Phys. Rept. **251**, 267 (1995), arXiv:hep-th/9405029 [hep-th] .
124. E. Witten, Adv. Theor. Math. Phys. **2**, 505 (1998), arXiv:hep-th/9803131 [hep-th] .
125. C. P. Herzog, Phys. Rev. Lett. **98**, 091601 (2007), arXiv:hep-th/0608151 [hep-th] .
126. C. A. Ballon Bayona, H. Boschi-Filho, N. R. F. Braga, and L. A. Pando Zayas, Phys. Rev. **D77**, 046002 (2008), arXiv:0705.1529 [hep-th] .
127. U. Gursoy, E. Kiritsis, and F. Nitti, JHEP **02**, 019 (2008), arXiv:0707.1349 [hep-th] .
128. O. Andreev and V. I. Zakharov, Phys. Rev. **D74**, 025023 (2006), arXiv:hep-ph/0604204 [hep-ph] .
129. O. Andreev and V. I. Zakharov, Phys. Lett. **B645**, 437 (2007), arXiv:hep-ph/0607026 [hep-ph] .
130. Y. Yang and P.-H. Yuan, JHEP **12**, 161 (2015), arXiv:1506.05930 [hep-th] .
131. M.-W. Li, Y. Yang, and P.-H. Yuan, Phys. Rev. **D96**, 066013 (2017), arXiv:1703.09184 [hep-th] .

132. I. Aref'eva and K. Rannu, JHEP **05**, 206 (2018), arXiv:1802.05652 [hep-th] .
133. S. He, S.-Y. Wu, Y. Yang, and P.-H. Yuan, JHEP **04**, 093 (2013), arXiv:1301.0385 [hep-th] .
134. D. Dudal and S. Mahapatra, Phys. Rev. **D96**, 126010 (2017), arXiv:1708.06995 [hep-th] .
135. U. Gursoy, E. Kiritsis, L. Mazzanti, G. Michalogiorgakis, and F. Nitti, *5th Aegean Summer School: FROM GRAVITY TO THERMAL GAUGE THEORIES: THE AdS/CFT CORRESPONDENCE Adamas, Milos Island, Greece, September 21-26, 2009*, Lect. Notes Phys. **828**, 79 (2011), arXiv:1006.5461 [hep-th] .
136. J. Erlich and C. Westenberger, Phys. Rev. D **79**, 066014 (2009), arXiv:0812.5105 [hep-ph] .
137. H. J. Kwee and R. F. Lebed, Phys. Rev. D **77**, 115007 (2008), arXiv:0712.1811 [hep-ph] .
138. T. Gherghetta, J. I. Kapusta, and T. M. Kelley, Phys. Rev. D **79**, 076003 (2009), arXiv:0902.1998 [hep-ph] .
139. H. Forkel, T. Frederico, and M. Beyer, J. High Energy Phys. **2007**, 077 (2007), arXiv:0705.1857 [hep-ph] .
140. A. Vega and I. Schmidt, Phys. Rev. D **82**, 115023 (2010), arXiv:1005.3000 [hep-ph] .
141. Z. Fang, Y.-L. Wu, and L. Zhang, Phys. Lett. B **762**, 86 (2016), 1604.02571v1 .
142. A. Cherman, T. D. Cohen, and E. S. Werbos, Phys. Rev. C **79**, 045203 (2009), arXiv:0804.1096 [hep-ph] .
143. W. de Paula and T. Frederico, Phys. Lett. B **693**, 287 (2010), arXiv:0908.4282 [hep-ph] .
144. Y.-Q. Sui, Y.-L. Wu, Z.-F. Xie, and Y.-B. Yang, Phys. Rev. D **81**, 014024 (2010), arXiv:0909.3887 [hep-ph] .
145. S. Afonin, Mod. Phys. Lett. A **22**, 1359 (2007), arXiv:hep-ph/0701089 .
146. M. Shifman and A. Vainshtein, Phys. Rev. D **77**, 034002 (2008).
147. S. Afonin, Phys. Rev. C **83**, 048202 (2011), arXiv:1102.0156 [hep-ph] .
148. S. Narison, Phys. Lett. B **624**, 223 (2005), arXiv:hep-ph/0412152 .
149. J. Hirn, N. Rius, and V. Sanz, Phys. Rev. D **73**, 085005 (2006), arXiv:hep-ph/0512240v2 .
150. C. Csaki and M. Reece, J. High Energy Phys. **05**, 062 (2007), arXiv:hep-

ph/0608266 [hep-ph] .
151. S. S. Afonin, Phys. Lett. B **576**, 122 (2003), arXiv:hep-ph/0309337 [hep-ph] .
152. S. S. Afonin, A. A. Andrianov, V. A. Andrianov, and D. Espriu, J. High Energy Phys. **04**, 039 (2004), arXiv:hep-ph/0403268 [hep-ph] .
153. S. S. Afonin and D. Espriu, J. of High Energy Phys. **2006**, 047 (2006), arXiv:hep-ph/0602219 .
154. F. Jugeau, S. Narison, and H. Ratsimbarison, Phys. Lett. B **722**, 111 (2013), arXiv:1302.6909 [hep-ph] .
155. S. Amendolia *et al.*, Nucl. Phys. B **277**, 168 (1986).
156. G. M. Huber *et al.* (The Jefferson Lab F_π Collaboration), Phys. Rev. C **78**, 045203 (2008).
157. C. J. Bebek *et al.*, Phys. Rev. D **17**, 1693 (1978).
158. G. P. Lepage and S. J. Brodsky, Phys. Lett. B **87**, 359 (1979).
159. D. B. Kaplan and H. Georgi, Physics Letters B **136**, 183 (1984).
160. D. B. Kaplan, H. Georgi, and S. Dimopoulos, Physics Letters B **136**, 187 (1984).
161. H. Georgi, D. B. Kaplan, and P. Galison, Physics Letters B **143**, 152 (1984).
162. H. Georgi and D. B. Kaplan, Physics Letters B **145**, 216 (1984).
163. M. J. Dugan, H. Georgi, and D. B. Kaplan, Nuclear Physics B **254**, 299 (1985).
164. G. 't Hooft, NATO Sci. Ser. B **59**, 135 (1980).
165. G. Ferretti and D. Karateev, JHEP **03**, 077 (2014), arXiv:1312.5330 [hep-ph] .
166. R. Contino, Y. Nomura, and A. Pomarol, Nucl. Phys. B **671**, 148 (2003), arXiv:hep-ph/0306259v1 .
167. K. Agashe, R. Contino, and A. Pomarol, Nucl. Phys. B **719**, 165 (2005), arXiv:hep-ph/0412089 .
168. K. Agashe and R. Contino, Nucl. Phys. B **742**, 59 (2006), arXiv:hep-ph/0510164 .
169. J. Setford, JHEP **01**, 092 (2018), arXiv:1710.11206 [hep-ph] .
170. R. Contino, L. Da Rold, and A. Pomarol, Phys. Rev. D **75**, 055014 (2007), arXiv:hep-ph/0612048 .
171. G. Aad *et al.* (The ATLAS collaboration), J. High Energy Phys. **2015**, 206 (2015), arXiv:1509.00672v2 [hep-ex] .
172. J. de Blas, O. Eberhardt, and C. Krause, JHEP **07**, 048 (2018),

arXiv:1803.00939 [hep-ph] .

173. A. Falkowski and M. Perez-Victoria, J. High Energy Phys. **2008**, 107 (2008), arXiv:0806.1737 [hep-ph] .
174. B. Bellazzini, C. Csáki, and J. Serra, Eur. Phys. J. C **74**, 2766 (2014), arXiv:1401.2457 [hep-ph] .
175. G. Panico and A. Wulzer, *The Composite Nambu-Goldstone Higgs* (Springer International Publishing, 2016) arXiv:1506.01961v2 [hep-ph] .
176. G. Altarelli and R. Barbieri, Phys. Lett. B **253**, 161 (1991).
177. M. E. Peskin and T. Takeuchi, Phys. Rev. D **46**, 381 (1992).
178. S. Weinberg, Phys. Rev. Lett. **18**, 507 (1967).
179. R. L. Delgado, A. Dobado, D. Espriu, C. Garcia-Garcia, M. J. Herrero, X. Marcano, and J. J. Sanz-Cillero, JHEP **11**, 098 (2017), arXiv:1707.04580 [hep-ph] .
180. A. Erdélyi, ed., *Higher transcendental functions (Bateman Manuscript Project)*, Vol. 1 (McGraw-Hill, New York, 1953).